

Behaviour of food-grade Pickering emulsions stabilized by plant-based particles under *in vitro* digestion conditions

Shuning Zhang

Submitted in accordance with the requirements for the degree of

Doctor of Philosophy

The University of Leeds

School of Food Science and Nutrition

July, 2022

The candidate confirms that the work submitted is her own, except where work which has formed part of jointly-authored publications has been included. The contribution of the candidate and the other authors to this work has been explicitly indicated below. The candidate confirms that appropriate credit has been given within the thesis where reference has been made to the work of others. Details of the jointly-authored publications and the contributions of the candidate and the other authors to the work are outlined on the next page

This copy has been supplied on the understanding that it is copyright material and that no quotation from the thesis may be published without proper acknowledgement.

The right of Shuning Zhang to be identified as Author of this work has been asserted by Shuning Zhang in accordance with the Copyright, Designs and Patents Act 1988.

© 2022 The University of Leeds and Shuning Zhang

Further details of the jointly-authored publications and the contributions of the candidate and the other authors to the work are included below:

Chapter 2

Sarkar A, Zhang S, Holmes M, Ettelaie R. (2018) Colloidal aspects of digestion of Pickering emulsions: Experiments and theoretical models of lipid digestion kinetics. *Adv Colloid Interface Sci.* 263:195-211.

Chapter 3

Zhang, S., Holmes, M., Ettelaie, R., Sarkar, A. (2020) Pea protein microgel particles as Pickering stabilizers of oil-in-water emulsions: Responsiveness to pH and ionic strength. *Food Hydrocolloids*, 102, 105583.

Chapter 4

Zhang, S., Murray, B. S., Suriyachay, N., Holmes, M., Ettelaie, R., & Sarkar, A. (2021). Synergistic interactions of plant protein microgels and cellulose nanocrystals at the interface and their inhibition of the gastric digestion of Pickering emulsions. *Langmuir*, 37(2), 827-840.

Chapter 5

Zhang, S., Murray B S., Holmes, M., Ettelaie, R., Sarkar, A. (2022) Gastrointestinal fate and fatty acid release of Pickering emulsions stabilized by mixtures of plant protein microgels + cellulose particles: an *in vitro* static digestion study. *Food Biophysics* (accepted on 06.07.2022)

Details of authorship contributions:

Chapter 2. Shuning Zhang: gathered the literature, arranged the tables and figures as well as drafted and edited the manuscripts and replied to the comments from reviewers. Melvin Holmes and Rammile Ettelaie: contributed to the mathematical modelling section, provided supervision, feedback and contributed to the proofreading and editing of the manuscript. Anweshha Sarkar: designed the research question for the literature review, rearranged the structure of the review, provided supervision, feedback and contributed to the proofreading and editing of the manuscript and answering questions upon receiving comments from the reviewers. % Contribution of Shuning Zhang, Anweshha Sarkar, Melvin Holmes and Rammile Ettelaie for Chapter 2 was 40%, 40%, 10% and 10% respectively.

Chapter 3. Shuning Zhang: designed the research question, experiments and conducted the measurements, data analysis and interpretation as well as drafted and edited the manuscripts and replied to the comments from reviewers. Melvin Holmes and Rammile Ettelaie: contributed to the fitting section, provided supervision, feedback and contributed to the proofreading and editing of the manuscript. Anweshha Sarkar: provided supervision, feedback and contributed to the proofreading and editing of the manuscript.

Chapter 4. Shuning Zhang: designed the research question, experiments and conducted the measurements, data analysis and interpretation as well as drafted and edited the manuscripts and replied to the comments from reviewers. Melvin Holmes and Rammile Ettelaie: provided supervision, feedback and contributed to the proofreading and editing of the manuscript. Brent S. Murray: provided supervision, helped designing the monolayer experiments and contributed to the proofreading and editing of the manuscript. Nuttaporn Suriyachay: conducted preliminary experiments for gastric digestion step of few emulsions. Anweshha Sarkar: provided

supervision, feedback and contributed to the proofreading and editing of the manuscript.

Chapter 5. Shuning Zhang: designed the research question, experiments and conducted the measurements, data analysis and interpretation as well as drafted and edited the manuscripts and replied to the comments from reviewers. Melvin Holmes and Rammile Ettelaie: contributed to the fitting section, provided supervision, feedback and contributed to the proofreading and editing of the manuscript. Brent S. Murray: provided supervision and contributed to the proofreading of the manuscript. Anwasha Sarkar: provided supervision, feedback and contributed to the proofreading and editing of the manuscript upon receiving comments from the reviewers.

List of accepted conference abstracts

Poster presentations

Zhang, S., Holmes, M., Ettelaie, R., Sarkar, A. (2018). A mathematical model for interpreting *in vitro* digestion of Pickering emulsions. 17th Food Colloids Conference: Application of Soft Matter Concepts – Leeds, UK.

Zhang, S., Holmes, M., Ettelaie, R., Sarkar, A. (2019). Behaviour of Pickering emulsions stabilized by pea protein-based microgel particles under *in vitro* digestion conditions. Industry networking event: Food Innovation for Delivering Health, Nutrition and Wellness – Leeds, UK.

Zhang, S., Holmes, M., Ettelaie, R., Sarkar, A. (2019). Pea protein microgel particles-stabilized Pickering emulsions: Influence of pH and ionic strength. 8th International Symposium on “Delivery of Functionality in Complex Food Systems” – Porto, Portugal. (Best poster award).

Zhang, S., Murray, B. S., Suriyachay, N., Holmes, M., Ettelaie, R., Sarkar, A. (2021). Designing gastric stable Pickering emulsions using synergistic plant-based particle-particle interaction at the oil-water interface The Designed Assembly of Colloids at Interfaces - Fundamentals to Applications Conference – online

Oral presentations

Zhang, S., Holmes, M., Ettelaie, R., Sarkar, A. (2018). Behaviour of Pickering emulsions stabilized by pea protein-based microgel particles. 5th PhD Conference. University of Leeds, UK

Zhang, S., Holmes, M., Ettelaie, R., Sarkar, A. (2019). UK Pickering emulsions stabilized by pea protein microgel particles: Influence of pH and ionic strength. The Food Hydrocolloids Trust: 20th Gums & Stabilizers for the Food Industry Conference – San Sebastian, Spain.

Zhang, S., Murray, B. S., Russell, J. A., Boxal, S., Sarkar, A, Modulating *in vitro* gastric digestion of emulsions using composite whey protein-cellulose nanocrystal interfaces (2019). 4th UK Hydrocolloids Symposium, from Food to Bioprocessing – Leeds, UK.

Zhang, S., Holmes, M., Ettelaie, R., Sarkar, A. (2019). Modulating *in vitro* gastric digestion of Pickering emulsions coated by cellulose nanocrystal interfaces. 6th PhD Conference. University of Leeds, UK

Zhang, S., Murray, B. S., Suriyachay, N., Holmes, M., Ettelaie, R., Sarkar, A. (2020). *In vitro* gastric digestion of Pea protein microgel particle stabilized Pickering emulsions coated by cellulose nanocrystals. Physics in Food Manufacturing Conference – Leeds, UK.

Zhang, S., Murray, B. S., Suriyachay, N., Holmes, M., Ettelaie, R., Sarkar, A. (2020). Overcoming gastric destabilization of pea protein microgel particle-stabilized Pickering emulsions using electrostatic coating with cellulose nanocrystals. 34th EFFoST International Conference – online

Zhang, S., Murray, B. S., Suriyachay, N., Holmes, M., Ettelaie, R., Sarkar, A. (2021). Synergistic Interactions of Plant Protein Microgels and Cellulose Nanocrystals at the Interface and Their Inhibition of the Gastric Digestion of Pickering Emulsions. 4th Food Structure and Functionality Symposium – online

Zhang, S., Murray, B. S., Suriyachay, N., Holmes, M., Ettelaie, R., Sarkar, A. (2021). Synergistic interactions of plant protein microgels and cellulose nanocrystals at interface and their inhibition of gastric digestion of Pickering emulsions. 6th PhD Conference . University of Leeds – online

Zhang, S., Murray, B. S., Suriyachay, N., Holmes, M., Ettelaie, R., Sarkar, A. (2021). Synergistic Interactions of Plant Protein Microgels and Cellulose Nanocrystals at the Interface and Their Inhibition of the Gastric Digestion of Pickering Emulsions. 35th Conference of European Colloid & Interface Society – online

Acknowledgements

First of all, I would like to sincerely thank my main supervisor Professor Anwesha Sarkar for her guidance, consistent help, patience as well as motivation throughout my PhD. Her support was truly from the start of this research project up to the submission of my thesis. I truly believe that she is the best supervisor in the world. I am deeply grateful for her continued help when I was in trouble of surgery and depression, and for her encouragement when I doubted my abilities. I was so lucky to have such an incredible and supportive person in this research project.

I also greatly indebted to my other supervisors, Dr Melvin Holmes and Dr Rammile Ettelaie for their instructive advice and useful suggestions on my thesis. I am deeply grateful for their help in my PhD. I would like to express my heartfelt gratitude to Professor Brent S. Murray, who have instructed and helped me a lot in the past three years. Next, I would like to extend my thanks to all staff in the School of Food Science and Nutrition, who helped me directly or indirectly throughout my research. I particularly would like to thank: Dr. Andrea Araiza Calahorra, Dr. Emma Krop, Dr. Efren Andablo, Miles Ratcliff, Dr. Joanne Brown, Ian Hardy, Dr. Nataricha Phisarnchananan and Neil Rigby, many thanks for always be there to help and offer valuable technical support during my PhD.

Last but not least, I would like to express my gratitude to my parents. Sincerely thanks for giving me a lot of help, support and encouragement in their own special ways. Their unconditional love and unlimited support help me overcome difficult times during these years. This thesis is dedicated to all of you.

Abstract

Lipid digestion of emulsions is a bio-interfacial process that is largely driven by the anchoring of the lipase-colipase-biosurfactant (bile salts) complex onto the surface of emulsified lipid droplets. Therefore, engineering oil-water interfaces that prevent competitive displacement by bile salts and/or delay the transportation of lipase to the lipidoidal substrate can be an effective strategy to modulate lipolysis in human physiology. Among various emulsions, particle-stabilized, so-called “Pickering emulsions” are particularly interesting in modulating the fundamental biological process of lipid digestion due to their distinctive stability against coalescence and resilience to desorption by intestinal biosurfactants such as bile salts and fatty acids. In this thesis, plant protein-based microgel particles were designed to create Pickering emulsions because of the known benefits of plant proteins with respect to sustainability, and the *in vitro* gastrointestinal digestion fate of these particle-laden droplets was investigated. The hypothesis was plant protein microgels alone cannot protect the droplet against gastric coalescence but a secondary coating by a non-enzymatically-responsive polysaccharide such as cellulose nanocrystals at the protein microgel interfaces can help tailoring gastrointestinal digestion of such emulsion. A range of physicochemical and microstructural characterization across length scales were used to investigate the colloidal design and digestion of Pickering emulsions with simple (protein microgels) and complex interfaces (protein microgels + cellulose nanocrystals).

Pea protein microgels were designed using a facile top-down approach of heat-set protein gel formation followed by controlled shearing. The aqueous dispersion of pea protein microgel particles at pH 7.0 were sub-micron size (~250 nm) with high negative charge (-35 mV) whilst the isoelectric point (pI) of the microgel particles was at pH 5.0. The high adsorption efficiency of such microgel particles at the oil-water interface (>98%) at pH 7.0, demonstrated excellent ability to inhibit coalescence of oil droplets providing the evidence for these pea protein microgels to act as a Pickering stabilizers. Adjusting the pH of such pea protein

microgel-stabilized emulsions to pI demonstrated aggregation of adsorbed microgels at the particle-laden interface providing a higher degree of adsorption as well as enhancing inter-droplet flocculation and the shear-thinning character as compared to those at pH 7.0 or pH 3.0. Moreover, microgel-microgel aggregation and viscosity enhancement in emulsions in presence of 100 mM NaCl were shown due to charge screening effects, which were further supported by theoretical considerations.

As hypothesized the plant protein microgels were pepsin-sensitive and thus were not offering protection to droplets against coalescence on their own. Engineering of the oil-water interface *via* synergistic particle–particle interactions using mutually oppositely-charged pea protein microgels and cellulose nanocrystals provided a barrier against gastric coalescence of Pickering emulsions whereas systems stabilized solely by pea protein microgels were digested immediately leading to droplet coalescence in the gastric regime. Further, increasing concentrations of cellulose nanocrystals and consequently increasing the bulk viscosity of emulsions, also enabled delaying gastric breakdown behaviour of underlying protein microgel-laden interface. Coalescence occurred during the intestinal digestion stage, irrespective of the concentration of cellulose nanocrystals used added. The presence of cellulose nanocrystals lowered the lipolysis kinetics but raised the extent of free fatty acid release as compared to in its absence, this is largely attributed to the lower levels of gastric coalescence, *i.e.*, a smaller droplet size and consequently higher interfacial area. The trends were similar when just lipase was added with no prior gastric phase, although the extent and rate of free fatty acids release decreased in all emulsions, highlighting the importance of prior proteolysis in lipolysis of such systems.

Findings of this thesis provides guidelines on designing complex interfacial structure using two types of oppositely charged particles that forms an electrostatically self-assembled particulate structure at the oil-water interface (at gastric pH). Such complex interfaces might be a particularly useful strategy to improve the delivery of lipophilic bioactive compounds that require protection in the stomach but release in the intestines.

Table of Contents

List of accepted conference abstracts.....	vi
Acknowledgements	viii
Abstract.....	ix
Table of Contents	xi
List of Tables	xvi
List of Figures.....	xvii
List of Abbreviations	xxvi
List of Symbols	xxx
Chapter 1. General Introduction.....	- 1 -
1.1 Overall research aim	- 1 -
1.2 Background	- 2 -
1.2.1 Pickering emulsions	- 2 -
1.3 Rationale behind the selection of biopolymers	- 3 -
1.3.1 Plant protein.....	- 4 -
1.3.1.1 Pea protein isolate for designing microgel particles	- 6 -
1.3.2 Polysaccharides.....	- 7 -
1.4 Rationale behind the selection of characterization techniques.....	- 8 -
1.4.1 Microgel particles and emulsions characterization	- 8 -
1.4.1.1 Dynamic light scattering (DLS).....	- 9 -
1.4.1.2 Static light scattering (SLS).....	- 11 -
1.4.1.3 Zeta-potential	- 12 -
1.4.1.4 Protein assay	- 15 -
1.4.1.5 Microscopy across scales.....	- 15 -
1.4.1.5.1 Light microscopy	- 15 -
1.4.1.5.2 Confocal laser scanning microscopy	- 16 -
1.4.1.5.3 Scanning electron microscopy (SEM)	- 18 -
1.4.1.6 Monolayer experiments	- 19 -
1.4.1.7 Interfacial shear viscosity	- 21 -
1.4.1.8 Rheology	- 24 -
1.4.2 <i>In vitro</i> gastrointestinal processing	- 27 -
1.4.2.1 Protein electrophoresis (sodium dodecyl sulphate polyacrylamide gel electrophoresis).....	- 30 -
1.4.2.2 Free fatty acid release	- 31 -
1.5 Outline of the thesis.....	- 32 -

1.6 Reference.....	- 35 -
Chapter 2. Literature review	- 46 -
Abstract	- 46 -
2.1 Introduction	- 47 -
2.2 Key players in colloidal structuring of lipids in human physiology ..	- 53 -
2.2.1 Oral phase	- 55 -
2.2.2 Gastric phase.....	- 56 -
2.2.3 Intestinal phase.....	- 57 -
2.3 Experimental investigations on colloidal digestion of Pickering emulsions.....	- 59 -
2.3.1 Enzyme-unresponsive particles	- 64 -
2.3.1.1 Silica nanoparticles.	- 64 -
2.3.1.2 Polysaccharide-based particles.	- 65 -
2.3.1.3 Flavonoid crystals	- 66 -
2.3.2 Enzyme-responsive particles	- 67 -
2.3.2.1 Starch particle	- 67 -
2.3.2.2 Protein particles from animal sources.....	- 68 -
2.3.2.3 Protein particles from plant sources.....	- 70 -
2.4 Future interfacial design strategies to control digestion profiles	- 71 -
2.4.1 Particle to droplet size ratio	- 71 -
2.4.2 Particle charge.....	- 73 -
2.4.3 Particle fusion at interface	- 74 -
2.4.4 Particle shape	- 75 -
2.4.5 Particle loading at the interface.....	- 77 -
2.4.6 Material chemistry of particle.....	- 78 -
2.5 Mathematical models for lipid digestion kinetics	- 79 -
2.6 Conclusions	- 88 -
2.7 References	- 90 -
Chapter 3. Pea protein microgel particles as Pickering stabilizers of oil-in-water emulsions: Responsiveness to pH and ionic strength.....	- 103 -
Abstract	- 103 -
3.1 Introduction	- 104 -
3.2 Materials and Methods.....	- 107 -
3.2.1 Materials	- 107 -
3.2.2 Methods	- 108 -

3.2.2.1	Preparation of pea protein microgel (PPM)	- 108 -
3.2.2.2	Preparation of PPM-stabilized Pickering emulsions (PPM-E)	- 108 -
3.2.2.3	Coalescence stability of PPM-E during storage.....	- 109 -
3.2.2.4	pH and ion treatment.....	- 110 -
3.2.2.5	Size and ζ -potential measurements	- 110 -
3.2.2.6	Adsorption efficiency of PPM at the oil-water interface	- 111 -
3.2.2.7	Apparent viscosity measurement	- 112 -
3.2.2.8	Microscopy	- 113 -
3.2.2.9	Sodium dodecyl sulphate-polyacrylamide gel electrophoresis (SDS-PAGE).....	- 113 -
3.2.2.10	Statistical analysis	- 114 -
3.3	Results and Discussion.....	- 114 -
3.3.1	Characteristics of aqueous dispersion of PPM.....	- 114 -
3.3.2	Colloidal stability of aqueous dispersions of PPM	- 115 -
3.3.3	Characteristics of Pickering O/W emulsions stabilized by PPM (PPM-E)	- 121 -
3.3.3.1	Stability of PPM-E prepared using various concentration of PPM	- 121 -
3.3.3.2	Composition of proteins in the adsorbed phase of E1.0.....	- 125 -
3.3.3.3	Influence of pH on behaviour of E1.0 droplets.....	- 126 -
3.3.3.4	Influence of background electrolyte concentration on behaviour of E1.0 droplets	- 132 -
3.4	Conclusions	- 134 -
3.5	References	- 136 -
Chapter 4. Synergistic interactions of plant protein microgels and cellulose nanocrystals at the interface and their inhibition of gastric digestion of Pickering emulsions		- 143 -
Abstract		- 143 -
4.1	Introduction	- 144 -
4.2	Material and Methods.....	- 146 -
4.2.1	Materials.	- 146 -
4.2.2	Methods	- 147 -
4.2.2.1	Preparation of pea protein microgel particles (PPM).....	- 147 -
4.2.2.2	Preparation of O/W emulsions.....	- 147 -
4.2.2.3	<i>In vitro</i> gastric digestion	- 148 -
4.2.2.4	Measurement of PPM and emulsion droplet size.....	- 149 -
4.2.2.5	Measurement of zeta-potential.....	- 149 -

4.2.2.6	Microscopy	- 149 -
4.2.2.7	Rheology	- 150 -
4.2.2.8	Electrophoresis of proteins and their digestants.	- 151 -
4.2.2.9	Langmuir trough monolayer experiments.....	- 151 -
4.2.2.10	Pepsin activity assay.	- 152 -
4.2.2.11	Statistical analyses	- 153 -
4.3	Results and Discussion.....	- 153 -
4.3.1	Characteristics of aqueous dispersions of PPM.	- 153 -
4.3.2	<i>In vitro</i> gastric digestion of aqueous dispersions of PPM.....	- 153 -
4.3.3	PPM-stabilized Pickering emulsions (PPM-E).	- 157 -
4.3.4	<i>In vitro</i> gastric digestion of PPM-E.	- 159 -
4.3.5	Interactions between CNCs and PPM-E at pH 3.0.	- 162 -
4.3.6	Monolayer experiments on PPM and PPM + CNC.	- 164 -
4.3.7	Particle size distributions of PPM-E with different CNC concentrations.	- 168 -
4.3.8	Rheological properties of PPM-E + CNC emulsions.....	- 169 -
4.4	Conclusions	- 175 -
4.5	References	- 177 -
Chapter 5. Gastrointestinal fate and fatty acid release of Pickering emulsions stabilized by mixtures of plant protein microgels + cellulose particles: an <i>in vitro</i> static digestion study		
	Abstract	- 184 -
5.1	Introduction	- 185 -
5.2	Material and Methods.....	- 187 -
5.2.1	Materials	- 187 -
5.2.2	Fabrication of pea protein microgel particles (PPM).....	- 188 -
5.2.3	Preparation of O/W Pickering emulsions (PPM-E)	- 189 -
5.2.4	<i>In vitro</i> gastrointestinal digestion.....	- 189 -
5.2.5	Sizing of PPM and emulsion droplets.....	- 190 -
5.2.6	Zeta-potential	- 191 -
5.2.7	Confocal laser scanning microscopy and visual imaging	- 191 -
5.2.8	Kinetics of free fatty acids (FFAs) release.....	- 192 -
5.2.9	Statistical analyses	- 193 -
5.3	Results and discussion.....	- 193 -
5.3.1	Colloidal stability of PPM dispersions during simulated gastrointestinal digestion	- 193 -

5.3.2	Behaviour of Pickering emulsions during simulated gastrointestinal digestion	- 196 -
5.3.2.1	Evolution of size of droplets	- 196 -
5.3.2.2	Microstructural changes.....	- 201 -
5.3.2.3	ζ - potential.....	- 205 -
5.3.3	Lipid digestion kinetics.....	- 206 -
5.3.4	Lipid digestion kinetics bypassing the gastric phase and using pure lipase	- 209 -
5.3.5	Lipid digestion kinetics of heat-treated emulsions.....	- 211 -
5.4	Conclusion.....	- 212 -
5.5	References	- 214 -
	Chapter 6. General discussion	- 221 -
6.1	Introduction	- 221 -
6.2	Summary of main results obtained in this thesis.....	- 223 -
6.3	Future directions.....	- 231 -
A.	Materials	- 231 -
B.	Advanced characterization techniques.....	- 234 -
C.	Modelling of digestion.....	- 237 -
6.4	Reference.....	- 239 -
	Appendix A	- 244 -
	Appendix B	- 248 -

List of Tables

Table 1.1. Summary of enzymes used in INFOGEST model.	- 29 -
Table 2.1. Summary of literature reports on Pickering O/W emulsions where in vitro lipid digestion kinetics was followed.	- 61 -
Table 3.1. Mean droplet size and zeta-potential of PPM-stabilized Pickering emulsions prepared using different concentrations of PPM (0.05-1.0 wt%) during 28 days of storage at 4 °C.	- 123 -
Table 3.2. Mean droplet size and zeta-potential of PPM-stabilized Pickering emulsions (E1.0) as a function of pH and ionic strengths.	- 124 -
Table 3.3. Consistency coefficient (K) and flow behaviour index (n) of PPM-stabilized Pickering emulsions (E1.0) at different pH and at ionic strengths.	- 131 -
Table 4.1. Consistency index (K) and flow behaviour index (n) of PPM-E + 1, 2 or 3 wt% CNC.	- 171 -
Table 4.2. Mean zeta-potential of PPM-E with 1, 2 and 3 wt% CNC after 0, 30 and 120 min in vitro gastric digestion. Time 0 min represents the emulsion + SGF mixture at pH 3.0 without the addition of pepsin.	- 173 -
Table 4.3. Pepsin activity assay with 2 % w/v hemoglobin mixed with 1 wt% or 2 wt% CNC.	- 174 -
Table 5.1. Average droplet size of PPM-stabilized Pickering emulsion (PPM-E), PPM-E coated with 1.0 wt% CNC (PPM-E + CNC _{1.0}) and PPM-E coated with 3.0 wt% CNC (PPM-E + CNC _{3.0}) during in vitro during intestinal digestion.	- 200 -
Table 5.2. Kinetic data from free fatty acid release i.e. FFA release at 10 min (Φ_{10} , %), maximum quantity of FFA release (Φ_{max} , %), lipid-FFA conversion rate constant (k , $\mu\text{mols}^{-1} \text{m}^{-2}$) and the time to achieve 50% Φ_{max} ($t_{1/2}$, min) during in vitro gastrointestinal digestion of PPM-E and PPM-E+ CNC _{1.0-3.0}	- 209 -
Table 5.3. Kinetic data from free fatty acid release i.e. FFA release at 10 min (Φ_{10} , %), maximum quantity of FFA release (Φ_{max} , %), lipid-FFA conversion rate constant (k , $\mu\text{mols}^{-1} \text{m}^{-2}$) and the time to achieve 50% Φ_{max} ($t_{1/2}$, min) during in vitro intestinal digestion i.e. by passing the gastric phase of PPM-E and PPM-E+CNC _{1.0-3.0} , using pure lipase from porcine pancreas Type II.	- 210 -
Table S4.1. Mean droplet size of PPM-E with 1, 2 and 3 wt% CNC after 0, 30 and 120 min in vitro gastric digestion. Time 0 min represents the emulsion + SGF mixture at pH 3.0 without the addition of pepsin. Different superscripts (a-b) in the same column indicate significant differences between different samples at $p < 0.05$ level.	- 253 -

List of Figures

- Figure 1.1.** Schematic representation of Pickering O/W emulsion i.e. emulsions stabilized by solid particles with a variety of particle shapes; spherical, rods, cubs and peanut-shape..... - 3 -
- Figure 1.2.** Molecular structure of cellulose. - 8 -
- Figure 1.3.** Schematic representation of dynamic light scattering measuring principle. - 9 -
- Figure 1.4.** Hydrodynamic diameter in DLS being larger than the 'core' diameter due to the concentration and type of ions in medium (A) or any surface structure (B) i.e. adsorbed polymer..... - 11 -
- Figure 1.5.** Schematic representation of light scattered from small and large droplets, as well as scattered light patterns of 1 mm and 10 μm droplets as example, respectively, which were illuminated using a commercial laser pointer (Microtrac, 2022). - 12 -
- Figure 1.6.** Schematic representation of a negatively charged particle in dispersed solution containing counter ions, figure reproduced from Malvern (2009)..... - 13 -
- Figure 1.7.** Schematic representation of confocal laser scanning microscopy.- 17 -
- Figure 1.8.** Schematic illustration of the Langmuir trough arrangement (A) and a Wilhelmy plate partially immersed in water phase (B). Key: (a) container (b) location of Wilhelmy plate; (c) barrier; (d) direction of the force for compression of interface; (e) indication of the change in shape of barrier on compression (Xu et al., 2007). - 20 -
- Figure 1.9.** Schematic representation of surface pressure (π) versus area per molecule (A) plot of a surface-active molecule. The π -A plot is divided to different regimes (gas, liquid, solid and collapse) during compression. - 21 -
- Figure 1.10.** Schematic representation of biconical geometry system and interfacial shear gradient at interface (Lauger, 2007). - 22 -
- Figure 1.11.** Relationship between the force and velocity of an applied stress on the displacement of a material (Mezger, 2014). - 25 -
- Figure 1.12.** Schematic representation of the oscillatory rheology of a viscoelastic material, showing the sinusoidal applied stress (σ), the sinusoidal measured strain (γ) and the phase shift angle (δ) occurring between the applied stress and measured strain response (Mezger, 2014)..... - 26 -

Figure 1.13. Schematic representation of sodium dodecyl sulphate polyacrylamide gel electrophoresis (SDS-PAGE). - 31 -

Figure 1.14. Schematic framework of this thesis. - 32 -

Figure 2.1. Possible positions of spherical solid particle at curved liquid-liquid interface representing particles preferentially wetted by aqueous phase (particle-stabilized O/W emulsions) (a) and by oil phase (particle-stabilized W/O emulsions), respectively (b), and position of a single spherical particle at a planar oil-water interface for a contact angle (θ), measured through the aqueous phase (c), with $\theta < 90^\circ$ (left), $= 90^\circ$ (center), $> 90^\circ$ (right), respectively. - 51 -

Figure 2.2. Schematic representation of the possible fate of Pickering emulsions based as they traverse through the oral to gastrointestinal regimes based on in vitro digestion studies. For simplicity reason, spherical particle is shown as enzyme-responsive and rod-shaped particle is shown as enzyme-unresponsive. - 54 -

Figure 2.3. Schematic showing particle fusion at the O/W interface by heat treatment, (a) with examples of relative barrier properties in modified starch-stabilized interface as a function of heat treatment (Reprinted with permission from Yang et al. (2014) and Ge et al. (2017)), (b) and release of FFA in whey protein-microgel (WPM)-stabilized interface with/ without heat treatment (HT-WPM) as a function of duodenal digestion time (image redrawn with permission from Sarkar et al. (2016d)) (c). Insets in (b): (left) is a non-heat treated quinoa starch granule-stabilized droplet and (right) a heat treated droplet illustrating the creation of a partially gelatinized starch layer. Insets in (c): (left) is WPM-stabilized droplet with corresponding transmission electron micrograph (gray solid line – theoretical fit, solid circle – observed value) and (right) is Heat treated droplet (HT-WPM) with corresponding transmission electron micrograph (black dashed line, empty circle – observed value). - 75 -

Figure 2.4. Examples of anisotropic particles, rod-shaped (a), peanut shaped (b) and cubic-shaped (c) with schematic, electron micrograph of the particles, arrangement of the particles at the interface and microstructure of the Pickering emulsion droplets stabilized by the respective anisotropic particles. Microscopic images of peanut- and cube-shaped particles and corresponding emulsion droplets are reprinted with permission from Tavacoli et al. (2012) and those of rod-shaped particles are reprinted with permission from de Folter et al. (2014b). - 76 -

Figure 2.5. Schematic representation of the mathematical models applicable to the pathways relevant to surfactant-stabilized or particle-stabilized emulsions. Under the assumptions or rapid adsorption/desorption of surface enzymes and permissible reduction in droplet size, equations (2.16) and (2.17) are relevant where short time digestion and subsequent asymptotic equilibrium are achieved. Where droplet size

remains stable, *i.e.* Pickering emulsion, equation (2.9) is the appropriate route and where further equation (2.10) selection is required for rapid adsorption and where interfacial dynamics are included, equation (2.12) is appropriate. Here it is notable that interfacial adsorption at short-times results in delayed digestion and that the large-time behaviour (in red) of both equations (2.10) and (2.12) are asymptotic. . - 87 -

Figure 3.1. Schematic flow diagram for preparation of pea protein microgel particles (PPM) and O/W Pickering emulsion (PPM-E). - 109 -

Figure 3.2. Particle size distribution of pea protein microgel particles (PPM) at pH 7.0..... - 115 -

Figure 3.3. Influences of pH on hydrodynamic diameter (●) and polydispersity index (PDI) (○) (a), ζ -potential (●) (b), and optical microscopic images (scale bar of 1.0 μm) (c), respectively. Error bars represent standard deviations. - 116 -

Figure 3.4. Influences of ionic strength on hydrodynamic diameter (■) and polydispersity index (PDI) (□) (a), ζ -potential (■), and optical images (scale bar of 2.0 μm) (c), respectively. Error bars represent standard deviations. - 117 -

Figure 3.5. Total interaction potential ($U/k_{\text{B}}T$) of PPM at various pH (a) and at different ionic strengths (b), calculated as a function of separation distance (h). ... - 118 -

Figure 3.6. Visual images of storage stability of Pickering emulsions stabilized by 0.05-1.0 wt% PPM (E0.05-E1.0) during 28 days of storage at 4 °C. - 122 -

Figure 3.7. SDS-PAGE pattern of pea protein concentrate (PPI) dispersion, PPM dispersions and the adsorbed phase of PPM-E (E1.0), all containing 1 wt% pea protein. Lane M represents the protein marker of 80-250 kDa molecular weight range. The samples included PPM dispersions, PPM dispersions which are pH-treated (adjusting the pH of PPM to pH 3.0, 5.0 and 7.0) and salt-treated (100 mM NaCl), as well as the adsorbed phases of PPM-E (E1.0) at different pHs (pH 3.0, 5.0 and 7.0) and ionic strength (100 mM NaCl). - 126 -

Figure 3.8. Mean droplet size distribution (a) of Pickering emulsions (E1.0) at pH 7.0 (green solid line), pH 5.0 (black dotted line) and pH 3.0 (red dashed line), respectively, and apparent viscosities (b) of PPM-E at pH 7.0 (green square), pH 5.0 (black circles) and pH 3.0 (red triangles) at shear rates from 0.1 to 1000 s^{-1} , respectively. - 126 -

Figure 3.9. Confocal micrographs (2D, and 3D, b) of freshly prepared Pickering emulsions (E1.0) and insets of visual images of PPM-E (after 3 months storage) as a function of pH, respectively. - 129 -

Figure 3.10. Mean droplet size distribution (a) of freshly prepared Pickering emulsions (E1.0) at 1 mM (green solid line), 10 mM (red dashed line) and 100 mM NaCl (black dotted line) respectively, and apparent viscosities (b) of E1.0 at 1 mM (green inverted triangle), 10 mM (red rhombus) and 100 mM NaCl (black hexagon) at shear rates from 0.1 to 1000s⁻¹, respectively..... - 132 -

Figure 3.11. Confocal micrographs of freshly prepared Pickering emulsions (E1.0) with insets of visual images of PPM-E (after 3 months storage) at 1 mM, 10 mM and 100 mM NaCl, respectively. For the 100 mM NaCl, a 3D confocal micrograph is also shown in the right hand side of the corresponding 2D image. - 133 -

Figure 4.1. (a) PSD of pea protein microgel particles (PPM) at pH 7.0 with inset table showing the hydrodynamic diameter (d_h), polydispersity index (PDI) and zeta-potential. (b) and (c) Evolution of the mean d_h (■), PDI (□) and zeta-potential (■), respectively, of PPM at pH 3.0 after *in vitro* gastric digestion at different time points (0-120 min). The insets in (c) are images of aqueous dispersions of PPM before and after 120 min of gastric digestion, respectively. Time 0 min represents the PPM + SGF mixture at pH 3.0 without the addition of pepsin. Error bars represent standard deviations..... - 156 -

Figure 4.2. SDS-PAGE electrogram of aqueous dispersions of PPM at pH 3.0 after *in vitro* gastric digestion at different times (0-150 min). Lane M represents the protein markers of 10-250 kDa M_w range..... - 157 -

Figure 4.3. . (a) Droplet size distribution of 20 wt% oil-in-water emulsions stabilized by PPM (PPM-E) at pH 7.0 (●), pH 3.0 (○) and PPM + SGF mixture at pH 3.0 without the addition of pepsin (-) with insets showing corresponding volume-average mean diameter (d_{43}) and zeta-potential of all the samples. Different superscripts (a-c) in the same columns of the inset of (a) represent significant differences between different samples at $p < 0.05$ level. (b) cryo-SEM micrograph of PPM-E at pH 7.0. Scale bar in (b) represents 10 μm - 158 -

Figure 4.4. (a) Droplet size distribution, (b) d_{32} (○) and d_{43} , (●) and (c) zeta-potential (●), of PPM-E as a function of *in vitro* gastric digestion time with SGF containing pepsin. The insets in (b) are images of the emulsions before and after 120 min of gastric digestion. Time 0 min represents the PPM-E + SGF mixture at pH 3.0 without the addition of pepsin. Error bars represent standard deviations. - 161 -

Figure 4.5. Confocal micrographs of 20 wt% oil-in-water emulsions stabilized by PPM (PPM-E) as a function of *in vitro* gastric digestion time (0-120 mins) at pH 3.0 (refer to **Supplementary Figure S4.1** for tiled confocal micrographs covering larger fields of view). Green color represents PPM (stained by Nile Blue); red color represents oil (stained by Nile Red); black color represents air or water. Time 0 min

represents the PPM-E + SGF mixture at pH 3.0 without the addition of pepsin. Scale bar represents 10 μm - 162 -

Figure 4.6. (a) Influence of concentration of cellulose nanocrystal (CNC) on zeta-potential (\bullet); (b) corresponding visual images of PPM-E with added CNC. Error bars on (a) represent standard deviations. - 163 -

Figure 4.7. Surface pressure (π) versus area per particle (A/N_p) spread at the A-W interface for various systems. (a) 0.466 wt% PPM at pH 7.0 ($\blacksquare, \blacktriangle$) and pH 3.0 (\triangle, Δ): 1st compressions \blacksquare, \triangle ; 2nd compressions \blacktriangle, Δ . (b) 0.04 wt% CNC alone at pH 3.0: 1st compression \triangle ; 2nd compression \square . (c) 0.466 wt% PPM spread first at pH 3.0, followed by spreading of 0.04 wt% CNC on top of PPM: 1st compression \blacksquare ; 2nd compression; \square 3rd compression \triangle ; average π - A/N_p result for 0.466 wt% PPM alone at pH 3.0 from (a) above \square . (d) Mixture of 0.02 wt% CNC + 0.233 wt% PPM at pH 3.0: 1st compression \blacksquare ; 2nd compression; \square 3rd compression \triangle ; average π - A/N_p result for 0.466 wt% PPM alone at pH 3.0 from (a) above \square . The dashed curve in the inset of Figure (a) shows the isotherm for whey protein microgels (WPM) taken from reference (Zembyla et al., 2019) compared to the pH 3.0 data for PPM in (a). The dashed straight lines in (a) are the extrapolations to estimate the dimensions of the adsorbed microgels (see text). - 166 -

Figure 4.8. (a) PSDs of freshly prepared 20 wt% O/W emulsions at pH 3.0: stabilized by PPM only (PPM-E) (-); PPM-E with 1 wt% CNC (\bullet), PPM-E with 2 wt% CNC (\blacksquare); PPM-E with 3 wt% CNC (\blacktriangle). Cryo-SEM micrograph and partial enlarged detail of PPM-E with: (b) 1 wt% CNC (c) 2 wt% CNC, (d) 3 wt% CNC (d). Scale bars represent in (b) 10 μm , in (c) and (d) 5 μm . The red arrows indicate what are thought to be CNC particles. - 168 -

Figure 4.9. (a) Flow curves, (b) strain amplitude sweep curves, (c) frequency sweep curves of freshly prepared 20 wt% oil-in-water emulsions at pH 3 stabilized by PPM (PPM-E) with 1 wt% CNC (PPM-E + CNC_{1.0}) (\bullet), 2 wt% CNC (PPM-E + CNC_{2.0}) (\blacksquare) and 3 wt% CNC (PPM-E + CNC_{3.0}) (\blacktriangle). Error bars represent standard deviations. - 170 -

Figure 4.10. PSDs of PPM-E with: (a) 1 wt%, (b) 2 wt%, (c) 3 wt% CNC after different *in vitro* gastric digestion times. Time 0 min represents the emulsion + SGF mixture at pH 3.0 without the addition of pepsin. (d) Shows d_{32} (\cdots) and d_{43} (-) at 0, 30 and 120 min for 1 (\bullet), 2 (\blacksquare) and 3 wt% CNC (\blacktriangle). Error bars represent standard deviations. - 172 -

Figure 4.11. Confocal micrographs of 20 wt% oil-in-water emulsions stabilized by PPM (PPM-E) and 1 wt% CNC (PPM-E + CNC_{1.0}), 2 wt% CNC (PPM-E + CNC_{2.0}), and 3 wt% CNC (PPM-E + CNC_{3.0}) as a function of *in vitro* gastric digestion time (0, 120 min) at pH 3.0. The green color represents PPM (stained by

Nile Blue); the red color represents the oil phase (stained by Nile Red); the blue color represents the CNC (stained by Calcofluor White); the black color represents air or water. Time 0 min represents the PPM-E + SGF mixture at pH 3.0 without the addition of pepsin. Scale bar represents 50 μm - 175 -

Figure 5.1. Evolution of mean hydrodynamic diameter (■), polydispersity index (PDI) (□) after intestinal digestion without gastric step (a), ζ -potential (■) of PPM after *in vitro* intestinal digestion as a function of time (0, 30 and 120 mins) (b) or evolution of mean hydrodynamic diameter (■), polydispersity index (PDI) (□) after intestinal digestion with gastric step (c). Insets in (b) represent the visual images of aqueous dispersion of PPM during intestinal digestion at different time points, respectively. Digestion time 0 min in (a) shows the original PPM+ SIF+ bile salt mixture at pH 7.0 without the addition of pancreatin. Digestion time of 0 min in (c) represents the gastric-digested PPM+ SIF+ bile salt mixture at pH 7.0 without the addition of pancreatin at pH 6.8. Standard deviations are shown by error bars. - 195 -

Figure 5.2. Mean size distribution of gastric-digested Pickering oil-in-water emulsions stabilized by PPM containing 20 wt% oil (PPM-E) (a), PPM-E further coated by 1.0 wt% CNC (PPM-E+ CNC_{1.0}) or (b) 3.0 wt% CNC (PPM-E+ CNC_{3.0}) (c) during *in vitro* intestinal digestion. Digestion time of 0 min SIF shows the gastric-digested emulsion + SIF mixture without the addition of pancreatin and bile salts at pH 7.0. Time 0 min SIF + bile represents the gastric- digested emulsion+ SIF+ bile salt mixture without the addition of pancreatin at pH 7..... - 199 -

Figure 5.3. Confocal micrographs, visual images and schematic representations of PPM-stabilized emulsion (PPM-E) after sequential *in vitro* gastrointestinal digestion. Green colour (Nile Blue stain) represents PPM; the red colour (Nile Red stain) represents the oil phase and the black background is air or water. Digestion time of 0 min SIF represents the gastric- digested emulsion + SIF mixture without the addition of pancreatin and bile salts at pH 7.0. Digestion time of 0 min SIF+ bile represents the gastric- digested emulsion + SIF + bile salt mixture without the addition of pancreatin at pH 7.0. Scale bar in the micrographs correspond to 20 μm - 202 -

Figure 5.4. Confocal micrographs and visual images of PPM stabilized emulsion coated with 1.0 wt% CNC after sequential *in vitro* gastrointestinal digestion. Green colour (Nile Blue stain) represents PPM; the red colour (Nile Red stain) represents the oil phase; the blue colour (Calcofluor White stain) represents the CNC and the black background represents air or water. Digestion time of 0 min SIF represents the gastric-digested emulsion + SIF mixture without the addition of pancreatin and bile salts at pH 7.0. Digestion time of 0 min SIF + bile represents the gastric-

digested emulsion + SIF + bile salt mixture without the addition of pancreatin at pH 7.0. Scale bar in the micrographs correspond to 20 μm - 203 -

Figure 5.5. Confocal micrographs and visual images of PPM stabilized emulsion coated with 3.0 wt% CNC after sequential in vitro gastrointestinal digestion. Green colour (Nile Blue stain) represents PPM; the red colour (Nile Red stain) represents the oil phase; the blue colour (Calcufluor White stain) represents the CNC and the black background represents air or water. Digestion time of 0 min SIF represents the gastric-digested emulsion + SIF mixture without the addition of pancreatin and bile salts at pH 7.0. Digestion time of 0 min SIF + bile represents the gastric-digested emulsion + SIF + bile salt mixture without the addition of pancreatin at pH 7.0. Scale bar in the micrographs correspond to 20 μm - 204 -

Figure 5.6. Mean ζ -potential of gastric-digested PPM-E, PPM-E+CNC_{1.0} and PPM-E+CNC_{3.0} at pH 7.0. Digestion time of 0 min SIF represents the gastric-digested emulsion + SIF mixture without the addition of pancreatin or bile salts at pH 7.0. Digestion time of SIF + bile represents the gastric- digested emulsion + SIF + bile salt mixture without the addition of pancreatin at pH 7.0. Standard deviations are represented by error bars. - 206 -

Figure 5.7. Release of free fatty acid during intestinal digestion (after prior-gastric digestion) of WPI-stabilized emulsion (black diamond), PPM-E (green circle), PPM-E + CNC_{1.0} (red square), and PPM-E + CNC_{3.0} (blue triangle). Error bars represent the standard deviations. The solid lines in each of the %FFA curves connecting the symbols (data points) are the best theoretical fits to the experimental data predicted using the mathematical model (Eq. (5.1)). - 208 -

Figure 5.8. Release of free fatty acids (FFA%) during in vitro intestinal digestion bypassing the gastric phase (using pure lipase) with inset showing the zoomed image over time of PPM-E (green circle), PPM-E+CNC_{1.0} (red square), and PPM-E+CNC_{3.0} (blue triangle). Error bars represent standard deviations. Solid lines connecting the symbols (data points) in each of the %FFA curves are the best theoretical fits to the experimental data predicted using the mathematical model (Eq. 5.1). - 210 -

Figure 5.9. Release of free fatty acids (%FFA) during in vitro intestinal digestion bypassing the gastric phase (using pure lipase with no added proteases) over time of (a) PPM-E and (b) PPM-E+CNC_{1.0} with (open circle) or without heat treatment (solid circle). Error bars represent standard deviations. - 212 -

Figure 6.1. Schematic framework of the thesis. - 222 -

Figure 6.2. Flow chart of producing protein hydrogel using commercial pea protein isolate. *: Cooling: Heated gel was cooled to room temperature via flowing water,

and stored at 4 °C for 24 h. # Solubility fraction was determined by Lowry assay via DC protein assay, absorbance measured at 750 nm. - 223 -

Figure 6.3. Particle size distribution (PSD) of pea protein microgel particles (PPM-N) formed by S85 Plus N at pH 7.0 with inset table showing the hydrodynamic diameter (d_h), polydispersity index (PDI) and zeta-potential. The insets are visual and optical images of aqueous dispersions of PPM-N (S85 Plus N). Scale bar represents 20 μm - 224 -

Figure 6.4. SDS-PAGE electrogram of aqueous dispersions of PPM (S85 XF), PPM-N (S85 Plus N) and the supernatant of aqueous dispersions of PPM-N (PPM-S) at pH 7.0. Lane M represents the protein markers of 10-250 kDa M_w range. - 225 -

Figure 6.5. Droplet size distribution of 20 wt% oil-in-water emulsions stabilized by PPM-N (S 85 Plus N) at pH 7.0 (●) with insets showing corresponding surface-average mean diameter (d_{32}), volume-average mean diameter (d_{43}) and zeta-potential. The insets are confocal visual and optical images of emulsion stabilized by PPM-N (S85 Plus N). Scale bar of confocal image represents 5 μm , Scale bar of optical image represents 20 μm - 226 -

Figure 6.6. Graphical summary for **Chapter 3** showing how Pickering emulsion droplets stabilized by PPM show a pH dependent transition from being intact particles to aggregated network at the oil-water (O/W) interface. - 229 -

Figure 6.7. Graphical abstract for **Chapter 4** showing how Pickering emulsion droplets stabilized by PPM resulted in gastric coalescence whereas addition of CNC as a second layer via electrostatic complexation with PPM at the interface protects against such destabilization. - 230 -

Figure 6.8. Interfacial shear viscosity of 1.0 wt % PPM at pH 7.0(●) with phosphate buffer at 25°C, and the 1.0 wt% PPM at pH 3.0 (■) with SGF in in vitro gastric digestion regime. A: changing temperature of PPM dispersion from 25°C to 37°C. B: temperature reaches at 37°C. C: Pepsin + SGF mixture was added into PPM dispersion. - 236 -

Figure 6.9. Schematic representation of adding pepsin dispersion during the measurement of interfacial shear viscosity. - 237 -

Figure 6.10. Schematic representation of various strategies to influence gastrointestinal digestion kinetics of Pickering emulsion where 1) no barrier i.e. lipase gets access to the lipid core through gaps in the microgel layer, 2) lipase binds to polysaccharide in bulk phase reducing overall available activity, 3) lipase activity is affected as the polysaccharide forms network in the bulk phase and 4)

- lipase activity is affected as the polysaccharide forms a barrier layer at the interface. - 238 -
- Figure S3.1.** Correlation function of PPM as function of pH (a) and as function of ionic strength (b), respectively. - 244 -
- Figure S3.2.** Electrostatic ($U_R/k_B T$) and Van der Waals interaction ($U_{VW}/k_B T$) of PPM at various pH (a) and at different ionic strengths (b), calculated as a function of separation distance (h). - 245 -
- Figure S3.3.** Visual images of coalescence stability of diluted PPM-stabilized Pickering emulsions (E0.05-E1.0) (1:4 w/w with buffer) prepared using different concentrations of PPM (0.05-1.0 wt%) during 28 days of storage at 4 °C. Red circles indicate the oil droplets. - 246 -
- Figure S3.4.** Visual images of centrifuged and diluted subnatants of PPM-stabilized Pickering emulsion (E1.0) (1:4 w/w buffer) at different pH values (a) or 100 mM NaCl (b), respectively. - 247 -
- Figure S4.1.** Confocal micrograph tiles covering different fields within the sample of 20 wt% oil-in-water emulsions stabilized by PPM (PPM-E) after (a) 0 min and (b) 120 min of *in vitro* gastric digestion at pH 3.0. Green colour represents PPM (stained by Nile Blue); red colour represents the oil phase (stained by Nile Red); black colour represents air or water. Note 0 min in Figure (a) represents the PPM-E+SGF mixture at pH 3.0 *without* the addition of pepsin. Scale bar represents 20 μm - 248 -
- Figure S4.2.** Influence of concentration of cellulose nanocrystals (CNC) on: (a) the mean ζ -potential values (\circ) of aqueous dispersion of PPM and (b) the flowability of these mixtures. Error bars represent standard deviations. - 249 -
- Figure S4.3.** Surface pressure (π) versus area per particle (A/N_p) spread at the A-W interface for 0.466 wt% PPM: standard deviations about the means are shown for 9 separate compressions at pH 7.0 (black line and error bars) and pH 3.0 (red line and error bars). - 250 -
- Figure S4.4.** Frequency sweep curves of freshly prepared 20 wt% O/W emulsions stabilized by PPM (PPM-E) at pH 3.0 ($G' \bullet$, $G'' \circ$). Error bars represent standard deviations. - 251 -
- Figure S4.5.** (a) Flow curves and (b) frequency sweep curves of freshly prepared PPM (1 wt%) at pH 3 mixed with 1 wt% CNC (PPM + CNC_{1.0}) (\bullet), 2 wt% CNC (PPM + CNC_{2.0}) (\blacksquare) and 3 wt% CNC (PPM + CNC_{3.0}) (\blacktriangle). These samples are aqueous dispersions of particles without any oil droplets. Error bars represent standard deviations. - 252 -

List of Abbreviations

A-W	Air-water interface
AFM	Atomic force microscopy
BSE	Back-scattered electrons
BSA	Bovine serum albumin
CNC	Cellulose nanocrystal
CN	Chitin nanoparticles
ChN	Chitosan nanoparticles
CLSM	Confocal laser scanning microscopy
Cryo-SEM	Cryo scanning electron microscopy
2D	Two-dimensional
3D	Three-dimensional
DLS	Dynamic light scattering
DLVO	Derjaguin-Landau-Verwey-Overbeek
DTT	Diothiothreitol
E0.05	Pickering emulsion stabilized with 0.05wt% pea protein
E0.1	Pickering emulsion stabilized with 0.1wt% pea protein
E0.25	Pickering emulsion stabilized with 0.25wt% pea protein
E0.5	Pickering emulsion stabilized with 0.5wt% pea protein
FFA/FFAs	Free fatty acids
GCP	Gliadin colloidal particles

GI	Gastrointestinal tract
HT-WPM	Whey protein microgel particles with heat treatment
KFN	Karifin nanoparticles
LFnp/ LFN	Lactoferrin nanoparticles
LF-ALG	Lactoferrin nanoparticles complexed with alginate
LF-CAR	Lactoferrin nanoparticles complexed with carrageenan
LVER	Linear viscoelastic region
MAG	Monoacylglycerol
Mw	Protein molecular weight
MUC5B	Glycosylated salivary mucin
NFC	Nanofibrillated cellulose
OSA	Octenyl succinic anhydride
O/W	Oil-in-water
O-W	Oil-water interface
PDCAAS	Protein digestibility corrected amino acid score
PDI	Polydispersity index
pI	Isoelectric point
PPI	Pea protein isolate
PPM	Pea protein microgel particle
PPM-E/E1.0	Pea protein microgel particle- stabilized Pickering emulsion
PPM + CNC	Pea protein microgel particles complexed with cellulose nanoparticles
PPM + CNC _{0.5-3.0}	Pea protein microgel particles complexed with 0.5-3.0 wt% cellulose nanocrystals

PPM-E + CNC _{0.5-3.0}	Pea protein microgel particle-stabilized Pickering emulsion coated with 0.5-3.0 wt% cellulose nanocrystals
PPM-N	Pea protein microgel particle formed by using S85 Plus N protein powder
PPM-N-E	Pickering emulsion stabilized by pea protein microgel particles which formed by using S85 Plus N protein powder
PPM-S	The supernatant of aqueous dispersion of pea protein microgel particle formed by using S85 Plus N powder
PPP	Pea protein particles
PSD	Particle size distribution
PTFE	Polytetrafluoroethylene
SDS	Sodium dodecyl sulphate
SDS-PAGE	Sodium dodecyl sulphate polyacrylamide gel electrophoresis
SE	Secondary electrols
SEM	Scanning electron microscopy
SGF	Simulated gastric fluid
SIF	Simulated intestinal fluid
SLS	static light scattering
SPN	Soy protein nanoparticles/ soy protein nanoparticle aggregates
SPHE	Soy protein nanoparticles-stabilized Pickering emulsions
S ⁻ /SS	Sulfhydryl/disulfide bonds
TAG	Triacylglycerols
TOBC	TEMPO-oxidized bacterial cellulose

Vi ₁₋₃	Vicilin protein subunits
W/O	Water-in-oil
WPI	Whey protein isolate
WPM	Whey protein microgel
ZCP	Zein colloidal particles
ZMP	Zein microparticle
ZPCP	Zein-propylene glycol alginate composite particles

List of Symbols

A	Area
A_{280} Test	Absorbance measurement at 280 nm
A_H	Hamaker constant
a	Particle radius
a_s	Interfacial area covered by solid particles
B_o	Boussinesq number
B_o	Bond number
B	Buoyant force
c_i^∞	Number density of i^{th} type of ion
D	Diffusion coefficient
D_m	Displacement
d_p	Diameter of the particle
d_H	Hydrodynamic diameter
d_{32}	Sauter mean diameter
d_{43}	De Broukere mean diameter
ΔE	Desorption energy
F	Forces
$f(k_a)$	Henry's function
G'	Storage or elastic modulus
G''	loss or viscous modulus
ΔG	Gibbs free energy change
g	Gravity acceleration
ΔH	Enthalpy change

h	Height
h	Separation distance between particle-particle surface
K	Consistency coefficient
κ^{-1}	Debye length
k	Thickness
k	Rate of lipid digestion
k_B	Boltzmann's constant
k_o	Rate of hydrolysis per unit area
L	Lengths
M	Molar
M_{Base}	Molarity of the base
M	Torque
m	Mass
N_A	Avogadro's number
N_p	Number of particles
n_i	Number of droplets with a diameter, d_i
n	Power-law index
n	Flow index
P	Weight
P	Perimeter
R	Radius
R^2	Regression coefficient
r	Radius
ΔS_{config}	The configurational entropy change

S_p	Surface covered by the particles
T	Temperature
t	Thickness of plate
t	Time
$t_{1/2}$	Half-life
Δt	Duration of the reaction,
U	Human Enzyme Unresponsive
U	Interaction potential
U_E	Electrophoretic modility
U_R	Electrostatic repulsion
U_{VW}	Van der Waals attraction
V	Volume
V	Velocity
v_p	velocity of particle
W_w	Weight of the lipid
w	Width of plate
X	Concentration of pepsin
z_i	Valency of i^{th} type of ion
η	viscosity
η_i	Interfacial viscosity
δ	Standard deviation
δ	Phase angle
θ	Angle

ζ	Zeta-potential
ψ	Surface potential
π	Surface pressure
Ω	Angular velocity
σ	Shear stress
γ	Shear strain
$\dot{\gamma}$	Shear rate
γ_{ow}	Interfacial tension at oil-water interface
γ_{po}	Interfacial tension at particle-oil interface
γ_{pw}	Interfacial tension at particle-water interface
$\gamma_{ow}\Delta A$	The change in interfacial free energy
ρ_p	Density of particle
ρ_c	Density of continuous phase
ρ_o	Density of oil phase
λ	Thickness of barrier layer
ε	Dielectric constant of the medium
ε	Permittivity of the system
ε_0	Permittivity of vacuum
ε_r	Permittivity of water
Φ	Amount of free fatty acids
$\varphi(t)$	Fatty acid release at time t
Φ_{10}	FFA released at 10 min
φ_{max}	Maximum extent of FFA release

$\Gamma(t)$	Surface coverage by enzyme at any given time t
Γ^{Max}	Maximum surface coverage

Chapter 1:

General Introduction

1.1 Overall research aim

Emulsions are widely used formulation vehicles in various industries, such as food, cosmetics, pharmaceuticals, agrochemicals, fine chemicals, among others. The emulsion system is useful because of its general ease of preparation and innocuousness, and also emulsion allows ways to protect the active materials which it encapsulates from oxidation, bacterial attack, physiological or environmental degradation. This delivery system has significant advantages like delivering active materials with an optimal concentration to improve effectiveness of delivery, as well as controlling the targeted release of the functional encapsulated substances. The principles of emulsion science are commonly applied in food industry to create various emulsified food products with desirable appearances, textures, flavor and mouthfeels, as well as to design functional products for encapsulation and effective delivery of bioactives. However, conventional emulsion has some drawbacks, such as a limited stability against environmental and physiological stresses, and does not allow controlled release of bioactive compounds. In order to improve delivery, bioavailability and optimized release of bioactive compounds, there has been growing interests in designing advanced emulsion systems, including nanoemulsions, high internal phase emulsion, multilayer emulsions, multiple emulsion, emulsion gel particles, and lately particle-stabilized emulsions, also called “Pickering emulsions”.

Thesis objective: In this thesis, the overarching objective was to design novel Pickering emulsion stabilized by particles from plant source to allow the control digestion during gastrointestinal processing to serve as a unique delivery vehicle. Different biopolymers (proteins and polysaccharide based particles, either lab-synthesized or naturally-derived) and processing technologies were used to design Pickering stabilizers and to engineer Pickering emulsions with complex interfaces that can respond to physiological conditions effectively, allowing to

control the lipid digestion performance. The innovative aspect of this thesis is that soft protein microgel particles from plant source were designed to electrostatically interact with polysaccharides (cellulose nanocrystals) to create complex particle-laden interfaces to offer outstanding gastric stability of lipid droplets but allowing release of lipids in the intestinal phase.

Thesis hypothesis: The hypothesis of this thesis was that by creating a complex interfacial layer at the oil droplet surface, the oil droplets could be better protected against gastric degradation where most destabilization occurs in protein-stabilized matrices.

1.2 Background

This thesis is focused on food grade Pickering emulsion co-stabilized by plant-based protein particles and polysaccharides and their influence on lipid digestion kinetics. The rationale behind the selection of pea protein and cellulose nanocrystals are discussed in the following section.

1.2.1 Pickering emulsions

Emulsion is a mixed dispersion of two or more immiscible liquids that one liquid (the dispersed phase) is presented as micron or sub-micron scale in the other (the continuous phase or bulk phase) (McClements, 2004, Singh and Sarkar, 2011b). When the emulsion is stabilized using solid particles alone, it is called as Pickering emulsion (Pickering, 1907b), which was firstly mentioned by Ramsden (1904b) since the beginning of 20th century. However, the gradual interests in Pickering emulsions in the food colloids community has only picked up in the last decade (Berton-Carabin and Schroen, 2015) as reflected in two narrative reviews by Dickinson (2010a, 2012). Dickinson (2010a) initially highlighted that the application of Pickering particles directly to food was rather limited. However, after two years with the substantial amounts of published studies on food-grade Pickering emulsions, he summarized the ability of various Pickering particles in food-grade oil-in-water (O/W) emulsion stabilization, like modified starch microparticles and chitin nanocrystals (Dickinson, 2012). The fast increasing

interests of this emulsion system in food field was due to the high ability of Pickering particles to protect the emulsion droplets against coalescence and Ostwald ripening under environmental stress, such as heating, pH extremes and high ionic concentration (Ettelaie and Lishchuk, 2015b, Aveyard et al., 2003a), as well as the high inhibition of bile salts displacement of the particle-laden interface in the gastrointestinal phase. This latter one is also one of the key rationales to use Pickering emulsions in this thesis for controlling gastrointestinal behaviour *via* designing the complex nature of particulate interfacial layer.

Solid particles which could stabilize Pickering emulsion has various shape (**Figure 1.1**), such as spherical, rods, cubes, peanut-shape *etc.* (de Folter et al., 2014a, Kalashnikova et al., 2011). The spherical particle is selected and synthesized in this thesis since it is the common shape of protein-based particle and easy to prepare using homogenization techniques that are readily available in food industries but more importantly, classical thermodynamic theory of model particle adsorption can be applied to understand the particle properties (Dickinson, 2012).

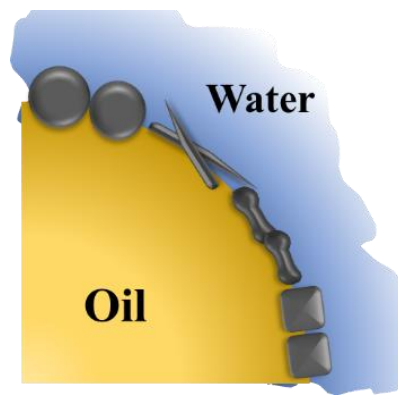


Figure 1.1. Schematic representation of Pickering O/W emulsion *i.e.* emulsions stabilized by solid particles with a variety of particle shapes; spherical, rods, cubs and peanut-shape.

1.3 Rationale behind the selection of biopolymers

Pickering particles and emulsions were designed based on physicochemical characteristics of specific biopolymers (proteins and polysaccharides) at specific conditions. In order to understand the interfacial structure in Pickering emulsions,

the choice of pea protein as the biopolymer, pea protein concentration, designed microgel particles and their use as Pickering stabilizer in O/W emulsions are discussed in the following section. For the more complex interfacial layer *i.e.* particle-particle-laden interface, this section also includes the structure of polysaccharide particle *i.e.* cellulose nanocrystal used and its choice to allow electrostatic binding to the adsorbed pea protein microgel particle at the O/W interface.

1.3.1 Plant protein

Recently, the protein found in plant foods has received growing attention, and is considered as the sustainable alternative to daily proteins such as whey protein in milk. It is now clear that plant proteins result in orders of magnitude lower greenhouse gas emissions as compared to animal protein counterparts (Poore and Nemecek, 2018). There has been increasing literature demonstrating the health benefits of plant proteins, including cardiovascular health, metabolic risk, diabetes type II, chronic disease, weight management as well as mortality reduction (Hertzler et al., 2020, Ahnen et al., 2019, Ge et al., 2020).

Legumes (chickpeas, lentil, cowpea, black bean, soy bean and pea) great source of plant-based proteins due to the high level of protein concentration as well as high protein quality of certain legume protein. The protein digestibility corrected amino acid score (PDCAAS) is used quantify the protein quality accorded to the essential amino acid content and true fecal protein digestibility. Soy protein has a high protein quality, which is similar to egg, milk and whey protein on PDCAAS (0.9-1.0) (Rizzo and Baroni, 2018). We focused on pea protein in this thesis, even the score of PDCAAS of pea protein is slightly lower to the range from 0.7 to 0.9 (Hertzler et al., 2020). The key rationales behind selection of pea protein is not only due to its great fat- and water-binding ability, the properties of emulsification and gelation as well as a high nutritional value, but also it is recognized as a protein with limited allergenicity and thus suitable for food applications (Sandberg, 2011, Krefting, 2017, Day, 2013).

Pea protein isolate (PPI) is produced by wet processing *via* isoelectric precipitation or ultrafiltration process (Boye et al., 2010), which is a group of protein with albumins, two major globulins (legumin and vicilin) and one minor (convicilin) proteins (Laguna et al., 2017b). Pea legumin has a molecular weight of 300-410 kDa made up of six polypeptides, which contains an acidic subunit (38-40 kDa) and a basic subunit (19-33 kDa) linked *via* disulfide bond. Although the isoelectric point (pI) of legumin depend on its heterogenetic subnunit, the true pI is pH 4.7 (Gatehouse et al., 1980). Vicilin with a lot of smaller polypeptides ranging from 12.5-33 kDa is considered as one subunit (O'Kane et al., 2004a, O'Kane et al., 2004b). Convicilin with a polypeptide of 70 kDa has a similar amino acid profile to vicilin except with a N-terminal extension highly charged (Croy et al., 1980). PPI presents negative charges at neutral pH because of the overall pI being close to pH 4.3 (Liu et al., 2009). The pea protein isolate, which has been used in this thesis (**Chapters 3-5**) to create microgel particles, has a high protein concentration of 85%, and 15% of other components include ash and crude fiber. The pea fiber may promote emulsion stability in cooperation with pea protein (Huang et al., 2019), however, the protein is expected to play the key role in stabilization. The influence of ash or fibre on the colloidal properties of Pickering emulsion is expected to be negligible, because of an extremely low concentration of 0.0017% in the final emulsion system. In addition, the presence of pea fiber could have affected the colloidal stability due to interactions with PPI, but the microgel which is monomeric unit of the hydrogel consists of a strong network structure in which any insoluble components may be blocked inside of gel-like network structure and thus not available to interact with the oil phase. In addition, there was no sedimentation or phase separation in the dispersion of pea protein microgel particle post high speed centrifugation (data not shown). Hence, the overall role of ash or fibre in microgel-stabilized emulsion is not considered in this thesis.

1.3.1.1 Pea protein isolate for designing microgel particles

Gel is a colloid system which may be defined as a cross-linked network structures formed by a polymer in a fluid. It could be soft and weak, or hard and strong depending upon on its network density and flow behavior. When the hydrophobic, three-dimensional polymeric network structures is able to hold with 99% water, it is defined as hydrogel (Ahmed, 2015). Hydrogel formation of proteins has been wide investigated with key influencing factors being pH conditions, ionic strengths as well as temperature (Bora et al., 1994b, Mession et al., 2015, Mori et al., 1982, Shand et al., 2007). Pea protein can self-assemble to form the heat-induced gel particularly at high concentrations when heated at above 75 °C due to thermal denaturation and cross-linking of two main globular protein, Legumin 11S and Vicillin 7S that contain free thio groups. Legumin is denatured at 69-77 °C because of the broken disulphide-linking between the acidic and basic subunits, and followed by exposure of the free active sulfhydryl groups in hydrophobic amino acids. With the increasing temperature (75-85 °C), both hydrophobic interaction and sulfhydryl/disulfide bonds (S⁻/SS) exchange reaction lead to rearrangements of legumin and protein aggregation (Mession et al., 2015, Shand et al., 2007, Mession et al., 2013). Meanwhile, vicililin denatures and aggregates mainly *via* non-covalent interactions such as hydrophobic interactions and hydrogen bonding.

The term microgel can be used to describe monomeric units of a hydrogel *i.e.* particles of hydrogel with length scale varying from nanometer to micrometre (Thorne et al., 2011). And the term “microgel particles” is defined as a dispersed system that *i.e.* the hydrogel particles are dispersed throughout the solvent. For example, soybean proteins have been used in literature to form a thermally cross-linked gel, which was broken to micrometre scale microgels using a high pressure homogenizer (Matsumiya and Murray, 2016). Using the same processing principle, pea protein heat-set gel was created and hypothesized to be broken down into microgel particles by controlled shearing using a high pressure homogenizer, which was further used to stabilize O/W Pickering emulsions (**Chapter 3**). And this pea protein microgel particle was also used to form the initial adsorbed layer of

polysaccharide-coated Pickering emulsion for gastric digestion and lipolysis (**Chapter 4** and **5**).

1.3.2 Polysaccharides

Polysaccharides produced from plants are major components of the human diet and an important source of dietary fiber intake. Polysaccharides not only are widely applied in biochemical and pharmacological fields due to safety and non-toxicity (Huang et al., 2015, Sakurai and Shinkai, 2000), but also have increasing interest as functional material in food because of their bioactivities including antineoplastic, immunomodulation, anti-oxidant, and anti-inflammatory, as well as their potential advantages in the management of energy balance, satiety, glycemia and colonic health (Lovegrove et al., 2017). Functional properties of polysaccharides depend on their physiochemistry and molecular structure rather than the source (Ferreira et al., 2015, Nie and Xie, 2011, Liu et al., 2021). Polysaccharides have an extremely diverse structure but share some common features such as long linear chains of carbohydrate molecules composed with at least ten different smaller monosaccharides using glycosidic bonds. Depending on the type of composed monosaccharides, polysaccharides are divided into homopolysaccharides and heteropolysaccharides. Cellulose is a common homopolysaccharides, which is the most abundant naturally occurring polymer. It consists of long chains of the same type of β -1,4-linked glycosides monosaccharides (**Figure 1.2**). In this thesis, cellulose nanocrystal was used in **Chapter 4** and **5** to create complex interface *via* electrostatic interaction with adsorbed plant protein microgel-based particle.

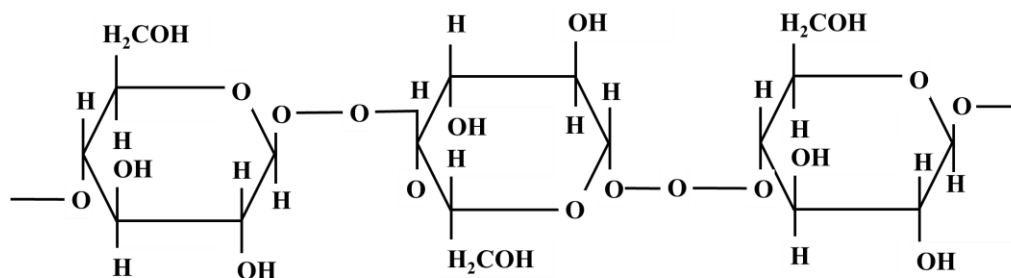


Figure 1.2. Molecular structure of cellulose.

The cellulose nanocrystals (CNCs) used in this thesis were produced *via* sulfuric acid hydrolysis, containing approximately 10,000 glucose units (Sjostrom, 1993). When wood cellulose fibers undergo acid treatment, disordered and/or paracrystalline regions tend to be completely hydrolyzed, however, crystalline regions remain due to their higher acid resistance, and generate rod-like nanocrystals (Habibi et al., 2010, Matos Ruiz et al., 2012). Meanwhile, surface hydroxyl groups of cellulose react with sulfate ions, generating strong acid groups and negatively-charged surface sulfate esters, and leading to high hydrophilicity and no time-dependent viscosity (Araki et al., 1998). On the other hand, sulfuric-treated CNCs present intrinsic properties, such as nanoscale dimensions, high surface area, unique morphology, low density and mechanical strength, leading to a plethora of applications of CNCs for interactions with biopolymers, especially protein such as whey protein, sodium caseinate, core zein protein as well as soy protein (Sarkar et al., 2017b, Pindakova et al., 2019, Ben Shalom et al., 2021, Zhang et al., 2019). For example, a novel multilayered microparticles were created at pH 4.0 by using positively-charged zein microparticles (ZMPs) as the core, coated with negatively-charged CNCs as primary layer, and followed with positively charged whey protein microgels (WPMs) as the second layer (Wei et al., 2021a). The interparticle interactions of both ZMP-CNC and CNC-WPM were dependent on the electrostatic binding at acidic condition. In this thesis, CNCs were mixed into Pickering emulsion primarily stabilized by pea protein microgel particles at pH 3.0 to create a complex protein-particle-polysaccharide crystal hybrid interfacial structure for the first time (**Chapter 4 and 5**)

1.4 Rationale behind the selection of characterization techniques

1.4.1 Microgel particles and emulsions characterization

In order to fully understand the evolution of microstructures and physicochemical characteristics of both particles and emulsions with or without the presence of

polysaccharides and their fate while going through *in vitro* gastrointestinal regime, several analytical instruments were employed. The theoretical and technical properties of the main characterization tools employed in this PhD thesis are discussed below.

1.4.1.1 Dynamic light scattering (DLS)

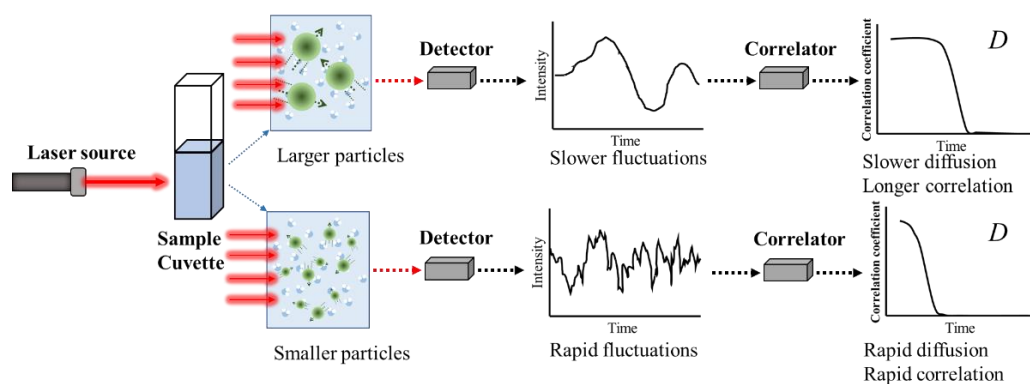


Figure 1.3. Schematic representation of dynamic light scattering measuring principle.

Dynamic light scattering (DLS) was employed to determine the particle size of pea protein microgel particles (PPM) and to analyze the aggregation of these particles as they undergo various pH adjustment, ionic concentration (**Chapter 3**) as well as interact with *in vitro* gastrointestinal metabolites (**Chapters 4 and 5**). DLS is one of classical methods used to measure the size of particle at range from 1 nm to 1 μm , such as nano-scale emulsion, aggregated proteins, surfactant micelles, and other nanoparticles. In the solution, particles undergo Brownian motion which is a random movement, resulting from thermally induced collisions with solvent molecules (Malvern, 2015a). Smaller particles have higher degree of Brownian motion, whilst the larger particles tend to diffuse more slowly. When particles are illuminated *via* a laser beam in DLS, the fluctuation of scattered waves arriving at the detector randomly in time reflects the fluctuations in the position of particles

(**Figure 1.3**) (Nobmann et al., 2007). Briefly, small particles rapidly diffuse resulting in a rapid fluctuations of the intensity signal, whereas larger particles have slower fluctuations (Dalglish and Hallett, 1995). To create auto-correlation functions, snapshots of the scattering signals are taken at nano or micro-seconds comparing to the original signal. These auto-correlation functions are used to extract the translational diffusion coefficients (D), which quantify the rate of Brownian motion of particles. To calculate the hydrodynamic diameter of particles (d_H), D is used in Stokes-Einstein equation (equation 1.1) as follows:

$$d_H = \frac{k_B T}{3\pi\eta D} \quad (1.1)$$

where, k_B is the Boltzmann's constant (1.380649×10^{-23} joule per kelvin (K)), T is the absolute temperature, η is the viscosity of medium and D is the translational diffusion coefficients. Hydrodynamic diameter is the size of a sphere that diffuses at the same rate as the particle being measured. This means that the reported diameter is influenced not only by the size of "core" particles, but also by any surface structure (*i.e.* adsorbed polymer) and the ions condition in medium (**Figure 1.4**) (Malvern, 2015a). The true particle size distribution, meanwhile, can also be analyzed based on the auto-correlation function. Measuring the width of the particle size distribution, polydispersity index (PDI), as another important parameter, is calculated using the equation (1.2):

$$PDI = \left(\frac{\delta}{d_H}\right)^2 \quad (1.2)$$

where, δ is the standard deviation. The value of PDI could change from 0 to 1.0 (Danaei et al., 2018). If the $PDI < 0.3$, the particles could be considered as monodisperse. When the PDI is close to 1.0, the sample dispersion has multiple

particle sized populations and considered to be highly polydispersed. Although DLS was used for PPM characterization, it was not that useful for CNC as latter was rod-shaped and the approximations were not valid.

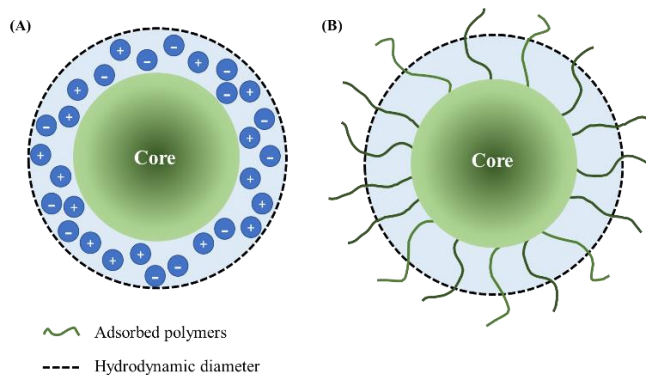


Figure 1.4. Hydrodynamic diameter in DLS being larger than the 'core' diameter due to the concentration and type of ions in medium (A) or any surface structure (B) *i.e.* adsorbed polymer.

1.4.1.2 Static light scattering (SLS)

Static laser light scattering (SLS) is another measurement technique used for size characterization, but for an emulsion droplet ranging from 0.01 to 1000 μm . SLS was used to characterize the droplet size of Pickering emulsions undergoing various adjustments in pH, ionic concentrations (**Chapter 3**) as well as *in vitro* gastrointestinal processing (**Chapters 4 and 5**). When light interacts with droplets, diffraction, refraction, reflection, and absorption occur, leading to a phenomenon called as static light scattering. For droplet, which has significantly larger size than the light wavelength, diffraction occurred at the particle surface, playing a dominant role based on Fraunhofer diffraction theory, and resulting in an angular variation of the scattered light (Microtrac, 2022, Malvern, 2022). Diffraction of large droplet has a small angle (θ) with strong intensity, while smaller droplet scatters light as a larger angle with weak intensity (**Figure 1.5**). Three laser beams hit the sample dispersion from different angles, therefore, the angle and intensity of the scattered light are detected under a particularly wide range of angles. The information of detected intensity of scattered light is transitioned to droplet size distribution using “Mie theory”, assuming that droplets are sphere and dispersed in the homogeneous

solution, as well as knowing the refractive index of both particles and dispersion medium (Born and Wolf, 2013).

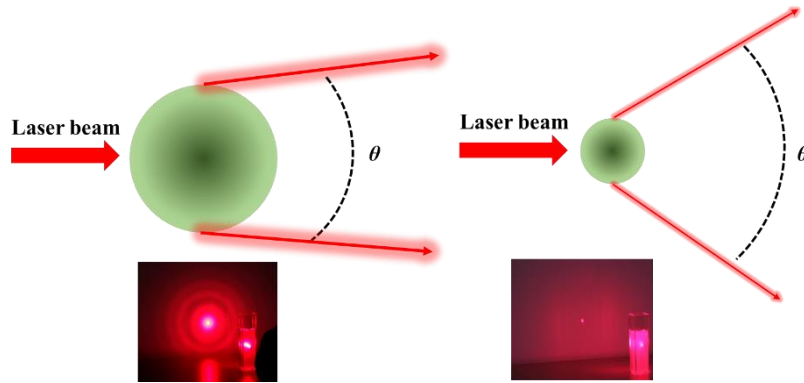


Figure 1.5. Schematic representation of light scattered from small and large droplets, as well as scattered light patterns of 1 mm and 10 μm droplets as example, respectively, which were illuminated using a commercial laser pointer (Microtrac, 2022).

SLS results are commonly reported as the d_{43} (De Brouckere mean diameter), which relate with the volume-average diameter of the droplet and is sensitive to large droplets, as well as d_{32} (Sauter mean diameter) which relate with the surface area mean diameter, latter is sensitive to the presence of the fine droplets. These two values are calculated using the equations (1.3) and (1.4), respectively:

$$d_{43} = \frac{\sum_1^n d_i^4 v_i}{\sum_1^n d_i^3 v_i} \quad (1.3)$$

$$d_{32} = \frac{\sum_1^n d_i^3 v_i}{\sum_1^n d_i^2 v_i} \quad (1.4)$$

1.4.1.3 Zeta-potential

In this thesis, the Zeta (ζ)-potential of particles and different emulsion droplets was measured undergoing the various pH and ionic strength adjustment (**Chapter 3**) as well as *in vitro* gastrointestinal conditions (**Chapters 4** and **5**). The electrical

characteristics are not only important parameter to analyse the electrostatic stability and physicochemical properties of both particles and emulsions, but also are key indices to dictate the interparticle interaction between CNC and adsorbed PPM at the O/W interface.

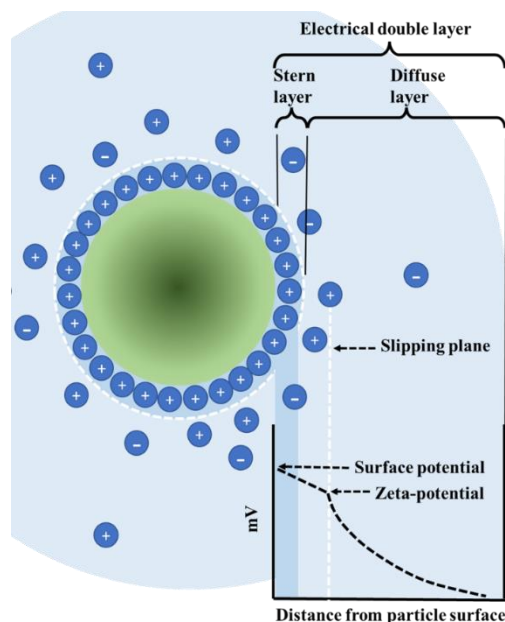


Figure 1.6. Schematic representation of a negatively charged particle in dispersed solution containing counter ions, figure reproduced from Malvern (2009).

The electrical properties of particles or droplets depend on the surface charge, those are strongly influenced by both charged functional groups and the types as well as the concentrations of ions in the dispersed medium. For example with a negatively-charged particle (**Figure 1.6**), the surface charge of particles attracts counter ions (ions of positive charge), while repels ions of similar charge. The increased concentration of ions surrounding the particle results in an electrical double layer, which exists as an inner region and an outer region. The inner region also called as “Stern layer” is created by strong attraction between the charged particle surfaces, meanwhile, the outer region is called the “diffuse layer”, latter is formed with loosely attracted ions, which is far away from particle surface. There is a notional stable boundary formed by the cooperation of particles and ions within the outer region. When the particle move, *e.g.* due to Brownian motion, ions within the boundary move together, however any ions beyond the boundary does not

affected by the particle movement. The electrostatic potential at this boundary (also called as “hydrodynamic shear” or “slipping plane”) is known as the ζ -potential (Malvern, 2009).

ζ -potential is determined by measuring electrophoretic mobility *via* electrophoresis and particle velocity measurement. The sample dispersion is added into a capillary cell which have two oppositely charged electrodes. Once an electric field is applied ($E_f = \text{Voltage applied} / \text{Distance between electrodes}$), charged particles tend to move towards opposite charged electrode. However, this movement is opposed by the viscous forces. Ultimately, the particles move at a constant velocity when the two opposing forces reach equilibrium. The velocity of particles, which is measured using laser doppler velocimetry, depends on the strength of electric field, the dielectric constant of the medium (ϵ), the viscosity of medium (η) and the ζ -potential of the particle. The velocity of particle (v_p) is related to electrophoretic mobility ($U_E = v_p / E_f$), and then the electrophoretic mobility is applied in Henry's equation (1.5) for calculation of ζ -potential:

$$U_E = \frac{2\epsilon\zeta f(k_a)}{3\eta} \quad (1.5)$$

where, $f(k_a)$ is the Henry's function which refers to the ratio of the particle radius (a) to the thickness of electrical double layer (k). Electrophoretic experiments are normally conducted in aqueous media with moderate concentration of electrolyte. Generally, $f(k_a)$ used two values as approximations: 1.5 and 1.0. In case of 1.5 for $f(k_a)$, particles exposed to higher salt concentrations lead to “thinner” electric double layer as comparing with radius of particle, Henry's equation is modified into the Helmholtz-Smoluchowski equation ($U_E = \epsilon\zeta / \eta$). On the other hand, the value of $f(k_a)$ is used as 1 when the thickness of electric layer is larger than the particle radius and Henry's equation is modified as the Hückel equation ($U_E = 2\epsilon\zeta / 3\eta$) (Malvern, 2015b).

1.4.1.4 Protein assay

The protein concentration was determined using Bio-Rad DC Protein Assay. This assay is similar to the Lowry Assay, a colorimetric assay for protein concentration following detergent solubilization. Based on the reaction of protein with an alkaline copper tartrate solution and Folin reagent, there are two steps which lead to colour development: 1) The reaction between the pea protein and copper in an alkaline medium, and 2) the subsequent reduction of Folin reagent by the copper-treated pea protein (Lowry et al., 1951). Colour development is primarily due to the amino acids tyrosine and tryptophan, and to a lesser extent linked to cystine, cysteine, and histidine. The copper-treated protein was reduced by Folin reagent, producing one or more of several possible reduced species by loss of 1, 2, or 3 oxygen atoms. The subsequent reductions were blue color with maximum absorbance at 750 nm and minimum absorbance at 405 nm (Lowry et al., 1951, Peterson, 1979). In addition, standard protein curve was freshly created using bovine serum albumin (BSA) standard containing 0.2 mg/ mL to 1.5 mg/ mL protein. The pea protein samples were normally diluted to the range from 0.2 to 1.0 mg/mL.

1.4.1.5 Microscopy across scales

The morphology and surface of the particles and the Pickering emulsion droplets with or without covering with CNCs were studied using different types of microscopy across scales (*i.e.*, optical, confocal and electron microscope) relying on different physical principles.

1.4.1.5.1 Light microscopy

Light microscopy is the most simple, basic microscopy where the surface of samples is imaged by reflected light. Most light microscopes have the same components that include several objective lenses, a light source with a mirror and an eyepiece or digital camera. The optical microscopes use a wide-field illumination leading to the uniform illumination of the whole focus plane, including the plane

above and below the focal plane. Therefore, only thin and relatively transparent samples could be clearly imaged (Auty, 2013). Although the resolution of an optical microscope is governed by the wavelength of the light source (which can be as low as 200 nm) and the objective, objects smaller than 1 μm are hardly detectable, such as the fresh prepared PPM in this thesis. In this thesis, light microscopy was used to monitor the possible aggregation of particles when subjected to various pH values and ionic concentrations (**Chapter 3**). In addition, the limited contrast between different components in a sample due to their similar refractive indices is another limitation of the optical microscope (McClements, 2014). To overcome this limitation, other types of microscope was used, such as confocal laser scanning microscopy (CLSM) to image both two-dimensional (2D) and three-dimensional (3D) structure in emulsions *via* a fluorescence technique.

1.4.1.5.2 Confocal laser scanning microscopy

Confocal laser scanning microscopy (CLSM) often called as confocal microscopy (**Figure 1.7**) is a type of optical microscopy with significant feature that the image of a light source and a detector are focused on a single volume element at a well-defined depth in the sample (Auty, 2013). Similar to an epifluorescence microscope, the fluorophores of sample absorb incident light, and then release again at longer wavelength. This emitted light is deflected by a dichroic mirror onto a photomultiplier detector with emission pinhole in front of the detector. The spatial pinhole is used to block out-of-focus light in image formation, leading to increasing optical resolution and contrast of a micrograph (Auty, 2013, Pawley, 2006). The signal intensity accepted in detector is further amplified and converter into pixels. Only one focal point in the sample is illuminated at a time. Therefore, 2D imaging requires regularly scanning over a consecutive x - y horizontal planes in the sample by using one or more dichroic mirrors. In addition, 3D structure is reconstructed by imaged 2D pixels at different depths. Nevertheless, depths of the focal point is dependent on the wavelength of the used light divided by the numerical aperture of the objective lens (Pawley, 2006).

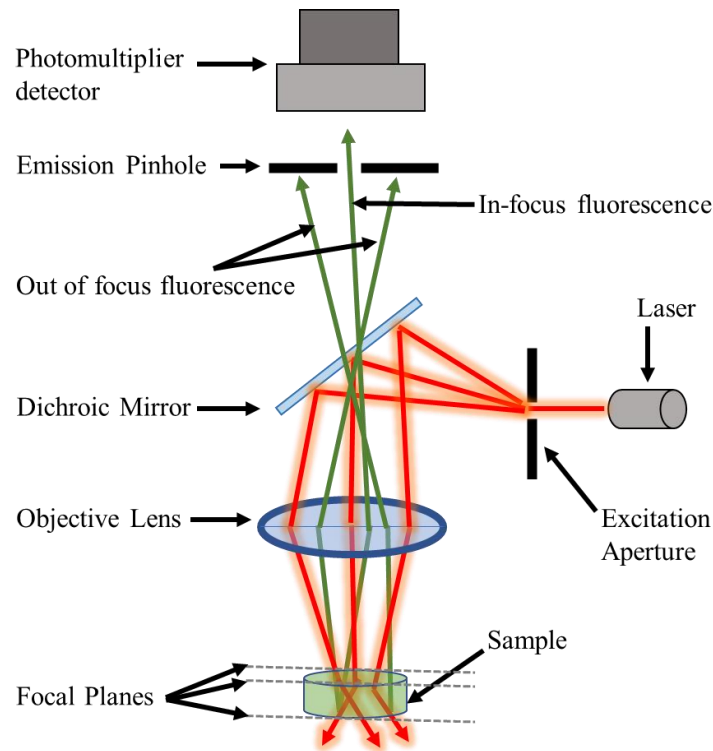


Figure 1.7. Schematic representation of confocal laser scanning microscopy.

CLSMs are widely applied in the investigation of food microstructures, but most food ingredients are not naturally fluorescent. In order to easily analyse the morphology and microstructure of sample, fluorescent dyes are required to stain different components in the sample, such as proteins and oil droplets in emulsions. In this thesis, Nile Blue was used to stain pea protein microgel particles by electrostatic interactions, Nile Red stained oil droplets through hydrophobic interactions as well as the polysaccharide (CNC) was stained by calcofluor white (Auty, 2013, Mokobi, 2021). Thus, CLSM was used to recognize the position and aggregated behaviour of PPM at O/W interface, to observe the shape and size of oil droplets, as well as to monitor coalesced oil droplets (**Figure 3-5**).

1.4.1.5.3 Scanning electron microscopy (SEM)

Scanning electron microscopy (SEM) is a common electron microscopy technique to characterize organic and inorganic materials on a scale ranging from nanometer (3-20 nm) to micrometer (Mohammed and Abdullah, 2018, McClements, 2014). The electron focus beam used in SEM scan the surface of a sample and interact with atoms within the sample, resulting in secondary electrons (SE), reflected or back-scattered electrons (BSE), characteristic X-rays and light. These signals contain information of the samples about their surface characteristic and composition, and is collected by an electron detector. The intensity of detected signal is measured and combined with the beam position to image using a software. Unlike optical microscopy, SEM resolution is not affected by the diffraction limit, or fineness of either lenses or mirrors. This resolution is determined primarily by both the size of the electron spot formed by the beam on the sample surface which in turn depends on the wavelength of the electrons, and the size of volume that generates a detectable signal below the spot (Greiser, 2009).

In order to limit the scatter and attenuate of electron beam by gas molecules, most of electron microscopy require samples to be imaged under high vacuum. To achieve vacuum environment during operation, the sample must not release gas. However, required drying or evaporation process may often destroy the inherent structure, shape and size of interest in the sample. Cryo-scanning electron microscopy (cryo-SEM) using a low temperatures is an useful technique in this regard as it could provide compatibility with the vacuum environment, preventing evaporation in hydrated sample, and in turn enable retaining the original structure of the sample (Greiser, 2009). Therefore, samples are treated by rapid freezing with liquid nitrogen to reduce the loss of structure during the imaging process. The frozen sample is transferred in the preparation cryo-chamber under vacuum with a low-temperature. In this chamber, the sample is cut with cold knife to explore internal structure. The cleaved surface is etched *via* ice sublimation with heater as needed. And then a conductive metal such as gold or platinum is sprayed and coat the sample, to enhance the intensity signal of the secondary electron as well as to

dissipate charge deposited at the surface by the electron beam during imaging (JEOL, 2011, Greiser, 2009).

In this thesis, cryo-SEM was used to observe the position of both protein-based particles and polysaccharide crystals at the heptane-water interface (**Chapter 4**). In order to avoid interference by oil crystallization during the freezing step, heptane was used in emulsions as a perfect substitute for sunflower oil. Heptane helped droplets to remain spherical with a smooth interface, due to accelerated solidification (Destribats et al., 2014b). Both emulsion systems (heptane or sunflower oil) presented the same macroscopic and microscopic characteristics. Thus, the cryo-SEM images for heptane emulsion was suitable to represent the morphological characteristics of sunflower oil emulsions.

1.4.1.6 Monolayer experiments

Langmuir trough has been used to measure surface phenomena of a monolayer undergoing compression of adsorbed film at a given interface, usually air-water interface or oil-water interface (Murray, 1997). The colloidal behaviour of adsorbed particles with expansion or compression at interface is one of the key factors to determine the formation and stability of colloidal system. In this thesis, Langmuir trough monolayer experiment was used to provide evidences of formation of particle-particle complex between CNC and PPM particles at the interface.

As described in **Figure 1.8A** about Langmuir trough, a moveable barrier (15 cm long \times 4) is capable of changing the area of the interface, which is placed in a container that holds the aqueous phase for analysis. A Wilhelmy plate, which is very thin, dip into the interface to measure the forces (F) acting on it due to surface tension, weight (P), and buoyant force (B). Thus, the surface tension can be calculated by equation (1.6) (Maget-Dana, 1999):

$$F = P + 2(t + w)\gamma \cos \theta - B \quad (1.6)$$

where, γ is the surface tension of aqueous phase, t is the thickness of plate, w is the width of plate and θ is the contact angle. Since the weight of the plate and the effect of buoyancy can be set to zero by instrument operation, and the surface pressure (π) is simply defined as a change of the surface tension due to the monolayer (see equation (1.7)):

$$\pi = \gamma_0 - \gamma \quad (1.7)$$

where, γ_0 is the surface tension of the pure phase. If the plate is completely wetted by aqueous phase leading to contact angle as zero (Erbil, 2006), the surface pressure can be obtained from the equation (1.8):

$$\pi = -\Delta\gamma = -\left[\frac{\Delta F}{2(t+w)}\right] = -\frac{\Delta F}{2w}, \text{ if } w \gg t \quad (1.8)$$

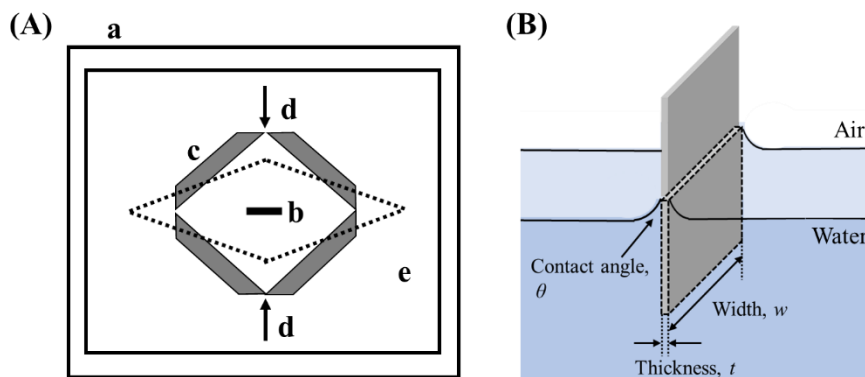


Figure 1.8. Schematic illustration of the Langmuir trough arrangement (A) and a Wilhelmy plate partially immersed in water phase (B). Key: (a) container (b) location of Wilhelmy plate; (c) barrier; (d) direction of the force for compression of interface; (e) indication of the change in shape of barrier on compression (Xu et al., 2007).

After surface-active particles are spread at interface, the surface pressure is continuously measured while the surface area with the barriers reduce at a constant

rate. It is carried out at constant temperature and is reported as a surface pressure – area isotherm (π - A isotherm). **Figure 1.9** shows the schematic of a typical π - A isotherm. The isotherm presents different regions (also called as phases) during compression depending on the interaction strength between particles (McClements, 2004). At high interfacial areas, the particles are far away from each other without interaction. This region is called as “gas” phase where the characteristics of individual particle determine the surface pressure. With increasing of surface pressure lead to reduction of interfacial area, the particle-particle interactions occur, leading to increase in surface pressure. “Liquid” phase is region that particles start to interact each other, but are still have space to freely move. In the next region called as “solid” phase, the particles closely packed together with a strong repulsive force, leading to rapid increase in the surface pressure. In any further compression, particles are going to aggregate and the monolayer film would collapses.

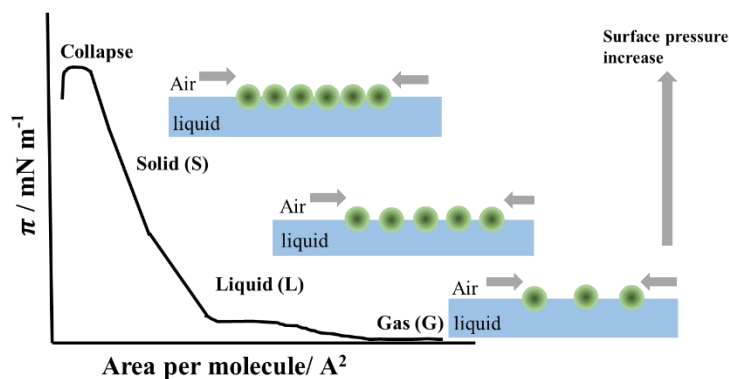


Figure 1.9. Schematic representation of surface pressure (π) versus area per molecule (A) plot of a surface-active molecule. The π - A plot is divided to different regimes (gas, liquid, solid and collapse) during compression.

1.4.1.7 Interfacial shear viscosity

Interfacial rheology is a branch of rheology that focus on the mechanical and flow properties of matter at the gas-liquid or liquid-liquid interface which are two immiscible phases (Murray and Dickinson, 1996). Interfacial rheology only makes sense when surface active compounds are present as a film at the interface because

interfacial rheology explains how the stresses used on interface influence the stability of adsorbed layer. The methods used to measure the rheological properties of an interfacial layer thus can be divided as dilatational and shear rheology methods (Murray and Dickinson, 1996, Renggli et al., 2020). For shear rheological methods with inducing shear, the area of adsorbed film remains the same. The interfacial viscosities characterize an important interfacial behaviour of adsorbed films that this interface has resistance to flow and deformation under the forces from the neighboring phase (Soo-Gun and Slattery, 1978).

Interfacial shear viscosity is a useful approach to monitor the formation and structure of the adsorbed films. In this thesis, interfacial shear viscosity was measured using Anton Paar rheometer to understand the structure of protein-based particle layer at various pH values as well as with the addition of pepsin. These information can be related to the formation and stability of emulsion, as well as the deformation of adsorbed film under attack from pepsin (**Chapter 6**).

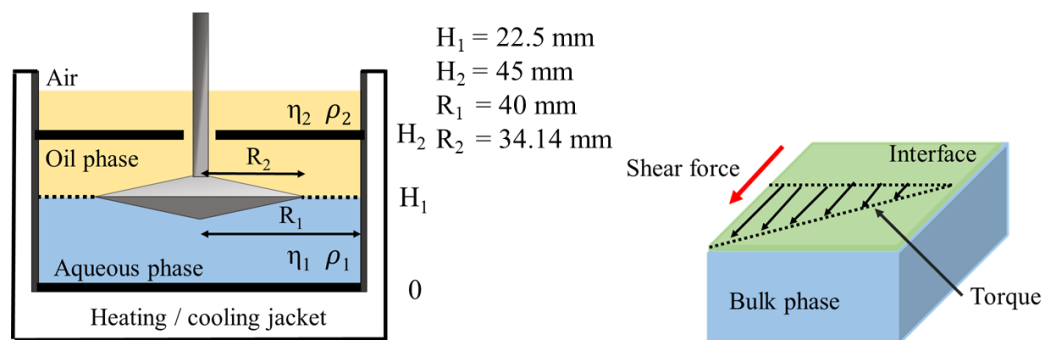


Figure 1.10. Schematic representation of biconical geometry system and interfacial shear gradient at interface (Läuger, 2007).

The biconical measuring system combined with an MCR rheometer is used for two-dimensional rheological measurements (**Figure 1.10**). For O/W emulsion sample, surface active components disperse in aqueous phase and are loaded into the vessel with certain volume. The biconical geometry with very sharp edges ($2 \times 5^\circ$) is placed on the top of aqueous phase, and in turn generally, carefully covered with oil phase to achieve the perfect position of the disc at O/W interface finally.

For the viscosity measurements, the biconical geometry rotates at a constant shear rate resulting in torque, as shown in **Figure 1.10**. Once the raw data of torque (M) and angular velocity (Ω) are measured, the interfacial viscosity could be obtained *via* relating reduced torque with the Boussinesq number (B_o) (Erni et al., 2003). A macroscopic Boussinesq number is used (Renggli et al., 2020), which is defined as equation (1.9):

$$B_o = \frac{\text{Interface}}{\text{Bulk phase}} = \frac{\eta_i \frac{V}{L_i} P}{(\eta_1 + \eta_2) \frac{V}{L_b} A} = \frac{\eta_i}{(\eta_1 + \eta_2) R} \quad (1.9)$$

where, η_i is the interfacial viscosity, η_1 and η_2 are the viscosity of lower and upper phase, respectively, R is a characteristic distance of the flow geometry, L_i and L_b are the lengths over which the velocity V decays in the interface and bulk phase, P is the perimeter between the probe and interface, and A is the contact area between the probe and bulk phase, whilst, V/L_i is assumed equal to V/L_b . It is worth to note that the relation of reduced torque and B_o is linear at high value of B_o . In this case, the interfacial shear viscosity is easily calculated from torque (equation (1.10)) (Chachanidzea et al., 2021, Erni et al., 2003):

$$\eta_i = \frac{M - \frac{8}{3} R_2^3 (\eta_1 + \eta_2) \Omega}{4\pi R_2^2 \Omega} \quad (1.10)$$

where, R_2 is the radius of the diss. Since biconical measuring system is sensitive to interactions between the adsorbed molecules and the possible change of interfacial structure, interfacial rheological parameters change as function of the ageing time of the adsorbed layer (Roth et al., 2000). Therefore, the interfacial shear viscosity is characterized every 15 min over 24 hours in this PhD thesis.

1.4.1.8 Rheology

Rheology describes the deformation and flow behaviour of liquid, semi-solid or solid matter. As shown in **Figure 1.11**, a specific force is applied to a material, leading to flow and /or deformation of the material. Shear stress (σ), shear strain (γ) and shear rate ($\dot{\gamma}$) are the terms that are usually used to describe the relationship between the applied force and the flow or deformation, and then to determine the rheological properties of the materials. Shear stress (equation (1.11)) is defined as the amount of force (F) per unit area (A), shear strain (equation (1.12)) is the displacement of the material due to stress, whilst shear rate (equation (1.13)) is the rate at which shear progresses (Mezger, 2014).

$$\sigma = \frac{F}{A} \quad (1.11)$$

$$\gamma = \frac{D_m}{h} \quad (1.12)$$

$$\dot{\gamma} = \frac{v}{h} \quad (1.13)$$

where, D_m is the displacement, h is the height and v is the velocity, which is obtained with t representing time ($v = \frac{D_m}{t}$).

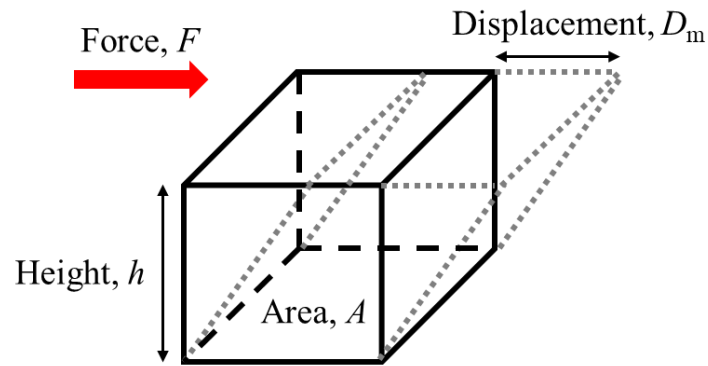


Figure 1.11. Relationship between the force and velocity of an applied stress on the displacement of a material (Mezger, 2014).

In this thesis (**Chapter 3 and 4**), rotational rheology for shear viscosity was studied using a cone and plate geometry to understand the properties of O/W emulsions stabilized by PPM undergoing the various pH adjustment, ionic concentration. Dynamic oscillatory rheology was studied to understand the influence of the addition of CNC on the properties of PPM dispersion and PPM-stabilized emulsions. Both a cone and plate geometry and concentric cylinder geometry were used for dynamic oscillatory rheology in this thesis.

For liquid materials, shear viscosity is used to describe their flow behaviour, which measuring the resistance of materials to flow when a certain shear stress is applied. Depending on the flowing behaviour, fluids can be classed as Newtonian and non-Newtonian. For ideal Newtonian fluids, shear viscosity (η) is defined as the ratio between shear stress (σ) and shear rate ($\dot{\gamma}$) ($\eta = \frac{\sigma}{\dot{\gamma}}$). It means that the viscosity of materials is independent to the shear rate as a constant temperature. In the other hand, non-Newtonian fluids are those where the viscosity of materials depends on the shear rate. The behaviour of non-Newtonian fluids can be classed as shear-thinning (pseudoplastic behaviour) or shear-thickening (dilatant behaviour). In the case of shear-thinning, the viscosity of materials decreases with increasing shear rate due to the deformation and re-arrangement of molecules. Oppositely, viscosity of materials increases with decreasing shear rate due to the flocculation or compression of the dispersed particles in shear-thickening systems (Mezger, 2014).

In addition, semi-solid materials are often characterized *via* dynamic oscillatory rheology, which examines viscoelastic properties of the material, *i.e.* complex shear modulus G^* , determined by equation (1.14):

$$G^* = \frac{\sigma}{\dot{\gamma}} \tag{1.14}$$

In this measurement, materials applied with a constant sinusoidal stress are measured their resulting strain as a function of amplitude stress, frequency, temperature or time (**Figure 1.12**). During shearing, the deformation energy is stored by the material, described as the storage or elastic modulus (G'). Meanwhile, the loss or viscous modulus (G'') represents the loss of the deformation energy of materials. Another parameter of dynamic oscillatory rheology is the phase angle (δ), which is the lag angle between the applied shear and the strain. The phase angle is the ratio between the viscous and elastic modulus (equation (1.15)), describing the damping ability of materials.

$$\tan \delta = \frac{G''}{G'} \quad (1.15)$$

If $\tan \delta > 1$, viscous modulus plays the key role. Oppositely, when the elastic modulus dominates, $\tan \delta < 1$. When G' is equal to G'' ($\tan \delta = 1$), it is the sol/gel transition point (Mezger, 2014).

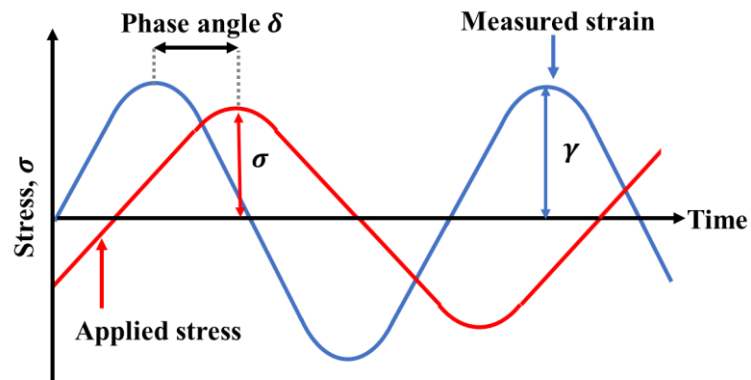


Figure 1.12. Schematic representation of the oscillatory rheology of a viscoelastic material, showing the sinusoidal applied stress (σ), the sinusoidal measured strain (γ) and the phase shift angle (δ) occurring between the applied stress and measured strain response (Mezger, 2014).

In this thesis, an amplitude sweep and a frequency sweep were used in oscillatory measurements of PPM stabilized emulsion covering with CNC (**Chapter 4**). An amplitude sweep test is conducted as function of amplitude shear strain, while keeping the temperature and frequency constant. This measurement allows to understand the linear viscoelastic region (LVER) of the material as well as determining the limiting value of the LVER. This limiting value is known as breaking point, usually representing that the material irreversibly starts to break down. Frequency sweep measurement is conducted in the LVER (Mezger, 2014). The frequency sweep test is conducted as function of frequency, while keeping shear and temperature constant. This test allows to examine the time-dependent deformation behaviour. High frequency simulates rapid motion/short-term behaviour while low frequency simulates slow motion/long-term behaviour. On the other hand, a frequency sweep test also allows to understand the degree of cross-link in materials, *e.g.* the network in the bulk phase of emulsion which is important for this thesis. A cross-linking in bulk phase with a high degree will show exhibit constant rigidity. In this case, both elastic and viscous moduli are almost constant over frequency, while $G' \gg G''$ and G' being almost parallel to G'' . In case of a lower degree of cross-linking, materials show more flexibility with G' increasing until reaching a plateau, while G'' also increases until reaching a maximum value and then dropping. Additionally, the values of G' and G'' will be closer to each other (Mezger, 2014).

1.4.2 *In vitro* gastrointestinal processing

In vitro methods are particularly used to study the gastrointestinal behaviour of colloidal particles or systems as well as to understand their controlled release mechanisms (bioaccessibility), because they mimic the physiological conditions *in vivo*, such as pH, ions concentration and enzymes, in a fast, inexpensive, less labour-intensive, standardized approach without the need of ethical permission, as compared with the use of *in vivo* methods (Alegría et al., 2015). *In vitro* methods have been developed in three main models, which are the static, the semi-dynamic

and dynamic models. All the standardized *in vitro* digestion generally contain two or three phases, *i.e.* oral, gastric and intestinal, and try to mimic digestion steps and physiological conditions in human physiology.

Static models are considered as the simplest models, which are the usual choice for digestion studies of a simple food or purified food components, such as milk, bread, or nutrients. The main disadvantage of static models is that they neglect dynamic physiological properties, such as the changes in pH and enzyme concentration over time, gradual removal of digestion products, hydration as well as dynamic peristalsis (Alegría et al., 2015). Therefore, dynamic and semi-dynamic models have been developed. Dynamic models is the closest model to “real” digestion since the design of this model is based on extensive researches into human physiology, as well as simulating the physiology from both biochemical and mechanical aspects (Dupont et al., 2019, Wickham et al., 2012). Although dynamic models are successful to directly compare with the results of *in vivo* or clinical studies due to their abilities to process any complex real food items and meals, the application of this system is limited in food research. The dynamic models only simulate the behaviour of gastric phase, while simulations of oral and intestinal phases are relatively scarce (Dupont et al., 2019). In addition, the dynamic models request feeding a meal enough for an adult, which perhaps is another limitation (Dupont et al., 2019). On the other hand, semi-dynamic models are developed to overcome limitation of both static and dynamic models as well as to fill the gap between them.

In this thesis, the INFOGEST model, which is a static *in vitro* model developed by Minekus et al. (2014), was considered enough to investigate protection and breakdown mechanisms of PPM particles and the O/W emulsions during gastrointestinal digestion (**Chapter 4** and **5**). The enzymes used in INFOGEST model were listed in **Table 1.1**. In addition, an artificial version when gastric digestion was bypassed was also explored in **Chapter 5** to understand the importance of proteolysis (if any) during the gastric phase on subsequent lipolysis.

Table 1.1. Summary of enzymes used in INFOGEST model.

<i>In vitro</i> digestion regime	Enzyme	Structure	Molecule weight (kDa)	Substrate	Concentration (mg/ml)	Reference
Gastric phase	Porcine pepsin	Bilobal	34.5	Protein	3.077	(Worthington, 2020)
Intestinal phase	Porcine pancreatic Lipase from porcine pancreas Type II				24.201 29.412	
	lipase	Globular	50-52	lipid		(Mendes et al., 2012)
	colipase	Rectangular	10	-		(Egloff et al., 1995)
	trypsin	Single chain	23.3	Protein		(Walsh, 1970)
	chymotrypsin	Rhombic	25	Protein		(Appel, 1986)
	amylase	Globular	51-54	Starch		(Cozzone et al., 1970)

1.4.2.1 Protein electrophoresis (sodium dodecyl sulphate polyacrylamide gel electrophoresis)

Sodium dodecyl sulphate polyacrylamide gel electrophoresis (SDS-PAGE) is a discontinuous electrophoretic system which is used to separate charged protein under an electric field based on their molecular weights. Generally, protein samples are denatured using sodium dodecyl sulphate (SDS), which binds to the protein backbone leading to the dissociation and unfolding of the protein. A reducing agent, such as mercaptoethanol or dithiothreitol, is used to further disrupt disulphide bonds, resulting in total unfolding to linear chains. In addition, the presence of SDS and broken S-S bonds lead to negative charge on the proteins, proportionally to their peptide chain length. Then, the negatively charged proteins are loaded into a polyacrylamide-based discontinuous gel, which has different sizes of pores. Under an electric field, the negatively-charged proteins move towards the positively-charged electrode, and is separated depending on their molecular size (**Figure 1.13**). Smaller protein with lower molecular weights move rapidly while larger proteins move slowly due to the pore structure of gel. Finally, the treated sample is stained with Coomassie Blue in order to detect the protein bands in the gel matrix. The molecular weight of each separated protein is calculated by comparing to a protein standard using densitometry.

In this thesis, SDS-PAGE was used to determine the composition of pea protein-based microgel particles (**Chapter 3**), as well as to analyze the extent of protein hydrolysis of the particles during and after *in vitro* gastric digestion stage (**Chapter 4**). However, this method cannot be applied to analyze the extent of protein hydrolysis in our emulsion system in *in vitro* gastric digestion, due to the limitation that some protein within the gel particles were covered by CNC, which were not hydrolysed to a great extent.

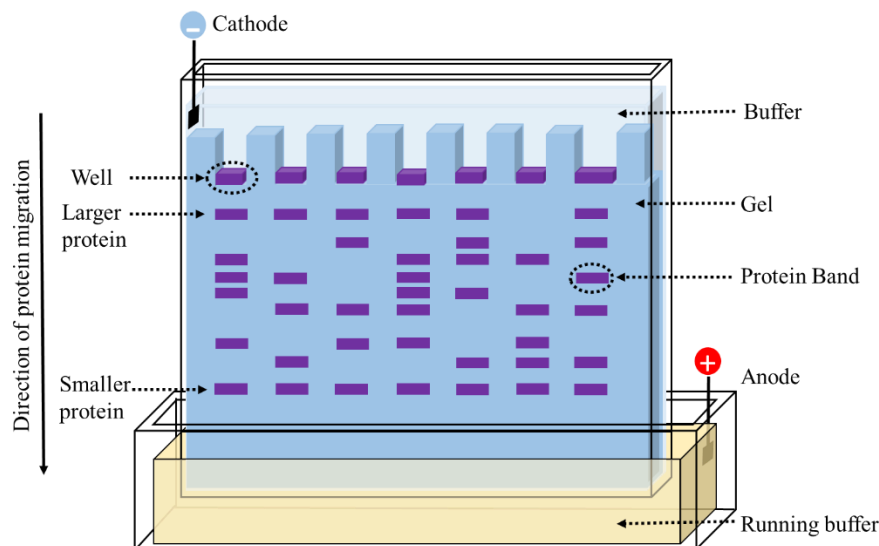


Figure 1.13. Schematic representation of sodium dodecyl sulphate polyacrylamide gel electrophoresis (SDS-PAGE).

1.4.2.2 Free fatty acid release

The pH-stat titration method is a classical approach to analyse the free fatty acid released during the *in vitro* intestinal digestions systems. Lipid is hydrolysed by the lipase at pH 6.8, resulting in the release of two free fatty acids (FFAs) and one monoacylglycerol (MAG) from one triacylglycerols (TAG) molecule leading to a reduction in pH value. Therefore, by maintaining the pH at the initial constant value (pH 6.8) *via* titration of sodium hydroxide (NaOH), the amount of released FFAs is calculated depending on the volume of added sodium hydroxide over time (Li and McClements, 2010b). It is assumed that two moles of NaOH are needed to achieve neutralization of one mole of digested triglyceride.

In this thesis, pH-stat titration was used to understand the different release rates of FFAs in PPM stabilized emulsion with the addition of CNCs as compared to the PPM stabilized emulsion without added CNCs (**Chapter 5**).

1.5 Outline of the thesis

Having discussed the rationale of selection of materials and methods for this thesis, the overall structure of this thesis is illustrated in **Figure 1.14**. This thesis includes a comprehensive narrative review on the application of different particles at the O/W interface that can play an integral role in modifying the kinetics of lipid digestion including discussion of mathematical models to derive specific kinetic parameters. It then continues with a series of research studies from the design and characterization of plant-based Pickering particles and corresponding emulsions prepared using complex interfaces, to *in vitro* gastrointestinal lipid digestion.

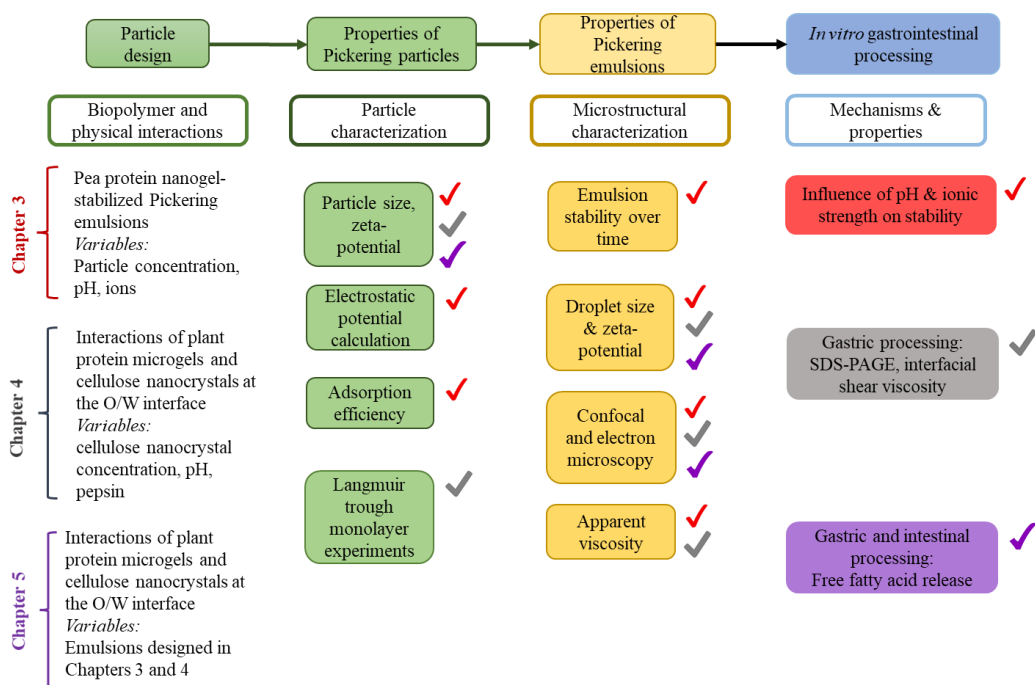


Figure 1.14. Schematic framework of this thesis.

Chapter 2 includes a literature review giving an overview of the key players in colloidal structuring of lipid digestion in human physiology. A summary of types of Pickering particles, and interfacial design strategies to control digestion profiles that have been investigated in recent years is discussed, while the theoretical models which is crucial to quantify lipid digestion kinetics are elaborated. A clear knowledge gap is identified to pursue the experimental studies on plant-based particles and also complex particle-particle interfaces. The literature

review forming this chapter was published in a peer-reviewed journal, *Advances in Colloid and Interface Science*.

Chapter 3 discusses the design of plant-based (pea protein) microgel particles using the top-down approach, followed by the characterization of colloidal stability of these microgel particles as functions of pH and ions concentrations. The ability of these particles as Pickering emulsifier was investigated from the influence of particle concentration and storage stability. Furthermore, the effects of pH and ionic strength on microstructure and stability of the emulsions stabilized by these microgel particles were investigated using experiments supported by theoretical calculations. The formation of pea protein microgel particles *via* the top-down approach acting as Pickering stabilizers was reported for the first time. This chapter was published in peer-reviewed journal, *Food Hydrocolloids*.

Chapter 4 presents the ability of cellulose nanoparticles to protect oil droplets in PPM stabilized emulsions, from coalescence during *in vitro* gastric digestion. The proteolysis of pea protein microgel particles and coalescence in Pickering emulsion stabilized by these particles during *in vitro* gastric digestion were evaluated from aspects of size, ζ -potential, microstructure (confocal microscopy) and protein hydrolysis *via* SDS-PAGE. In addition, a complex particle layer of Pickering emulsion was designed through covering adsorbed PPMs with CNC *via* an electrostatic interaction, to resist droplets coalescence in gastric digestion. The stability of the corresponding Pickering emulsion droplets was evaluated as a function of different CNC concentrations using ζ -potential measurements, Langmuir trough experiments and shear viscosity measurements. This chapter was published in the peer-reviewed journal, *Langmuir*.

Chapter 5 demonstrates coalescence occurring during the intestinal digestion stage to various extents on addition of CNC, as well as highlights the importance of prior proteolysis in lipid digestion of such systems. This chapter has been submitted to the peer-reviewed journal, *Food Biophysics*.

Chapter 6 includes a general summary and discussion of the main results of this thesis, and conclusions in relation to the principal research problem and areas for future studies.

1.6 Reference

- AHMED, E. M. 2015. Hydrogel: Preparation, characterization, and applications: A review. *J Adv Res*, 6, 105-21.
- AHNEN, R. T., JONNALAGADDA, S. S. & SLAVIN, J. L. 2019. Role of plant protein in nutrition, wellness, and health. *Nutr Rev*, 77, 735-747.
- ALEGRÍA, A., GARCIA-LLATAS, G. & CILLA, A. 2015. Static digestion models: General introduction. *The impact of food bioactives on health*, 3-12.
- APPEL, W. 1986. Chymotrypsin: Molecular and catalytic properties. *Clinical biochemistry*, 19, 317-322.
- ARAKI, J., WADA, M., KUGA, S. & OKANO, T. 1998. Flow properties of microcrystalline cellulose suspension prepared by acid treatment of native cellulose. *Colloids and Surfaces A: Physicochemical and Engineering Aspects*, 142, 75-82.
- AUTY, M. A. E. 2013. Confocal microscopy: principles and applications to food microstructures. *Food Microstructures*.
- AVEYARD, R., BINKS, B. P. & CLINT, J. H. 2003. Emulsions stabilised solely by colloidal particles. *Advances in Colloid and Interface Science*, 100-102, 503-546.
- BEN SHALOM, T., BELSEY, S., CHASNITSKY, M. & SHOSEYOV, O. 2021. Cellulose Nanocrystals and Corn Zein Oxygen and Water Vapor Barrier Biocomposite Films. *Nanomaterials (Basel)*, 11.
- BERTON-CARABIN, C. C. & SCHROEN, K. 2015. Pickering emulsions for food applications: background, trends, and challenges. *Annu Rev Food Sci Technol*, 6, 263-97.
- BORA, P. S., BREKKE, C. J. & POWERS, J. R. 1994. Heat Induced Gelation of Pea (*Pisum sativum*) Mixed Globulins, Vicilin and Legumin. *Journal of Food Science*, 59, 594-596.
- BORN, M. & WOLF, E. 2013. *Principles of optics: electromagnetic theory of propagation, interference and diffraction of light*, Elsevier.

- BOYE, J. I., AKSAY, S., ROUFIK, S., RIBÉREAU, S., MONDOR, M., FARNWORTH, E. & RAJAMOHAMED, S. H. 2010. Comparison of the functional properties of pea, chickpea and lentil protein concentrates processed using ultrafiltration and isoelectric precipitation techniques. *Food Research International*, 43, 537-546.
- CHACHANIDZEA, R., XIE, K., MASSAAD, H., ROUX, D., LÉONETTI, M. & DE LOUBENS, C. 2021. Structural characterization of the interfacial self-assembly of polyelectrolytes. *arXiv preprint arXiv:2110.03519*.
- COZZONE, P., PASERO, L., BEAUPOIL, B. & MARCHIS-MOUREN, G. 1970. Characterization of Porcine Pancreatic Isoamylases Chemical and Physical Studies. *Biochimica et biophysica acta*, 207, 490-504.
- CROY, R., GATEHOUSE, J. A., TYLER, M. & BOULTER, D. 1980. The purification and characterization of a third storage protein (convicilin) from the seeds of pea (*Pisum sativum* L.). *Biochemical Journal*, 191, 509-516.
- DALGLEISH, D. G. & HALLETT, F. R. 1995. Dynamic light scattering: applications to food systems. *Food Research International*, 28, 181-193.
- DANAEI, M., DEGHANKHOLD, M., ATAEI, S., HASANZADEH DAVARANI, F., JAVANMARD, R., DOKHANI, A., KHORASANI, S. & MOZAFARI, M. R. 2018. Impact of Particle Size and Polydispersity Index on the Clinical Applications of Lipidic Nanocarrier Systems. *Pharmaceutics*, 10.
- DAY, L. 2013. Proteins from land plants – Potential resources for human nutrition and food security. *Trends in Food Science & Technology*, 32, 25-42.
- DE FOLTER, J. W., HUTTER, E. M., CASTILLO, S. I., KLOP, K. E., PHILIPSE, A. P. & KEGEL, W. K. 2014. Particle shape anisotropy in pickering emulsions: cubes and peanuts. *Langmuir*, 30, 955-964.
- DESTREBATS, M., ROUVET, M., GEHIN-DELVAL, C., SCHMITT, C. & BINKS, B. P. 2014. Emulsions stabilised by whey protein microgel

- particles: towards food-grade Pickering emulsions. *Soft matter*, 10 36, 6941-54.
- DICKINSON, E. 2010. Food emulsions and foams: Stabilization by particles. *Current Opinion in Colloid & Interface Science*, 15, 40-49.
- DICKINSON, E. 2012. Use of nanoparticles and microparticles in the formation and stabilization of food emulsions. *Trends in Food Science & Technology*, 24, 4-12.
- DUPONT, D., ALRIC, M., BLANQUET-DIOT, S., BORNHORST, G., CUEVA, C., DEGLAIRE, A., DENIS, S., FERRUA, M., HAVENAAR, R., LELIEVELD, J., MACKIE, A. R., MARZORATI, M., MENARD, O., MINEKUS, M., MIRALLES, B., RECIO, I. & VAN DEN ABEELE, P. 2019. Can dynamic in vitro digestion systems mimic the physiological reality? *Crit Rev Food Sci Nutr*, 59, 1546-1562.
- EGLOFF, M. P., SARDA, L., VERGER, R., CABBILLAU, C. & TILBEURGH, H. V. 1995. Crystallographic study of the structure of colipase and of the interaction with pancreatic lipase. *Protein science*, 4, 44-57.
- ERBIL, H. Y. 2006. *Surface chemistry of solid and liquid interfaces*, Wiley-Blackwell.
- ERNI, P., FISCHER, P., WINDHAB, E. J., KUSNEZOV, V., STETTIN, H. & LÄUGER, J. 2003. Stress- and strain-controlled measurements of interfacial shear viscosity and viscoelasticity at liquid/liquid and gas/liquid interfaces. *Review of Scientific Instruments*, 74, 4916-4924.
- ETTELAIE, R. & LISHCHUK, S. V. 2015. Detachment force of particles from fluid droplets. *Soft Matter*, 11, 4251-65.
- FERREIRA, S. S., PASSOS, C. P., MADUREIRA, P., VILANOVA, M. & COIMBRA, M. A. 2015. Structure-function relationships of immunostimulatory polysaccharides: A review. *Carbohydr Polym*, 132, 378-96.

- GATEHOUSE, J. A., CROY, R. R. D. & BOULTER, D. 1980. Isoelectric-focusing properties and carbohydrate content of pea (*Pisum sativum*) legumin. *Biochemical Journal*, 185, 497-503.
- GE, J., SUN, C. X., CORKE, H., GUL, K., GAN, R. Y. & FANG, Y. 2020. The health benefits, functional properties, modifications, and applications of pea (*Pisum sativum* L.) protein: Current status, challenges, and perspectives. *Compr Rev Food Sci Food Saf*, 19, 1835-1876.
- GREISER, J. 2009. *Advances in Cryo-SEM: From Micrometers to Nanometers* [Online]. Available: <https://www.americanlaboratory.com/914-Application-Notes/577-Advances-in-Cryo-SEM-From-Micrometers-to-Nanometers/> [Accessed].
- HABIBI, Y., LUCIA, L. A. & ROJAS, O. J. 2010. Cellulose Nanocrystals: Chemistry, Self-Assembly, and Applications. *Chemical Reviews*, 110, 3479-3500.
- HERTZLER, S. R., LIEBLEIN-BOFF, J. C., WEILER, M. & ALLGEIER, C. 2020. Plant Proteins: Assessing Their Nutritional Quality and Effects on Health and Physical Function. *Nutrients*, 12.
- HUANG, L., CAI, Y., LIU, T., ZHAO, X., CHEN, B., LONG, Z., ZHAO, M., DENG, X. & ZHAO, Q. 2019. Stability of emulsion stabilized by low-concentration soybean protein isolate: Effects of insoluble soybean fiber. *Food Hydrocolloids*, 97.
- HUANG, M., WANG, F., ZHOU, X., YANG, H. & WANG, Y. 2015. Hypoglycemic and hypolipidemic properties of polysaccharides from *Enterobacter cloacae* Z0206 in KKAY mice. *Carbohydrate Polymers*, 117, 91-98.
- JEOL, L. 2011. Introducing Cryo Scanning Electron Microscopy. In: JEOL APPLICATION DATA SHEET, S. (ed.). JEOL Application Data Sheet, SEM SM-B-004-00E. .

- KALASHNIKOVA, I., BIZOT, H., CATHALA, B. & CAPRON, I. 2011. New Pickering emulsions stabilized by bacterial cellulose nanocrystals. *Langmuir*, 27, 7471-7479.
- KREFTING, J. 2017. The Appeal of Pea Protein. *Journal of Renal Nutrition*, 27, e31-e33.
- LAGUNA, L., PICOUET, P., GUÀRDIA, M. D., RENARD, C. M. G. C. & SARKAR, A. 2017. In vitro gastrointestinal digestion of pea protein isolate as a function of pH, food matrices, autoclaving, high-pressure and re-heat treatments. *Lwt*, 84, 511-519.
- LÄUGER, J. 2007. Interfacial Shear Rheology of Coffee Samples. Metrohm Siam: Anton Paar.
- LI, Y. & MCCLEMENTS, D. J. 2010. New mathematical model for interpreting pH-stat digestion profiles: impact of lipid droplet characteristics on in vitro digestibility. *J Agric Food Chem*, 58, 8085-92.
- LIU, H., XU, J., XU, X., YUAN, Z., SONG, H., YANG, L. & ZHU, D. 2021. Structure/function relationships of bean polysaccharides: A review. *Crit Rev Food Sci Nutr*, 1-15.
- LIU, S., LOW, N. H. & NICKERSON, M. T. 2009. Effect of pH, Salt, and Biopolymer Ratio on the Formation of Pea Protein Isolate–Gum Arabic Complexes. *Journal of Agricultural and Food Chemistry*, 57, 1521-1526.
- LOVEGROVE, A., EDWARDS, C. H., DE NONI, I., PATEL, H., EL, S. N., GRASSBY, T., ZIELKE, C., ULMIOUS, M., NILSSON, L., BUTTERWORTH, P. J., ELLIS, P. R. & SHEWRY, P. R. 2017. Role of polysaccharides in food, digestion, and health. *Crit Rev Food Sci Nutr*, 57, 237-253.
- LOWRY, O., ROSEBROUGH, N., FARR, A. L. & RANDALL, R. 1951. Protein Measurement with the Folin Phenol Reagent. *Journal of Biological Chemistry*, 193, 265-275.

- MAGET-DANA, R. 1999. The monolayer technique: a potent tool for studying the interfacial properties of antimicrobial and membrane-lytic peptides and their interactions with lipid membranes. *Biochimica et Biophysica Acta (BBA) - Biomembranes*, 1462, 109-140.
- MALVERN, I. L. 2009. *Zetasizer Nano Series User Manual MAN0317*, Worcestershire, UK: Malvern Instruments Ltd. .
- MALVERN, I. L. 2015a. *A basic guide to particle characterization*, Worcestershire, UK: Malvern Instruments Ltd. .
- MALVERN, I. L. 2015b. *Zeta potential - An introduction in 30 minutes*, Worcestershire, UK: Malvern Instruments Ltd. .
- MALVERN, P. L. 2022. *Laser Diffraction (LD): Particle size distributions from nanometers to millimeters*. [Online]. Malvern Panalytical Ltd: Malvern Panalytical Ltd. Available: <https://www.malvernpanalytical.com/en/products/technology/light-scattering/laser-diffraction> [Accessed].
- MATOS RUIZ, M., CAVAILLÉ, J. Y., DUFRESNE, A., GÉRARD, J. F. & GRAILLAT, C. 2012. Processing and characterization of new thermoset nanocomposites based on cellulose whiskers. *Composite Interfaces*, 7, 117-131.
- MATSUMIYA, K. & MURRAY, B. S. 2016. Soybean protein isolate gel particles as foaming and emulsifying agents. *Food Hydrocolloids*, 60, 206-215.
- MCCLEMENTS, D. J. 2004. *Food emulsions: principles, practices, and techniques*, CRC press.
- MCCLEMENTS, D. J. 2014. *Nanoparticle-and microparticle-based delivery systems: Encapsulation, protection and release of active compounds*, CRC press.
- MENDES, A. A., OLIVEIRA, P. C. & DE CASTRO, H. F. 2012. Properties and biotechnological applications of porcine pancreatic lipase. *Journal of molecular catalysis. B, Enzymatic*, 78, 119-134.

- MESSION, J.-L., CHIHI, M. L., SOK, N. & SAUREL, R. 2015. Effect of globular pea proteins fractionation on their heat-induced aggregation and acid cold-set gelation. *Food Hydrocolloids*, 46, 233-243.
- MESSION, J. L., SOK, N., ASSIFAOU, A. & SAUREL, R. 2013. Thermal denaturation of pea globulins (*Pisum sativum* L.)-molecular interactions leading to heat-induced protein aggregation. *J Agric Food Chem*, 61, 1196-204.
- MEZGER, T. G. 2014. *The rheology handbook : for users of rotational and oscillatory rheometers*, Hanover, Vincentz Network.
- MICROTRAC. 2022. *STATIC LASER LIGHT SCATTERING* [Online]. <https://www.microtrac.com/knowledge/static-laser-light-scattering/>:
Microtrac *MRB.* Available:
<https://www.microtrac.com/knowledge/static-laser-light-scattering/>
[Accessed].
- MINEKUS, M., ALMINGER, M., ALVITO, P., BALLANCE, S., BOHN, T., BOURLIEU, C., CARRIÈRE, F., BOUTROU, R., CORREDIG, M., DUPONT, D., DUFOUR, C., EGGER, L., GOLDING, M., KARAKAYA, S., KIRKHUS, B., LE FEUNTEUN, S., LESMES, U., MACIERZANKA, A., MACKIE, A., MARZE, S., MCCLEMENTS, D. J., MÉNARD, O., RECIO, I., SANTOS, C. N., SINGH, R. P., VEGARUD, G. E., WICKHAM, M. S., WEITSCHIES, W. & BRODKORB, A. 2014. A standardised static in vitro digestion method suitable for food - an international consensus. *Food Funct*, 5, 1113-24.
- MOHAMMED, A. & ABDULLAH, A. Scanning electron microscopy (SEM): A review. Proceedings of the 2018 International Conference on Hydraulics and Pneumatics—HERVEX, Băile Govora, Romania, 2018. 7-9.
- MOKOBI, F. 2021. *Calcofluor White Staining- Principle, Procedure, Results, Applications* [Online]. Available: <https://microbenotes.com/calcofluor-white-staining/> [Accessed].

- MORI, T., NAKAMURA, T. & UTSUMI, S. 1982. Gelation Mechanism of Soybean 11S Globulin: Formation of Soluble Aggregates as Transient Intermediates. *Journal of Food Science*, 47, 26-30.
- MURRAY, B. S. 1997. Equilibrium and dynamic surface pressure-area measurements on protein films at air-water and oil-water interfaces. *Colloids and Surfaces A: Physicochemical and Engineering Aspects*, 125, 73-83.
- MURRAY, B. S. & DICKINSON, E. 1996. Interfacial Rheology and the Dynamic Properties of Adsorbed Films of Food Proteins and Surfactants. *Food Science and Technology International, Tokyo*, 2, 131-145.
- NIE, S.-P. & XIE, M.-Y. 2011. A review on the isolation and structure of tea polysaccharides and their bioactivities. *Food Hydrocolloids*, 25, 144-149.
- NOBBMANN, U., CONNAH, M., FISH, B., VARLEY, P., GEE, C., MULOT, S., CHEN, J., ZHOU, L., LU, Y., SHEN, F., YI, J. & HARDING, S. E. 2007. Dynamic light scattering as a relative tool for assessing the molecular integrity and stability of monoclonal antibodies. *Biotechnol Genet Eng Rev*, 24, 117-28.
- O'KANE, F. E., HAPPE, R. P., VEREIJKEN, J. M., GRUPPEN, H. & VAN BOEKEL, M. A. 2004a. Characterization of pea vicilin. 1. Denoting convicilin as the α -subunit of the Pisum vicilin family. *Journal of Agricultural and Food Chemistry*, 52, 3141-3148.
- O'KANE, F. E., HAPPE, R. P., VEREIJKEN, J. M., GRUPPEN, H. & VAN BOEKEL, M. A. 2004b. Characterization of pea vicilin. 2. Consequences of compositional heterogeneity on heat-induced gelation behavior. *Journal of Agricultural and Food Chemistry*, 52, 3149-3154.
- PAWLEY, J. 2006. *Handbook of biological confocal microscopy*, Springer Science & Business Media.

- PETERSON, G. L. 1979. Review of the folin phenol protein quantitation method of lowry, rosebrough, farr and randall. *Analytical Biochemistry*, 100, 201-220.
- PICKERING, S. U. 1907. Cxcvi.—emulsions. *Journal of the Chemical Society, Transactions*, 91, 2001-2021.
- PINDAKOVA, L., KASPARKOVA, V. & BORDES, R. 2019. Role of protein-cellulose nanocrystal interactions in the stabilization of emulsion. *J Colloid Interface Sci*, 557, 196-206.
- POORE, J. & NEMECEK, T. 2018. Reducing food's environmental impacts through producers and consumers. *Science*, 360, 987-992.
- RAMSDEN, W. 1904. Separation of solids in the surface-layers of solutions and 'suspensions'(observations on surface-membranes, bubbles, emulsions, and mechanical coagulation).—Preliminary account. *Proceedings of the royal Society of London*, 72, 156-164.
- RENGGLI, D., ALICKE, A., EWOLDT, R. H. & VERMANT, J. 2020. Operating windows for oscillatory interfacial shear rheology. *Journal of Rheology*, 64, 141-160.
- RIZZO, G. & BARONI, L. 2018. Soy, Soy Foods and Their Role in Vegetarian Diets. *Nutrients*, 10.
- ROTH, S., MURRAY, B. S. & DICKINSON, E. 2000. Interfacial Shear Rheology of Aged and Heat-Treated β -Lactoglobulin Films: Displacement by Nonionic Surfactant. *Journal of Agricultural and Food Chemistry*, 48, 1491-1497.
- SAKURAI, K. & SHINKAI, S. 2000. Molecular recognition of adenine, cytosine, and uracil in a single-stranded RNA by a natural polysaccharide: Schizophyllan. *Journal of the American Chemical Society*, 122, 4520-4521.
- SANDBERG, A. S. 2011. 15 - Developing functional ingredients: a case study of pea protein. In: SAARELA, M. (ed.) *Functional Foods (Second Edition)*. Woodhead Publishing.

- SARKAR, A., ZHANG, S., MURRAY, B., RUSSELL, J. A. & BOXAL, S. 2017. Modulating in vitro gastric digestion of emulsions using composite whey protein-cellulose nanocrystal interfaces. *Colloids and Surfaces B: Biointerfaces*, 158, 137-146.
- SHAND, P. J., YA, H., PIETRASIK, Z. & WANASUNDARA, P. K. J. P. D. 2007. Physicochemical and textural properties of heat-induced pea protein isolate gels. *Food Chemistry*, 102, 1119-1130.
- SINGH, H. & SARKAR, A. 2011. Behaviour of protein-stabilised emulsions under various physiological conditions. *Adv Colloid Interface Sci*, 165, 47-57.
- SJOSTROM, E. 1993. *Wood chemistry: fundamentals and applications*, Gulf professional publishing.
- SOO-GUN, O. H. & SLATTERY, J. C. 1978. Disk and biconical interfacial viscometers. *Journal of Colloid and Interface Science*, 67, 516-525.
- THORNE, J. B., VINE, G. J. & SNOWDEN, M. J. 2011. Microgel applications and commercial considerations. *Colloid and Polymer Science*, 289, 625-646.
- WALSH, K. A. 1970. [4] Trypsinogens and trypsins of various species. Elsevier Science & Technology.
- WEI, Y., GUO, A., LIU, Z., ZHANG, L., LIAO, W., LIU, J., MAO, L., YUAN, F. & GAO, Y. 2021. Development of curcumin loaded core-shell zein microparticles stabilized by cellulose nanocrystals and whey protein microgels through interparticle interactions. *Food Funct*, 12, 6936-6949.
- WICKHAM, M. J. S., FAULKES, R. M., MANN, J. & MANDALARI, G. 2012. The Design, Operation, and Application of a Dynamic Gastric Model. *Dissolution Technologies*, 19, 15-22.
- WORTHINGTON. 2020. *Pepsin - Manual* [Online]. Worthington Biochemical Corporation. Available: <https://www.worthington-biochem.com/products/pepsin/manual> [Accessed 2022].

- XU, R., DICKINSON, E. & MURRAY, B. S. 2007. Morphological Changes in Adsorbed Protein Films at the Air–Water Interface Subjected to Large Area Variations, as Observed by Brewster Angle Microscopy. *Langmuir*, 23, 5005-5013.
- ZHANG, X., LIU, Y., WANG, Y., LUO, X., LI, Y., LI, B., WANG, J. & LIU, S. 2019. Surface modification of cellulose nanofibrils with protein nanoparticles for enhancing the stabilization of O/W pickering emulsions. *Food Hydrocolloids*, 97, 105180.

Chapter 2^a

Literature review

Abstract

Lipid digestion is a bio-interfacial process that is largely governed by the binding of the lipase-colipase-biosurfactant (bile salts) complex onto the surface of emulsified lipid droplets. Therefore, engineering oil-water interfaces that prevent competitive displacement by bile salts and/or delay the transportation of lipase to the lipidoidal substrate can be an effective strategy to modulate lipolysis in human physiology. In this review, we present the mechanistic role of Pickering emulsions *i.e.* emulsions stabilized by micron-to-nano sized particles in modulating the important fundamental biological process of lipid digestion by virtue of their distinctive stability against coalescence and resilience to desorption by intestinal biosurfactants. We provide a systematic summary of recent experimental investigations and mathematical models that have blossomed in the last decade in this domain. A strategic examination of behaviour of various particle-laden interfaces, where the particles are synthetic, natural or laboratory-synthesized from biological sources and mechanism of the lipid digestion of the droplets stabilized by these particles in simulated biophysical environments (oral, gastric, intestinal regimes) was carried out. This allowed us to categorize these particles into two classes based on their mechanistic role in modifying lipid digestion. These are ‘human enzyme-unresponsive particles’ (*e.g.* silica, cellulose, chitin, flavonoids) *i.e.* the ones that cannot to be digested by human enzymes, such as amylase, protease and ‘human enzyme-responsive particles’ (*e.g.* protein microgels, starch granules), which can be readily digested by humans. We focused on the role of particle shape (spherical, anisotropic) on modifying both interfacial and bulk phases during lipolysis. Also, the techniques currently used to alter the kinetics of lipid digestion using intelligent physical or chemical treatments to control interfacial

^a Published as a peer-reviewed publication: Sarkar A, Zhang S, Holmes M, Ettelaie R.(2018) Colloidal aspects of digestion of Pickering emulsions: Experiments and theoretical models of lipid digestion kinetics. *Adv Colloid Interface Sci.* 263:195-211.

particle spacing were critically reviewed. A comparison of how various mathematical models reported in literature predict free fatty acid release kinetics during lipid digestion highlighted the importance of the clear statement of the underlying assumptions. We provide details of the initial first order kinetic models to the more recent models, which account for the rate of adsorption of lipase at the droplet surface and include the crucial aspect of interfacial dynamics. We provide a unique decision tree on model selection, which is appropriate to minimize the difference between experimental data of free fatty acid generation and model predictions based on precise assumptions of droplet shrinkage, lipase-binding rate, and nature of lipase transport process to the particle-laden interface. Greater insights into the mechanisms of controlling lipolysis using particle-laden interfaces with appropriate mathematical model fitting permit better understanding of the key lipid digestion processes. Future outlook on interfacial design parameters, such as particle shape, size, polydispersity, charge, fusion, material chemistry, loading and development of new mathematical models that provide closed-loop equations from early to later stages of kinetics are proposed. Such future experiments and models hold promise for the tailoring of particle-laden interfaces for delaying lipid digestion and/or site-dependent controlled release of lipidic active molecules in composite soft matter systems, such as food, personal care, pharmaceutical, healthcare and biotechnological applications.

2.1 Introduction

Emulsions are ubiquitous in nature (*e.g.* milk, butter) and in engineered systems (*e.g.* cosmetics, processed food, pharmaceuticals, paints). Emulsions are intimate dispersions of two immiscible liquids, such as oil and water. In general, the liquid, which is present as micron- or sub-micron-sized droplets in the other liquid is known as the dispersed, discontinuous or internal phase (Singh and Sarkar, 2011a, Sarkar and Singh, 2016, McClements, 2015). And, the liquid into which the droplets are dispersed is known as the dispersion medium, continuous or external phase. From a thermodynamic perspective, emulsions are metastable *i.e.* they are in a state far from the equilibrium. Thus, emulsions tend to separate into their individual phases to attain an equilibrium configuration over a period

of time. This thermodynamic instability is commonly represented using Gibbs free energy change, ΔG , during emulsification. Emulsification at a constant temperature of T alters both the configurational entropy of the droplets, S_{config} , and the contact area between the immiscible phases, A , such that ΔG is given by:

$$\Delta G = \Delta H - T\Delta S_{config} + \gamma_{ow}\Delta A \quad (2.1)$$

where, ΔH is the enthalpy change, which is almost zero for emulsification, and γ_{ow} is the interfacial tension between the oil and water phases. The change in interfacial free energy ($\gamma_{ow}\Delta A$) is always net-positive as the interfacial area increases after the homogenization process, and is generally much larger than the term containing the configurational entropy change, ΔS_{config} , and thus the latter can be ignored (McClements, 2015). Hence, ΔG is mainly governed by $\gamma_{ow}\Delta A$. In the presence of an emulsifier, the magnitude of $\gamma_{ow}\Delta A$ is diminished due to reduction of the interfacial tension between the two phases enabled by adsorption of the emulsifier at the oil–water interface, consequently reducing the free energy. Though interfacial energy is the key driving force for emulsion formation, the properties of emulsifiers, such as surface charge and steric hindrance are crucial for providing kinetic stability to the emulsions. Emulsifiers, such as mono or di-acylglycerols, proteins, modified starches play an important role in imparting this kinetic stability to the oil droplets, however they tend to phase separate over a period of weeks to few months.

Besides conventional surfactants, emulsions can also be stabilized by rigid or soft solid particles that form a mechanical barrier *via* the Pickering stabilization mechanism (Aveyard et al., 2003a, Binks, 2002a). In fact, such Pickering emulsions are often encountered in the crude oil refining process (McLean and Kilpatrick, 1997), homogenized milk stabilized by casein micelles and aggregated milk proteins (Dickinson, 2010b) and are engineered for soft material applications (Aveyard et al., 2003a, Piao et al., 2015). In comparison to classical surfactant-stabilized emulsions, Pickering emulsions that are stabilized by solid particles are distinctively more stable to coalescence and

Ostwald ripening (Aveyard et al., 2003a, Binks, 2002a). This is due to the large amount of desorption energy (ΔE) required to dislodge the particles from the interface (Ettelaie and Lishchuk, 2015a). In other words, for emulsions to destabilize, the free energy (ΔG) of the system has to significantly increase at first, as the particles move from their preferred positions on the interface to one of the two phases. The adsorption energy for a single particle can be expressed using equation (2.2) (Binks, 2002a, Leal-Calderon and Schmitt, 2008, Lam et al., 2014):

$$\Delta G = -\Delta E = -\gamma_{ow}\pi r_p^2(1 - |\cos \theta|)^2 \quad (2.2)$$

where, r_p is the radius of the particle and θ is the equilibrium three-phase contact angle (Binks, 2002a, Binks and Horozov, 2006) highlighting the wettability of the particles by oil or water phases. The actual energy required to dislodge a particle from the surface has been shown to be even higher, at several times that given by equation (2.2). This is due to dissipation of energy stored in the liquid neck, formed between the particle and interface, as the liquid relaxes back once the particle has departed from the surface (Ettelaie and Lishchuk, 2015a, Lishchuk and Ettelaie, 2016). Hence, even nano-sized solid particles with $r \approx 50$ nm at a contact angle of 90° at the oil-water interface (typical value of $\gamma_{ow} \approx 50$ mN m⁻¹) will have $\Delta E \approx 10^5 k_B T$, where k_B is the Boltzmann's constant. This is several orders of magnitude higher than that for classical surfactants, which typically have $\Delta E \approx 5 k_B T$ and therefore tend to continuously “hop on and off” from the interface (French et al., 2016b). Thus, it is almost certain that solid particles once adsorbed under partial wetting conditions by the two phases, will remain irreversibly anchored to the interface making Pickering emulsions highly resilient to coalescence, when compared to similar droplets stabilized by typical molecular surfactants. Theoretically, wetting is represented by the classical Young's equation (equation 2.3), which is related to the balance of interfacial forces per unit length of the contact line at particle–oil (γ_{po}), particle–water (γ_{pw}), and oil–water (γ_{ow}) surfaces:

$$\cos \theta = \frac{\gamma_{po} - \gamma_{pw}}{\gamma_{ow}} \quad (2.3)$$

If one of the liquids wets the solid particles more than the other, the better wetting liquid becomes the continuous phase and the other one becomes the dispersed phase. For instance, if θ measured in the aqueous phase is smaller than 90° (Figure 2.1a), then particles are preferentially wetted by the aqueous phase (*i.e.* $\gamma_{pw} < \gamma_{po}$), with a large fraction of such particles residing in the continuous phase and stabilizing an O/W emulsion. Such hydrophilic biocompatible particles include protein microgels, zein particles and chitin nanocrystals (Destribats et al., 2014a, Sarkar et al., 2016d, Tzoumaki et al., 2011, de Folter et al., 2012). However, if θ is $>90^\circ$ (Figure 2.1b), the particles tend to be preferentially wetted by oil phase and stabilizes a W/O emulsion, as demonstrated using zein particles in presence of lecithin (Rutkevičius et al., 2018). Particles wetted equally by oil and water have contact angle of 90° (Figure 2.1c). It is noteworthy that when θ is relatively close to 90° , then particles effectively act as a Pickering stabilizer as particles tend to remain dispersed in either phases if they are too hydrophilic ($\theta \ll 90^\circ$) or too hydrophobic ($\theta \gg 90^\circ$) (Binks and Lumsdon, 2000). In order to overcome this latter issue, many studies have modified natural particles to varying degrees in order to make them partially wetted by both the polar and non-polar phases. For example, modified starch granules, prepared *via* reaction with octenyl succinic anhydride (Yusoff and Murray, 2011) or modified cellulose prepared using stearoyl chloride (Pang et al., 2018) have been used as effective Pickering stabilizers of oil-in-water or water-in-oil emulsions, respectively.

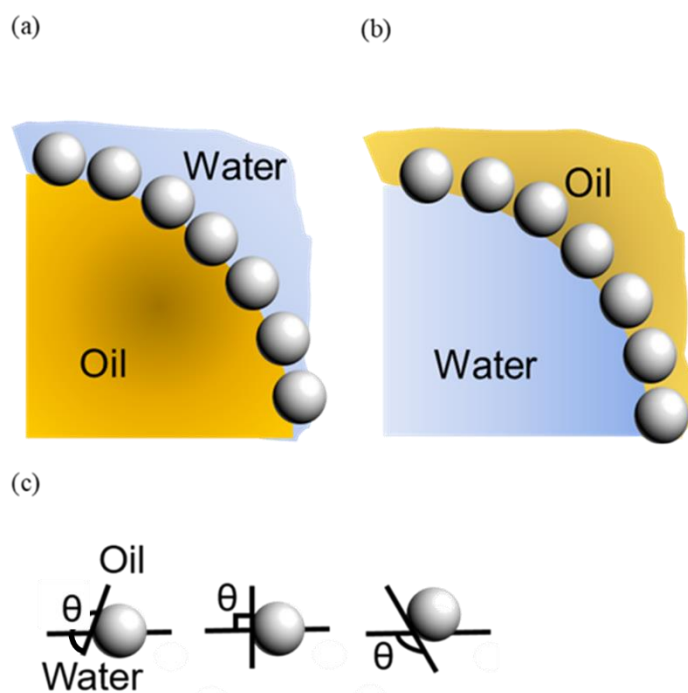


Figure 2.1. Possible positions of spherical solid particle at curved liquid-liquid interface representing particles preferentially wetted by aqueous phase (particle-stabilized O/W emulsions) (a) and by oil phase (particle-stabilized W/O emulsions), respectively (b), and position of a single spherical particle at a planar oil-water interface for a contact angle (θ), measured through the aqueous phase (c), with $\theta < 90^\circ$ (left), $= 90^\circ$ (center), $> 90^\circ$ (right), respectively.

Pickering stabilization of colloids using particles is a century-old concept, first introduced by Ramsden (1904a) and proven experimentally by Pickering few years later (Pickering, 1907a). The earliest theoretical treatment, demonstrating how fine particles can stabilize emulsions and foams, seems to be developed by Levine *et al.* dating back to 1989 (Levine *et al.*, 1989). Nevertheless, the study of particle-laden interface has revived through a renaissance of research attention in the last two decades. This can partly be attributed to the growing demands for designing ultra-stable emulsions using surfactant-free and ‘clean-label’ emulsifiers. In part, such a resurgence of research interests in particle-stabilized interfaces are also associated with tremendous progress in mining biocompatible particles from natural sources and laboratory-scale synthesis of relatively low-cost biocompatible colloidal particles with tunable size (micron-to-nanometers) (Dickinson, 2015b, Dickinson, 2017, Lam *et al.*, 2014) for use in food, pharmaceutical, cosmetics and other allied soft matter applications. In such applications sustainability and

biocompatibility are key requirements. Last but not the least, particle-laden interfaces have been lately recognized as promising templates by colloid scientists to address key biological processes, such as delaying lipid digestion (Sarkar et al., 2016d, Sarkar et al., 2017b, Sarkar et al., 2018b, Tzoumaki et al., 2013b), drug delivery (Marto et al., 2016), nutraceutical delivery (Araiza-Calahorra et al., 2018) and controlled release of lipophilic molecules *via* oral and topical administration routes (Chevalier et al., 2015, Frelichowska et al., 2009).

In particular, lipid digestion is a fundamental biological process that represents a major bottleneck in the pathway to controlled delivery of lipophilic drugs and nutrients when administered through oral routes in human physiology. Lipid digestion is an interfacial process and the kinetics of lipid digestion is governed by the binding of enzymes (lipases, proteases, amylases), biosurfactants (bile salts) and other cofactors onto the surface of emulsified droplets (Wilde and Chu, 2011b). Simplistically, one might expect lipid digestion to be controlled by tailoring and/or tuning the interfacial network. Hence, research efforts have been directed in recent years to alter the kinetics of lipid digestion by modification of the interfacial structures (Sarkar et al., 2018b, Sarkar et al., 2016d, Sarkar et al., 2016e, Sandra et al., 2008, Singh and Sarkar, 2011a, Golding and Wooster, 2010). In particular, solid particles have shown encouraging outcomes in this direction in the past decade by a variety of interfacial mechanisms, which necessitates this review. Progress on Pickering emulsion research has been well-described in the excellent reviews by Binks (2003a, 2002a, 2017), Dickinson (2010b, 2012, 2015b, 2015a, 2017) and few other research groups (Lam et al., 2014, Berton-Carabin and Schroën, 2015, Jie and Guang-Hui, 2016, Rousseau, 2013, Leal-Calderon and Schmitt, 2008, Chevalier and Bolzinger, 2013, Tavernier et al., 2016), who have discussed the physical chemistry, stabilization principle as well as design of elegant Pickering emulsions stabilized by organic (biologically derived) particles. However, to our knowledge, there exists no review that has discussed the mechanistic role of Pickering emulsions in modulating the important fundamental biological process of lipid digestion.

Hence, the purpose of this review is to focus on the experimental

investigations and theoretical models on lipid digestion of Pickering emulsions stabilized by nano-to-micron-sized particles within the last decade. In this review, only O/W emulsions are considered. We start with briefly discussing the key physiological players in the biophysics of lipid digestion in the oral, gastric and intestinal regimes. The ultimate step of conversion of lipids into self-assemblies, such as micelles, vesicles, and liquid crystals that are essential for lipid absorption in the lower intestines is beyond the scope of this review. A description of the colloidal aspects of digestion sets the scene for understanding how parameters associated with the particle, such as size, shape, concentration, charge, packing density affect the resilience of the particle-covered droplets to harsh physiological conditions. We have then summarized the current knowledge of how such particles on their own or *via* suitable physical/ chemical tuning at the interface play an integral role in modifying the kinetics of lipid digestion. Attention is then directed towards reviewing the mathematical models in literature, highlighting the early first order kinetic models to the more recent models attempting to account for the adsorption kinetics of enzymes at the droplet surface and the associated role of interfacial structure. We provide a decision tree on model selection appropriate to likely to represent a given digestion behaviour (*e.g.* droplets shrinking, enzyme binding rate, nature of enzyme transport process to the surface of droplets). Finally, we provide suggestions for future work in both theoretical and experimental domains to maximize the potential of Pickering emulsions in order to address fundamental biological and biochemical challenges associated with emulsified lipid digestion. Such knowledgebase can enable us to rationally design particle-laden interfaces for site-dependent controlled release of lipid soluble active molecules in composite soft matter systems, such as food, personal care and pharmaceutical applications.

2.2. Key players in colloidal structuring of lipids in human physiology

In this review, we are concerned mainly with the physiological re-structuring or resilience-to-destabilization of Pickering emulsion during the trajectory of lipid digestion. Nevertheless, we provide a concise summary of the three sequential

regimes (**Figure 2.2**) *i.e.* oral, gastric and intestinal, where complex colloidal structuring might occur with the eventual conversion of lipids to free fatty acids (FFAs) monomers. In particular, we highlight the interfacial role of the key enzymes and biosurfactants, such as mucin (oral), amylase (oral, intestinal), pepsin (gastric), trypsin and chymotrypsin (intestinal), bile salts (intestinal) and most importantly, lipase (gastric and intestinal). This is by no means to underestimate the roles of the inorganic ions (Na^+ , K^+ , Ca^{2+} , HCO_3^-), pH (full spectrum effects from saliva to gastrointestinal juices), and a range of shear-to-surface forces (oral shear, peristalsis, mixing regimes, interactions with mucus-coated surfaces) throughout the aqueous oral-to-gastrointestinal tract on colloidal structuring, aggregation of droplets and phase separation. Detailed information about colloidal aspects of lipid digestion in surfactant stabilized systems can be found in number of review articles (Sarkar and Singh, 2016, Singh and Sarkar, 2011a, McClements, 2018, Wilde and Chu, 2011b, Golding and Wooster, 2010, Favé et al., 2004, Reis et al., 2009).

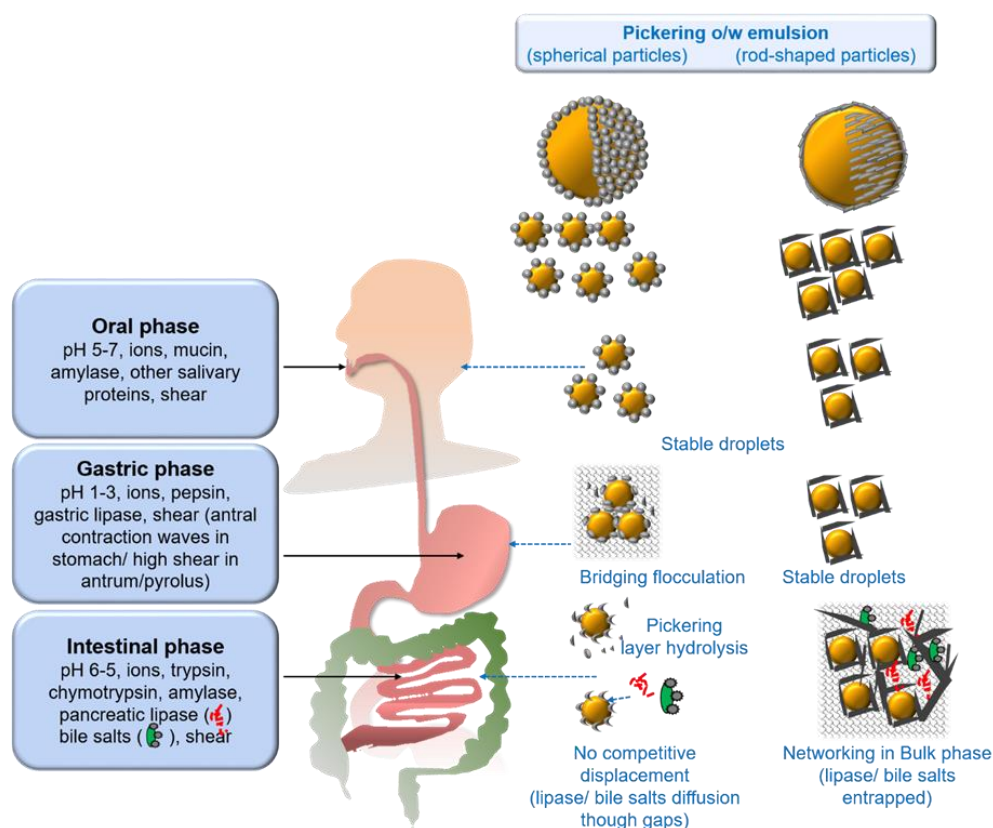


Figure 2.2. Schematic representation of the possible fate of Pickering emulsions based as they traverse through the oral to gastrointestinal regimes based on *in vitro* digestion studies. For simplicity reason, spherical particle is shown as enzyme-responsive and rod-shaped particle is shown as enzyme-unresponsive.

2.2.1 Oral phase

Saliva is the first complex fluid that an emulsion encounters upon oral consumption. Emulsions reside in the oral cavity for only a few seconds to minutes, depending upon the oral viscosity and coating abilities. Nonetheless, during this short time period, the emulsion droplets can undergo a diverse palette of destabilization routes from flocculation (bridging, depletion) to coalescence and phase separation depending upon their interactions with salivary components (Sarkar and Singh, 2012, Sarkar et al., 2016f, Laguna and Sarkar, 2017, Mosca and Chen, 2017). Human saliva has a neutral pH and contains a range of ions, proteins (*e.g.* mucin, immunoglobulin, statherins, proline-rich proteins, lysozymes, serum albumin), enzymes (amylase) and bacterial cells that are dispersed in 99% aqueous phase (Schipper et al., 2007).

Highly glycosylated salivary mucin (MUC5B), which contributes to 10–25% of total salivary proteins is deemed as one of the main components in the dilute saliva that can modify an emulsion's dispersion state. Structurally, salivary mucins are 20% polypeptide core and 80% carbohydrates and have a high molecular weight ($\geq 10^6$ Da) (Bansil and Turner, 2006). Emulsion structuring for ionic surfactant-stabilized or protein-coated droplets in the mouth can occur by virtue of electrostatic interactions with mucin, which is negatively charged at oral pH. The charge density of the mucin is associated with the sulphates and sialic acid (N-acetylneuraminic acid) parts of the glycosylated constructs. Hence, positively charged emulsions, such as, lactoferrin-coated droplets may undergo bridging flocculation with simulated or real saliva whereas weakly negatively-charged emulsions, such as, β -lactoglobulin-coated droplets undergo depletion flocculation in oral phase (Sarkar et al., 2009a, Sarkar et al., 2016f, Sarkar et al., 2017a, Silletti et al., 2007, Vingerhoeds et al., 2009). The second important component that can have a serious impact on colloidal instability is the enzyme, *salivary α -amylase*, latter initiates the hydrolysis of α -1-4 glycosidic bonds in starch in the oral phase. Therefore, α -amylase can rupture the interfacial layer and lead to oil droplet accretion, conditional to the scenario that the interfacial layer contain starch as structural motifs (Dresselhuis et al., 2008b, Torres et al., 2018). Besides mucin and α -amylase, salivary ions may induce oral flocculation of droplets *via*

electrostatic charge screening and/or ion binding effects (Sarkar et al., 2009a, Sarkar and Singh, 2012, Sarkar et al., 2016f). Oral shear-, surface- and air- (Aken et al., 2005, Dresselhuis et al., 2008b, Dresselhuis et al., 2008a) induced interactions may also result in droplet coalescence or partial coalescence, latter being dependent on the proportion of solid fat content in the droplets at oral temperature.

2.2.2 Gastric phase

After this relatively short oral residence, emulsions travel through the oesophagus and are subjected to harsh acidic environments (pH 1-3), ions, digestive enzymes (*pepsin* and *gastric lipase*) and mixing vortexes induced by antral contractions as well as shear forces when they reach the stomach (Golding and Wooster, 2010, Singh and Sarkar, 2011a, McClements, 2018) (**Figure 2.2**). The physicochemical conditions (pH, ionic strengths) in the stomach may lead to aggregation of the emulsion droplets in the stomach (Sarkar et al., 2010a). From a biochemical perspective, proteins are significantly hydrolysed by pepsin to smaller peptides, lipids are only partially digested by acid stable gastric lipase and carbohydrates see almost no breakdown in the gastric regime.

Pepsin is a proteolytic enzyme that breaks down the peptide bonds between hydrophobic groups, preferably aromatic amino acids, such as phenylalanine, tryptophan, and tyrosine. Thus, pepsin-induced cleavage can result in modification of the interfacial structure if the droplet surface that contains proteinaceous materials. Pepsin-induced proteolysis may result in interfacial film drainage eventually leading to droplet coalescence (Singh and Ye, 2013, Singh et al., 2009, Mackie and Macierzanka, 2010, Sarkar et al., 2009b, Singh and Sarkar, 2011a). Although the majority of lipolysis occurs in the intestinal phase, gastric lipase can contribute to nearly 10-30% of lipid digestion resulting in generation of FFAs in the stomach (Miled et al., 2000, Armand et al., 1996). Gastric lipase is active in the pH range of pH 3–6, which suggests that gastric lipase-induced lipid hydrolysis can occur even in the first hours of gastric digestion where the pH of the stomach is still elevated owing to the meal buffering capacity (Golding and Wooster, 2010). The gastric lipase-

mediated fatty acids released in the stomach may have some surface activity and competitive adsorption behaviour versus the parent material at the interface and thus alter the interfacial composition of lipid droplets. However, studies reported in literature on the interfacial aspects of gastric lipase-mediated lipolysis of emulsified lipids are relatively scarce to enable commenting on the interfacial modification with any certainty. This is because of the unavailability of reliable sources of lipases that behave like human gastric lipases until very recently (Sams et al., 2016). Depending on the initial interfacial structure (*e.g.* protein, surfactants), lipid composition (*e.g.* solid/ liquid lipid ratio) and degree of interactions with organic and inorganic players in the gastric phase, the fate of emulsion structure can vary from remaining intact to flocculated, coalesced, partially coalesced and phase separated (Golding et al., 2011, Sarkar et al., 2009b, Sarkar et al., 2010a, Singh and Sarkar, 2011a).

2.2.3 Intestinal phase

The majority of the interfacial alteration of the droplets and lipid digestion (70–90%) occurs in the upper part of the small intestine. The intestinal digestion is a complex process due to the presence of a cocktail of amylolytic, lipolytic and proteolytic enzymes, biosurfactant and inorganic components. As the droplets transcend from the stomach to intestine, the pH of the physiological medium reverts back to nearly neutral (Singh and Ye, 2013). Many, if not most colloid scientists have highlighted the key intestinal players to be *trypsin* and *chymotrypsin* for proteolytic action on protein-coated interfaces (Singh and Ye, 2013), *pancreatic amylase* for hydrolysis of starch-stabilized interfaces (Feher, 2017) and biosurfactant (*bile salts*) and *pancreatic lipase* (Wilde and Chu, 2011b) for generating fatty acids, mono and/or diacylglycerols from the hydrophobic lipid core besides cofactors (*colipase*) (Brockman, 2002, van Tilbeurgh et al., 1999) and other enzymes. For instance, trypsin predominantly catalyses the peptide chains at the C-terminal of aliphatic amino acids, mainly lysine and arginine, whereas chymotrypsin favours large aromatic residues, such as phenylalanine, tyrosine and tryptophan. Such interfacial cleavage can have consequences on altering the interfacial composition in the case of protein-stabilized droplets, such as those stabilized by β -lactoglobulin generating small

molecular weight peptides which might not have sufficient viscoelasticity like the parent protein film to prevent droplet deformation (Sarkar et al., 2010c).

The interfacial dynamics becomes most exciting in the intestinal phase as intestinal lipid digestion is an interfacial process that involves a complex interplay between competitive adsorption of lipase/colipase and bile salts at the O/W interface (**Figure 2.2**). Bile salts are a very unconventional, planar-type of biosurfactant that, unlike classical surfactants, do not have a typical hydrophobic head and a hydrophilic tail group (Maldonado-Valderrama et al., 2011). The facial amphiphilicity of bile salts originates from the flat steroidal structure, with the polar hydroxyl groups on the concave side and methyl groups on the convex side. Because of their high surface active properties, bile salts play a crucial role in lipid digestion by displacing the initial adsorbed materials from the interface (Euston et al., 2013, Maldonado-Valderrama et al., 2008) *via* orogenic displacement if the parent interfacial film is viscoelastic, permitting lipase/colipase complex to act on the bile-coated oil droplets. The role of the initial charge density at the droplet surface determines to a large extent the kinetics of the sequential binding of negatively charged bile salts to the interfacial material or displacement of the initial adsorbed layer by intestinal bile salts (Sarkar et al., 2010b, Singh and Sarkar, 2011a). Besides surface activity, bile salts also facilitate the solubilisation of lipid digestion products into lamellar phase or mixed micelles. Often, bile salts can also remove inhibitory surfactants, such as lipid digestion products (fatty acids, mono/diglycerides) from the interface *via* competitive displacement mechanism, thus accelerating and enabling continuation of digestion of emulsified lipid droplets (Sarkar et al., 2016e).

Pancreatic lipase is active approx. between pH 5.5 to pH 7.5 and hydrolyses the emulsified lipids producing two FFAs and a 2-monoacylglycerol (Reis et al., 2009, Golding and Wooster, 2010, Wilde and Chu, 2011b). Lipase can only act in the presence of co-lipase and in some cases the presence of co-lipase and bile salts. For lipid hydrolysis to take place, the pancreatic lipase-colipase complex must first adsorb to bile salt-covered interface. Thus, interactions of the adsorbed layer at the droplet surface and lipase are critical in determining the rate of lipid hydrolysis. As lipolysis progresses there is a build-

up of fatty acids and monoglycerides at the emulsion interface, which might displace the adsorbed materials. Noteworthy that these lipid digestion products may be surface active but not essentially colloidal stabilizers. Thus, the emulsions generally suffer from droplet coalescence in case of most surfactant-stabilized emulsions in the intestinal stage (Sarkar et al., 2010c, Singh and Sarkar, 2011a, Golding et al., 2011). Nevertheless, bile salts play a key role here in facilitating the desorption of fatty acids and monoglycerides and their solubilisation into the micellar phase promoting further lipid digestion, and some of the bile salts may remain adsorbed to the surface conferring a high negative charge, thus promoting stability (Sarkar et al., 2010b, Sarkar et al., 2016e)

2.3 Experimental investigations on colloidal digestion of Pickering emulsions

As it is obvious from the biophysical aspects of digestion in human physiology, conventional emulsion droplets prepared using surfactants, such as polysorbates or proteins may eventually shrink as the emulsified lipids in the interior of the droplets undergo easy conversion to FFAs during lipid digestion. Therefore, engineering complex interfacial architecture (*e.g.* interface composition and structural attributes) can be one of the promising solutions to modulate the colloidal aspects of lipid digestion. Indeed, the significant advantage of particle-stabilized emulsions over biopolymers- or other surfactant-stabilized emulsions for altering lipid digestion is their unique resilience against coalescence, dissolution and shrinkage mechanisms (Binks, 2002a, Dickinson, 2017). The mechanism behind such minimal decrease in the volume of the droplets during lipid digestion is the significant energy barrier for particles to detach from the interface offering an almost impossible exchange by the surface active materials in the physiological regimes (*e.g.* bile salts, lipid digestion products). Moreover, the interfacial thickness and surface load are much greater for particle-laden interface offering barrier properties to physiological restructuring in comparison with conventional surfactant-stabilized counterparts (Berton-Carabin and Schroën, 2015).

Questions arise as to what happens to such particles and particle-covered droplets, when they traverse the various stages of the human oral-to-gastrointestinal tract. Of course, the fate of these systems might be affected by interference from the competing biochemical processes, such as breakdown of Pickering layers of intact starch-based particles by α -amylase (Marefati et al., 2017) or protein-based particles by pepsin and/or trypsin (Sarkar et al., 2016d). However, such factors might not affect polysaccharide-based particle- (*e.g.* chitin nanocrystals) (Tzoumaki et al., 2013b), organic crystal- (*e.g.* flavonoids) (Luo et al., 2011) or inorganic particle- covered droplets (*e.g.* silica) (Ruiz-Rodriguez et al., 2014), which are unaffected by gastrointestinal enzymes. This section thus summarizes the key colloidal mechanisms from the experimental investigations of *in vitro* digestion of Pickering emulsions carried out in the last decade (see **Figure 2.2** for the schematic). We have categorised particle-laden interfaces into two discrete classes, namely, ‘human enzyme-unresponsive’ particles *i.e.* the ones that cannot be digested by human enzymes (*e.g.* amylase, protease) and ‘human enzyme-responsive particles’, latter that can be readily digested by human enzymes. Characteristics of the Pickering emulsions and their digestion data are listed in **Table 2.1**.

Table 2.1. Summary of literature reports on Pickering O/W emulsions where *in vitro* lipid digestion kinetics was followed.

Type of particles (<i>E</i> = Human Enzyme responsive, <i>U</i> = Human Enzyme Unresponsive)	Particle Shape & Size Range (d_p = diameter, l_p = length, h_p = height, t = shell thickness)	Emulsion droplet size (μm)	<i>In vitro</i> digestion regimes	Intestinal lipid digestion with kinetic data			Reference
				k	ϕ_{max} (%)	$t_{1/2}$ (min)	
Silica nanoparticles (<i>U</i>)	Spherical, d_p = 50-500 nm	4 – 8	Oral, Intestinal	\approx control	\sim 50%*, <control	-	Ruiz-Rodriguez et al. (2014); Tikekar et al. (2013)
Nanofibrillated cellulose (NFC) (<i>U</i>)	Fibre, d_p = 57 nm l_p = Several μms	9 – 24 μm	Sequential (Oral-Gastric-Intestinal)	7.5-12% FFA/min*, <control	\sim 78-84%*, <control	-	Winuprasith et al. (2018)
Chitin nanocrystal (<i>U</i>)	Rod, d_p = 18 nm l_p = 240 nm	5 – 7 μm	Intestinal	$2.0 \times 10^{-4} \text{ s}^{-1}$, <control	33%, <control	-	Tzoumaki et al. (2011); Tzoumaki et al. (2013b); Tzoumaki et al. (2010)
Chitosan-tripolyphosphate nanoparticles (<i>U</i>)	Spherical, d_p = 214–522 nm	19 – 86 μm	Sequential (Oral-Gastric-Intestinal)	-	33%, <control	-	Shah et al. (2016b); Shah et al. (2016a)
Flavonoid glycosides from	-	1 μm	Intestinal	0.13 $\mu\text{mol s}^{-1} \text{ m}^{-2}$,	33%, <control	9.8, >control	Yang et al. (2014)

<i>Ginkgo biloba</i> extracts (U)				<control			
Starch granules (E)	Polyhedral, $d_p = 1.8 \mu\text{m}$	27 – 32 μm	Oral, Gastric, Intestinal	Relative lipolysis rate: heated < not heated	-	-	Marefati et al. (2017); Rayner et al. (2014); Sjöo et al. (2015)
Starch granules with heat treatment (E)					-	-	
Whey protein microgel particles (WPM) (E)	Spherical, $d_p = 300 \text{ nm}$	43 μm	Sequential (Gastric-Intestinal), Only Intestinal step without proteases**	0.31** $\mu\text{mol s}^{-1} \text{ m}^{-2}$, <control	42%, 20%**, <control	6.6, 16.5**, >control	Sarkar et al. (2016d)
Whey protein microgel particles with heat treatment (HT-WPM) (E)				0.35** $\mu\text{mol s}^{-1} \text{ m}^{-2}$, <control	42%, 16%**, <control	6.6, 44.4** >control	
Lactoferrin nanoparticles (LFnp)	Spherical, $d_p = 200 - 400 \text{ nm}$	1 – 11 μm	Sequential (Oral-Gastric), Intestinal	\approx control	\sim 64%*, \approx control	-	Shimoni et al. (2013); Meshulam and Lesmes (2014a); Peinado et al. (2010b)
Lactoferrin nanoparticles complexed with alginate (LF-ALG) (E/U)		1 – 56 μm		<control	\sim 50%*, <control	-	
Lactoferrin nanoparticles		3 – 9 μm		>control	\sim 70%*, >control	-	

complexed with carrageenan (LF-CAR) (E/U)							
Zein particle shell (E)	Spherical, $t = 1.5 - 4 \mu\text{m}$	30 – 40 μm	Sequential (Gastric-Intestinal I)	<control	~40-100%*, <control	-	Emmanouela et al. (2014)
Zein + tannic acid (E)	-, $d_p = 96 - 203 \text{ nm}$	25 – 45 μm	Sequential (Gastric-Intestinal)	<control	~4-6%*, <control	-	Yuan et al. (2017)
Gliadin + aproanthocynaidins (E)	Spherical, $d_p = 87-290 \text{ nm}$	53-94 μm	Sequential (Gastric-Intestinal)	<control	~40%, <control	~40*, >control	Zhou et al. (2018a)
Kafirin nanoparticles (E)	$d_p = 92 - 434 \text{ nm}$		Gastric, Intestinal	<control	~38%, <control	-13.23***, > control	Xiao et al. (2015a); Xiao et al. (2016b)

- k = rate of lipid digestion, ϕ_{max} = maximum extent of FFA release (observed or theoretical), $t_{1/2}$ = time interval whereby half of the initial concentration of lipids has been converted to FFA (observed or theoretical)
 No data (-), Derived data from the graphs (*), Bypassed proteolysis (**), Indicative

2.3.1 Enzyme-unresponsive particles

2.3.1.1 Silica nanoparticles.

In the case of inorganic particles, silica particles have captured lot of attention not only for stabilize Pickering emulsions (Binks and Lumsdon, 1999) but also for their role in altering the extent of lipid digestion (Ruiz-Rodriguez et al., 2014). Using artificial saliva formulation, Ruiz-Rodriguez *et al.* (2014) showed that Pickering emulsion droplets of mean size of 3-8 μm stabilized by silica nanoparticles (0.5-5 wt%) had an inter-particle (in other words intra-droplet) aggregation at the interface influenced by the charge screening effects of the salivary salts providing enhanced physical stability to the emulsion droplets. This is unlike the inter-droplet aggregation behaviour observed in ionic surfactant- or protein-stabilized emulsions in presence of artificial or real saliva (Silletti et al., 2007, Sarkar et al., 2009a) (**Figure 2.2**).

Interestingly, such silica-stabilized emulsions were stable across the physiological range of pH values from 3.0 to 7.0, which is advantageous over many oral emulsion formulations that suffer from pH-induced gastric instability. Finally, Ruiz-Rodriguez *et al.* (Ruiz-Rodriguez et al., 2014) highlighted that bile salts were unable to displace the practically irreversibly adsorbed silica nanoparticles from the interface, in line with another study on silica-laden interface showing similar results with enhanced curcumin retention (Tikekar et al., 2013). The presence of silica particles at the interface reduced the maximum extent of lipid digestion (ϕ_{max} , %), but interestingly did not affect the initial rate of lipolysis (k , s^{-1}) (Ruiz-Rodriguez et al., 2014) (**Table 2.1**). This might be explained primarily using the size of the gaps (interfacial pores) in the silica particle-laden interfaces. Such gaps can be expected to be sufficiently large to allow the diffusion of angstrom-sized lipase/bile salts complex to the surface to allow instantaneous onset of digestion, but small enough to allow the migration of the FFAs generated during lipid digestion into the continuous phase. In addition, one might recognize that for Pickering emulsions, there is ideally no shrinkage of droplets, so the volume of droplets should not alter and a large portion of FFA produced must remain within the droplets. Hence, one might consider not only measuring FFAs using ‘gold-standard’ titrimetric techniques that measures FFA only after it is released in the continuous phase but also

consider measuring the undigested triglycerides together with other digestion products that might have been retained within the dispersed phase or still somehow anchored to the adsorbed phase.

2.3.1.2 Polysaccharide-based particles.

Besides inorganic particles, biodegradable polysaccharide-based particles, such as cellulose nanocrystals (CNC) or nanofibrillated cellulose (NFC) (Sarkar et al., 2018b, Sarkar et al., 2017b, Winuprasith et al., 2018, Scheuble et al., 2014a) and chitin nanocrystals (CN) (Tzoumaki et al., 2013b) have been recognized among the most opportune materials as they are not digested by human gastrointestinal enzymes yet are biodegradable. Both cellulose and chitin obtained from plant cell walls and animal sources (sea food wastes), respectively, are essentially naturally-abundant polysaccharides with semi-crystalline architecture containing alternate nanocrystalline and amorphous domains (Salas et al., 2014, Duan et al., 2018, Ling et al., 2018). Strong acid hydrolysis can remove the amorphous domains leading to the formation of stiff rod-shaped nanocrystals of high aspect ratio (typically 5–50 nm in width and between 100 nm to several micrometers in lengths). Another favorable aspect of using these nanocrystals at the O/W interface is that these anisotropic particles pack in a more ordered fashion but inhomogeneously (Lou et al., 2016), thus, providing improved steric hindrance and mechanical strengths at the interface even at lower particle loadings, and thus can bring advantage over spherical particles in modulating lipid digestion.

One of the earliest studies in the field of digestion of Pickering emulsion was conducted by Tzoumaki *et al.* (2013b) where authors compared the digestibility of Pickering O/W emulsions stabilized by CN with that of the conventional emulsions stabilized by milk proteins. Interestingly, CN at interface not only decreased the extent of lipid digestion (φ_{max} , %) by two-folds to 33% FFA release (**Table 2.1**), as compared to that stabilized by milk proteins, but also significantly reduced the initial rate of digestion (k , s⁻¹). This distinctive reduction in rate of digestion was also shown in studies using NFC (Winuprasith et al., 2018), which is unlike the behaviour that was observed in the spherical silica-laden interface as discussed previously (Ruiz-Rodriguez et al., 2014).

In addition to the irreversible adsorption of these rod-shaped particles at the interface and inability to be desorbed by bile salts/ lipid digestion products, two other mechanisms (Tzoumaki et al., 2013b, Winuprasith et al., 2018, Sarkar et al., 2018b, Tzoumaki et al., 2010) were proposed for this delay in lipid digestion (**Figure 2.2**) - 1) the rod shaped particles formed a rigid inter-particle (*i.e.* intra-droplet) network at the oil–water interface providing a strong mechanical barrier of considerable interfacial viscosity around the droplets, 2) the rod shaped particles underwent isotropic to nematic phase transition forming highly ordered and densely packed network structures in the *aqueous phase*, which might have mechanically entrapped the emulsion droplets and decreased their access to bile salts or lipase. Mechanism 1) is largely associated with packing of rods that can be much more efficient than that of spheres at the interface. Mechanism 2) is similar to trapping emulsion droplets in a gel-like network to create a tortuous path for lipase/colipase complex to reach the hydrophobic lipid core (Sarkar et al., 2015a, Guo et al., 2017a), which is achieved in these CN and CNC particle-laden interfaces without using an additional gelling agent. This highlights that particles can have interesting interfacial as well as bulk rheology that can be carefully engineered to tailor lipid digestion kinetics and develop controlled delivery applications. For instance, Pickering emulsions stabilized by chitosan tripolyphosphate nanoparticles that are engineered *via* ionic gelation technique with lower extent of FFA release have been applied to enhance bioaccessibility of encapsulated bioactive molecules, such as curcumin as compared to nanoemulsion counterparts (Shah et al., 2016b, Shah et al., 2016a).

2.3.1.3 Flavonoid crystals

Another important class of organic particles from biological origin that have been investigated in literature are flavonoid crystals, which are secondary metabolites from plants. Flavonoids, such as tiliroside, rutin and naringin have shown tendency to absorb at oil-water interface (Luo et al., 2011, Duffus et al., 2016). In fact, there has been only one study on flavonoid particles from *Ginkgo biloba* extract that has investigated *in vitro* lipid digestion profile. Yang *et al.* (2014) demonstrated that such particles behaved as Pickering stabilizers,

however the size and shape of the particles were not mentioned. Such particles reduced both the rate ($k = 0.13 \mu\text{mol s}^{-1} \text{m}^{-2}$) and extent of FFA release ($\varphi_{max} \sim 24\%$) (**Table 2.1**) from the flavonoid covered-lipid droplets by nearly two- and four-folds, respectively, as compared to a surfactant-stabilized emulsion.

2.3.2 Enzyme-responsive particles

Assiduous research have been devoted to the lipid digestion of Pickering emulsions using digestive particles (**Table 2.1**). These particles include starch granules and nanoparticles with or without hydrophobic modification with octenyl succinic anhydride (OSA) and a range of protein particles from animal (whey protein microgel, lactoferrin nanoparticles) sources and more recently plant (karifin nanoparticles, zein protein particles, pea protein microgel particles). Such digestible particles have been widely used in scientific investigation for lipid digestion as they are not only safe in theory as they are digestible by human gastrointestinal enzymes but also perceived as relatively more natural, “clean label” and “green” (Rayner et al., 2014).

2.3.2.1 Starch particle

Native starch granule is semi-crystalline (Zobel, 1988, Borah et al., 2018) and second-most abundant particle after cellulose. The forms of starch used for making Pickering emulsion in literature has ranged across length scales from native to OSA-modified relatively starch granules of mean diameter of 1-50 μm (Rayner et al., 2012, Li et al., 2013, Timgren et al., 2011) to starch nanoparticles and nanocrystals of mean diameter of few nanometers that have been engineered physically or chemically (Yang et al., 2018, Lu et al., 2018, Ge et al., 2017). Although overwhelming amount of research has been done on starch particle-laden interface, investigations are relatively scarce when dealing with lipid digestion of such droplets.

In fact, only two systematic studies from the Swedish research group (Marefati et al., 2017, Sjöo et al., 2015) demonstrated lipid digestion behaviour of emulsions stabilized by hydrophobically modified quinoa starch granules (Marefati et al., 2017). Marefati *et al.* (2017) demonstrated that amolytic digestion in oral phase by α -amylase resulted in significant size reduction of the

emulsion droplets and release of some free starch particles. However, a major proportion of the modified starch granule-coated droplets still retained their integrity and were resilient to coalescence even after 60 min of salivary exposure, unlike the conventional emulsions stabilized by OSA-modified starch, where the latter underwent dramatic coalescence within seconds (Dresselhuis et al., 2008b, Torres et al., 2018). The gastric digestion had no effect on these Pickering emulsions as it can be expected owing to lack of any amylolysis. Interesting conclusions were highlighted about the lipid digestion profile in the intestinal phase (Marefati et al., 2017). Although the starch granules were not likely to be displaced by bile salts, the gaps between these micron-sized starch granules at the interface allowed rather easy accessibility of bile salts and lipolytic enzymes to the interface in the particle-free area, leading to droplet coalescence.

2.3.2.2 Protein particles from animal sources.

The acceptability of animal proteins and versatility to create microgel, nanogel or nanoparticles using their heat-sensitivity (*e.g.* whey protein, lactoferrin) (Sarkar et al., 2016d, Shimoni et al., 2013, Destribats et al., 2014a) have enabled creation of laboratory synthesized particle of tuneable size to create Pickering emulsions. The distinctive feature of using protein-based particle is that they can offer both electrostatic stabilization and steric hindrance when present as Pickering layers as opposed to starch granules, in latter, the droplets are only sterically stabilized unless modified.

Work carried in our laboratory (Sarkar et al., 2016d) has demonstrated interesting gastric and intestinal digestion profile of emulsion droplets (mean diameter of 43 μm) stabilized using negatively-charged spherical whey protein microgel particles (WPM, 300 nm). These particles were created using a top-down approach of breaking a 10 wt% whey protein gel in a jet homogenizer as opposed to the bottom up approach used previously (Destribats et al., 2014a). The Pickering emulsions stabilized by WPM showed interesting resilience to gastric coalescence unlike conventional whey protein-stabilized emulsions (Sarkar et al., 2009b), where dramatic increase in the droplet size has been

reported due to pepsin-induced rupture of the interfacial protein layer. Looking at confocal microstructure and polyacryl amide gel electrogram of the protein bands from the adsorbed phase of the Pickering layer of WPM, it was concluded that pepsin was not able to fully access some of the hydrophobic sites due to the reburial of those domains within the microgel particles. Noteworthy is that the interfacial loading ($\sim 14 \text{ mg m}^{-2}$) was nearly 12-fold higher than a whey protein monolayer at the interface indicating a substantial increase in substrate required to be digested by pepsin (Destribats et al., 2014a) (**Figure 2.2**). Such interesting gastric stability of protein particle versus protein monolayer was also demonstrated in our laboratory also using lactoferrin nanogel particles (Sarkar et al., 2018a), which was further enhanced when electrostatically complexed with another enzyme-unresponsive polysaccharide particle (inulin nanoparticles). Similar results were obtained by Shimoni *et al.* (2013), where kinetic stability to gastric coalescence was imparted when lactoferrin nanoparticles were complexed with polysaccharide, such as alginate and carrageenan.

In the intestinal phase, there was stark difference in the digestion profile of protein microgel particle-stabilized interface if the digestion was sequential versus if only bile salts-lipase-catalysed (without any protease) scenario was considered. For instance, if it was a sequential gastric and intestinal digestion (Destribats et al., 2014a), presence of WPM particles versus whey protein monolayer at the interface did not affect the rate or extent of fatty acid release as it was a proteolysis-dominated lipid digestion phenomenon. Similar results were obtained using lactoferrin nanoparticle-laden interface that the extent or rate of FFA release was similar to that of a lactoferrin monolayer at droplet surface (Meshulam and Lesmes, 2014a), which might be associated with the proteolytic effect of the pancreatic lipase used that might have contained proteolytic enzyme residues.

To understand this better, we carried out lipid digestion investigations with WPM-laden interface in our laboratory using pure lipase and bile salts without any of the proteolysis that normally occurs during the gastric or intestinal digestion stage (Destribats et al., 2014a). The extent of FFA release was reduced by two folds (20%) and initial rate of digestion was diminished

(**Table 2.1**) when exposed to just pure lipase as opposed to proteolytic-lipolytic mixture. This suggests the inability of bile salts to displace the intact non-proteolysed WPM from the interface. In other words, a large portion of the surface was not available for the adsorption of the lipase/colipase complex. This reduced the overall rate of FFA generation. However, it is noteworthy that the Pickering layer of particles was not impervious but rather semipermeable. Bile salts and lipase being small molecules could access the interface through the gaps in the microgel-stabilized interface, similar to that discussed in starch granule-stabilized interface (Marefati et al., 2017), but bile salts could not displace the microgel particles, due to the very strong binding of the WPM to the interface.

2.3.2.3 Protein particles from plant sources.

There is burgeoning research interest in designing biocompatible particles derived from plant proteins due to their limited contribution to environmental footprints as compared to the counterparts derived from animal proteins. Filippidi *et al.* (2014) took the advantage of water insolubility and slow protease-induced digestibility of zein particles (a prolamin rich protein from corn) to create Pickering emulsions. As discussed in the WPM digestion study (Destribats et al., 2014a), the rate-limiting step was again the full or partial hydrolysis of zein particles by gastric/ intestinal proteases, which eventually allowed access of the lipase to the inner lipid core. However, intelligent design of the zein-particulate shell created by solvent precipitation to a greater thickness (4 μm versus 1.5 μm in the thinner layer) slowed the rate and extent of digestion remarkably (Emmanouela et al., 2014). Another study highlighted that creating particles using zein hydrogen bonded with tannic acid can be an alternative approach to provide protection to Pickering emulsion droplets against a harsh gastric environment (Yuan et al., 2017), facilitating to slow down the release of FFA during *in vitro* intestinal digestion. Similar Pickering layer approach has been also used using gliadin, another (prolamine-rich protein) precipitated with a flavonoid (proanthocyanidins) to create particles that was successful to reduce FFA release extent ($\varphi_{max} \sim 40\%$) (Zhou et al., 2018a) (**Table 2.1**).

Interestingly, the gastric instability of the plant protein particles was also observed in Pickering emulsions stabilized by karifin particles (Xiao et al., 2015a, Xiao et al., 2016b) (**Figure 2.2**), another water-insoluble prolamin protein derived from sorghum. In fact the oil droplets lost their integrity at the end of simulated gastric digestion resulting in macroscopic phase separation as the particle-laden interface was readily pepsinolysed. However, to investigate the possible effect of the kafirin particle layer on lipolysis of emulsified oil droplets, the karifin particle-stabilized emulsions were subjected to intestinal digestion bypassing the gastric regime. As expected, karifin-stabilized droplets showed three-fold slower FFA release kinetics and extent of FFA release ($\varphi_{max} \sim 40\%$) (**Table 2.1**) as compared to the surfactant counterpart.

Work on Pickering stabilized emulsions created using pea protein nanoparticle aggregates at pH 3 (Shao and Tang, 2016a) and heated soy glycinin particles (Liu and Tang, 2016a) have also shown enhanced protection for delivery of a bioactive (β -carotene). However, careful attention needs to be provided in these studies as the reduced extent of lipid digestion and bioactive release was associated with rheological properties of the gel-like emulsion driven by volume fraction of the droplets rather than interfacial architecture of the particles.

2.4 Future interfacial design strategies to control digestion profiles

Particle-laden interface offer new opportunities to control digestion profile in addition to the obvious energy barrier-associated mechanism *i.e.* almost irreversibly anchored particles are unable to be desorbed by bile salts and other lipid digestion metabolites. We now propose a list of design strategies that can be used to manipulate interfacial architecture and composition of particles to enable them to act as transient or complete mechanical barrier to the diffusion of lipases in both gastric and intestinal phases.

2.4.1 Particle to droplet size ratio

Particle size of the Pickering stabilizer plays a determinant role in decide the

fate of the lipid digestion kinetics. According to equation (2.2), the detachment energy for particles is proportional to the square of the radius of the particle. Thus, the larger the size of the particle, the higher the thermal energy required to dislodge them from the interface. However, one has to be careful about the role of gravitational force versus thermal energy in such a scenario. The ratio of gravity forces to surface tension forces for a particle adsorbed at an interface is represented by Bond number as shown in equation (2.4):

$$B_o = \frac{(\rho_p - \rho_c)gd_p^2}{\gamma_{ow}} \quad (2.4)$$

where, ρ_p and ρ_c are the densities of the particle and the continuous phase, respectively, d_p is the average diameter of the particle, γ_{ow} is the surface tension and g is acceleration due to gravity. So, it is only for particle with $B_o \ll 1$, surface-tension forces tends to dominate (Tavacoli et al., 2012). Furthermore, if the particles are too small, eventually the desorption energy required to dislodge the particles will be low, specifically in presence of the bile salts, where γ_{ow} is small. Thus, use of particle-laden interface might not be beneficial in such a case.

Also, it is worth to remind that mostly particle-laden interfaces are generally far from possessing a complete monolayer at the interface and even if the Pickering layer is complete, inter-particle gaps remain. These gaps will tend to allow the passage of the lipase-colipase/ bile salts to the bare interfaces, as discussed previously. For instance, for an idealized case of monodispersed spherical particles, the highest surface coverage is achieved when particles on the droplet surface are arranged on a regular 2D triangular lattice. In such a scenario, the typical dimensions of the gaps between the particles will be $(\sqrt{3} - 1)d_p/2 \cong 37 \text{ nm}$ for particles of size $d_p = 100 \text{ nm}$. This is nearly fifteen-folds higher than the typical dimension of lipase/colipase complex and thus may not have a substantial impact on creating a barrier against the diffusion of lipolytic catalysts to the droplet interface (Sarkar et al., 2016d). Even though the enzymes and bile will be able to access the droplet surface through the gaps

between the particles, the available amount of interface can be envisaged to be significantly reduced by the presence of the particles, hence limiting the rate of lipolysis.

It is noteworthy that size of particles also determine the size of the emulsion droplets and that the particles are significantly smaller than the targeted emulsion droplet size (at least one-to-two orders of magnitude). Thus, lipid digestion kinetics largely depends on the available surface area of the droplets. For example, emulsions with smaller droplet size will present a larger surface area and therefore a greater number of anchoring sites for lipase. Consequently, to reduce the rate and extent of lipolysis, a coarser emulsion with larger droplet size and lower surface area may be preferable. The alternative to reduce these interstitial spaces will be to employ “polydispersity” of size distribution as a tool to increase surface packing. Although colloid scientists have attempted to create monodisperse particles and eventually monodisperse droplets, polydispersity of particles can be an elegant technique to reduce inter-particle spaces and thus lipid digestion rate, provided such polydispersity is well-controlled. Therefore, there exists a delicate compromise for determining the particles of optimum size distribution to achieve the ideal energy barrier, gap dimension and consequently the droplet size. Ultimately, this may govern the rate of diffusion of lipase and surface area available for lipolysis. Finally, it is worth mentioning that it is always important to provide the FFA release data with the droplet size so that a comparison can be made with the literature, as Pickering emulsion droplets are generally larger in size as compared to surfactant-stabilized emulsions. So, it is important to understand whether the reduction in lipolysis kinetics is linked to the size of the droplets or interfacial architecture created by the Pickering layer of particles.

2.4.2 Particle charge

Adsorbed charged particles can be useful to provide electrostatic repulsion between the oil droplets of an o/w emulsion in a similar fashion as ionic emulsifiers. Moreover, they may also help to create an electrostatic barrier to the possible approach of negatively-charged bile salts to the vicinity of a

negatively-charged particle-laden interface. However, with increasing magnitude of charge of the particles, there will be a corresponding increase in the interstitial separation due to particle-particle electrostatic repulsion at the interface. Such an approach can be useful to create a porous membrane at the interface in order to accelerate digestion or enhance release of digestion products. However, if the objective is to slow down digestion, one might attempt to increase the salinity of the system to screen the charge so that the particles aggregate at the interface and provide the interfacial barrier effects to lipolysis as was observed in silica-nanoparticle-stabilized interfaces (Meshulam and Lesmes, 2014a).

2.4.3 Particle fusion at interface

One of the approaches that has been used to reduce this empty spaces at the interface has been “interfacial particle fusion” *i.e.* sintering of particles once they have been already adsorbed (**Figure 2.3a**). This helps to take the advantage of the energy barrier of the particles combined with a mechanical barrier effect of a cohesive “single” bulky layer. Interestingly, physical treatments, such as use of heat, has been shown to fuse the particles once they are already absorbed in the interfaces. This approach has been used in two independent studies using starch granules (Sjöö et al., 2015, Rayner et al., 2014) (**Figure 2.3b**) and whey protein microgels (Sarkar et al., 2016d) (**Figure 2.3c**) and has shown dramatic effects on improving the barrier property and delay in FFA release. Since the gaps are expected to be significantly smaller due to this particle fusion, the approach impedes all aspects of the process *i.e.* the diffusion of lipolysis-limiting digestion products, such as FFA away from the reaction sites, as well as that of the lipase/colipase-bile salt complex to the surface. Such fusion can also be brought about using pH shifts, using mono- and divalent ions and/or enzymatic crosslinking, depending upon the responsiveness of the particles to these aspects. A study of such aspects will demand future research work.

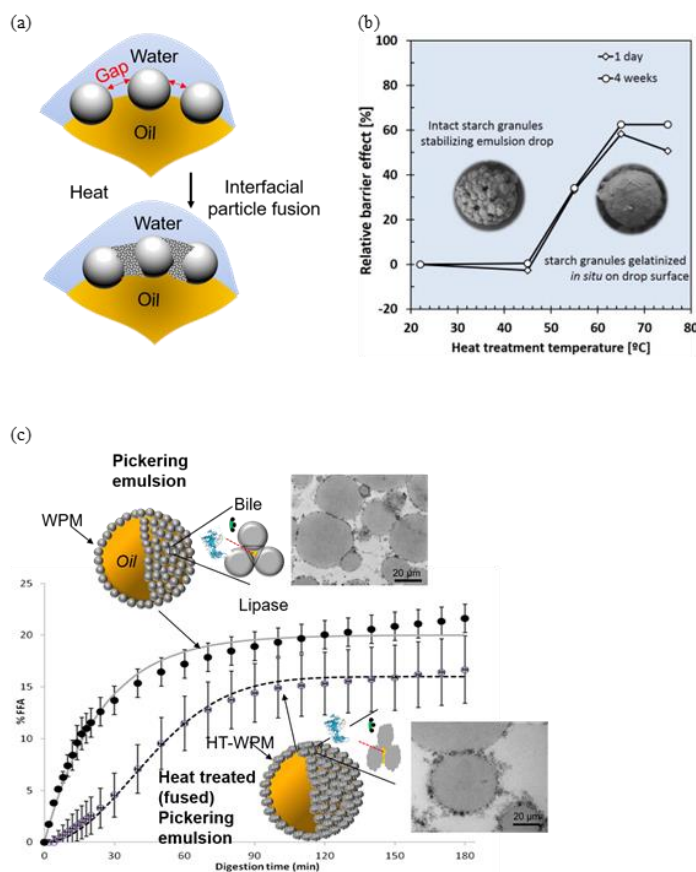


Figure 2.3. Schematic showing particle fusion at the O/W interface by heat treatment, (a) with examples of relative barrier properties in modified starch-stabilized interface as a function of heat treatment (Reprinted with permission from Yang et al. (2014) and Ge et al. (2017)), (b) and release of FFA in whey protein-microgel (WPM)-stabilized interface with/ without heat treatment (HT-WPM) as a function of duodenal digestion time (image redrawn with permission from Sarkar et al. (2016d)) (c). Insets in (b): (left) is a non-heat treated quinoa starch granule-stabilized droplet and (right) a heat treated droplet illustrating the creation of a partially gelatinized starch layer. Insets in (c): (left) is WPM-stabilized droplet with corresponding transmission electron micrograph (gray solid line – theoretical fit, solid circle – observed value) and (right) is Heat treated droplet (HT-WPM) with corresponding transmission electron micrograph (black dashed line, empty circle – observed value).

2.4.4 Particle shape

As expected, the “spherical” particles have primarily been investigated to create Pickering emulsions from inorganic silica nanoparticles to bio-derived protein microgels. However, the influence of particle shape on interfacial packing and emulsion stability has attracted relatively little research attention. The non-spherical particles, such as rods, cubes, peanut-shaped particles (**Figure 2.4**)

tend to have more positive effects on the emulsion stability *via* differences in packaging density (de Folter et al., 2014b, Kalashnikova et al., 2011). Even at a lower concentration, particles with higher aspect ratio, such as rod- and peanut-shaped particles can improve the interfacial loading tremendously by creating interfacial stacking, leading to some sort of interlocking structure at the interface. This is demonstrated by hermatite particles (de Folter et al., 2014b) and CNC particles (Kalashnikova et al., 2011) in **Figure 2.4**. For instance, Capron et al. (2013) created stable o/w emulsions using <0.1 wt% of CNC, as a result of the entanglements between the CNCs. Recently, lipid digestion work using rod-shaped cellulose nanocrystals either at the surface or as a barrier layer are showing interesting lipid digestion outcomes, as discussed previously (Sarkar et al., 2018b, Winuprasith et al., 2018, Sarkar et al., 2017b). In fact, now the time seems ripe for colloid scientists to explore bio-derived anisotropic shaped particles, considering biocompatible processing routes to create such particles and models to understand their emulsion stability during lipid digestion. Such particles may help to control lipid digestion rate by particle networking attributes, not only at the interface but also in the bulk phase as shown in **Figure 2.2** (Tzoumaki et al., 2013b).

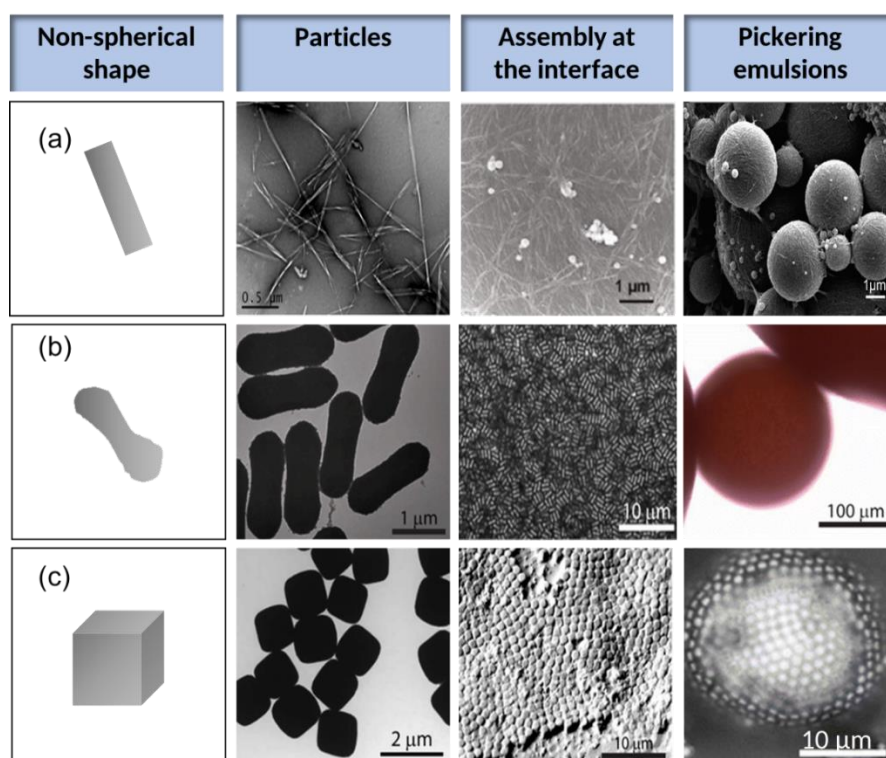


Figure 2.4. Examples of anisotropic particles, rod-shaped (a), peanut shaped (b) and cubic-shaped (c) with schematic, electron micrograph of the particles,

arrangement of the particles at the interface and microstructure of the Pickering emulsion droplets stabilized by the respective anisotropic particles. Microscopic images of peanut- and cube-shaped particles and corresponding emulsion droplets are reprinted with permission from Tavecchi et al. (2012) and those of rod-shaped particles are reprinted with permission from de Folter et al. (2014b).

2.4.5 Particle loading at the interface

Under given emulsification conditions, the initial particle loading can influence the interfacial packing behaviour and structure, furthermore affecting the average droplet size and emulsion stability. Once close-packing is established, the loading ceases to have an effect. For classical emulsions stabilized by surfactants, the average droplet size reduces with increasing surfactant concentration until reaching a critical concentration point and then droplet size reaches a plateau (Aveyard et al., 2003a). The decreasing trend of droplets size relates to the process that larger droplets breakdown into smaller droplets creating more surfaces due to the reduction of interfacial tension. Pickering emulsions also follow a similar trend in a classical emulsion (Jie and Guang-Hui, 2016).

Chevalier et al. (2013) summarized the three stages of Pickering emulsion formation based on the ratio between solid particles (M_p) and the oil mass (M_o). At the low concentration, coalescence occurs due to insufficient quantity of solid particles to cover the droplets. As the solid particles concentration increases, the larger droplets are broken into smaller droplets, leading to a reduction in average droplet diameter (D_o) as shown in equation (2.5):

$$D_o = \frac{6}{\rho_o a_s} \frac{M_o}{M_p} \quad (2.5)$$

where, ρ_o is the density of oil and a_s is the interfacial area covered by the solid particles. In the final stage, the average droplet size reaches a steady state where a complete saturation is achieved. With a high particle concentration, the excess

solid particles create either a multilayer or do not get absorbed to the interface and remain dispersed in the continuous phase. With fewer particles, a typical interfacial structure can be a single bridging layer stabilizing the interface between two droplets (French et al., 2015). Such bridged network can be actually useful to create a network and reduce the surface available for lipase to bind. Note that for incorrectly chosen contact angles, such bridging might instead cause coalescence of droplets. Another option can be to increase the mechanical barrier of the interface by creating a multilayered particle architecture (Brunier et al., 2016) and eventually increase the adsorbed particle loading. If carefully controlled, such multilayers of Pickering particles can help to form a tortuous path for the diffusion of bile salts and lipases' ability to anchor to the interface and thus control the kinetics of lipid digestion.

2.4.6 Material chemistry of particle

Of course, the material of the particles has a crucial role in determining their fate during the sequential lipid digestion. In mind of the previous discussion, it is clear that human enzyme-responsive particles, such as unmodified protein-based or starch-based particles might not be suitable to delay lipolysis if sequential three-phase digestion is considered. As the particles are significantly influenced by biochemical interferences due to their responsiveness to physiological enzymes, they lose their particulate integrity before and during the lipolysis step. Hence, enzyme-responsive particle-stabilized emulsions can only offer altered digestion profile if they are administered specifically at the site rather than typical oral administration routes. One way to avoid this is to modify the interfacial thickness of the particles by precipitation techniques (de Folter et al., 2012) or protect the droplets from instantaneous digestion by changing the particle material chemistry. Such modifications in particle chemistry can be obtained by complexation with human enzyme-unresponsive polysaccharides, such as alginate (Meshulam and Lesmes, 2014a, Liang et al., 2016, Peinado et al., 2010b), or tannic acid/ flavonoids (Yuan et al., 2017, Zhou et al., 2018a) or binding with or another layer of enzyme-unresponsive particles, such as inulin (Sarkar et al., 2018a).

Interestingly, from an environmental viewpoint plant proteins are preferred choice for creating emulsifiers. In fact most plant proteins have limited aqueous solubility (Sarkar et al., 2016a, Sarkar and Kaul, 2014, Adal et al., 2017, Laguna et al., 2017a) and are less digestible as compared to animal proteins (de Folter et al., 2012, Laguna et al., 2017a), which restricts their use as classical biopolymeric surfactants. This offers a great window of opportunity for colloid scientists to utilize plant protein aggregates or synthesize particles derived from plant proteins for altering lipid digestion profile. This has indeed started to capture attention of researchers relatively recently. Other opportunities include hydrophobic modification of enzyme-unresponsive polysaccharide particles for tailoring lipid digestion, though careful attention needs to be taken to allow compliance as being “safe” and also “clean-label”, if food application is the ultimate goal.

2.5 Mathematical models for lipid digestion kinetics

In this section, we shift our focus from experimental investigations to review theoretical models which is crucial to quantify lipid digestion kinetics and understand mathematically the similarities and dissimilarities of Pickering emulsions versus a classical surfactant stabilized emulsions. Typically, the pH-stat method is used to monitor the concentrations of FFAs released during the lipid digestion upon introduction of lipase at neutral pH levels. Experimental procedures may commit emulsions to simulated digestion processes by initial incubation in simulated gastric fluid (SGF) and then subsequently in simulated intestinal fluid (SIF). Monitoring and control of changes in pH permit quantification of the concentration of FFA generated during digestion of the emulsified lipids. The percentage of FFA released may be calculated from the number of moles of a base *e.g.* NaOH required to neutralize the FFA that could be produced from the triacylglycerols present in the lipid under the assumption that 2 FFAs per triacylglycerol molecules are generated as can be seen in equation (2.6) (Li and McClements, 2010a, Sarkar et al., 2016e):

$$\%FFAs = \frac{V_{Base} \times M_{Base} \times M_w}{2W_w} \quad (2.6)$$

where, V_{Base} is the volume (mL) and M_{Base} the molarity (M) of the base respectively, M_w is the average molecular weight of the lipid (kg mol^{-1}) and W_w is the initial weight of the lipid (g). We denote the fraction of converted lipid in the emulsion at time t by $\alpha(t)$, which is equivalent to the fatty acid released $\varphi(t)/\varphi_{max}$ where φ_{max} is the maximum fatty acid level attained after digestion.

A major consideration in developing models to capture possible delays in digestion of emulsion droplets is to correctly account for the kinetics of arrival and adsorption of enzymes onto their surface. This is particularly important given that much of the discussion above concerns development of suitable means of slowing down such adsorption process. It is reasonable to assume that at any time t , the reaction rate will be a first order one varying linearly as the fraction of unconverted oil in a droplet, namely $(1-\alpha(t))$. This situation is true for relatively small droplets one encounters in most practical emulsion systems. For these, the composition of the droplet remains homogenous throughout, as would be the case if there is rapid diffusion of unconverted/converted oil between the surface and interior of the droplet (*i.e.* concentration gradients within the fine droplets remain small). Furthermore, since such reactions only occur at the surface of the droplets where the lipase is adsorbed, the reaction rate is expected to be proportional to the coverage of surface by enzyme at any given time t , *i.e.* $\Gamma(t)$. Accordingly, sub-maximal conversion rate constant (per unit area) at time t may be expressed as:

$$\frac{\Gamma(t)}{\Gamma^{Max}} k \quad (2.7)$$

where it is assumed that the surface coverage achieves a maximum of Γ^{Max} , whereupon the lipid conversion rate constant also achieves its

maximum value. Here, k ($\text{mol s}^{-1} \text{m}^{-2}$) is defined as lipid conversion rate per unit area of the droplet surface, occurring at maximum lipase surface coverage. In its simplest form, we may expect the value of k to be proportional to the exposed part of the surface, namely $k = k_0(1 - S_p)$. Here, S_p is the fraction of the surface covered by the particles and k_0 represents the rate of hydrolysis per unit area if all the surface of the droplets was available for adsorption by lipase. The value of S_p itself is a sensitive function of the degree of polydispersity, the shape of the particles, the contact angle at surface and any possible inter-particle interactions. This makes it rather difficult to calculate S_p for a general case. However, for some specific ideal situations, a value may be given. For examples, if the particles were monodispersed hard spheres, then at maximum packing, obtained for a regular 2D triangular lattice arrangement (see section **2.4.1**), the value of $S_p \approx 0.9$ if the contact angle is 90° , and ≈ 0.45 when it is 45° (Sarkar et al., 2016d). Typically estimates for Γ^{Max} coverage can be calculated for the lipase-colipase complex using the molecular radius of gyration (*e.g.* 25\AA providing an estimate of $2.66 \times 10^{-7} \text{ moles m}^{-2}$) (Pignol et al., 2000). Thus, for a droplet of size d_0

$$\frac{\pi d_0^3}{6} \frac{\rho_0}{M_w} \frac{d\alpha}{dt} = \frac{\Gamma(t)}{\Gamma^{Max}} k \pi d_0^2 (1 - \alpha) \quad (2.8)$$

where πd_0^2 is the surface area of the droplet and M_w the molar weight of the lipid molecules. The general formal solution to the above equation is

$$\alpha(t) = 1 - \exp\left(-\frac{6M_w}{d_0\rho_0} \frac{k}{\Gamma^{max}} \int_0^t \Gamma(t') dt'\right) \quad (2.9)$$

Different more specific forms of equation (2.9) now emerge depending on how $\Gamma(t)$ varies with time. Historically, to gain insight into the dynamics of lipid digestion, a first order rate kinetics model was initially introduced by Ye *et al.* (2013). This early model amounts to assuming that the adsorption kinetics of lipase onto the droplet surface is very rapid. In such a case the full lipase coverage is achieved almost immediately and $\Gamma(t) \sim$

Γ^{Max} from the onset. This situation would be appropriate for Pickering type emulsions, since the gaps between the adsorbed particles on the interfacial surface are sufficiently large to allow unhindered access of the lipase (Sarkar et al., 2016d), given that the radius of gyration of the pancreatic lipase/co-lipase complex is approximately 25 Å (Pignol et al., 2000). Similarly, the long-time behaviour of any adsorption model, once full coverage has been achieved past a reasonable period of time, increasingly approaches that predicted by the model of Ye *et al.* (2013). With $\Gamma(t)$ set to Γ^{Max} throughout the digestion process, equation (2.9) simplifies to (2.10) below:

$$\varphi(t) = \varphi_{Max}(1 - \exp(-k_1 t)) \quad (2.10)$$

Here, k_1 (s^{-1}) is the rate of first order kinetics and t is the digestion time (s) in Ye *et al.* model and can be related to parameters of the more general model according to $k_1 = 6M_w k / (d_0 \rho_0)$. This model has successfully been used by the same authors to explain the effect of calcium concentration in promoting lipase adsorption at the interfacial surface. The model has also proved useful in interpretation of experimental data, allowing an understanding of differences in reaction rates of emulsions stabilized by different interfacial materials (*e.g.* bile salts, protein, protein-particle composites) (Sarkar et al., 2016e, Sarkar et al., 2018b) to be achieved.

When the dynamics of enzyme adsorption process is not sufficiently fast, it becomes important to take the variation of $\Gamma(t)$ with time into account. If arrival of the lipase to the interface is the limiting factor in determining the rate of adsorption to the surface, then for such a diffusion-limited process, $\Gamma(t) \approx [(2Dt/d_0) + 2(Dt/\square)^{1/2}]n$ in the early stages of adsorption, where D denotes the diffusion coefficient of the enzyme (typically $10^{-9} - 10^{-10} \text{ m}^2 \text{ s}^{-1}$) in the continuous aqueous phase and n is their molar concentration in the bulk solution. Substituting this form of $\Gamma(t)$ in equation (2.9) gives:

$$\alpha(t) = \frac{\varphi(t)}{\varphi_{Max}} = \left[1 - \exp \left(\frac{-6kM_w}{\rho_0 d_0^2 \Gamma^{Max}} \left(Dt^2 + \frac{4d_0\sqrt{D}}{3\sqrt{\pi}} t^{3/2} \right) \right) \right] \quad (2.11)$$

The second term in the above exponential becomes much smaller than the first one for time periods $t \gg d_0^2/D$. For typical values of D and emulsion drops of size say $10 \mu\text{m}$, this occurs very early on, $t \sim 0.1$ to 1s . Thus, while still in rather early stages of digestion, equation (2.11) can be further approximated to

$$\alpha(t) = \frac{\varphi(t)}{\varphi_{Max}} = \left(1 - \exp \left(\frac{-6kM_w D n t^2}{\rho_0 d_0^2 \Gamma^{Max}} \right) \right) \quad (2.12)$$

Equation (2.12) has a more convenient form for fitting to experimental data. The half-life ($t_{1/2}$) *i.e.* the time interval whereby half of the initial amount of lipids has been converted to FFA, for each of the two cases discussed above can be obtained by setting $\alpha(t)=1/2$ in equations (2.10) or (2.12). This yields

$$t_{\frac{1}{2}} = \left(\ln(2) \frac{d_0^2 \rho_0 \Gamma^{Max}}{6k D n M_w} \right)^{\frac{1}{2}} \quad (2.73)$$

$$t_{1/2} = \ln(2) \frac{d_0 \rho_0}{6k M_w} \quad (2.14)$$

Utilising the parameters k and half-life ($t_{1/2}$) provide valuable information with which to compare the digestion profiles of different emulsion samples. For example, Sarkar *et al.* (2016d) successfully used the above models to understand the differences in the digestion behaviour of Pickering type emulsions, stabilized by whey protein microgel particles, before and after their heat treatment. An interesting prediction of equation (2.12) is a rather slow start to hydrolysis and an initial ‘‘convex shaped’’

curve (**Figure 3c**) for the variation of amount of converted lipid with time. Though regularly seen in experiments, prior to the work of Sarkar *et al.* (2016d), this feature was not fully appreciated and had often been ignored during the fitting of the data.

The linear variation of the coverage of interface by lipase with time, can also be applied to analyse the early stages of digestion in systems where the adsorption is barrier limited. For these

$$\Gamma(t) \cong \lambda nt \tag{2.13}$$

where instead of $\lambda = 2D/d_0$ as for the diffusion limited case, now the value of λ depends on the thickness, the material and porosity of the barrier layer formed around the droplets. Once again it should be noted that equation (2.13) applies to time frame where the surface of droplets are only scarcely covered and as yet far from reaching their maximum saturation by bile salt/lipase. There are many models for the variation of $\Gamma(t)$, encompassing the entire adsorption period for the barrier limited situation. However, the usefulness of these in the context of digestion of lipid emulsions is as yet to be fully established. Therefore, for now at least, we refrain from discussing these type of models in any greater detail, leaving such discussion to possible future reviews.

The models discussed thus far all assume emulsion droplets that more or less maintain their original size, as lipid is converted to FFA. This is a reasonable assumption for Pickering type emulsions, as was discussed earlier. When the emulsions are stabilized by molecular layers of surfactants or proteins, the picture alters significantly. For now such emulsifiers are displaced by bile salt and in turn any generated FFA can favourably partition into the aqueous phase without much difficulty, resulting in a shrinkage of droplet size. At the same time, the decrease in the surface area that such shrinkage entails may result in desorption of bile salt/lipase, depending on the kinetic of desorption and amount of enzyme

already accumulated on the surface at any given time. It is quite reasonable to consider droplets as entirely consisting of unconverted lipids throughout the process, given that originally the aqueous phase is devoid of FFA and the strong tendency of fatty acids to partition into water. This is to say that all generated FFA migrate immediately out of oil droplets. With this assumption, and once again considering the fact that hydrolysis only occurs at the surface, the governing equation for the variation of droplet size, d , with elapsed time t becomes:

$$\frac{\pi\rho_0 d^2}{2M_w} \frac{d}{dt}(d) = -\pi d^2 k \frac{\Gamma(t)}{\Gamma^{max}} \quad (2.14)$$

Equation (2.14) together with the initial condition $d=d_0$ at time $t=0$, admits the following general solution

$$d(t) = d_0 \left(1 - \frac{2M_w k}{d_0 \rho_0 \Gamma^{max}} \int_0^t \Gamma(t') dt' \right) \quad (2.15)$$

which in turn gives the amount of converted lipid as

$$\varphi(t) = \varphi_{Max} \left[1 - \left(1 - \frac{2M_w k}{d_0 \rho_0 \Gamma^{max}} \int_0^t \Gamma(t') dt' \right)^3 \right] \quad (2.16)$$

In general it is quite difficult to theoretically determine the form of $\Gamma(t)$, given the possibility of competitive adsorption occurring between the bile salt/lipase and an already existing protein, particularly where such protein has formed a viscoelastic cross-linked surface layer. This situation is further complicated if any subsequent enzyme desorption kinetics is slow compared to the rate of droplet shrinkage, thus giving rise to the possibility of $\Gamma(t)$ exceeding Γ^{Max} at some point during the shrinkage. However, for situations involving none-film forming proteins, as for

example casein, or where the emulsion was stabilized by a relatively low molecular weight surfactants one may plausibly assume that such complications do not arise. In other words the kinetic of adsorption and possible desorption of lipase/bile salt are fast enough for enzyme surface coverage to always be maintained at Γ^{Max} , from the very early stages of digestion all the way to the end of the process. With this reasonable assumption, it is easy to see that the general equation ((2.16) readily simplifies to (2.17):

$$\varphi(t) = \varphi_{Max} \left[1 - \left(1 - \frac{2M_w k}{d_0 \rho_0} t \right)^3 \right] \quad (2.17)$$

whereas before ρ_0 and M_w are density and molar weight of lipid, respectively and d_0 the initial droplet diameter. The model encompassing the above assumption was first proposed by McClements and Li (2010a, 2015) and later solved by Gaucel *et al.* (2015) to yield equation (2.17). The model predict a fixed finite time at which droplets will be completely hydrolyzed (*i.e.* shrank to zero). This time is $\tau = \frac{d_0 \rho_0}{2M_w k}$, beyond which equation (2.17) is no longer physical. Another aspect of the model is that as droplets shrink, the surface to volume ratio increases and hence the model predicts a rather rapid upturn in the rate of hydrolysis towards the end of the process. This is thought to not be all that realistic. A possible modifications to overcome this issue has been discussed by Gaucel *et al.* (2015). Once again if one is interested in the half-life ($t_{1/2}$), then using (2.17) this is found to be

$$t_{1/2} = \frac{\rho d_0}{2kM_w} \left(1 - \frac{1}{\sqrt[3]{2}} \right) \quad (2.18)$$

In **Figure 2.5**, a schematic representation of the mathematical models applicable to the pathways relevant to surfactant-stabilized or particle-stabilized emulsions. Herein, we provide the modelling pathways relevant to the various droplet

behaviour and interfacial dynamics during digestion. Under the assumptions of rapid adsorption/desorption of surface enzymes and permissible reduction in droplet size, equations (2.16) and (2.17) are relevant where short time digestion and subsequent asymptotic equilibrium is observable. Under conditions where the droplet size remains stable during digestion, *i.e.* in the case of Pickering emulsion, equation (2.9) is the appropriate modelling route and where equation (2.10) is selected for rapid interfacial adsorption and in the cases where interfacial dynamics are anticipated, equation (2.12) is appropriate. In the latter case it is notable that interfacial adsorption at short-times results in delayed digestion and that the large-time behaviour (marked in red) of both equations (2.10) and (2.12) asymptotically stable, approach a constant plateau value.

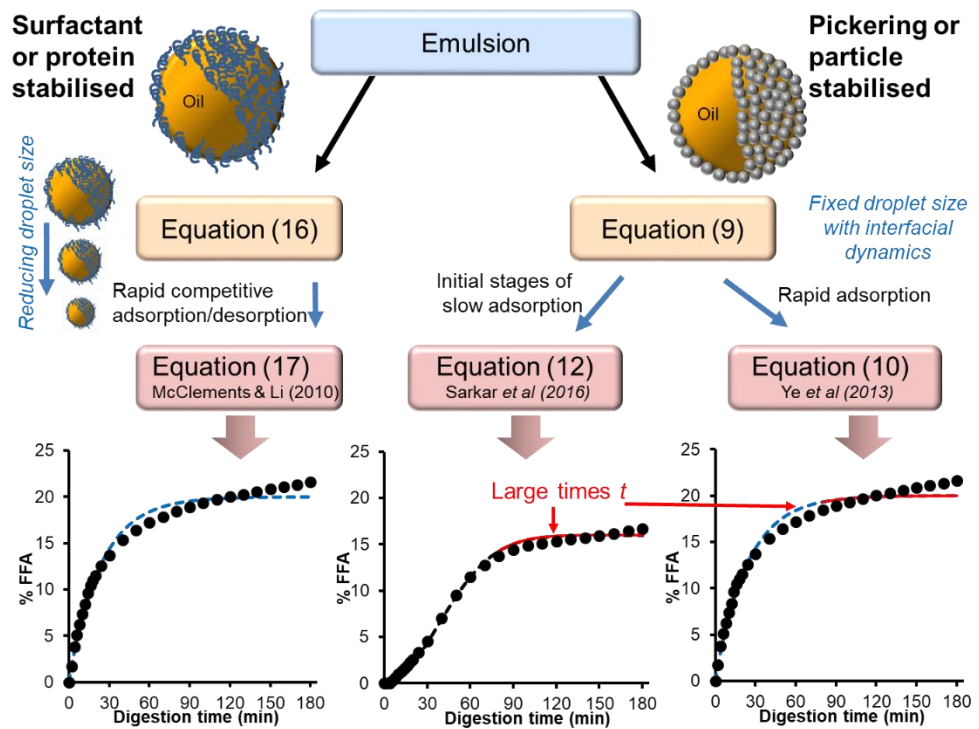


Figure 2.5. Schematic representation of the mathematical models applicable to the pathways relevant to surfactant-stabilized or particle-stabilized emulsions. Under the assumptions or rapid adsorption/desorption of surface enzymes and permissible reduction in droplet size, equations (2.16) and (2.17) are relevant where short time digestion and subsequent asymptotic equilibrium are achieved. Where droplet size remains stable, *i.e.* Pickering emulsion, equation (2.9) is the appropriate route and where further equation (2.10) selection is required for rapid adsorption and where interfacial dynamics are included, equation (2.12) is appropriate. Here it is notable that interfacial adsorption at short-times results in delayed digestion and that the large-time behaviour (in red) of both equations (2.10) and (2.12) are asymptotic.

In this section, we have discussed several different models currently being used in the literature to fit experimental data on digestion of emulsion systems. We have sought to provide a clearer understanding of the connection between various models, by discussing them as limiting cases of a more generalised situation. In doing so, we highlight the limits of validity and underlying assumption in each case. It is important that some thought be given to the type of model that best captures the situation one is investigating, rather than a forced attempt to fit the data to equations for which the underlying model is not necessarily appropriate. When this is done carefully, these models provide useful means to compare the digestion of emulsion systems that possess different surface properties and will facilitate standard parameters to compare reaction behaviour *e.g.* the case where, particles at interface remain intact or fuse together either with or without heat treatments, respectively. We envisage that the future models will provide closed form equations which will accommodate more complex systems where surface and droplet shrinkage dynamics both occur simultaneously.

2.6 Conclusions

The biophysical aspects of lipid digestion of particle-stabilized emulsions is a rapidly growing research domain owing to its fundamental importance to human biology and numerous industrial applications in food, pharmaceutical, personal care, biomedical sectors, such as, designing systems allowing sustained release of lipophilic molecules. Recently, there has been a substantial improvement in the understanding the role of particle-laden interface on modifying colloidal aspects of lipid digestion. We have provided the first systematic, balanced and comprehensive summary of experimental investigations as well as mathematical models for lipid digestion of Pickering emulsion droplets within this review. The key benefits of using Pickering emulsions is the ability of these particles to resist any competitive displacement by surface active bile salts by virtue

of high desorption energies of these particles. Although the gaps between the particles may provide access to the lipolysis enzymes, but the area available for lipase to bind is significantly reduced due to the presence of the particle on the droplet surface, providing further benefits to reduce the kinetics and extent of digestion. Besides intact particles, some attempts have been made in literature to include particle fusion, such as using heat treatments after thermos-labile particles have been adsorbed at the interface in order to reduce those interstitial pores and consequently, delay lipid digestion. Particle shape anisotropy has also been shown to offer interesting features in altering digestion profile by not only influencing interfacial adsorption and surface packing to reduce interfacial porosity but also impacting bulk interactions with key lipid digestion players. In order to adequately compare different mathematical models ranging from simple first order kinetics to those that account for kinetics of lipase-binding and interfacial dynamics, a decision tree has been proposed based on underlying assumptions and boundary conditions to ensure validity of the models. In summary, in order to adequately manipulate lipid digestion kinetics, we propose specific interfacial design strategies for future investigations focussing on particle physics and chemistry as well as the development of closed-loop mathematical models.

Based on the identified knowledge gaps, this thesis investigates a novel soft heat-set microgel particles from plant-based protein isolate and complex interfaces using microgels and polysaccharide particles to create Pickering emulsions with stimuli-responsive properties. The stability of Pickering emulsions stabilized by pea protein microgel particles (PPM) was studied as a function of different environmental stimuli *i.e.* pH values and ionic strengths (**Chapter 3**). Then, Pickering emulsions with complex particle-particle interface due to the electrostatic interactions between PPM and cellulose nanocrystals (CNC) were studied and emulsion responsiveness to gastric enzymes during *in vitro* gastric regime was investigated (**Chapter 4**). Finally, the degree and the rate of free fatty acids (FFAs) release after *in vitro* gastrointestinal digestion were assessed and compared between simple and complex interfaces (**Chapter 5**) followed by a general discussion (**Chapter 6**).

2.7 References

- ADAL, E., SADEGHPOUR, A., CONNELL, S., RAPPOLT, M., IBANOGLU, E. & SARKAR, A. 2017. Heteroprotein complex formation of bovine lactoferrin and pea protein isolate: A multiscale structural analysis. *Biomacromolecules*, 18, 625-635.
- AKEN, V., & HOOG (2005), AKEN, G. A. V., VINGERHOEDS, M. H. & HOOG, E. H. A. D. 2005. Colloidal behaviour of food emulsions under oral conditions. *In: DICKINSON, E. (ed.) Food colloids: Interaction, microstructure and processing*. Cambridge, UK: The Royal Society of Chemistry.
- ARAIZA-CALAHORRA, A., AKHTAR, M. & SARKAR, A. 2018. Recent advances in emulsion-based delivery approaches for curcumin: From encapsulation to bioaccessibility. *Trends in Food Science & Technology*, 71, 155-169.
- ARMAND, M., BOREL, P., PASQUIER, B., DUBOIS, C., SENFT, M., ANDRE, M., PEYROT, J., SALDUCCI, J. & LAIRON, D. 1996. Physicochemical characteristics of emulsions during fat digestion in human stomach and duodenum. *American Journal of Physiology-Gastrointestinal and Liver Physiology*, 271, G172-G183.
- AVEYARD, R., BINKS, B. P. & CLINT, J. H. 2003. Emulsions stabilized solely by colloidal particles. *Advances in Colloid and Interface Science*, 100-102, 503-546.
- BANSIL, R. & TURNER, B. S. 2006. Mucin structure, aggregation, physiological functions and biomedical applications. *Current Opinion in Colloid & Interface Science*, 11, 164-170.
- BERTON-CARABIN, C. C. & SCHROËN, K. 2015. Pickering emulsions for food applications: Background, trends, and challenges. *Annual Review of Food Science and Technology*, 6, 263-297.
- BINKS, B. P. 2002. Particles as surfactants—similarities and differences. *Current Opinion in Colloid & Interface Science*, 7, 21-41.
- BINKS, B. P. 2017. Colloidal particles at a range of fluid–fluid interfaces. *Langmuir*, 33, 6947-6963.
- BINKS, B. P. & HOROZOV, T. S. 2006. Colloidal particles at liquid interfaces: An introduction. *In: BINKS, B. P. & HOROZOV, T. S. (eds.) Colloidal*

- Particles at Liquid Interfaces*. Cambridge: Cambridge University Press.
- BINKS, B. P. & LUMSDON, S. O. 1999. Stability of oil-in-water emulsions stabilized by silica particles. *Physical Chemistry Chemical Physics*, 1, 3007-3016.
- BINKS, B. P. & LUMSDON, S. O. 2000. Influence of particle wettability on the type and stability of surfactant-free emulsions. *Langmuir*, 16, 8622-8631.
- BORAH, P. K., RAPPOLT, M., DUARY, R. K. & SARKAR, A. 2018. Effects of folic acid esterification on the hierarchical structure of amylopectin corn starch. *Food Hydrocolloids*.
- BROCKMAN, H. 2002. Colipase-induced reorganization of interfaces as a regulator of lipolysis. *Colloids and Surfaces B: Biointerfaces*, 26, 102-111.
- BRUNIER, B., SHEIBAT-OTHMAN, N., CHEVALIER, Y. & BOURGEAT-LAMI, E. 2016. Partitioning of laponite clay platelets in pickering emulsion polymerization. *Langmuir*, 32, 112-124.
- CAPRON, I. & CATHALA, B. 2013. Surfactant-free high internal phase emulsions stabilized by cellulose nanocrystals. *Biomacromolecules*, 14, 291-296.
- CHEVALIER, Y. & BOLZINGER, M.-A. 2013. Emulsions stabilized with solid nanoparticles: Pickering emulsions. *Colloids and Surfaces A: Physicochemical and Engineering Aspects*, 439, 23-34.
- CHEVALIER, Y., BOLZINGER, M.-A. & BRIANÇON, S. 2015. Pickering emulsions for controlled drug delivery to the skin. In: DRAGICEVIC, N. & MAIBACH, H. I. (eds.) *Percutaneous Penetration Enhancers Chemical Methods in Penetration Enhancement: Drug Manipulation Strategies and Vehicle Effects*. Berlin, Heidelberg: Springer Berlin Heidelberg.
- DE FOLTER, J. W. J., HUTTER, E. M., CASTILLO, S. I. R., KLOP, K. E., PHILIPSE, A. P. & KEGEL, W. K. 2014. Particle shape anisotropy in pickering emulsions: Cubes and peanuts. *Langmuir*, 30, 955-964.
- DE FOLTER, J. W. J., VAN RUIJVEN, M. W. M. & VELIKOV, K. P. 2012. Oil-in-water Pickering emulsions stabilized by colloidal particles from the water-insoluble protein zein. *Soft Matter*, 8, 6807-6815.

- DESTRIKATS, M., ROUVET, M., GEHIN-DELVAL, C., SCHMITT, C. & BINKS, B. P. 2014. Emulsions stabilized by whey protein microgel particles: towards food-grade Pickering emulsions. *Soft Matter*, 10, 6941-6954.
- DICKINSON, E. 2010. Food emulsions and foams: Stabilization by particles. *Current Opinion in Colloid & Interface Science*, 15, 40-49.
- DICKINSON, E. 2012. Use of nanoparticles and microparticles in the formation and stabilization of food emulsions. *Trends in Food Science & Technology*, 24, 4-12.
- DICKINSON, E. 2015a. Microgels — An alternative colloidal ingredient for stabilization of food emulsions. *Trends in Food Science & Technology*, 43, 178-188.
- DICKINSON, E. 2015b. Structuring of colloidal particles at interfaces and the relationship to food emulsion and foam stability. *Journal of Colloid and Interface Science*, 449, 38-45.
- DICKINSON, E. 2017. Biopolymer-based particles as stabilizing agents for emulsions and foams. *Food Hydrocolloids*, 68, 219-231.
- DRESSELHUIS, D. M., DE HOOG, E. H. A., COHEN STUART, M. A. & VAN AKEN, G. A. 2008a. Application of oral tissue in tribological measurements in an emulsion perception context. *Food Hydrocolloids*, 22, 323-335.
- DRESSELHUIS, D. M., DE HOOG, E. H. A., COHEN STUART, M. A., VINGERHOEDS, M. H. & VAN AKEN, G. A. 2008b. The occurrence of in-mouth coalescence of emulsion droplets in relation to perception of fat. *Food Hydrocolloids*, 22, 1170-1183.
- DUAN, B., HUANG, Y., LU, A. & ZHANG, L. 2018. Recent advances in chitin based materials constructed via physical methods. *Progress in Polymer Science*, 82, 1-33.
- DUFFUS, L. J., NORTON, J. E., SMITH, P., NORTON, I. T. & SPYROPOULOS, F. 2016. A comparative study on the capacity of a range of food-grade particles to form stable O/W and W/O Pickering emulsions. *Journal of Colloid and Interface Science*, 473, 9-21.
- EMMANOUELA, F., R., P. A., M., B. E. C., PANAYIOTIS, V. & P., V. K. 2014. All-natural oil-filled microcapsules from water-insoluble proteins.

- Advanced Functional Materials*, 24, 5962-5968.
- ETTELAIE, R. & LISHCHUK, S. V. 2015. Detachment force of particles from fluid droplets. *Soft Matter*, 11, 4251-4265.
- EUSTON, S. R., BAIRD, W. G., CAMPBELL, L. & KUHN, M. 2013. Competitive adsorption of dihydroxy and trihydroxy bile salts with whey protein and casein in oil-in-water emulsions. *Biomacromolecules*, 14, 1850-1858.
- FAVÉ, G., COSTE, T. C. & ARMAND, M. 2004. Physicochemical properties of lipids: New strategies to manage fatty acid bioavailability. *Cellular and molecular biology (Noisy-le-Grand, France)*, 50, 815-831.
- FEHER, J. 2017. 8.5 - Digestion and Absorption of the Macronutrients. *Quantitative Human Physiology (Second Edition)*. Boston, US: Academic Press.
- FRELICHOWSKA, J., BOLZINGER, M.-A., VALOUR, J.-P., MOUAZIZ, H., PELLETIER, J. & CHEVALIER, Y. 2009. Pickering w/o emulsions: Drug release and topical delivery. *International Journal of Pharmaceutics*, 368, 7-15.
- FRENCH, D. J., BROWN, A. T., SCHOFIELD, A. B., FOWLER, J., TAYLOR, P. & CLEGG, P. S. 2016. The secret life of Pickering emulsions: particle exchange revealed using two colours of particle. *Scientific Reports*, 6, 31401.
- FRENCH, D. J., TAYLOR, P., FOWLER, J. & CLEGG, P. S. 2015. Making and breaking bridges in a Pickering emulsion. *Journal of Colloid and Interface Science*, 441, 30-38.
- GAUCEL, S., TRELEA, I. C. & LE FEUNTEUN, S. 2015. Comment on new mathematical model for interpreting pH-stat digestion profiles: Impact of lipid droplet characteristics on in vitro digestibility. *Journal of Agricultural and Food Chemistry*, 63, 10352-10353.
- GE, S., XIONG, L., LI, M., LIU, J., YANG, J., CHANG, R., LIANG, C. & SUN, Q. 2017. Characterizations of Pickering emulsions stabilized by starch nanoparticles: Influence of starch variety and particle size. *Food Chemistry*, 234, 339-347.
- GOLDING, M. & WOOSTER, T. J. 2010. The influence of emulsion structure and stability on lipid digestion. *Current Opinion in Colloid & Interface*

- Science*, 15, 90-101.
- GOLDING, M., WOOSTER, T. J., DAY, L., XU, M., LUNDIN, L., KEOGH, J. & CLIFTON, P. 2011. Impact of gastric structuring on the lipolysis of emulsified lipids. *Soft Matter*, 7, 3513-3523.
- GUO, Q., BELLISSIMO, N. & ROUSSEAU, D. 2017. Role of gel structure in controlling in vitro intestinal lipid digestion in whey protein emulsion gels. *Food Hydrocolloids*, 69, 264-272.
- JIE, W. & GUANG-HUI, M. 2016. Recent studies of pickering emulsions: Particles make the difference. *Small*, 12, 4633-4648.
- KALASHNIKOVA, I., BIZOT, H., CATHALA, B. & CAPRON, I. 2011. New pickering emulsions stabilized by bacterial cellulose nanocrystals. *Langmuir*, 27, 7471-7479.
- LAGUNA, L., PICOUET, P., GUÀRDIA, M. D., RENARD, C. M. G. C. & SARKAR, A. 2017. In vitro gastrointestinal digestion of pea protein isolate as a function of pH, food matrices, autoclaving, high-pressure and re-heat treatments. *LWT - Food Science and Technology*, 84, 511-519.
- LAGUNA, L. & SARKAR, A. 2017. Oral tribology: update on the relevance to study astringency in wines. *Tribology - Materials, Surfaces & Interfaces*, 11, 116-123.
- LAM, S., VELIKOV, K. P. & VELEV, O. D. 2014. Pickering stabilization of foams and emulsions with particles of biological origin. *Current Opinion in Colloid & Interface Science*, 19, 490-500.
- LEAL-CALDERON, F. & SCHMITT, V. 2008. Solid-stabilized emulsions. *Current Opinion in Colloid & Interface Science*, 13, 217-227.
- LEVINE, S., BOWEN, B. D. & PARTRIDGE, S. J. 1989. Stabilization of emulsions by fine particles I. Partitioning of particles between continuous phase and oil/water interface. *Colloids and Surfaces*, 38, 325-343.
- LI, C., LI, Y., SUN, P. & YANG, C. 2013. Pickering emulsions stabilized by native starch granules. *Colloids and Surfaces A: Physicochemical and Engineering Aspects*, 431, 142-149.
- LI, Y. & MCCLEMENTS, D. J. 2010. New mathematical model for interpreting ph-stat digestion profiles: Impact of lipid droplet characteristics on in

- vitro digestibility. *Journal of Agricultural and Food Chemistry*, 58, 8085-8092.
- LIANG, H., ZHOU, B., LI, J., HE, Y., PEI, Y. & LI, B. 2016. Engineering functional alginate beads for encapsulation of Pickering emulsions stabilized by colloidal particles. *RSC Advances*, 6, 101267-101276.
- LING, S., KAPLAN, D. L. & BUEHLER, M. J. 2018. Nanofibrils in nature and materials engineering. *Nature Reviews Materials*, 3, 18016.
- LISHCHUK, S. V. & ETTALAIE, R. 2016. Detachment force of particles with pinning of contact line from fluid bubbles/droplets. *Langmuir*, 32, 13040-13045.
- LIU, F. & TANG, C.-H. 2016. Reprint of "Soy glycinin as food-grade Pickering stabilizers: Part. III. Fabrication of gel-like emulsions and their potential as sustained-release delivery systems for β -carotene". *Food Hydrocolloids*, 60, 631-640.
- LOU, F., YE, L., KONG, M., YANG, Q., LI, G. & HUANG, Y. 2016. Pickering emulsions stabilized by shape-controlled silica microrods. *RSC Advances*, 6, 24195-24202.
- LU, X. X., XIAO, J. & HUANG, Q. R. 2018. Pickering emulsions stabilized by media-milled starch particles. *Food Research International*, 105, 140-149.
- LUO, Z., MURRAY, B. S., YUSOFF, A., MORGAN, M. R. A., POVEY, M. J. W. & DAY, A. J. 2011. Particle-stabilizing effects of flavonoids at the oil-water interface. *Journal of Agricultural and Food Chemistry*, 59, 2636-2645.
- MACKIE, A. & MACIERZANKA, A. 2010. Colloidal aspects of protein digestion. *Current Opinion in Colloid & Interface Science*, 15, 102-108.
- MALDONADO-VALDERRAMA, J., WILDE, P., MACIERZANKA, A. & MACKIE, A. 2011. The role of bile salts in digestion. *Advances in Colloid and Interface Science*, 165, 36-46.
- MALDONADO-VALDERRAMA, J., WOODWARD, N. C., GUNNING, A. P., RIDOUT, M. J., HUSBAND, F. A., MACKIE, A. R., MORRIS, V. J. & WILDE, P. J. 2008. Interfacial characterization of β -lactoglobulin networks: Displacement by bile salts. *Langmuir*, 24, 6759-6767.

- MAREFATI, A., BERTRAND, M., SJÖÖ, M., DEJMEK, P. & RAYNER, M. 2017. Storage and digestion stability of encapsulated curcumin in emulsions based on starch granule Pickering stabilization. *Food Hydrocolloids*, 63, 309-320.
- MARTO, J., ASCENSO, A., SIMOES, S., ALMEIDA, A. J. & RIBEIRO, H. M. 2016. Pickering emulsions: Challenges and opportunities in topical delivery. *Expert Opinion on Drug Delivery*, 13, 1093-1107.
- MCCLEMENTS, D. J. 2015. *Food emulsions: Principles, practices, and techniques*, Boca Raton, US, CRC Press.
- MCCLEMENTS, D. J. 2018. The biophysics of digestion: lipids. *Current Opinion in Food Science*, 21, 1-6.
- MCCLEMENTS, D. J. & LI, Y. 2015. Response to comment on new mathematical model for interpreting pH-stat digestion profiles: Impact of lipid droplet characteristics on in vitro digestibility. *Journal of Agricultural and Food Chemistry*, 63, 10354-10354.
- MCLEAN, J. D. & KILPATRICK, P. K. 1997. Effects of asphaltene solvency on stability of water-in-crude-oil emulsions. *Journal of Colloid and Interface Science*, 189, 242-253.
- MESHULAM, D. & LESMES, U. 2014. Responsiveness of emulsions stabilized by lactoferrin nano-particles to simulated intestinal conditions. *Food & Function*, 5, 65-73.
- MILED, N., CANAAN, S., DUPUIS, L., ROUSSEL, A., RIVIÈRE, M., CARRIÈRE, F., DE CARO, A., CABBILLAU, C. & VERGER, R. 2000. Digestive lipases: From three-dimensional structure to physiology. *Biochimie*, 82, 973-986.
- MOSCA, A. C. & CHEN, J. 2017. Food-saliva interactions: Mechanisms and implications. *Trends in Food Science & Technology*, 66, 125-134.
- PANG, B., LIU, H., LIU, P., PENG, X. & ZHANG, K. 2018. Water-in-oil Pickering emulsions stabilized by stearylated microcrystalline cellulose. *Journal of Colloid and Interface Science*, 513, 629-637.
- PEINADO, I., LESMES, U., ANDRÉS, A. & MCCLEMENTS, J. D. 2010. Fabrication and morphological characterization of biopolymer particles formed by electrostatic complexation of heat treated lactoferrin and anionic polysaccharides. *Langmuir*, 26, 9827-9834.

- PIAO, S. H., KWON, S. H., ZHANG, W. L. & CHOI, H. J. 2015. Celebrating Soft Matter's 10th Anniversary: Stimuli-responsive Pickering emulsion polymerized smart fluids. *Soft Matter*, 11, 646-654.
- PICKERING, S. U. 1907. CXCVI.-Emulsions. *Journal of the Chemical Society, Transactions*, 91, 2001-2021.
- PIGNOL, D., AYVAZIAN, L., KERFELEC, B., TIMMINS, P., CRENON, I., HERMOSO, J., FONTECILLA-CAMPS, J. C. & CHAPUS, C. 2000. Critical role of micelles in pancreatic lipase activation revealed by small angle neutron scattering. *Journal of Biological Chemistry*, 275, 4220-4224.
- RAMSDEN, W. 1904. Separation of solids in the surface-layers of solutions and 'suspensions' (observations on surface-membranes, bubbles, emulsions, and mechanical coagulation).—Preliminary account. *Proceedings of the Royal Society of London*, 72, 156-164.
- RAYNER, M., MARKU, D., ERIKSSON, M., SJÖÖ, M., DEJMEK, P. & WAHLGREN, M. 2014. Biomass-based particles for the formulation of Pickering type emulsions in food and topical applications. *Colloids and Surfaces A: Physicochemical and Engineering Aspects*, 458, 48-62.
- RAYNER, M., TIMGREN, A., SJOO, M. & DEJMEK, P. 2012. Quinoa starch granules: a candidate for stabilising food-grade Pickering emulsions. *Journal of the Science of Food and Agriculture*, 92, 1841-1847.
- REIS, P., HOLMBERG, K., WATZKE, H., LESER, M. E. & MILLER, R. 2009. Lipases at interfaces: A review. *Advances in Colloid and Interface Science*, 147-148, 237-250.
- ROUSSEAU, D. 2013. Trends in structuring edible emulsions with Pickering fat crystals. *Current Opinion in Colloid & Interface Science*, 18, 283-291.
- RUIZ-RODRIGUEZ, P. E., MESHULAM, D. & LESMES, U. 2014. Characterization of pickering O/W emulsions stabilized by silica nanoparticles and their responsiveness to *in vitro* digestion conditions. *Food Biophysics*, 9, 406-415.
- RUTKEVIČIUS, M., ALLRED, S., VELEV, O. D. & VELIKOV, K. P. 2018. Stabilization of oil continuous emulsions with colloidal particles from water-insoluble plant proteins. *Food Hydrocolloids*, 82, 89-95.

- SALAS, C., NYPELÖ, T., RODRIGUEZ-ABREU, C., CARRILLO, C. & ROJAS, O. J. 2014. Nanocellulose properties and applications in colloids and interfaces. *Current Opinion in Colloid & Interface Science*, 19, 383-396.
- SAMS, L., PAUME, J., GIALLO, J. & CARRIERE, F. 2016. Relevant pH and lipase for in vitro models of gastric digestion. *Food & Function*, 7, 30-45.
- SANDRA, S., DECKER, E. A. & MCCLEMENTS, D. J. 2008. Effect of interfacial protein cross-linking on the in vitro digestibility of emulsified corn oil by pancreatic lipase. *Journal of Agricultural and Food Chemistry*, 56, 7488-7494.
- SARKAR, A., ADEMUYIWA, V., STUBLEY, S., ESA, N. H., GOYCOOLEA, F. M., QIN, X., GONZALEZ, F. & OLVERA, C. 2018a. Pickering emulsions co-stabilized by composite protein/ polysaccharide particle-particle interfaces: Impact on *in vitro* gastric stability. *Food Hydrocolloids*, 84, 282-291.
- SARKAR, A., GOH, K. K. T. & SINGH, H. 2009a. Colloidal stability and interactions of milk-protein-stabilized emulsions in an artificial saliva. *Food Hydrocolloids*, 23, 1270-1278.
- SARKAR, A., GOH, K. K. T. & SINGH, H. 2010a. Properties of oil-in-water emulsions stabilized by β -lactoglobulin in simulated gastric fluid as influenced by ionic strength and presence of mucin. *Food Hydrocolloids*, 24, 534-541.
- SARKAR, A., GOH, K. K. T., SINGH, R. P. & SINGH, H. 2009b. Behaviour of an oil-in-water emulsion stabilized by β -lactoglobulin in an in vitro gastric model. *Food Hydrocolloids*, 23, 1563-1569.
- SARKAR, A., HORNE, D. S. & SINGH, H. 2010b. Interactions of milk protein-stabilized oil-in-water emulsions with bile salts in a simulated upper intestinal model. *Food Hydrocolloids*, 24, 142-151.
- SARKAR, A., HORNE, D. S. & SINGH, H. 2010c. Pancreatin-induced coalescence of oil-in-water emulsions in an in vitro duodenal model. *International Dairy Journal*, 20, 589-597.
- SARKAR, A., JUAN, J.-M., KOŁODZIEJCZYK, E., ACQUISTAPACE, S., DONATO-CAPEL, L. & WOOSTER, T. J. 2015. Impact of protein gel

- porosity on the digestion of lipid emulsions. *Journal of Agricultural and Food Chemistry*, 63, 8829-8837.
- SARKAR, A., KAMARUDDIN, H., BENTLEY, A. & WANG, S. 2016a. Emulsion stabilization by tomato seed protein isolate: Influence of pH, ionic strength and thermal treatment. *Food Hydrocolloids*, 57, 160-168.
- SARKAR, A. & KAUL, P. 2014. Evaluation of tomato processing by-products: A comparative study in a pilot scale setup. *Journal of Food Process Engineering*, 37, 299-307.
- SARKAR, A., LI, H., CRAY, D. & BOXALL, S. 2018b. Composite whey protein–cellulose nanocrystals at oil-water interface: Towards delaying lipid digestion. *Food Hydrocolloids*, 77, 436-444.
- SARKAR, A., MURRAY, B., HOLMES, M., ETTALAIE, R., ABDALLA, A. & YANG, X. 2016b. In vitro digestion of Pickering emulsions stabilized by soft whey protein microgel particles: Influence of thermal treatment. *Soft Matter*, 12, 3558-3569.
- SARKAR, A. & SINGH, H. 2012. Oral behaviour of food emulsions. *Food Oral Processing*. Wiley-Blackwell.
- SARKAR, A. & SINGH, H. 2016. Emulsions and foams stabilized by milk proteins. In: MCSWEENEY, P. L. H. & O'MAHONY, J. A. (eds.) *Advanced Dairy Chemistry: Volume 1B: Proteins: Applied Aspects*. New York, NY: Springer New York.
- SARKAR, A., YE, A. & SINGH, H. 2016c. On the role of bile salts in the digestion of emulsified lipids. *Food Hydrocolloids*, 60, 77-84.
- SARKAR, A., YE, A. & SINGH, H. 2016d. Oral processing of emulsion systems from a colloidal perspective. *Food & Function*, 8, 511-521.
- SARKAR, A., YE, A. & SINGH, H. 2017a. Oral processing of emulsion systems from a colloidal perspective. *Food & Function*.
- SARKAR, A., ZHANG, S., MURRAY, B., RUSSELL, J. A. & BOXAL, S. 2017b. Modulating in vitro gastric digestion of emulsions using composite whey protein-cellulose nanocrystal interfaces. *Colloids and Surfaces B: Biointerfaces*, 158, 137-146.
- SCHEUBLE, N., GEUE, T., WINDHAB, E. J. & FISCHER, P. 2014. Tailored interfacial rheology for gastric stable adsorption layers. *Biomacromolecules*, 15, 3139-3145.

- SCHIPPER, R. G., SILLETTI, E. & VINGERHOEDS, M. H. 2007. Saliva as research material: Biochemical, physicochemical and practical aspects. *Archives of Oral Biology*, 52, 1114-1135.
- SHAH, B. R., LI, Y., JIN, W., AN, Y., HE, L., LI, Z., XU, W. & LI, B. 2016a. Preparation and optimization of Pickering emulsion stabilized by chitosan-tripolyphosphate nanoparticles for curcumin encapsulation. *Food Hydrocolloids*, 52, 369-377.
- SHAH, B. R., ZHANG, C., LI, Y. & LI, B. 2016b. Bioaccessibility and antioxidant activity of curcumin after encapsulated by nano and Pickering emulsion based on chitosan-tripolyphosphate nanoparticles. *Food Research International*, 89, 399-407.
- SHAO, Y. & TANG, C.-H. 2016. Gel-like pea protein Pickering emulsions at pH3.0 as a potential intestine-targeted and sustained-release delivery system for β -carotene. *Food Research International*, 79, 64-72.
- SHIMONI, G., SHANI LEVI, C., LEVI TAL, S. & LESMES, U. 2013. Emulsions stabilization by lactoferrin nano-particles under in vitro digestion conditions. *Food Hydrocolloids*, 33, 264-272.
- SILLETTI, E., VINGERHOEDS, M. H., NORDE, W. & VAN AKEN, G. A. 2007. The role of electrostatics in saliva-induced emulsion flocculation. *Food Hydrocolloids*, 21, 596-606.
- SINGH, H. & SARKAR, A. 2011. Behaviour of protein-stabilized emulsions under various physiological conditions. *Advances in Colloid and Interface Science*, 165, 47-57.
- SINGH, H. & YE, A. 2013. Structural and biochemical factors affecting the digestion of protein-stabilized emulsions. *Current Opinion in Colloid & Interface Science*, 18, 360-370.
- SINGH, H., YE, A. & HORNE, D. 2009. Structuring food emulsions in the gastrointestinal tract to modify lipid digestion. *Prog Lipid Res*, 48, 92-100.
- SJÖÖ, M., EMEK, S. C., HALL, T., RAYNER, M. & WAHLGREN, M. 2015. Barrier properties of heat treated starch Pickering emulsions. *Journal of Colloid and Interface Science*, 450, 182-188.
- TAVACOLI, J. W., KATGERT, G., KIM, E. G., CATES, M. E. & CLEGG, P. S. 2012. Size limit for particle-stabilized emulsion droplets under gravity.

Physical Review Letters, 108, 268306.

- TAVERNIER, I., WIJAYA, W., VAN DER MEEREN, P., DEWETTINCK, K. & PATEL, A. R. 2016. Food-grade particles for emulsion stabilization. *Trends in Food Science & Technology*, 50, 159-174.
- TIKEKAR, R. V., PAN, Y. & NITIN, N. 2013. Fate of curcumin encapsulated in silica nanoparticle stabilized Pickering emulsion during storage and simulated digestion. *Food Research International*, 51, 370-377.
- TIMGREN, A., RAYNER, M., SJÖÖ, M. & DEJMEK, P. 2011. Starch particles for food based Pickering emulsions. *Procedia Food Science*, 1, 95-103.
- TORRES, O., ANDABLO-REYES, E., MURRAY, B. S. & SARKAR, A. 2018. Emulsion Microgel Particles as High-Performance Bio-Lubricants. *ACS Applied Materials & Interfaces*, 10, 26893-26905.
- TZOUMAKI, M. V., MOSCHAKIS, T. & BILIADERIS, C. G. 2010. Metastability of nematic gels made of aqueous chitin nanocrystal dispersions. *Biomacromolecules*, 11, 175-181.
- TZOUMAKI, M. V., MOSCHAKIS, T., KIOSSEOGLOU, V. & BILIADERIS, C. G. 2011. Oil-in-water emulsions stabilized by chitin nanocrystal particles. *Food Hydrocolloids*, 25, 1521-1529.
- TZOUMAKI, M. V., MOSCHAKIS, T., SCHOLTEN, E. & BILIADERIS, C. G. 2013. In vitro lipid digestion of chitin nanocrystal stabilized o/w emulsions. *Food & Function*, 4, 121-129.
- VAN TILBEURGH, H., BEZZINE, S., CABBILLAU, C., VERGER, R. & CARRIÈRE, F. 1999. Colipase: structure and interaction with pancreatic lipase. *Biochimica et Biophysica Acta (BBA) - Molecular and Cell Biology of Lipids*, 1441, 173-184.
- VINGERHOEDS, M. H., SILLETTI, E., DE GROOT, J., SCHIPPER, R. G. & VAN AKEN, G. A. 2009. Relating the effect of saliva-induced emulsion flocculation on rheological properties and retention on the tongue surface with sensory perception. *Food Hydrocolloids*, 23, 773-785.
- WILDE, P. J. & CHU, B. S. 2011. Interfacial & colloidal aspects of lipid digestion. *Advances in Colloid and Interface Science*, 165, 14-22.
- WINUPRASITH, T., KHOMEIN, P., MITBUMRUNG, W., SUPHANTHARIKA, M., NITITHAMYONG, A. & MCCLEMENTS, D. J. 2018. Encapsulation of vitamin D3 in pickering emulsions

- stabilized by nanofibrillated mangosteen cellulose: Impact on in vitro digestion and bioaccessibility. *Food Hydrocolloids*, 83, 153-164.
- XIAO, J., LI, C. & HUANG, Q. 2015. Kafirin nanoparticle-stabilized pickering emulsions as oral delivery vehicles: Physicochemical stability and *in vitro* digestion profile. *Journal of Agricultural and Food Chemistry*, 63, 10263-10270.
- XIAO, J., WANG, X. A., PEREZ GONZALEZ, A. J. & HUANG, Q. 2016. Kafirin nanoparticles-stabilized pickering emulsions: Microstructure and rheological behaviour. *Food Hydrocolloids*, 54, 30-39.
- YANG, D., WANG, X.-Y., JI, C.-M., LEE, K.-T., SHIN, J.-A., LEE, E.-S. & HONG, S.-T. 2014. Influence of Ginkgo biloba extracts and of their flavonoid glycosides fraction on the in vitro digestibility of emulsion systems. *Food Hydrocolloids*, 42, 196-203.
- YANG, T., ZHENG, J., ZHENG, B.-S., LIU, F., WANG, S. & TANG, C.-H. 2018. High internal phase emulsions stabilized by starch nanocrystals. *Food Hydrocolloids*, 82, 230-238.
- YE, A., CUI, J., ZHU, X. & SINGH, H. 2013. Effect of calcium on the kinetics of free fatty acid release during in vitro lipid digestion in model emulsions. *Food Chemistry*, 139, 681-688.
- YUAN, Z., JINGJING, Z., RUNTING, P., ZHILI, W., JIAN, G., JINMEI, W., SHOUWEI, Y. & XIAOQUAN, Y. 2017. Zein/tannic acid complex nanoparticles-stabilized emulsion as a novel delivery system for controlled release of curcumin. *International Journal of Food Science & Technology*, 52, 1221-1228.
- YUSOFF, A. & MURRAY, B. S. 2011. Modified starch granules as particle-stabilizers of oil-in-water emulsions. *Food Hydrocolloids*, 25, 42-55.
- ZHOU, F.-Z., YAN, L., YIN, S.-W., TANG, C.-H. & YANG, X.-Q. 2018. Development of pickering emulsions stabilized by gliadin/proanthocyanidins hybrid particles (gphps) and the fate of lipid oxidation and digestion. *Journal of Agricultural and Food Chemistry*, 66, 1461-1471.
- ZOBEL, H. 1988. Molecules to granules: A comprehensive starch review. *Starch-Stärke*, 40, 44-50.

Chapter 3^b

Pea protein microgel particles as Pickering stabilizers of oil-in-water emulsions: Responsiveness to pH and ionic strength

Abstract

The aim of this study was to design plant protein-based microgel particles to create Pickering emulsions (20 wt% sunflower oil, 0.05-1.0 wt% protein) and investigate the role of electrostatic interactions on colloidal behaviour of such emulsions. Pea protein microgels (PPM) were designed using a facile top-down approach of heat-set protein gel formation followed by controlled shearing. The aqueous dispersion of PPM had hydrodynamic diameters ranging from 200 to 400 nm at pH 7.0 to pH 9.0 with high negative charge (-30 to -35 mV) and pI was pH 5.0. With increasing ionic concentration from 1 to 250 mM NaCl, the ζ -potential of PPM changed to -8 mV due to charge screening effects, in line with theoretical calculations of the electrostatic potential. The Pickering emulsions with smallest droplet sizes (d_{43}) \sim 25 μ m exhibited excellent coalescence stability and high adsorption efficiency of PPM at the oil-water interface (>98%) at pH 7.0, with the latter being supported by confocal microscopy showing effective adsorption of the PPMs at the droplet surface. Adjusting the pH of the emulsions to pI demonstrated aggregation of adsorbed PPM at the particle-laden interface providing a higher degree of adsorption as well as enhancing inter-droplet flocculation and the shear-thinning character as compared to those at pH 7.0 or pH 3.0. Charge screening effects in presence of 100 mM NaCl resulted in PPM-PPM aggregation and enhanced viscosity of the emulsions. Findings from this study on pea protein microgels would open avenues for rational designing of sustainable Pickering emulsions in the future.

^b Published as a peer-reviewed publication: Zhang, S., Holmes, M., Ettelaie, R., Sarkar, A. (2020) Pea protein microgel particles as Pickering stabilizers of oil-in-water emulsions: Responsiveness to pH and ionic strength. *Food Hydrocolloids*, 102, 105583.

3.1 Introduction

In recent times, gradual dietary changes towards sustainable plant-based ingredients has increased and, consequently designing food emulsions using plant proteins have been the preferred direction for emulsifiers to reduce food-production associated environmental footprints (Rayner et al., 2014). Furthermore, plant proteins are appreciated by consumers as they are “green”, “vegan-friendly” and are considered to be less allergenic and are less expensive as compared to the most commonly used dairy proteins. A range of plant proteins, such as soybean, pea, chickpea, faba bean, lentil, cowpea, French bean, sweet lupin, tomato seed and zein protein (Ben-Harb et al., 2018b, Jayasena et al., 2010, Karaca et al., 2011, Kimura et al., 2008, Pan et al., 2015, Sarkar et al., 2016b) have been investigated for stabilizing oil-in-water (O/W) emulsions. However, many if not most, of these plant proteins have limited aqueous solubility (Sarkar et al., 2016b, Nesterenko et al., 2013, Makri and Doxastakis, 2006) and are less digestible as compared to the dairy proteins (de Folter et al., 2012, Laguna et al., 2017b). This restricts easy replacement of dairy proteins in food products by plant proteins.

In comparison to the conventional protein-stabilized emulsions, the investigation of plant protein-based particles to create Pickering emulsions can be particularly interesting as these emulsions involve particle-stabilization of the droplets and therefore do not need perfect solubilisation of these proteins in the aqueous phase. In other words, these emulsions need the particles to be partially wettable by the oil and aqueous phases. In addition, Pickering emulsions have gained remarkable research interest in the food colloids community in recent years due to their distinctive stability against coalescence and Ostwald ripening as well as their ability to alter lipid digestion kinetics of emulsions post consumption (Aveyard et al., 2003b, Binks, 2002b, Dickinson, 2012, Dickinson, 2013, Sarkar et al., 2019a). Hence, there is a strong demand in food industries to find cheaper plant protein-based Pickering stabilizer alternatives that can effectively stabilize emulsion droplets for longer term against coalescence.

As compared to the extensive studies on particles derived from animal-based proteins being used as Pickering stabilizers, *e.g.* whey protein microgels (Destribats et al., 2014a, Sarkar et al., 2016c) and lactoferrin nanoparticles or nanogels (David-Birman et al., 2013, Gal et al., 2013, Meshulam and Lesmes, 2014a, Sarkar et al., 2018a), those involving particles obtained from plant proteins are fairly recent and are attracting significant research attention. For example, Liu and co-authors (Zhu et al., 2017, Peng et al., 2018, Peng et al., 2020, Liu and Tang, 2014, Liu and Tang, 2016b, Liu and Tang, 2013, Liu et al., 2017) investigated the ability of soy protein nanoparticles aggregates (SPN) (~100 nm, created *via* heat-treatment at 95 °C for 15 min) to act as Pickering stabilizers. On the other hand, Chen et al. (2014) prepared heat denatured soy protein nanogel particles at various pH values (pH 2.0-7.0) and added ions (0-200 mM NaCl). In another recent study, Zhu et al. (2018) suggested the importance of the electrostatic screening by ions (100-200 mM NaCl) to improve freeze-thaw stability of Pickering emulsions stabilized by soy protein-based nanoparticles. Besides the commonly used soy protein-based particles, peanut protein microgel particles have been recently investigated, where these microgel particles were prepared *via* enzyme treatment and had hydrodynamic diameters ranging from 200 to 300 nm and were used to stabilize high-internal-phase Pickering emulsions with 87 % oil volume fractions (Jiao et al., 2018). Water-insoluble zein-based colloidal particles and kafirin nanoparticles have also been reported as possible Pickering stabilizers. For example, de Folter et al. (2012) fabricated zein-based colloidal particles with an average diameter of ~70 nm. Xiao et al. (2016a) used an anti-solvent precipitation method to produce kafirin nanoparticles with a mean diameter of 206.5 nm. Gliadin colloidal particles (GCPs) with average diameter of ~120 nm at acidic pH that were prepared by an anti-solvent procedure (Hu et al., 2016b) were suggested as Pickering stabilizers.

Due to the significant academic and industrial interests resulting from their low cost, Liang and Tang (2014a) created pea protein nanoparticles for the first time. In such a process, an aqueous dispersion of pea protein isolate (PPI) was adjusted at pH 3.0 to produce pea protein-based particles with hydrodynamic diameter of 100-200 nm. In addition, such particles generated

oil-in-water (O/W) Pickering emulsion with 20 wt% oil volume fraction. In another study, Shao and Tang (2015) found that such pea protein particle-stabilized Pickering emulsion enabled controlled release of lipophilic bioactive compounds during *in vitro* gastrointestinal digestion. Compared to the emulsion stabilized with untreated PPI, the Pickering-stabilized emulsion had a sustained release behaviour due to their gel-like inter-droplet network formation. Another recent study by Cochereau et al. (2019) designed pea protein microgel particles with protein concentration of 1-4 wt% at pH 6-8 *via* slow and modest heat treatment (*i.e.* 20- 40 °C).

It is thus clear from the literature that stabilizing Pickering emulsions using plant protein-based particles is a relatively recent endeavour. In particular, considering the strong research interests by food industries and academic community in pea protein, it is surprising that relatively little attention has been devoted to designing pea protein-based particles for the purpose of stabilizing Pickering emulsion droplets. Although the gelation properties of pea proteins (Bora et al., 1994a, Mession et al., 2015, Shao and Tang, 2015), pea protein-based aggregates, such as heat-treated fibrillar aggregates (Munialo et al., 2014), mixed pea globulin aggregates (Mession et al., 2017b), as well as thermal aggregates from mixed pea globulin and β -lactoglobulin (Chihi et al., 2016, Chihi et al., 2018), have been widely studied, there has only been two studies that have used pea protein particles to prepare Pickering emulsions (Liang and Tang, 2014a, Shao and Tang, 2015). Furthermore, these two studies have been performed using pea protein gelation at just one particular pH (pH 3.0), thus restricting the use of such emulsions over a wider range of pH and ionic strengths. To our knowledge, there has been no study that has systematically characterized the colloidal properties of thermally-crosslinked pea protein microgel in the aqueous phase, as well as when present at the droplet surface, and in particular also investigated the role of electrostatics on the colloidal behaviour of these types of emulsions. Considering the recent demand of plant-based protein particles, it is necessary to characterise the ability of such Pickering emulsions at a wide range of pH and ionic strengths to understand their responsiveness to

environmental conditions during their processing and indeed after consumption.

Hence, in this study, pea protein has been used to design pea protein microgels (PPM) using a top down approach for creating a heat-set hydrogel, followed by controlled shearing to investigate their potential to stabilize O/W Pickering emulsions, which has not been reported in literature to date. We hypothesized that pea protein microgel already adsorbed to the interface would aggregate at the droplet surface by suitably adjusting the pH to acidic pH, forming a densely packed layer of particles further protecting the oil droplets against coalescence. Colloidal stability of pea protein microgel particles (PPM) in aqueous phase and PPM-stabilized emulsions were systematically characterized as a function of pH (pH 2.0-9.0) and ionic strength (1-250 mM NaCl) using particle sizing (dynamic light scattering), droplet sizing (static light scattering), optical microscopy, confocal laser scanning microscopy (two dimensional (2D) as well as three dimensional (3D) images), apparent viscosity, adsorption efficiency assessment and ζ -potential measurements. The composition of PPM at the interface was assessed using sodium dodecyl sulphate polyacrylamide gel electrophoresis (SDS-PAGE). In addition, we calculated the interaction potentials of the particles as a function of pH and ionic strengths at close separation distances to identify the electrostatic contribution of these particles at the droplet surface during any droplet aggregation phenomena.

3.2 Materials and Methods

3.2.1 Materials

Commercial pea protein isolate (Nutralys S85XF) (PPI) with 85% protein content was kindly gifted by Roquette (Lestrem, France). Sunflower oil was purchased from local supermarket and used without any further purification. Mini-PROTEAN TGX Gels, ProtoBlue Safe Colloidal Coomassie G-250 stain and all sodium dodecyl sulphate polyacrylamide gel electrophoresis (SDS-PAGE) chemicals were purchased from Bio-Rad Laboratories, UK. Sodium

azide, Nile Red and Nile Blue were purchased from Sigma Aldrich (Dorset, UK). All other chemicals were of analytical grade and purchased from Sigma-Aldrich Dorset, UK) unless otherwise specified. All solutions were prepared with Milli-Q water (water purified by a Milli-Q apparatus, Millipore Corp., Bedford, MA, USA) with a resistivity of 18.2 M Ω cm at 25 °C.

3.2.2 Methods

3.2.2.1. Preparation of pea protein microgel (PPM)

Pea protein-based Pickering particles were prepared using slight modification of the top-down method developed by Sarkar et al. (2016c). Briefly, the PPI powder at 15 wt% powder *i.e.* 12.75 wt% protein was dispersed in 20 mM phosphate buffer at pH 7.0. The aqueous dispersion of PPI was mixed for 2 hours using magnetic stirring at 300 rpm, and then stored at 4 °C overnight. The PPI dispersion was heated at 90 °C for 1 hour to allow formation of heat-set gel (**Figure 3.1**). During heat treatment, the globular pea proteins were denatured and unfolded (Laguna et al., 2017b). And then the denatured proteins aggregated *via* the disulphide crosslinking forming a macroscopic protein-based hydrogel. After cooling to room temperature using flowing water at 25 °C, the pea protein hydrogel was stored at 4 °C overnight. These hydrogels were mixed with 20 mM phosphate buffer (1: 1 v/v) at pH 7.0 and were broken to macrogel particles using a blender (HB711M, Kenwood, UK) at speed 3 for 5 minutes. After removing the air bubbles generated during blending using vacuum (25-30 bar) for 15 min, the macroscopic gel particle dispersion was homogenized using two passes through a two-stage valve homogenizer (Panda Plus 2000, GEA Niro Soavi Homogeneizador Parma, Italy) operating at first/ second stage pressures of 250/ 50 bars, respectively. The resultant particles, termed as pea protein microgels (PPM) contained 6.375 wt% protein.

3.2.2.2 Preparation of PPM-stabilized Pickering emulsions (PPM-E)

Sunflower oil was mixed with appropriate quantities of PPM at 20:80 oil: protein (w/w) ratio using rotor-stator (L5M-A, Silverson machines, UK) mixing

at 8,000 rpm for 5 minutes. The PPM dispersion was diluted using phosphate buffer to have 0.05, 0.10, 0.25, 0.50 and 1.0 wt% protein content in the final emulsions, henceforth, such emulsions are referred as E0.05, E0.1, E0.25, E0.5 and E1.0, respectively. The pre-homogenized oil-PPM mixture was further homogenized by a two-stage valve homogenizer (Panda Plus 2000, GEA Niro Soavi Homogeneizador Parma, Italy) operating at two stages, of 250 and 50 bar pressures (**Figure 3.1**) resulting in Pickering emulsions (PPM-E, E0.05-E1.0). Sodium azide (0.02 wt%) was added as an antimicrobial agent.

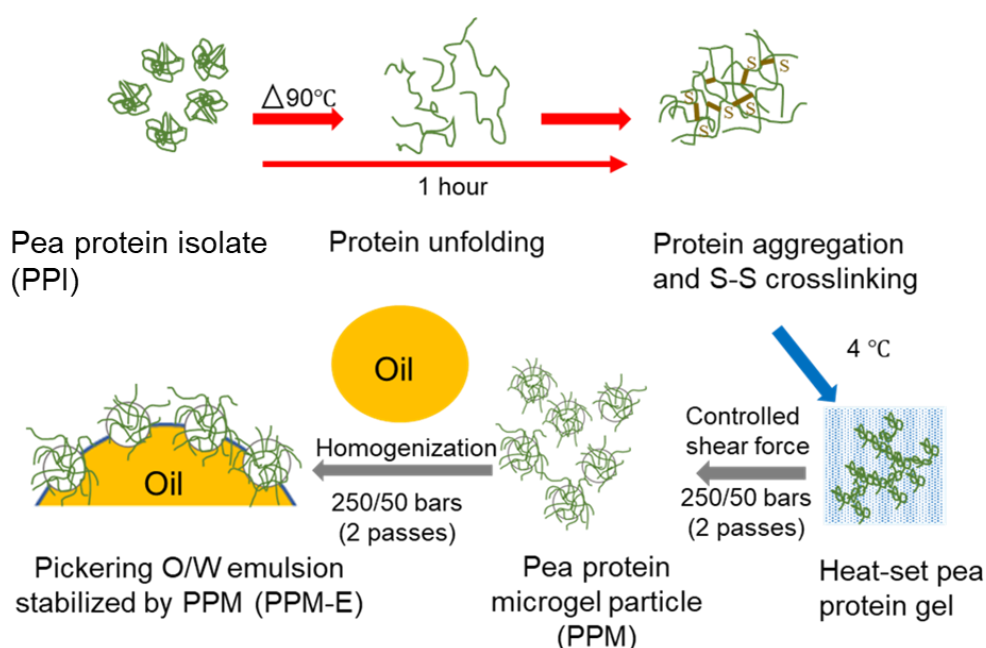


Figure 3.1. Schematic flow diagram for preparation of pea protein microgel particles (PPM) and O/W Pickering emulsion (PPM-E).

3.2.2.3 Coalescence stability of PPM-E during storage

The PPM-Es (E0.05, E0.10, E0.25, E0.50 and E1.0) were stored at 4°C for a period of 28 days and were monitored using droplet sizing, ζ -potential measurement and visual observation to select the most stable emulsions for pH and ion treatment.

3.2.2.4 pH and ion treatment

To investigate the colloidal stability of PPM and PPM-E (E1.0, chosen based on the coalescence stability study) under environmental conditions, the samples were subjected to different pH and ionic strengths. The pH adjustment (pH 2.0-9.0) was done by both “low to high” and “high to low” methods by adding 1 M HCl or 1 M NaOH, without any salt addition (Adal et al., 2017). For “high to low” pH adjustment, the PPM at pH 9.0 was rapidly adjusted to a target pH while mixing. For “low to high”, the PPM at pH 2.0 was adjusted to a target pH quickly while mixing. In case of E1.0, the pH responsiveness was checked at pH 3.0, 5.0 and 7.0. For ionic strengths, the pH value of PPM was kept constant at pH 7.0 and ionic strength was adjusted from 1-250 mM NaCl. For E1.0, the physicochemical stability was assessed by subjecting the emulsions to 1 mM, 10 mM and 100 mM NaCl, respectively.

3.2.2.5 Size and ζ -potential measurements

The hydrodynamic diameters of PPM dispersion at various pH and ionic strengths were measured at 25 °C using a Zetasizer Nano-ZS (Malvern Instruments Ltd, Malvern, Worcestershire, UK). The PPM sample was diluted to 0.004 wt% particle concentration with Milli-Q water before measurement. Assuming that there is no particle–particle interaction in the diluted sample, the hydrodynamic diameter (D_h) of the droplets was calculated using the Stokes–Einstein equation (3.1):

$$D_h = \frac{k_B T}{3\pi\eta D_t} \quad (3.1)$$

where D_t is the translational diffusion coefficient, k_B is Boltzmann’s constant, T is thermodynamic temperature, and η is dynamic viscosity. The refractive index of PPM was set at 1.52. The absorbance of the protein was assumed to be 0.001.

Droplet size distribution of PPM-Es (E0.05, E0.10, E0.25, E0.50 and E1.0) as a function of storage and E1.0 as a function of different pH or with various ionic strengths were determined using static light scattering (SLS) techniques using a Malvern MasterSizer 3000 (Malvern Instruments Ltd, Malvern, Worcestershire, UK) at 25 °C. Samples were added dropwise in distilled water until the instrument gave an obscuration rate between 4 and 6%. The average droplet size of the emulsion was reported as the volume mean diameter ($d_{43} = \frac{\sum n_i d_i^4}{\sum n_i d_i^3}$) and surface mean ($d_{32} = \frac{\sum n_i d_i^3}{\sum n_i d_i^2}$) where, n_i is the number of droplets with a diameter, d_i . The refractive index of sunflower oil and the dispersion medium were set at 1.46 and 1.33, respectively. The absorbance value of the emulsion droplets was set at 0.001.

Zetasizer Nano ZS was used to measure the ζ -potential of PPM dispersion, PPM-Es (E0.05, E0.10, E0.25, E0.50 and E1.0) as a function of storage and E1.0 as a function of pH and ionic strength. Before measurement, PPM dispersion at different pH values was diluted to 0.004 wt% particle concentration and E1.0 with different pH values was diluted to 0.005 wt% droplet concentration using Milli-Q water adjusted to relevant pH (2.0-9.0). Similarly, PPM or E1.0 containing different concentrations of NaCl was diluted Milli-Q water adjusted to relevant NaCl concentrations (1-250 mM). The diluted sample was then added into a folded capillary cell (DTS1070 cell, Malvern Instruments Ltd., Worcestershire, UK), which had two electrodes. After 120 seconds of equilibration in the Zetasizer at 25 °C, the PPM particles or E1.0 droplets moved towards oppositely charged electrodes. The magnitude of ζ -potential was determined from the terminal speed of the particle motion using Henry's equation, with Smoluchowski approximation appropriate here since the thickness of the diffused double layer is expected to be much smaller than the size of the particles.

3.2.2.6 Adsorption efficiency of PPM at the oil-water interface

To determine the adsorption efficiency of PPM at the oil-water interface after pH-treatment (adjusting the pH of PPM-E to pH 3.0, 5.0 and 7.0) or salt-treatment (100 mM NaCl), the quantity of PPM in the emulsion phase was

determined (Araiza-Calahorra and Sarkar, 2019b, Sarkar et al., 2016c). Briefly, PPM-E (E1.0) at different pHs (pH 3.0, 5.0 and 7.0) and ionic strength (100 mM NaCl) were diluted (1:4 w/w) with phosphate buffer (pH 7.0) or Milli-Q water (adjusted to pH 5.0 or pH 3.0) or phosphate buffer at H 7.0 containing 100 mM NaCl. All diluted emulsions were centrifuged for 40 mins at 10,000 rpm, 20 °C (Fresco 21 centrifuge, Thermo Fisher Scientific, Germany). The subnatants were carefully collected using a syringe and then measured using a DC protein assay kit (Bio-Rad Laboratories, Hercules, CA) on UV-Vis Spectrophotometer with an adsorption wavelength of 750 nm. The adsorption efficiency of PPM at the interface was calculated by subtracting the amount of PPM in the subnatant from the total amount of PPM used initially to prepare the emulsions as a percentage of total protein concentration in the emulsion.

3.2.2.7 Apparent viscosity measurement

The apparent viscosity of PPM-E (E1.0) as a function of pH and ionic strength were determined at 25 °C using a Kinexus ultra rheometer (Malvern Instruments Ltd, Malvern, UK). The apparent viscosities (η_a , Pa s) were recorded as a function of shear rates ranging from 0.1 to 1000 s⁻¹. All measurements were done in triplicates and were reported as the mean and standard deviation. In order to determine the flow type the emulsions as a function of pH and ionic strength, the flow curves were fitted using power-law model (Ostwald-de Waele model) (see Equation (3.2)):

$$\eta_a(\dot{\gamma}) = K(\dot{\gamma})^{n-1} \quad (3.2)$$

where, K is consistency coefficient (Pa sⁿ), n is power-law index and $\dot{\gamma}$ is shear rate (s⁻¹).

3.2.2.8 Microscopy

Optical microscopy (Nikon, SMZ-2T, Japan) was used to observe the microstructure of PPM and E1.0 as a function of pH and ionic strengths. The samples undergoing optical microscopy needed to be diluted 10 times in respective buffer. Zeiss confocal microscope (Model LSM 700, Carl Zeiss MicroImaging GmbH, Jena, Germany) was used for microstructural characterization of PPM at the interface of E1.0 droplets. The oil droplets in E1.0 were stained with 100 μL of Nile Red (2% w/v in dimethyl sulfoxide) and the protein stabilizing the oil droplets was stained with 500 μL of Nile Blue (10% w/v in Milli-Q water). Nile Red was excited by at 488 nm whereas Nile Blue was excited at 635 nm. The stained samples were mixed with an appropriate amount of xanthan gum (1 wt %) to reduce the Brownian motion of oil droplets. The prepared samples were placed onto a microscope slide, covered with a cover slip and observed at $63\times$ (oil) magnifications.

3.2.2.9 Sodium dodecyl sulphate-polyacrylamide gel electrophoresis (SDS-PAGE)

Sodium dodecyl sulphate polyacrylamide gel electrophoresis (SDS-PAGE) under reducing conditions was used to determine the composition of protein in the initial pea protein solution, PPM dispersions and the adsorbed phase of PPM-E (E1.0). The samples included PPM dispersions that are pH-treated (adjusting the pH of PPM to pH 3.0, 5.0 and 7.0) and salt-treated (100 mM NaCl) PPM dispersions as well as PPM-E (E1.0) at different pHs (pH 3.0, 5.0 and 7.0) and ionic strength (100 mM NaCl). To determine the protein compositions of adsorbed phase *i.e.* the particles at the interface, all the PPM-E samples after pH and ionic treatments were centrifuged at 14,500 g for 45 min, and then the cream phases were carefully collected, dispersed in Milli-Q water and centrifuged again for 45 min at 14,500 g . Approximately, 65 μL of pea protein dispersion, PPM samples and cream layer of PPM-E (E1.0) samples were mixed with 25 μL of SDS loading buffer (62.5 mM Tris-HCl, pH 6.8, 2% SDS, 25% glycerol, 0.01% bromophenol blue) and 10 μL of dithiothreitol (DTT, of a final concentration of 50 mM), heated at 95 $^{\circ}\text{C}$ for 5 min. The SDS-PAGE was carried out by loading 5 μL of protein marker

and 10 μL of these samples-SDS buffer mixtures in the Mini-PROTEAN 8-10% TGX Gels in a Mini-PROTEAN II electrophoretic unit Bio-Rad Laboratories, Richmond, CA, USA). The resolving gel contained 16% acrylamide and the stacking gel was made up of 4% acrylamide.

The running process had two stages; one at 100 V for 10 min at first stage and then 200 V of about 20 min for the second stage. After the run, the gel was stained for 2 hours using Coomassie Blue solution, which consisted of 90% ProtoBlue Safe Colloidal Coomassie G-250 stain and 10% ethanol. The gel was then destained using Milli-Q water overnight and scanned using the ChemiDoc™ XRS+ with image Lab™ Software (Bio- Rad Laboratories, Inc, USA). Each band within the lanes was selected automatically by the software to cover the whole band. Background intensity was subtracted after scanning an empty lane. The SDS-PAGE experiments were carried out in triplicates and band intensities was reported as an average and standard deviation of three reported readings.

3.2.2.10 Statistical analysis

All experimental results were reported as mean and standard deviations of five measurements on triplicate samples ($n = 5 \times 3$). The statistical analyses were conducted using one-way ANOVA and multiple comparison test using SPSS software (IBM, SPSS statistics, version 24) and the significant difference between samples were considered when $p < 0.05$.

3.3 Results and Discussion

3.3.1 Characteristics of aqueous dispersion of PPM

The aqueous dispersion of PPM in phosphate buffer at pH 7.0 had a narrow size distribution with single peak in the size range of 100 to 1000 nm (**Figure 3.2**). The PPM had a hydrodynamic diameter (D_h) of about 232 nm (polydispersity index (PDI) < 0.2) (**Figure 3.3a**). Although an aqueous dispersion of PPI showed multimodal size distribution with high PDI of nearly 1.0 (data not shown), preparing PPM *via* the top-down approach of heat-set gel formation and controlled shearing appears as a feasible approach to create plant protein-based particles with high colloidal stability. For instance, the PPM

were highly negatively charged (-40 mV) (**Figure 3.3b**) showing no particle aggregation or macroscopic sedimentation (**Figure 3.3c**) at pH 7.0, respectively over a year storage.

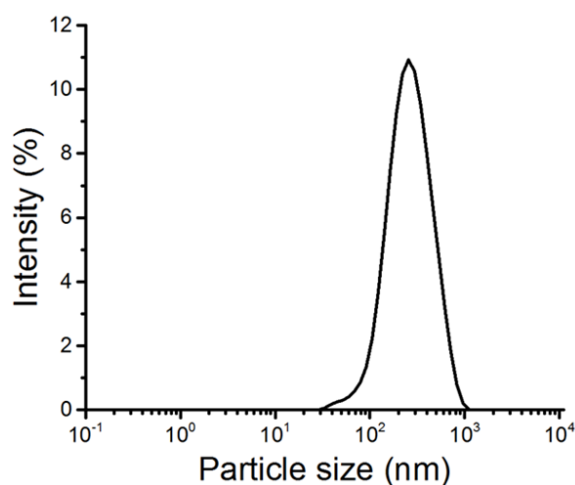


Figure 3.2. Particle size distribution of pea protein microgel particles (PPM) at pH 7.0.

3.3.2 Colloidal stability of aqueous dispersions of PPM

As shown in **Figure 3.3a**, D_h of PPM ranged from 200 to 400 nm at neutral to alkaline pH (pH 7.0 to pH 9.0) ($p > 0.05$). However, at pH 6.0, PPM showed a marked increase in D_h supported by correspondingly steep increase in PDI to 0.8 as compared to that at neutral pH ($p < 0.05$). The D_h of PPM dispersions increased to the highest values of $> 8,000$ nm at pH 5.0 followed by a decrease to $< 2,000$ nm at $3.0 < \text{pH} < 5.0$ (**Figure 3.3a**). High degree of particle aggregation and sedimentation observed using optical microscopy and macroscopic images, respectively, indicate pH 5.0 to be the isoelectric point (pI) (**Figure 3.3c**). Caution should be exercised while interpreting these D_h results with values above 1000 nm, when using dynamic light scattering (**Supplementary Figure S3-1**). Thus, focusing on the trend of increasing values of D_h , the colloidal stability of aqueous dispersions of PPM was limited at pH 6.0 with high PDI (**Figure 3.3a**) and excessive particle aggregation (**Figure 3.3c**).

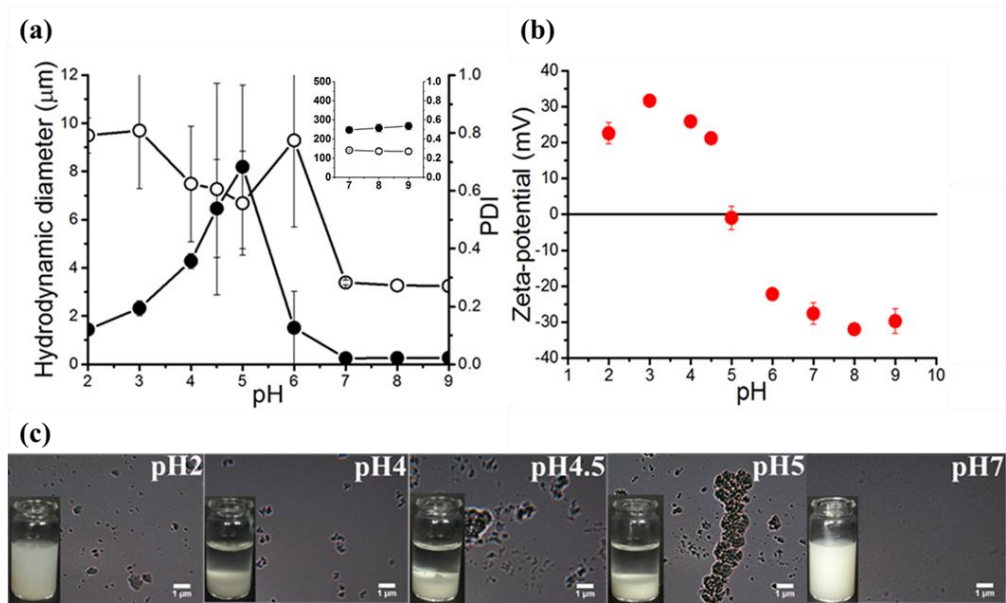


Figure 3.3. Influences of pH on hydrodynamic diameter (●) and polydispersity index (PDI) (○) (a), ζ -potential (●) (b), and optical microscopic images (scale bar of 1.0 μm) (c), respectively. Error bars represent standard deviations.

The colloidal behaviour of PPM as a function of pH was investigated using ζ -potential measurements of PPM (**Figure 3.3b**). The ζ -potential of PPM increased from -40 mV to +30 mV with pH change, from pH 9.0 to pH 2.0 ($p < 0.05$). Noticeably, the net surface charge was close to zero at pH 5.0 (**Figure 3.3b**) validating this to be the pI, corroborating with the largest hydrodynamic diameter and PDI (almost close to 1.0) data (**Figure 3.3a**). At this pH, the positively-charged amino-groups in PPM were balancing the negatively-charged carboxyl groups. Interestingly, the pI of PPM (**Figure 3.3b**) shifted slightly from that of the PPI, where latter is reported to be around 4.0 (Adal et al., 2017). Such discrepancy in pI values between protein concentrates and protein microgel particles are possible owing to the unfolding process during thermal treatment of the latter and consequently exposure of some charged groups. At or below pH 4.0, PPM showed net positive charge ranging from +20 to +30 mV. An interesting study by Destribats et al. (2014a) demonstrated that in whey protein microgel particles (WPM), some larger particle were present even when the pH value was far from the pI and the particles possessed electrostatic charge. The larger particles were postulated to be associated with the swelling of WPM *i.e.* the solvation of the exposed protein groups enabling WPM to swell. Nevertheless, in the present study even if some degree of

swelling of PPM might have occurred, due to the solvation of the protein groups that was promoted at acidic pH, such effects have been overshadowed by the dominant particle aggregation as observed in **Figure 3.3c**.

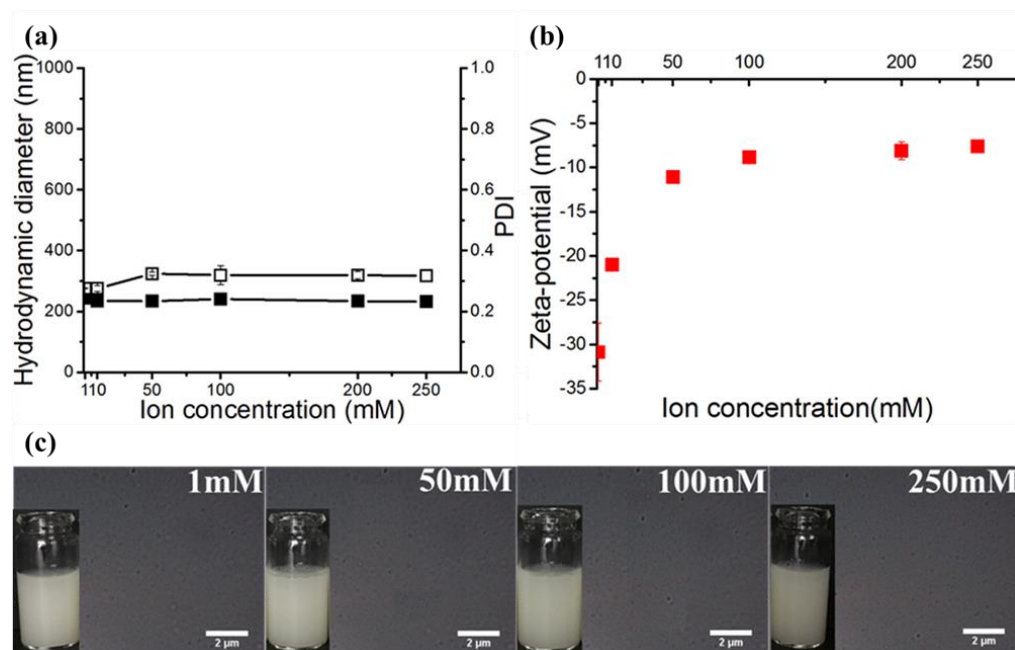


Figure 3.4. Influences of ionic strength on hydrodynamic diameter (■) and polydispersity index (PDI) (□) (a), ζ -potential (■), and optical images (scale bar of 2.0 μm) (c), respectively. Error bars represent standard deviations.

It is worth noting that the PPM in presence of electrolytes showed no significant difference in D_h and PDI (**Figure 3.4a**) as a function of ionic strengths. This was in close agreement with no aggregation or sedimentation observed in optical microscopy or macroscopic images (**Figure 3.4c**). However, a progressive decrease of ζ -potential magnitude from -31 to -7.5 mV was observed (**Figure 3.4b**) as the ionic strength increased from 1 to 250 mM NaCl. Similar salt-induced reduction in ζ -potential in plant protein-based particles has been observed in the case of soy protein-based nanoparticles, where Liu and Tang (2013) demonstrated that the increasing NaCl concentration (0-500 mM) led to the decrease of absolute magnitude of ζ -potential of soy protein nanoparticles. This is due to a decreased Debye length which for constant charged surfaces at any rate will lead to a lower ζ -potential.

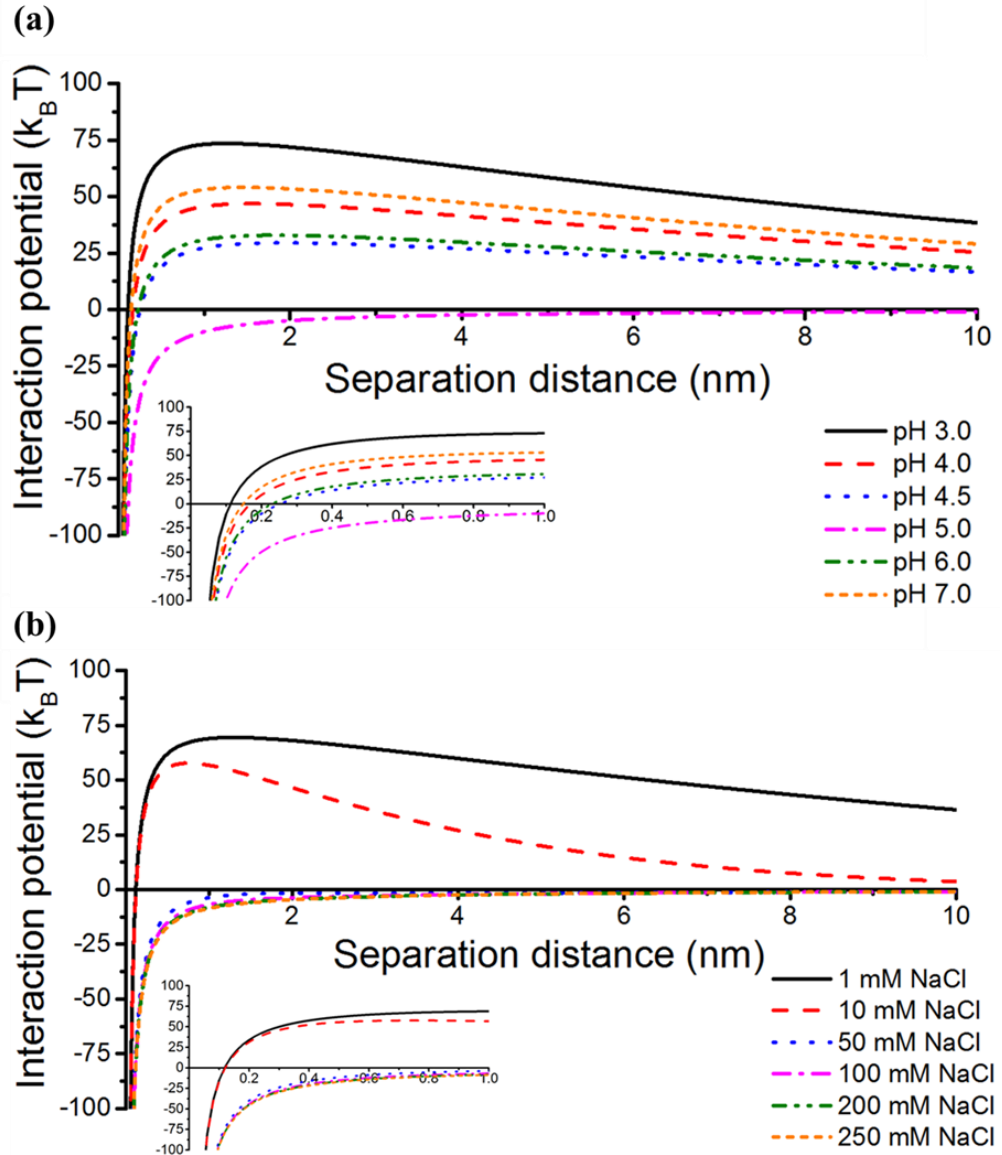


Figure 3.5. Total interaction potential ($U/k_B T$) of PPM at various pH (a) and at different ionic strengths (b), calculated as a function of separation distance (h).

Colloidal particles, such as PPM in this study, dispersed in aqueous solutions will experience Derjaguin-Landau-Verwey-Overbeek (DLVO) forces, other types of short-ranged, attractive non-DLVO forces (Hogg et al., 1966) as well as possible steric repulsion. To understand the role of interaction in the colloidal stability of PPM, we used DLVO theory to calculate the inter-particle electrostatic-mediated activation energy barrier between sub-micron sized PPMs, as two such particles approach each other at varying pHs and ionic strengths (**Figure 3.5**). This is done using equation (3.3) (Cosgrove, 2010):

$$U_R = 2\pi\epsilon\psi^2 a \ln[1 + \exp(-kh)] \quad (3.3)$$

for the electrostatic component of particle-particle interaction. For equation (3.3), ϵ is the permittivity of the system, *i.e.* $\epsilon_0\epsilon_r$ (ϵ_0 is the permittivity of vacuum, and ϵ_r is relative permittivity of water), ψ is the surface potential approximately equal to the ζ -potential values measured at different pHs or ionic strengths, a is the radius of PPM particle (*i.e.* 118 nm), h is the particle-particle surface separation distance ranging from 0.1 to 5 nm and κ^{-1} is the Debye length, which was calculated from equation (3.4):

$$\kappa = \left[\frac{N_A e^2}{\epsilon k T} \sum_i z_i^2 c_i^\infty \right]^{\frac{1}{2}} \quad (3.4)$$

Here, z_i is the valency of i^{th} type of ion, c_i^∞ is the number density of that ion, N_A is the Avogadro's number, and T is the temperature (298 K).

The total interaction potential (U) between PPMs is the summation of electrostatic repulsion (U_R) and van der Waals attraction (U_{VW}). In this calculation, the pH independent van der Waals attractive energy (U_{VW}) between two equal sized PPM was calculated using equation (3.5):

$$U_{VW} = -\frac{aA_H}{12h} \quad (3.5)$$

where, A_H is the Hamaker constant which has been assumed to be $1 k_B T$, similar to other reported protein particles (Tuinier and De Kruif, 2002).

The total interaction potential was higher than $100 k_B T$ at pHs < 3.0 and pHs > 6.0 (**Figure 3.5a**), suggesting an electrostatically-induced energy barrier being sufficient to slow down any aggregation to negligible rates (see **Supplementary Figure S3-2a** for electrostatic repulsion). However, the van der Waal's attractive forces particularly for PPM in the acidic pH *i.e.* pH 2.0-4.5 played a dominant role when at close PPM-PPM separation distance (< 0.15

nm). This caused the total energy maximum to fall below $\sim 10 k_B T$ (**Figure 3.5a**), in line with high D_h , high PDI (**Figure 3.3a**) and extensive particle aggregation (**Figure 3.3c**). The ζ -potential of PPM reflected minimal surface charge (almost close to zero, **Figure 3.3b**) at pH 5.0 and the correspondingly lack of sufficient electrostatic repulsion barrier, to provide a large energy in the presence of strong van der Waal's attraction (**Figure 3.5a**). A low energy barrier accelerated the aggregation of the particles (**Figures 3.3a** and **3.3c**).

The U_R and U_{VW} between PPMs with varying ionic strengths were also calculated using equations (3.3-3.5), as shown in **Figure 3.5b** (see **Supplementary Figure S3-2b** for U_R and U_{VW}). Interestingly, at 1-10 mM NaCl, the interaction was mainly dominated by electrostatic repulsive forces with PPM-PPM interaction potential of $> 100 k_B T$ overshadowing effects of van der Waal's attractive forces (**Figure 3.5b**) over most separation distances. As expected, the electrostatic repulsion between particles was screened, down to nearly zero, with the increase in the NaCl concentration (**Figure 3.5b**). Once the salt concentration was above 50 mM, the dominating van der Waal's attractive forces between PPMs should result in particle aggregation, leading to an unstable dispersion. However, this was not the case experimentally. In fact, larger particle aggregates were not observed (**Figure 3.4c**), and the size of PPM was stable at a range of 230 to 240 nm, with lower PDI values (**Figures 3.4a**). The possible explanation for the discrepancy between the theoretically predicted aggregation and an experientially observed stable dispersion might be attributed to the steric repulsion effects associated with the hairy PPM particles, which is not strongly influenced by electrolyte concentration. This requires experimental investigation in the future. This behaviour is unlike that of WPM, soy protein nanoparticles, zein colloid particles and kafirin nanoparticles (de Folter et al., 2012, Destribats et al., 2014a, Liu and Tang, 2013, Xiao et al., 2016a), where NaCl addition is known to cause aggregation of particles in the aqueous dispersions.

3.3.3 Characteristics of Pickering O/W emulsions stabilized by PPM (PPM-E)

3.3.3.1 Stability of PPM-E prepared using various concentration of PPM

To determine the optimum concentration of PPM to stabilize PPM-E, coalescence stability of PPM-Es stored under refrigerated conditions for a period of 28 days were characterized using size, charge and visual imaging of any oiling off. **Table 3.1** shows the emulsion droplet size and ζ -potential, and **Figure 3.7** presents the corresponding visual images of the freshly prepared PPM-Es (E0.50-1.0) after 7, 14 and 28 days storage, respectively, at 4 °C. The cream layer was evident in all the freshly prepared emulsions (E0.05-0.5), except in E1.0 (**Figure 3.7**), however, all the emulsions reverted back to a homogenous dispersion after gentle hand shaking without any visual evidence for coalescence. After a week of storage, although no phase separation was discernible in E0.05 and E0.1 macroscopically (**Figure 3.7**), larger oil droplets were visible after diluting the emulsions with buffer (**Supplementary Figure S3-3**) with clear signs of coalescence and hence the size and ζ -potential could not be measured (**Table 3.1**) in these emulsions. This is expected as the insufficient quantities of PPM in E0.05 and E0.1 prevented sufficient particle coverage to enable stabilization of the large surface area of such high fraction of oil droplets (20 wt%). The network formed by PPM in continuous phase appears to encapsulate the oil droplets, and this prevented the macroscopic oil phase separation (**Figure 3.7**).

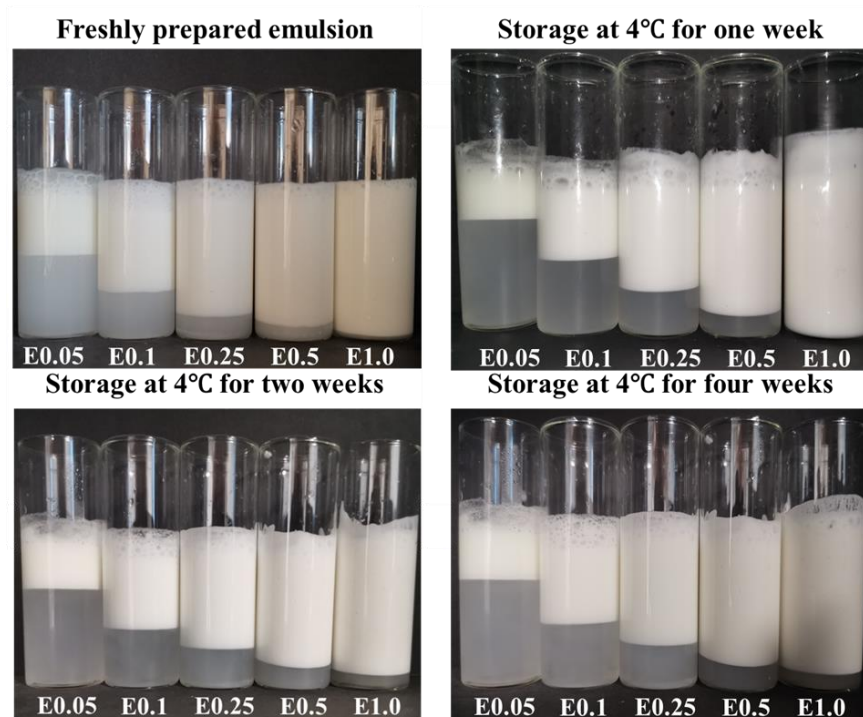


Figure 3.6. Visual images of storage stability of Pickering emulsions stabilized by 0.05-1.0 wt% PPM (E0.05-E1.0) during 28 days of storage at 4 °C.

The remaining three emulsions (E0.25, E0.5 and E1.0) did not show any coalescence upon dilution within the first week of storage (**Supplementary Figure S3-3**) and the ζ -potential values ranging from -38 to -41 mV (**Table 3.1**) indicated that the droplets had high net negative surface charge providing sufficient electrostatic stability to the droplets. After two weeks of storage, emulsions E0.25 and E0.5 showed an increase in droplet size ($p < 0.05$), however, no change in droplet size was observed in the case of E1.0 ($p > 0.05$) (**Table 3.1**). This was associated with decreasing values of ζ -potential for E0.25 and E0.5 ($p < 0.05$) and no significant change in ζ -potential value in the case of E1.0 ($p > 0.05$) over time (**Table 3.1**). More importantly, after storage over a month, oil droplets were detected in the diluted E0.25 and E0.5 emulsions (**Supplementary Figure S3-3**). There was no significant difference in droplet size and ζ -potential of emulsion E1.0 over this 28 day storage period ($p > 0.05$), which is also in line with results of other Pickering emulsions, where 1 wt% of particles were needed to provide sufficient surface coverage of the droplets (Araiza-Calahorra and Sarkar, 2019b, Du Le et al., 2020). In summary, 1.0 wt% PPM was sufficient to create small-sized ($d_{43} \sim 25 \mu\text{m}$) stable droplets that showed excellent resilience against coalescence (E1.0). Hence, hereafter, 1 wt

Table 3.1. Mean droplet size and zeta-potential of PPM-stabilized Pickering emulsions prepared using different concentrations of PPM (0.05-1.0 wt%) during 28 days of storage at 4 °C.

PPM concentration (wt%)	Emulsion characteristics	E0.05	E0.10	E0.25	E0.5	E1.0
Freshly prepared emulsions	d_{32} (μm)	13.3 ± 0.62 ^a	7.0 ± 0.7 ^b	4.2 ± 0.17 ^c	3.5 ± 0.37 ^d	2.8 ± 0.14 ^d
	d_{43} (μm)	53.6 ± 5.07 ^{ac}	51.9 ± 3.22 ^{ac}	49.8 ± 3.10 ^{ac}	32.5 ± 3.47 ^{ba}	24.6 ± 0.10 ^c
	ζ-potential (mV)	-36.1 ± 2.14 ^a	-36.4 ± 4.58 ^a	-36.8 ± 3.73 ^a	-37.3 ± 3.47 ^a	-40.9 ± 0.95 ^b
Day 07	d_{32} (μm)	-	-	9.06 ± 0.34 ^a	8.04 ± 0.17 ^b	3.21 ± 0.19 ^d
	d_{43} (μm)	-	-	45.14 ± 4.37 ^{ac}	44.4 ± 1.48 ^{ab}	24.57 ± 0.52 ^c
	ζ-potential (mV)	-	-	-36.46 ± 2.50 ^a	-37.13 ± 1.81 ^a	-40.8 ± 1.15 ^b
Day 14	d_{32} (μm)	-	-	9.87 ± 0.87 ^a	8.40 ± 0.14 ^b	5.59 ± 0.02 ^c
	d_{43} (μm)	-	-	50.54 ± 7.85 ^{ac}	49.08 ± 2.58 ^{ac}	25.00 ± 0.46 ^c
	ζ-potential (mV)	-	-	-30.44 ± 4.49 ^c	-36.68 ± 2.13 ^d	-40.78 ± 1.24 ^b
Day 28	d_{32} (μm)	-	-	-	-	6.39 ± 0.02 ^c
	d_{43} (μm)	-	-	-	-	24.9 ± 0.3 ^c
	ζ-potential (mV)	-	-	-	-	-39.96 ± 1.04 ^b

- Because of phase separation, measurement was not carried out.

Different superscripts (a-e) in the same row / column represent significant differences between different samples at $p < 0.05$ level.

Table 3.2. Mean droplet size and zeta-potential of PPM-stabilized Pickering emulsions (E1.0) as a function of pH and ionic strengths.

Emulsion characteristics	pH 7.0	pH 5.0	pH 3.0	1 mM NaCl	10 mM NaCl	100 mM NaCl
d_{32} (μm)	$2.8 \pm 0.14^{\text{a}}$	$4.2 \pm 0.14^{\text{b}}$	$3.2 \pm 0.10^{\text{c}}$	$2.9 \pm 0.04^{\text{a}}$	$2.9 \pm 0.02^{\text{a}}$	$3.1 \pm 0.26^{\text{a}}$
d_{43} (μm)	$24.6 \pm 0.10^{\text{a}}$	$24.5 \pm 0.90^{\text{a}}$	$24.3 \pm 0.43^{\text{a}}$	$24.8 \pm 0.93^{\text{a}}$	$23.0 \pm 2.20^{\text{a}}$	$24.5 \pm 1.19^{\text{a}}$
ζ -potential (mV)	$-40.9 \pm 0.95^{\text{a}}$	$-4.72 \pm 2.28^{\text{b}}$	$+41.5 \pm 0.09^{\text{c}}$	$-40.1 \pm 2.68^{\text{a}}$	$-28.1 \pm 2.04^{\text{d}}$	$-12.0 \pm 1.77^{\text{e}}$
Adsorption efficiency (%)	$98.5 \pm 0.2^{\text{a}}$	$99.2 \pm 0.01^{\text{b}}$	$98.7 \pm 0.03^{\text{a}}$	-	-	$98.7 \pm 0.01^{\text{a}}$

- Measurement was no carried out.

Different superscripts (a-e) in the same row represent significant differences between different samples at the $p < 0.05$ level.

PPM was chosen as the optimum concentration to create Pickering emulsions (E1.0) and test their response to pH and ionic strengths.

3.3.3.2 Composition of proteins in the adsorbed phase of E1.0

Compositions of PPI, PPM dispersions and the adsorbed phase of E1.0 were analysed by reduced SDS-PAGE to understand if there was any difference in composition of the protein subunits in bulk phase and those that were adsorbed at the interface in case of E1.0. The protein mixture in PPI or the laboratory-synthesized PPM had more than ten polypeptides (**Figure 3.6**) and the bands at range of 36-42 kDa had the highest proportion. The polypeptide composition of PPI or PPM was similar to those reported by Messian et al. (2015) and Peng et al. (2016) containing the three main proteins, legumin, vicilin and convicilin. Convicilin was the band at 66 kDa. Legumin is a globular protein with an acidic subunit ($L\alpha$) at about 42 kDa and basic subunit ($L\beta$) at 18- 24 kDa. Vicilin proteins consisted of three subunits (V_{i1-3}), which are respectively observed in fractions of around 50 kDa, 36-30 kDa and 20 kDa. Overall, SDS-PAGE results indicate that the formation of PPM from PPI involved all protein subunits, which is in accordance with results obtained previously that heat treatment did not affect the protein composition (Laguna et al., 2017b). In addition, the adsorbed phase of E1.0 showed similar molecular weight profiles to that of PPM that were not influenced by pH-treatment or exposure to ions. This suggests that adsorption or environmental stresses (pH or ions) applied to PPM had limited effect on the protein composition of the particles. In addition, a significant proportion of PPM did not enter the resolving gel and were retained in the stacking gel suggest that they were oligomers above 250 kDa. This suggests that DTT was not sufficient to break covalent disulphide bridges in the PPM effectively.

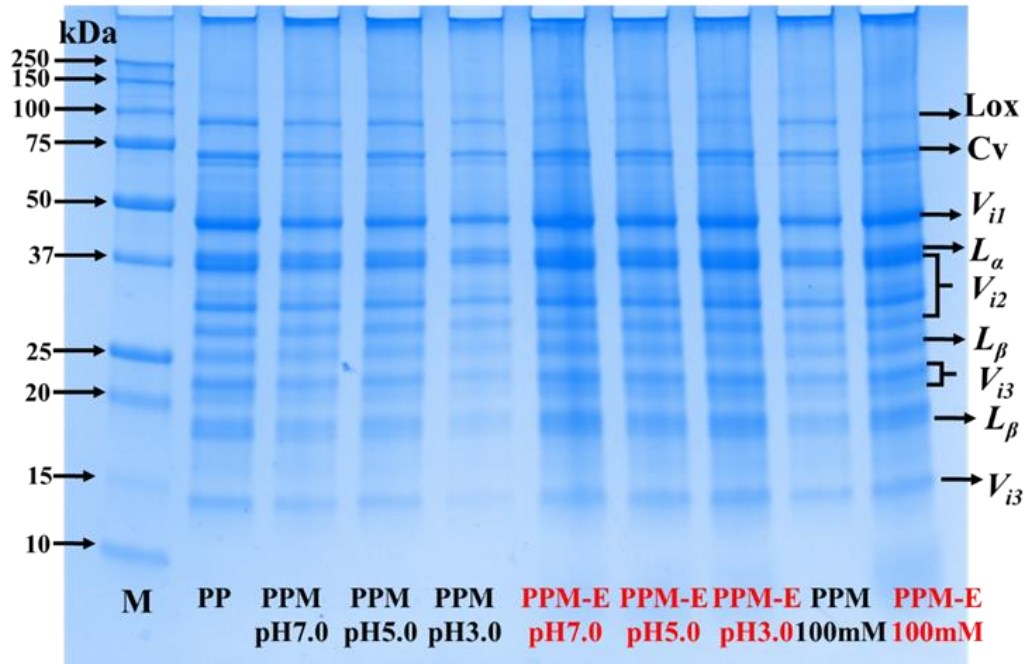


Figure 3.7. SDS-PAGE pattern of pea protein concentrate (PPI) dispersion, PPM dispersions and the adsorbed phase of PPM-E (E1.0), all containing 1 wt% pea protein. Lane M represents the protein marker of 80-250 kDa molecular weight range. The samples included PPM dispersions, PPM dispersions which are pH-treated (adjusting the pH of PPM to pH 3.0, 5.0 and 7.0) and salt-treated (100 mM NaCl), as well as the adsorbed phases of PPM-E (E1.0) at different pHs (pH 3.0, 5.0 and 7.0) and ionic strength (100 mM NaCl).

3.3.3.3 Influence of pH on behaviour of E1.0 droplets

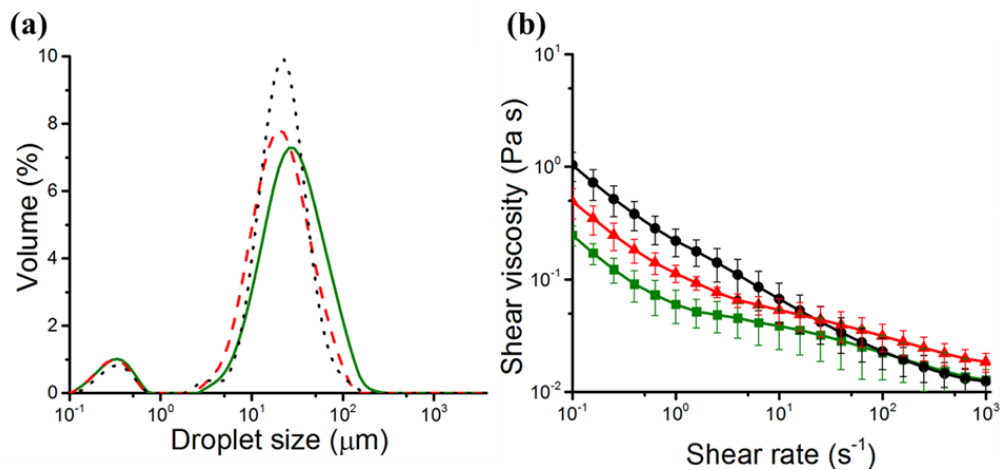


Figure 3.8. Mean droplet size distribution (a) of Pickering emulsions (E1.0) at pH 7.0 (green solid line), pH 5.0 (black dotted line) and pH 3.0 (red dashed line), respectively, and apparent viscosities (b) of PPM-E at pH 7.0 (green square), pH 5.0 (black circles) and pH 3.0 (red triangles) at shear rates from 0.1 to 1000 s⁻¹, respectively.

Figure 3.8a shows the mean droplet size distribution of E1.0 (20 wt% sunflower oil) as a function of pH (pH 3.0, pH 5.0 and pH 7.0) with corresponding Sauter mean diameter (d_{32}), De Brouckere mean diameter (d_{43}) and ζ -potential shown in **Table 3.2**. The initial E1.0 (pH 7.0) has a significantly larger proportion of droplets in the peak area of 10-100 μm . The smaller peak in the range of 0.1-1 μm as observed in **Figure 3.8a**, overlaps neatly with the size distribution of PPM estimated using dynamic light scattering (**Figure 3.2**), suggesting that these small particles in **Figure 3.8a** might be the free microgel particles that were not adsorbed to the droplet surface during the homogenization process (Sarkar et al., 2016c). Comparing the mean diameter of the PPM particles of ~ 230 nm (**Figure 3.3a**) and the mean size of the oil droplets (d_{43}) of ~ 25 μm (**Table 3.2**), the ratio of oil droplet size to PPM size ranges from 100:1 to 1000:1, which is a signature of a classical Pickering emulsion (Ettelaie and Lishchuk, 2015a, Sarkar et al., 2016c). The ζ -potential of E1.0 is about -41 mV (**Table 3.2**), similar to that of PPM (**Figure 3.3b**) at pH 7.0. This suggests that perhaps a monolayer of PPM might be present at the surface of droplets.

Interestingly, after adjusting the pH of E1.0 to pH 5.0 or pH 3.0, the d_{43} values were comparable to that of E1.0 at neutral pH ($p > 0.05$). However, d_{32} values of E1.0 at different pHs showed a significant difference ($p < 0.05$) (**Table 3.2**). This might be attributed to the fact that d_{32} value was more affected by the changes in free (unabsorbed) microgel peak as a function of pH as compared to d_{43} value, which is line with the behaviour of PPM in aqueous phase as observed in **Figure 3.3a**. The width of the peak at the range 10-100 μm in the droplet size distribution was narrower with a higher peak height at a lower pH (pH 3.0) than that seen for E1.0 at pH 7.0 (**Figure 3.8a**). Also, one might not expect such narrow droplet size distribution in E1.0, particularly at pH 5.0 considering it is the isoelectric point (pI) of PPM, where E1.0 droplets will also possess negligible surface charge (**Table 3.2**). This is a unique behaviour, unlike that observed in PPM in the aqueous phase (**Figures 3.3a and 3.3c**) as well as previous studies, where pH adjustment of emulsions stabilized by pea protein isolate to lower pH increased the emulsion droplet size and reduced the emulsion stability (Adebiyi and Aluko, 2011).

To understand the aggregation behaviour, the apparent viscosities of the emulsions (E1.0) at pH 7.0, pH 5.0 and pH 3.0 were determined using shear rate ranging from 0.1 to 1000 s⁻¹ (**Figure 3.8b**). The Ostwald de Waele model was applied to fit the flow curves and the corresponding fit parameters (consistency coefficient (K), flow index (n), regression coefficient (R^2)) were summarized in **Table 3.3**. The R^2 of all samples was ≥ 0.98 , confirming a good fit to the model. For E1.0 at different pH, n varied from 0.63 to 0.80, suggesting that E1.0 was a pseudoplastic fluid showing shear-thinning behaviour at all the tested pH values. Emulsions at pH 5.0 showed the highest K and the lowest n ($p < 0.05$) (**Table 3.3**). This is expected owing to strong inter-droplet flocculation in E1.0 at pI (pH 5.0) due to a reduction in electrostatic repulsive forces. Nevertheless, such aggregates were not strong and therefore possibly broken down by the shearing process during the static light scattering experiments and thus were not evident as a second peak in **Figure 3.8a**. Interestingly, at pH 3.0, the viscosity appeared to be higher than at pH 7.0 (**Figure 3.8b**), nevertheless, there was no significant difference ($p > 0.05$) in either K or n as compared to those at pH 7.0 ($p > 0.05$) (**Table 3.3**) suggesting that the droplet flocs that were broken down in the direction of shear were similar at pH 7.0 and pH 3.0.

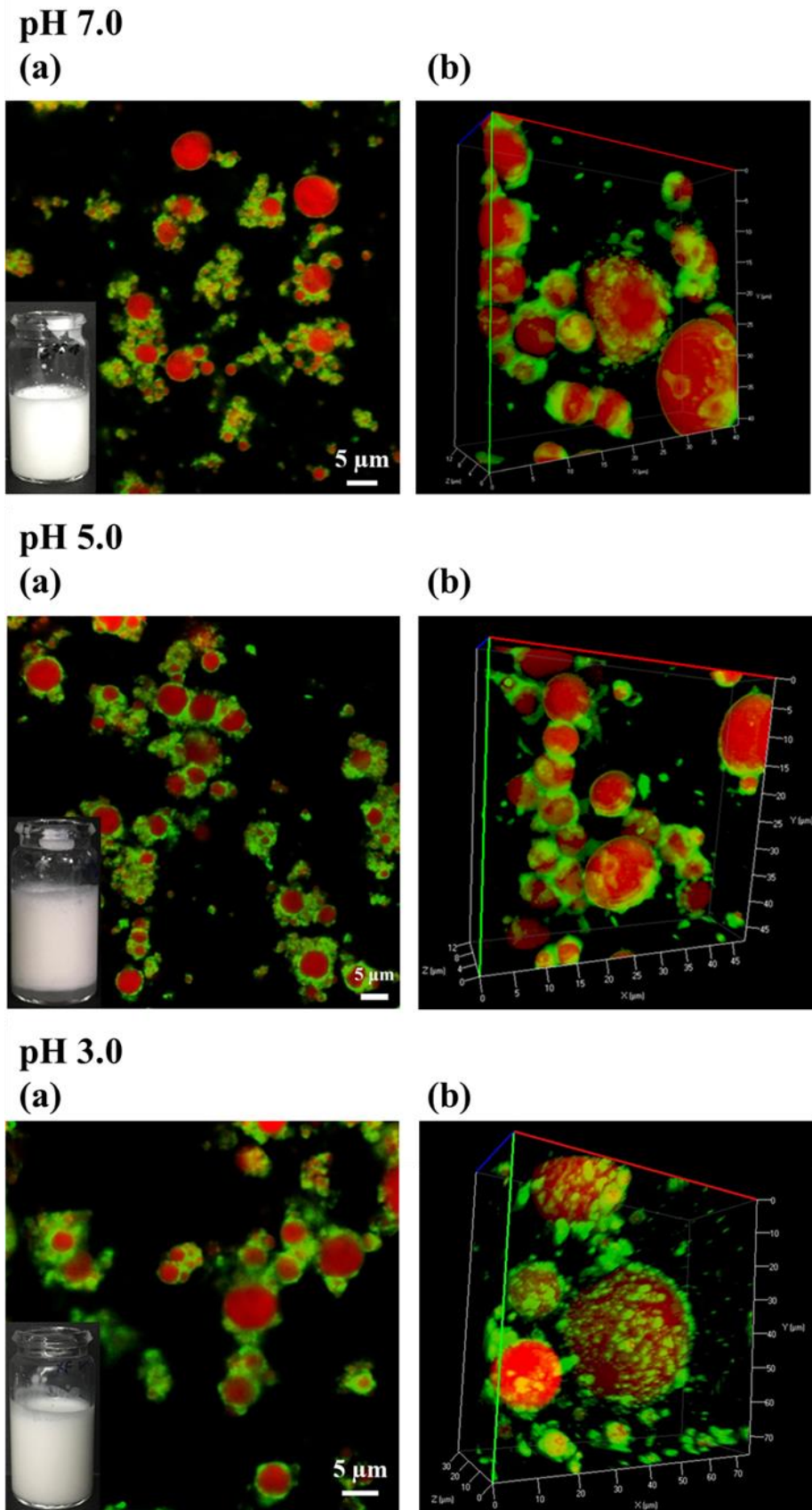


Figure 3.9. Confocal micrographs (2D, and 3D, b) of freshly prepared Pickering emulsions (E1.0) and insets of visual images of PPM-E (after 3 months storage) as a function of pH, respectively.

Visual images of E1.0 after 3 months of storage showed no distinct oil layers again confirming the ability of PPM to act as effective Pickering stabilizer (**Figure 3.9a**). Confocal laser scanning two-dimensional (2D) (**Figure 3.9a**) and three-dimensional (3D) (**Figure 3.9b**) micrographs revealed a thick layer of PPM (Nile Blue staining the protein microgels, displayed in green) adsorbed at oil-water interface (Nile Red staining the oil droplets, displayed in red), acting as a barrier to coalescence as observed visually. The confocal micrographs showed evidence of bridging flocculation as pH was reduced to pI (pH 5.0) with visual signs of creaming. This is in agreement with the higher viscosities and consequently higher consistency coefficients of the emulsions at pH 5.0 as compared to those at pH 7.0 and pH 3.0 ($p < 0.05$) (**Figure 3.8b**, **Table 3.3**). When the pH was adjusted to pH 3.0 (**Figure 3.9b**), the aggregation of adsorbed PPM at interface as well as bridging flocculation between the droplets were still evident. To understand whether the reduction of pH had an effect on PPM that were present at the interface, **Table 3.2** shows the adsorption efficiency of the PPM as a function of pH. The PPM had very high degree of adsorption (> 98%) to the droplet surface at all pH (**Table 3.2**), with slightly yet significantly higher adsorption at pH 5.0 as compared to those in pH 7.0 or pH 3.0 ($p < 0.05$). This is also evident visually from the images of the supernatant (**Supplementary Figure S3-4a**) after dilution and centrifugation of the emulsions suggesting that the majority of the PPM particles were either adsorbed at the droplet surface or somehow associated with interconnecting the neighbouring droplets in a PPM-PPM network. Overall, E1.0 maintained high stability to coalescence when the pH was adjusted from pH 7.0 down to pH 5.0 or pH 3.0, where the adsorbed PPM on the droplet surface increased aggregation as well as the PPM attached to neighbouring droplets.

Table 3.3. Consistency coefficient (K) and flow behaviour index (n) of PPM-stabilized Pickering emulsions (E1.0) at different pH and at ionic strengths.

Power-Law Model	<i>Ostwald de Waele fit for the apparent viscosity</i> (η_a)		R^2
	$\eta_a(\dot{\gamma}) = K(\dot{\gamma})^{n-1}$		
	n	K (Pa s ⁿ)	
pH 7.0 (E1.0)	0.80± 0.02 ^a	0.07± 0.005 ^a	0.982
pH 5.0	0.63± 0.01 ^b	0.13± 0.01 ^b	0.990
pH 3.0	0.80± 0.01 ^a	0.08± 0.003 ^a	0.993
1 mM NaCl at pH 7.0	0.80 ± 0.02 ^a	0.074 ± 0.005 ^a	0.982
10 mM NaCl at pH 7.0	0.81 ± 0.01 ^a	0.11 ± 0.008 ^a	0.969
100 mM NaCl at pH 7.0	0.67 ± 0.01 ^c	0.21 ± 0.09 ^c	0.999

Different superscripts (a-c) in the same column represent significant differences between different samples at $p < 0.05$ level.

3.3.3.4 Influence of background electrolyte concentration on behaviour of E1.0 droplets

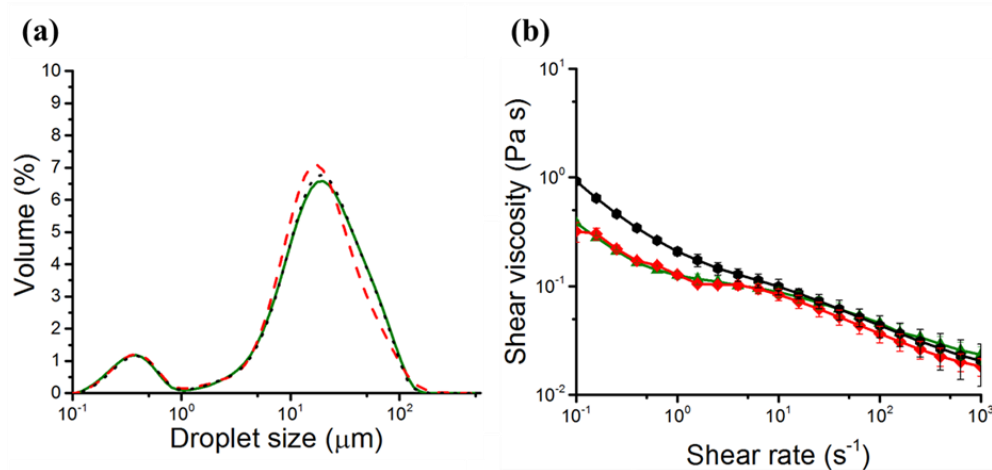


Figure 3.10. Mean droplet size distribution (a) of freshly prepared Pickering emulsions (E1.0) at 1 mM (green solid line), 10 mM (red dashed line) and 100 mM NaCl (black dotted line) respectively, and apparent viscosities (b) of E1.0 at 1 mM (green inverted triangle), 10 mM (red rhombus) and 100 mM NaCl (black hexagon) at shear rates from 0.1 to 1000 s⁻¹, respectively.

With the increase in ionic strength from 1 mM to 10 mM, the droplet size distribution (**Figure 3.10a**) and corresponding mean droplet diameters (d_{43} , d_{32}) (**Table 3.2**), showed no statistically significant differences ($p > 0.05$). Although the net surface potential of charged droplets became less negative (from -40 mV to -28 mV), the electrostatic repulsion was still sufficient to inhibit extensive flocculation in E1.0. The emulsions showed shear thinning behaviour irrespective of ionic strengths (**Figure 3.10b**). There was no significant difference between viscosities and the n values of these emulsions in the presence of 1 mM and 10 mM NaCl, especially in the region of 0.1-10 s⁻¹ shear rate ($p > 0.05$) (**Table 3.3**). Interestingly, the viscosity of emulsions in presence of 100 mM NaCl was higher than the other emulsions with consequently lower n value and higher K value ($p < 0.05$) (**Table 3.3**). The unaltered adsorption efficiency (**Table 3.2**, **Supplementary Figure S3-4b**) upon ion treatment (100 mM NaCl) and enhanced viscosity suggested inter-droplet flocculation in E1.0 with 100 mM NaCl, in line with lower net surface charge at the droplet surface (-12 mV) (**Table 3.2**). No oiling off or phase

separation were observed after rheology measurements, and even after an extended period of storage (**Figure 3.11**). Looking closely at confocal micrographs (**Figure 3.11**), droplet flocculation can be observed after addition of 100 mM NaCl corroborating with the bulk rheological measurements (**Figure 3.10b**). In a previous study, Pickering emulsions stabilized by kafirin nanoparticles showed a reduction in average droplet size on increasing ionic strength from 10 mM to 50 mM, which was mainly attributed to enhanced nanoparticle interaction *via* electrostatic screening effects. On the other hand, de Folter et al. (2012) suggested that Pickering emulsions stabilized by both positively- and negatively-charged zein particles at very high ionic strength (1 M) aggregated and exhibited an emulsion–gel phase. Comparing our results with these afore-mentioned plant protein-based Pickering emulsions, we hypothesize that a weak gel-like emulsion structure might have been formed which is apparent from the droplet aggregation observed in the confocal images (**Figure 3.11**). However, the structure of the O/W emulsion might not be as strong as that of a ‘true gel’, but may exhibit a small yield stress, which requires future rheological characterization.

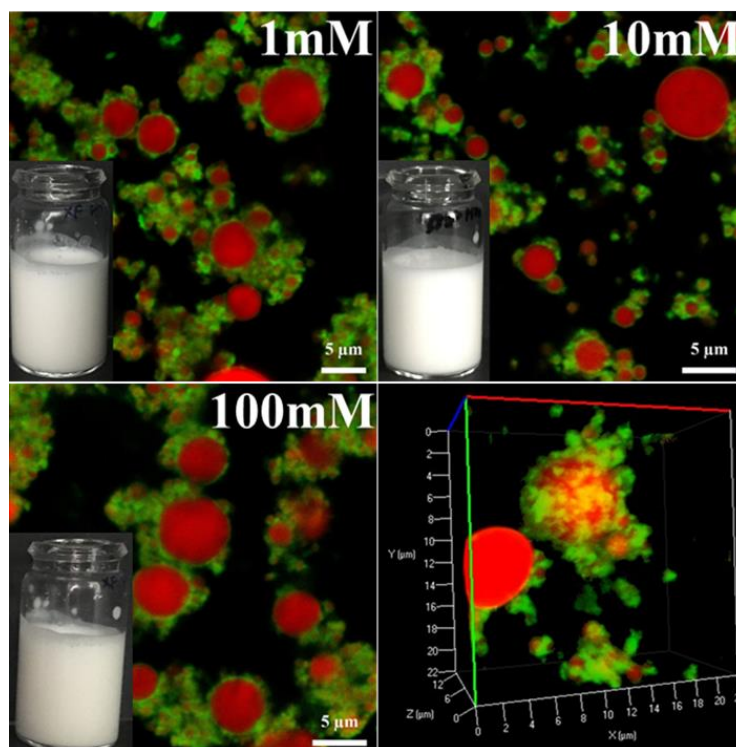


Figure 3.11. Confocal micrographs of freshly prepared Pickering emulsions (E1.0) with insets of visual images of PPM-E (after 3 months storage) at 1 mM, 10 mM and 100 mM NaCl, respectively. For the 100 mM NaCl, a 3D confocal micrograph is also shown in the right hand side of the corresponding 2D image.

3.4 Conclusions

Results from our research demonstrate the ability of a new class of plant protein particles *i.e.* pea protein microgels created using a facile top down approach to stabilize O/W Pickering emulsions with ultrastability against coalescence. To understand the characteristics of these Pickering O/W emulsion droplets as a function of microgel concentration, pH- or salt-treatment, the colloidal behaviour of pea protein microgel dispersions in aqueous phase was first investigated at various pH values (pH 2.0 to pH 9.0) or salt concentrations (1 to 250 mM NaCl) was investigated. Aqueous dispersions of pea protein microgels showed highest degree of particle aggregation at pH 5.0 as the activation energy barrier in particle-particle interaction potential was calculated to be extremely low at this pH. Meanwhile, high salt concentrations resulted in charge screening effects in PPM dispersion but the resulting reduction in electrostatic potential did not affect the hydrodynamic diameter of microgels, suggesting that other, possibly steric effects might also be playing a role in the colloidal stability of these particles. Interestingly, when the pea protein microgels were present at the oil-water interface, ultra-stable emulsion droplets were obtained only at microgels with 1.0 wt% protein concentration with all protein subunits *i.e.* legumin, vicillins and convicillins, being simultaneously present on the microgel-laden interface. The packed layer of PPM particles stabilizing the oil droplets allowed the emulsions to be stable over few months against coalescence. Upon pH reduction to pH 5.0, both intra-droplet and inter-droplet aggregation of PPM occurred resulting in higher adsorption efficiency and higher viscosity, respectively. The emulsions also showed responsiveness to ions, especially at 100 mM NaCl with enhancement in viscosity and shear-thinning character. To our knowledge, this is the first comprehensive study that has systematically demonstrated the role of electrostatics in the colloidal stability of the plant-based microgel particles in bulk phase versus particles adsorbed at the surface of the droplets. Findings from this comprehensive study might open door for applicability of these pea protein-based microgels in a range of food products and allied soft-matter applications, where alternative plant-based sustainable Pickering stabilizers are increasingly necessary.

To understand the gastric digestion properties of microgel particle-laden Pickering interfaces and additional complex particle-particle interfaces *i.e.* Pickering emulsions stabilized by PPM with/ without cellulose nanocrystals (CNC) during *in vitro* gastric digestion were monitored in the following **Chapter 4.**

3.5 References

- ADAL, E., SADEGHPOUR, A., CONNELL, S., RAPPOLT, M., IBANOGLU, E. & SARKAR, A. 2017. Heteroprotein Complex Formation of Bovine Lactoferrin and Pea Protein Isolate: A Multiscale Structural Analysis. *Biomacromolecules*, 18, 625-635.
- ADEBIYI, A. P. & ALUKO, R. E. 2011. Functional properties of protein fractions obtained from commercial yellow field pea (*Pisum sativum* L.) seed protein isolate. *Food Chemistry*, 128, 902-908.
- ARAIZA-CALAHORRA, A. & SARKAR, A. 2019. Pickering emulsion stabilized by protein nanogel particles for delivery of curcumin: Effects of pH and ionic strength on curcumin retention. *Food Structure*, 21, 100113.
- AVEYARD, R., BINKS, B. P. & CLINT, J. H. 2003. Emulsions stabilized solely by colloidal particles. *Advances in Colloid and Interface Science*, 100, 503-546.
- BEN-HARB, S., PANOUILLE, M., HUC-MATHIS, D., MOULIN, G., SAINT-EVE, A., IRLINGER, F., BONNARME, P., MICHON, C. & SOUCHON, I. 2018. The rheological and microstructural properties of pea, milk, mixed pea/milk gels and gelled emulsions designed by thermal, acid, and enzyme treatments. *Food Hydrocolloids*, 77, 75-84.
- BINKS, B. P. 2002. Particles as surfactants—similarities and differences. *Current opinion in colloid & interface science*, 7, 21-41.
- BORA, P. S., BREKKE, C. J. & POWERS, J. R. 1994. Heat Induced Gelation of Pea (*Pisum sativum*) Mixed Globulins, Vicilin and Legumin. *Journal of Food Science*, 59, 594-596.

- CHEN, N., LIN, L., SUN, W. & ZHAO, M. 2014. Stable and pH-Sensitive Protein Nanogels Made by Self-Assembly of Heat Denatured Soy Protein. *Journal of Agricultural and Food Chemistry*, 62, 9553-9561.
- CHIHAI, M.-L., MESSON, J.-L., SOK, N. & SAUREL, R. 2016. Heat-Induced Soluble Protein Aggregates from Mixed Pea Globulins and β -Lactoglobulin. *Journal of Agricultural and Food Chemistry*, 64, 2780-2791.
- CHIHAI, M.-L., NICOLAS, S. & SAUREL, R. 2018. Acid gelation of mixed thermal aggregates of pea globulins and β -lactoglobulin. *Food Hydrocolloids*, 85, 120-128.
- COCHEREAU, R., NICOLAI, T., CHASSENIEUX, C. & SILVA, J. V. C. 2019. Mechanism of the spontaneous formation of plant protein microcapsules in aqueous solution. *Colloids and Surfaces A: Physicochemical and Engineering Aspects*, 562, 213-219.
- COSGROVE, T. 2010. *Colloid science: principles, methods and applications*, Chichester, U.K, Wiley.
- DAVID-BIRMAN, T., MACKIE, A. & LESMES, U. 2013. Impact of dietary fibers on the properties and proteolytic digestibility of lactoferrin nanoparticles. *Food Hydrocolloids*, 31, 33-41.
- DE FOLTER, J. W. J., VAN RUIJVEN, M. W. M. & VELIKOV, K. P. 2012. Oil-in-water Pickering emulsions stabilized by colloidal particles from the water-insoluble protein zein. *Soft Matter*, 8, 6807-6815.
- DESTRIKATS, M., ROUVET, M., GEHIN-DELVAL, C., SCHMITT, C. & BINKS, B. P. 2014. Emulsions stabilized by whey protein microgel particles: towards food-grade Pickering emulsions. *Soft matter*, 10, 6941-6954.

- DICKINSON, E. 2012. Use of nanoparticles and microparticles in the formation and stabilization of food emulsions. *Trends in Food Science & Technology*, 24, 4-12.
- DICKINSON, E. 2013. Stabilising emulsion-based colloidal structures with mixed food ingredients. *Journal of the Science of Food and Agriculture*, 93, 710-721.
- DU LE, H., LOVEDAY, S. M., SINGH, H. & SARKAR, A. 2020. Pickering emulsions stabilized by hydrophobically modified cellulose nanocrystals: Responsiveness to pH and ionic strength. *Food Hydrocolloids*, 99, 105344.
- ETTELAIE, R. & LISHCHUK, S. V. 2015. Detachment force of particles from fluid droplets. *Soft Matter*, 11, 4251-4265.
- GAL, S., SHANI LEVI, C., TAL, S. & LESMES, U. 2013. Emulsions stabilization by lactoferrin nano-particles under in vitro digestion conditions. *Food Hydrocolloids*, 33, 264-272.
- HOGG, R., HEALY, T. W. & FUERSTENAU, D. 1966. Mutual coagulation of colloidal dispersions. *Transactions of the Faraday Society*, 62, 1638-1651.
- HU, Y.-Q., YIN, S.-W., ZHU, J.-H., QI, J.-R., GUO, J., WU, L.-Y., TANG, C.-H. & YANG, X.-Q. 2016. Fabrication and characterization of novel Pickering emulsions and Pickering high internal emulsions stabilized by gliadin colloidal particles. *Food Hydrocolloids*, 61, 300-310.
- JAYASENA, V., CHIH, H. J. & NASAR-ABBAS, S. 2010. Functional properties of sweet lupin protein isolated and tested at various pH levels. *Research Journal of Agriculture and Biological Sciences*, 6, 130-137.
- JIAO, B., SHI, A., WANG, Q. & BINKS, B. P. 2018. High-Internal-Phase Pickering Emulsions Stabilized Solely by Peanut-Protein-Isolate

Microgel Particles with Multiple Potential Applications. *Angewandte Chemie International Edition*, 57, 9274-9278.

KARACA, A. C., LOW, N. & NICKERSON, M. 2011. Emulsifying properties of chickpea, faba bean, lentil and pea proteins produced by isoelectric precipitation and salt extraction. *Food Research International*, 44, 2742-2750.

KIMURA, A., FUKUDA, T., ZHANG, M., MOTOYAMA, S., MARUYAMA, N. & UTSUMI, S. 2008. Comparison of Physicochemical Properties of 7S and 11S Globulins from Pea, Fava Bean, Cowpea, and French Bean with Those of Soybean □ French Bean 7S Globulin Exhibits Excellent Properties. *Journal of Agricultural and Food Chemistry*, 56, 10273-10279.

LAGUNA, L., PICOUET, P., GUÀRDIA, M. D., RENARD, C. M. G. C. & SARKAR, A. 2017. In vitro gastrointestinal digestion of pea protein isolate as a function of pH, food matrices, autoclaving, high-pressure and re-heat treatments. *LWT*, 84, 511-519.

LIANG, H.-N. & TANG, C.-H. 2014. Pea protein exhibits a novel Pickering stabilization for oil-in-water emulsions at pH 3.0. *LWT - Food Science and Technology*, 58, 463-469.

LIU, F., OU, S.-Y. & TANG, C.-H. 2017. Ca²⁺-induced soy protein nanoparticles as pickering stabilizers: Fabrication and characterization. *Food Hydrocolloids*, 65, 175-186.

LIU, F. & TANG, C.-H. 2013. Soy protein nanoparticle aggregates as Pickering stabilizers for oil-in-water emulsions. *Journal of agricultural and food chemistry*, 61, 8888-8898.

LIU, F. & TANG, C.-H. 2016. Soy glycinin as food-grade Pickering stabilizers: Part. III. Fabrication of gel-like emulsions and their potential as

- sustained-release delivery systems for β -carotene. *Food Hydrocolloids*, 56, 434-444.
- LIU, F. & TANG, C. H. 2014. Emulsifying properties of soy protein nanoparticles: influence of the protein concentration and/or emulsification process. *J Agric Food Chem*, 62, 2644-54.
- MAKRI, E. A. & DOXASTAKIS, G. I. 2006. Study of emulsions stabilized with *Phaseolus vulgaris* or *Phaseolus coccineus* with the addition of Arabic gum, locust bean gum and xanthan gum. *Food Hydrocolloids*, 20, 1141-1152.
- MESHULAM, D. & LESMES, U. 2014. Responsiveness of emulsions stabilized by lactoferrin nano-particles to simulated intestinal conditions. *Food & Function*, 5, 65-73.
- MESSION, J.-L., CHIHI, M. L., SOK, N. & SAUREL, R. 2015. Effect of globular pea proteins fractionation on their heat-induced aggregation and acid cold-set gelation. *Food hydrocolloids*, 46, 233-243.
- MESSION, J.-L., ROUSTEL, S. & SAUREL, R. 2017. Interactions in casein micelle – Pea protein system (part I): Heat-induced denaturation and aggregation. *Food Hydrocolloids*, 67, 229-242.
- NESTERENKO, A., ALRIC, I., SILVESTRE, F. & DURRIEU, V. 2013. Vegetable proteins in microencapsulation: A review of recent interventions and their effectiveness. *Industrial Crops and Products*, 42, 469-479.
- PAN, Y., TIKEKAR, R. V., WANG, M. S., AVENA-BUSTILLOS, R. J. & NITIN, N. 2015. Effect of barrier properties of zein colloidal particles and oil-in-water emulsions on oxidative stability of encapsulated bioactive compounds. *Food Hydrocolloids*, 43, 82-90.

- PENG, L.-P., XU, Y.-T., LI, X.-T. & TANG, C.-H. 2020. Improving the emulsification of soy β -conglycinin by alcohol-induced aggregation. *Food Hydrocolloids*, 98, 105307.
- PENG, W., KONG, X., CHEN, Y., ZHANG, C., YANG, Y. & HUA, Y. 2016. Effects of heat treatment on the emulsifying properties of pea proteins. *Food Hydrocolloids*, 52, 301-310.
- PENG, X. Q., XU, Y. T., LIU, T. X. & TANG, C. H. 2018. Molecular Mechanism for Improving Emulsification Efficiency of Soy Glycinin by Glycation with Soy Soluble Polysaccharide. *Journal of Agricultural and Food Chemistry*, 66, 12316-12326.
- RAYNER, M., MARKU, D., ERIKSSON, M., SJÖÖ, M., DEJMEK, P. & WAHLGREN, M. 2014. Biomass-based particles for the formulation of Pickering type emulsions in food and topical applications. *Colloids and Surfaces A: Physicochemical and Engineering Aspects*, 458, 48-62.
- SARKAR, A., ADEMUYIWA, V., STUBLEY, S., ESA, N. H., GOYCOOLEA, F. M., QIN, X., GONZALEZ, F. & OLVERA, C. 2018. Pickering emulsions co-stabilized by composite protein/ polysaccharide particle-particle interfaces: Impact on in vitro gastric stability. *Food Hydrocolloids*, 84, 282-291.
- SARKAR, A., KAMARUDDIN, H., BENTLEY, A. & WANG, S. 2016a. Emulsion stabilization by tomato seed protein isolate: Influence of pH, ionic strength and thermal treatment. *Food Hydrocolloids*, 57, 160-168.
- SARKAR, A., MURRAY, B., HOLMES, M., ETTOLAIE, R., ABDALLA, A. & YANG, X. 2016b. In vitro digestion of Pickering emulsions stabilized by soft whey protein microgel particles: influence of thermal treatment. *Soft Matter*, 12, 3558-69.
- SARKAR, A., ZHANG, S., HOLMES, M. & ETTOLAIE, R. 2019. Colloidal aspects of digestion of Pickering emulsions: Experiments and theoretical

models of lipid digestion kinetics. *Advances in Colloid and Interface Science*, 263, 195-211.

SHAO, Y. & TANG, C.-H. 2015. Gel-like pea protein Pickering emulsions at pH3.0 as a potential intestine-targeted and sustained-release delivery system for β -carotene. *Food Research International*, 79, 64-72.

TUINIER, R. & DE KRUIF, C. 2002. Stability of casein micelles in milk. *The Journal of chemical physics*, 117, 1290-1295.

XIAO, J., WANG, X. A., GONZALEZ, A. J. P. & HUANG, Q. 2016. Kafirin nanoparticles-stabilized Pickering emulsions: Microstructure and rheological behaviour. *Food Hydrocolloids*, 54, 30-39.

ZHU, X.-F., ZHANG, N., LIN, W.-F. & TANG, C.-H. 2017. Freeze-thaw stability of pickering emulsions stabilized by soy and whey protein particles. *Food Hydrocolloids*, 69, 173-184.

ZHU, X.-F., ZHENG, J., LIU, F., QIU, C.-Y., LIN, W.-F. & TANG, C.-H. 2018. Freeze-thaw stability of Pickering emulsions stabilized by soy protein nanoparticles. Influence of ionic strength before or after emulsification. *Food Hydrocolloids*, 74, 37-45.

Chapter 4^c

Synergistic interactions of plant protein microgels and cellulose nanocrystals at the interface and their inhibition of gastric digestion of Pickering emulsions

Abstract

Pickering emulsions have possibilities for optimizing transport of nutraceuticals, pharmaceuticals and other bioactive compounds in human physiology. So-called ultra-stable Pickering emulsions can often get destabilized in the gastric digestion regime if the particles are proteinaceous in nature. The present study seeks to test how the interfacial structure can be engineered *via* synergistic particle-particle interactions to impact gastric coalescence of Pickering emulsions. In this study, we designed plant-based protein particle stabilized oil-in-water emulsions (PPM-E, with 20 wt% sunflower oil,) *via* pea protein microgels (PPM at 1 wt%). The PPM hydrodynamic diameter \approx 250 nm. *In vitro* gastric digestion of PPM-E confirmed droplet coalescence within 30 min of pepsin addition. Supposedly surface active cellulose nanocrystals (CNCs, at 1-3 wt%) were added to PPM-E at pH 3.0, to see if could act as a barrier to interfacial pepsinolysis, due to the CNC and PPM being oppositely charged at this gastric pH value. A combination of confocal microscopy, zeta-potential and Langmuir trough measurements suggested that CNCs and PPMs might form a combined layer at the O/W interface, owing to the electrostatic attraction between them. CNCs at $>$ 2 wt% inhibited pepsinolysis of the adsorbed PPM film and thus droplet coalescence. However, increasing concentrations of CNC also increased the bulk viscosity of the PPM-E and eventually caused gelation of the emulsions, which would also delay their gastric breakdown. In conclusion, tuning bulk and interfacial structure of Pickering emulsions *via* synergistic interactions between two types of particles could be an effective strategy to

^c Published as a peer-reviewed publication: Zhang, S., Murray, B. S., Suriyachay, N., Holmes, M., Ettelaie, R., & Sarkar, A. (2021). Synergistic interactions of plant protein microgels and cellulose nanocrystals at the interface and their inhibition of the gastric digestion of Pickering emulsions. *Langmuir*, 37(2), 827-840.

modify enzymatic breakdown of such emulsions, which would have important applications in pharmaceuticals, foods and other soft matter applications.

4.1 Introduction

Pickering emulsions stabilized by biocompatible particles have aroused significant research interests recently owing to their extraordinary stability against coalescence due to their high desorption energies of the order of several thousands of $k_B T$ (where k_B is Boltzmann constant and T is temperature) as opposed to $< 5 k_B T$ for surfactant-stabilized emulsions and few hundreds of $k_B T$ for biopolymer stabilized emulsions (Sarkar et al., 2016c, Shimoni et al., 2013, Araiza-Calahorra and Sarkar, 2019b, Dickinson, 2012, Dickinson, 2015a, Sarkar and Dickinson, 2020, Murray, 2019b, Murray, 2019a) Of more interest here is that emulsions stabilized by rigid solid particles via the Pickering stabilization mechanism or soft solid particles, which are often referred to as Mickering emulsions (Gong et al., 2016, Murray, 2019b) which have been used as novel vehicles to modulate lipid digestion in the human gastrointestinal (GI) tract to allow delivery of lipid soluble active compounds for pharmaceutical and food applications. This is largely attributed to the ability of these particles to be resistant against competitive displacement by surface active agents in human physiology such as bile salts (Sarkar et al., 2019b). In particular, proteinaceous particles from animal sources have shown abilities to retard lipid digestion in the intestines in the presence of pure lipase and bile salts, *i.e.*, bypassing gastric digestion by preventing displacement by bile salt, such as in the case of emulsions stabilized by whey protein microgel (WPM) particles with or without heat treatment (Sarkar et al., 2016c) and lactoferrin nanoparticles (LFN) (Meshulam and Lesmes, 2014a, Peinado et al., 2010a, Shimoni et al., 2013). In addition, non-proteinaceous particles such as chitin nanocrystals (CN), (Tzoumaki et al., 2013a) have also shown abilities to retard lipid digestion by preventing displacement of particles by bile salt, as well as creating a network of chitin nanocrystals in the bulk phase, slowing down the transport of the enzyme to the oil-water (O-W) interface.

Although Pickering stabilization has shown promise in influencing

digestion in the intestinal phase in a highly artificial environment - where a gastric phase has been by-passed, Pickering stabilizers made from protein (French et al., 2016a, Peinado et al., 2010a, Sarkar et al., 2018a, Zhang et al., 2019) do not thrive in the preceding gastric regime, due to digestion by pepsin, and therefore will probably not offer any modulation of lipid digestion *in vivo*. For instance, protein particles, *e.g.* WPM,(Sarkar et al., 2016c) LFN,(Sarkar et al., 2018a) and kafirin nanoparticles (KFN) (Xiao et al., 2015b) can be hydrolyzed by pepsin under the usual acidic gastric environments (pH 1.0 to pH 3.0), causing a rupture of the interfacial particulate film, leading to aggregation or coalescence of the droplets. Thus, a more protective interfacial architecture is required in the gastric phase in the case of Pickering emulsions stabilized solely by protein-based particles.

Regarding more complex interfaces, recent studies have shown success on improving the stability of O/W emulsions during *in vitro* gastric digestion *via* the formation of multilayers consisting of protein gel particles and polysaccharides. For instance, examples include the co-operative effects of LFN + carrageenan, alginate or pectin (David-Birman et al., 2013, Meshulam and Lesmes, 2014a, Peinado et al., 2010a, Sarkar et al., 2018a), as well as between soy protein nanoparticles (SPN) and TEMPO-oxidized bacterial cellulose (TOBC) (Zhang et al., 2019). Layers coating the primary proteinaceous particle-stabilized interface, formed from polysaccharide-based particles such as cellulose nanocrystals (CNC), can act as an additional interfacial barrier, protecting the protein at the interface from being hydrolyzed by the gastric enzymes. This might be due to unique properties of CNC, in that is highly resistant to any human digestive enzymes and also the ability of CNCs to form particle networks in the continuous phase, which may slow down the transport of pepsin to the interface (Sarkar et al., 2019b).

In recent times, there has been a huge increase in the academic and commercial interest in exploiting and creating plant-based particles to design Pickering emulsions to replace animal-based proteins, due to their more ‘vegan-friendly’, ‘environment-friendly’, lower allergenicity and lower cost, *e.g.* zein particles,(Filippidi et al., 2014) kafirin particles,(Xiao et al., 2015b) soy protein nanoparticles (SPN) (Liu and Tang, 2016b). For instance, Shao and Tang (2016b)

created pea protein particles (PPP) at pH 3.0 and investigated the release of bioactive molecules from PPP-stabilized emulsions during lipid digestion. However, the required preparation of PPM at pH 3.0 limited the use of such emulsions during *gastrointestinal* lipid digestion. In the following study, a new range of thermally-crosslinked pea protein microgels were created that can be used to stabilize O/W emulsions at a range of pH values: the stability of these emulsions was investigated here during *in vitro* gastric digestion. Furthermore, in order to provide the required improved stability for protein-stabilized systems (Laguna et al., 2017b), a more complex interfacial structure was created by adding in CNCs (unmodified). Since the CNCs used were manufactured *via* sulfuric acid treatment, this introduces some sulfate groups and therefore some negative charge and increased hydrophilicity (George and Sabapathi, 2015, Younas et al., 2019). This results in the CNCs and PPMs having opposite charge at gastric pH values, so that they should form complexes at the interface and provide an additional barrier to the pepsin breaking down the primary PPM stabilizing film. Although several studies have shown mixed plant protein-polysaccharide particle interfaces can influence the rate of lipid digestion in a simulated digestion conditions (Li and de Vries, 2018), there have been relatively few reports of the effect of combining plant protein particle + unmodified CNC particles (Zhang et al., 2019, Zhou et al., 2018b). A combination of sizing, zeta-potential measurements, microscopy across several length scales (confocal laser scanning microscopy and cryo-scanning electron microscopy (cryo-SEM), sodium dodecyl sulfate polyacrylamide gel electrophoresis analysis (SDS PAGE), bulk rheology and Langmuir trough experiments have been employed to understand the gastric fate and stability of O/W emulsions stabilized by both set of particles: PPM + CNC.

4.2 Material and Methods

4.2.1 Materials.

Pea protein isolate (Nutralys S85X) containing 85% protein was provided by Roquette (Lestrem, France). Cellulose nanocrystal powder (CNC), which contained 100% sulfated CNC was purchased from Celluforce™ (Quebec,

Canada). Sunflower oil was purchased from the local supermarket (Tesco, UK). Pepsin (P7000) with measured enzymatic activity of 650 U/mg was purchased from Sigma-Aldrich (Dorset, UK). Mini-protein TGX gels, ProtoBlue safe colloidal Coomassie G-250 stain and all chemicals for sodium dodecyl sulfate polyacrylamide gel electrophoresis (SDS-PAGE) were purchased from Bio-Rad Laboratories, UK. All the chemicals, including sodium azide, Nile Red and Nile Blue, were of analytical grade and purchased from Sigma-Aldrich (Dorset, UK) unless otherwise specified. All solutions used were prepared using Milli-Q water which was purified by a Milli-Q apparatus (Millipore Corp., Bedford, MA, USA) with an ionic purity of 18.2 M Ω ·cm at 25°C.

4.2.2 Methods

4.2.2.1 Preparation of pea protein microgel particles (PPM).

Pea protein microgel particles (PPM) were prepared using a process previously described by Zhang and coworkers (Zhang et al., 2020). Briefly, pea protein concentrate (12.54 wt% protein) was dispersed in 20 mM phosphate buffer at pH 7.0 for 2 h and then the protein dispersion was heated at 90 °C for 60 min to form pea protein hydrogels and cooled to room temperature followed by storage at 4 °C overnight. The hydrogels were then mixed with phosphate buffer (1:1 w/w) at pH 7.0 and then pre-homogenized using a kitchen blender (HB711M, Kenwood, UK) for 5 min at level 3. The aqueous dispersion of the macrogel particles was subsequently homogenized using two passes through a two stage valve homogenizer (Panda, GEA Niro Soavi Homogeneizador Parma, Italy) at a pressure of 250/ 50 bar. The resulting microscopic PPM dispersion contained 6.28 wt% protein. Sodium azide (0.02 wt%) was added to prevent microbial growth. The PPM dispersion was diluted with phosphate buffer to 1.25 or 3.33 wt% protein before the emulsion preparation.

4.2.2.2 Preparation of O/W emulsions

PPM-E emulsions at pH 7.0 were prepared by homogenizing 20.0 wt% sunflower oil with 80.0 wt% PPM the latter containing 1.25 wt% protein, at pH 7.0. The mixture of oil and aqueous phases was pre-homogenized using a

Silverson rotor-stator type mixer (L5M-A, UK) at 8000 rpm for 5 min. The pre-emulsions were homogenized by two passes through the Panda homogenizer (GEA Niro Soavi Homogeneizador Parma, Italy) at 250/ 50 bar pressure. PPM-E + CNC emulsions were prepared as for PPM-E as above, but using 3.33 wt% protein in 60 wt% aqueous phase + 40 wt% oil, then adjusting the pH to pH 3.0 and mixing in a CNC dispersion (2-6 wt% in Milli-Q water at pH 3.0), waiting for 3 h, finally resulted in PPM-E + CNC emulsions containing 20 wt% oil, 1 wt% PPM (*i.e.*, the same as PPM-E) + 1 to 3 wt% CNC. In the following we denote the CNC concentration in the PPM-E + CNC systems with a subscript, *e.g.*, PPM-E + CNC_{1.0}, for the system containing 1 wt% CNC.

4.2.2.3 *In vitro* gastric digestion

The PPM dispersion, PPM-E and PPM-E + CNC were digested using a digestion protocol designed by Minekus et al. (2014) Briefly, 10 mL of PPM dispersion (1 wt% protein) or emulsion sample (20 wt% oil, 1 wt% protein) at pH 3.0 was mixed with 10 mL of simulated gastric fluid (SGF), which contained 0.514 g L⁻¹ KCl, 0.123 g L⁻¹ KH₂PO₄, 0.042 g L⁻¹ NaHCO₃, 0.06 g L⁻¹ NaCl, 0.0004 g L⁻¹ MgCl₂(H₂O)₆, 0.0009 g L⁻¹ (NH₄)₂CO₃ and 2000 U mL⁻¹ pepsin at pH 3.0 to simulate fed-state gastric digestion conditions. The mixture was incubated for 2.5 h at 37 °C using a shaking water bath (100 rpm, Grant Instruments Ltd, Cambridge, UK). To understand the changes in the physicochemical properties or structure of the microgel particles or droplets during the digestion, aliquots were collected at 0, 1, 5, 30, 60, 90, 120 and 150 min for size, zeta-potential, microscopy and SDS-PAGE analysis, and viscosity measurement. In the data collected during the digestion, “0 min” refers to the control sample, *i.e.*, the mixture of sample and SGF buffer without any added pepsin. For size and zeta-potential measurement, samples were measured immediately once collected from digested mixture. It is worth mentioning that the protocol’s recommended oral phase was not used in this study, because the systems do not contain any starch and thus were not expected to have any pepsinolysis digestion.

4.2.2.4 Measurement of PPM and emulsion droplet size.

Particle sizes of aqueous dispersions of PPM as function of digestion time were determined *via* dynamic light scattering (DLS) at 25 °C using a Zetasizer Nano-ZS (Malvern Instruments, Malvern UK) in a standard PMMA disposable cuvette. The samples before and after gastric digestion were diluted 200 times in SGF buffer (pH 3.0). The hydrodynamic diameter (D_h) of the PPM was calculated using the Stokes–Einstein equation ($D_h = \frac{k_B T}{3\pi\eta D_t}$), where, D_t is the translational diffusion coefficient, k_B is Boltzmann's constant, T is temperature in Kelvin, and η is dynamic viscosity of the aqueous dispersion of PPM. The refractive index of PPM was set at 1.52 with an absorbance of 0.001, as previously reported by Zhang et al. (2020)

Droplet size distributions of emulsions before and after digestion were determined *via* static light scattering (SLS) at 25 °C using Malvern MasterSizer 3000 (Malvern Instruments Ltd, Malvern, Worcestershire, UK). The samples were diluted to give an obscuration of between 4 and 6%. Refractive indices were set at 1.46 for sunflower oil and 1.33 for the aqueous medium, respectively. The average droplet size of the emulsion was reported as d_{43} (the volume mean diameter, $\frac{\sum n_i d_i^4}{\sum n_i d_i^3}$) and d_{32} (surface mean diameter, $\frac{\sum n_i d_i^2}{\sum n_i d_i}$) where, n_i is the number of droplets with a diameter, d_i .

4.2.2.5 Measurement of zeta-potential.

Zeta-potentials of PPM dispersions, PPM-E and PPM-E + CNC₁₋₃ before and after digestion were measured using a Zetasizer Nano ZS (Malvern Instruments, Worcestershire, UK). Before adding into a folded capillary cell (DTS1070 cell, Malvern Instruments Ltd., Worcestershire, UK), samples were diluted to 0.01 wt% particle concentration or 0.008 wt% droplet concentration using SGF buffer at pH 3.0.

4.2.2.6 Microscopy.

Cryogenic scanning electron microscopy (cryo-SEM) was used to visualize the adsorbed PPM and the arrangement of CNC at the interface of PPM-E or PPM-

E + CNC₁₋₃, respectively. To avoid influence by oil crystallization during the freezing step, (Araiza-Calahorra and Sarkar, 2019b, Destribats et al., 2013, Minekus et al., 2014) heptane was used as the dispersed phase instead of sunflower oil. A droplet of the emulsion sample was filled into a copper holder before being flash frozen in liquid nitrogen at $-180\text{ }^{\circ}\text{C}$. The samples were exposed to $-95\text{ }^{\circ}\text{C}$ for 5 min and then coated with 5 nm of platinum. Images were captured using a FEI Quanta 200 F ESEM with a Quorum Polar Prep 2000 cryo system at $-135\text{ }^{\circ}\text{C}$.

To perform microstructural characterization of PPM-E and PPM-E + CNC₁₋₃ before and after digestion, confocal laser scanning micrographs (CLSM) were captured using a Zeiss LSM 700 confocal microscope (Carl Zeiss MicroImaging GmbH, Jena, Germany). Approximately, 5 mL of sample was mixed with 100 μL of Nile Red (2% w/v in dimethyl sulfoxide), 500 μL of Fast Green (10% w/v in Milli-Q water) and 100 μL Calcofluor White to stain the oil, proteinaceous particles and CNC, respectively. Nile Red, Nile blue and Calcofluor White were excited at 514 nm, 633 nm and 410 nm, respectively. About 200 μL of xanthan gum (1 wt%) was added into the stained samples of the PPM-E and PPM-E + CNC₁₋₃ to reduce the Brownian motion of the oil droplets. The prepared samples were placed onto a microscope slide with cavity, covered with a cover slip and observed with a 63 \times (oil immersion) objective lens.

4.2.2.7 Rheology

The apparent viscosity (η_a) dynamic elastic modulus (G') and dynamic loss modulus (G'') of the freshly prepared PPM-E and PPM-E + CNC₁₋₃ were determined at $25\text{ }^{\circ}\text{C}$ using a Kinexus Ultra rheometer (Malvern Instruments Ltd, Malvern, UK). The apparent viscosities were recorded as a function of shear rates ranging from 0.1 to 1000 s^{-1} . Strain amplitude sweep tests were carried out with a shear strain range of 0.01-100% at 0.1 Hz frequency. Frequency sweep tests were then determined with an angular frequency range of $0.01\text{--}10\text{ s}^{-1}$ at a strain amplitude of 0.1% (*i.e.* in the linear viscoelastic regime). In order to characterize the flow type of the emulsions, the apparent viscosity curves were fitted using the Ostwald-de Waele model, $\eta_a(\dot{\gamma}) = K\dot{\gamma}^{n-1}$, where $\dot{\gamma}$ is the shear

rate, K is the consistency index and n is the flow behaviour index.

4.2.2.8 Electrophoresis of proteins and their digestants.

The protein and peptides compositions of the aqueous dispersions of PPM after hydrolysis by pepsin were determined *via* sodium dodecyl sulfate polyacrylamide gel electrophoresis (SDS-PAGE). Approximately, 50 μL of the PPM + SGF mixture after gastric digestion at different times (0, 1, 5, 10, 30, 60, 120 and 150 min) were mixed with 40 μL of SDS sample buffer (62.5 mM Tris-HCl, 2 wt% SDS, 25 wt% glycerol, 0.01 wt% bromophenol blue, pH 6.8) and 10 μL of dithiothreitol solution (DTT, 50 mM in final concentration), and heated at 95 °C for 5 min. Exactly, 5 μL of protein molecular weight (M_w) markers and 10 μL of each of the samples were loaded into pre-cast Mini-PROTEAN 8–10% TGX Gels in a Mini-PROTEAN II electrophoretic unit (Bio-Rad Laboratories, Richmond, CA, USA). After running the gel at 200 V for about 30 min, the gel was placed in a fixing solution (a 50:40:10 vol% ratio of Milli-Q water: methanol: acetic acid) for 2 h, and stained for 2 h with Coomassie Blue solution, which consisted of 90% ProtoBlue Safe Colloidal Coomassie G-250 stain and 10% ethanol. The gels were imaged using a ChemiDoc™ XRS + System with image Lab™ Software after de-staining overnight in Milli-Q water.

4.2.2.9 Langmuir trough monolayer experiments.

Langmuir trough monolayer experiments were carried out to understand the interaction between PPM and CNC at the interface, as described in a recent work measuring particle-particle interactions at the air-water (A-W) interface (Zembyla et al., 2019). Although these experiments were carried out at the A-W and not the oil-water (O-W) interface, they still should have revealed more information about the nature of the interactions at the surface of the emulsion droplets. The surface pressure was measured using a roughened mica Wilhelmy plate (3–5 cm in width), suspended from a force transducer (Maywood Instruments, Basingstoke, UK) at the centre of a polytetrafluoroethylene (PTFE) trough. Buffer (pH 7.0 or pH 3.0) was added to the trough until the plate dipped into the A–W interface. The A–W interfacial area in the trough was reduced to

the smallest possible and a vacuum line used to suck away the surface of the aqueous phase until the surface pressure π was $< 0.1 \text{ m N m}^{-1}$ and this remained $< 0.1 \text{ m N m}^{-1}$ on subsequent re-expansion (to the maximum trough area) and re-compression. For PPM experiments, a drop of an aqueous dispersion of PPM (0.46 wt% protein concentration) in a $100 \mu\text{l}$ syringe was slowly formed at the tip of the syringe and slowly lowered to touch the A-W interface, following by raising of the syringe tip. This was repeated until $100 \mu\text{L}$ of the PPM dispersion was spread. Suspensions of CNC alone (0.04 wt% CNC) were spread similarly. In all cases each $100 \mu\text{l}$ spreading process took 1 to 2 min and π versus area isotherms were measured 10 min after spreading. For experiments with PPM and CNC together, in one type of experiment 0.46 wt% PPM alone (at pH 3.0) was spread first, as above, then after 10 min $100 \mu\text{l}$ of a 0.04 wt% CNC dispersion at pH 3.0 was spread at top of the PPM film. Mixed dispersions of PPM and CNC were also spread (see later). Spread films were compressed at a constant low speed (Murray, 1997, Murray et al., 2002, Murray and Nelson, 1996) to measure the isotherms. In general, each spread film was compressed and expanded at least 2 times to check for reversibility, with all experiments conducted in triplicate.

4.2.2.10 Pepsin activity assay.

In order to determine the effect of the presence of CNCs on pepsin activity, hemoglobin was used as reacting protein. (Anson and Mirsky, 1932) $500 \mu\text{l}$ hemoglobin dispersion (2% w/v) with or without 1-2 wt% CNC at pH 2.0 was incubated in a shaking water bath at 37°C for 3 to 5 min to achieve temperature equilibration. Then $100 \mu\text{L}$ of pepsin solutions of different concentrations (5, 10, 15, 20, 25 and $30 \mu\text{g/mL}$) were added into the hemoglobin or hemoglobin + CNC dispersions. After incubation for 10 min, 1 mL TCA (5% w/v trichloroacetic acid) was added to stop the activity of pepsin. Finally, the reacted solution was centrifuged at 6000 g for 30 mins to collect a clear solution for absorbance measurement, at 280 nm, known as the A_{280} Test. Hemoglobin or hemoglobin + CNC dispersions without pepsin were used as blanks. The pepsin activity is calculated *via* equation 4.1.

$$\text{Units/mg} = \frac{A_{280} \text{ Test} \times 1000}{\Delta t \times X} \quad (4.1)$$

Where, Δt is the duration of the reaction, *i.e.* 10 mins and X is the concentration of pepsin.

4.2.2.11 Statistical analyses

All measurements were done three times on triplicate samples prepared on separate days and were reported as the mean and standard deviation ($n = 3 \times 3$). The statistical analyses were conducted using one-way (ANOVA) and the significant difference between samples were considered when $p < 0.05$ using Tukey test.

4.3 Results and Discussion

4.3.1 Characteristics of aqueous dispersions of PPM.

Pea protein microgel particles (PPM) dispersed in phosphate buffer at pH 7.0 were characterized to understand their properties before being used as Pickering emulsifiers. As shown in **Figure 4.1a**, DLS revealed a monomodal PSD (PSD) of PPM with a single peak in the size range of 100-1000 nm, with a mean hydrodynamic diameter (d_h) of 250 nm and a low polydispersity index (PDI \sim 0.2), in line with previous reports (Zhang et al., 2020). The PPM at pH 7.0 had a negative charge with a measured ζ -potential (about -40 mV), since the pH of the PPM was above the isoelectric point ($pI = 5.0$) (Zhang et al., 2020). The negatively-charged PPM suggests that the particles dispersed rather evenly in the aqueous solution without any visual separation due to the high particle-particle electrostatic repulsive forces.

4.3.2 *In vitro* gastric digestion of aqueous dispersions of PPM.

It can be observed from **Figure 4.1b** that d_h of PPM + SGF mixture at pH 3.0 without pepsin has similar values to those of fresh prepared PPMs at pH 7.0 (\sim 250 nm) (**Figure 4.1a**). Interestingly, PPM at pH 3.0 with SGF had a larger

size value, *i.e.* 2-3 μm , where data by DLS should be interpreted cautiously (Zhang et al., 2020). **Figure 4.1b** shows that the zeta-potential of PPM at 0 min digestion was positive (+25 mV) due to the protonation of the ionizable groups at pH 3.0. This zeta-potential value was slightly lower than that measured previously in water, (Torres et al., 2019, Zhang et al., 2020) presumably due to the presence of the SGF ions.

In the presence of SGF containing pepsin, d_h of PPMs dramatically increased (from 0.25 to 7 μm , **Figure 4.1b**) within the first 60 min, comparing with the d_h of PPMs at 0 min ($p < 0.05$). This marked increase in the particle size of PPM with correspondingly high PDI values can be attributed to protein particle aggregation due to proteolysis, resulting in their eventual sedimentation, as evidenced by **Figure 4.1c**. Interestingly, d_h decreased slightly to 4 μm in the later stages of digestion (post 90 min), possibly due to the eventual breakdown of these aggregates by pepsin (Nguyen et al., 2015b). The zeta-potential of PPM rapidly reduced to ~ 5 mV within the first 30 min of digestion, and decreased to nearly zero at longer times (**Figure 4.1c**), partly explaining the increase in d_h because of a decrease in electrostatic repulsion between the particles.

In order to better understand the gastric stability of PPM, the hydrolysis patterns of microgel particles containing 1 wt% protein were obtained using SDS-PAGE analysis, shown in **Figure 4.2**. In agreement with the evolution in d_h and zeta-potential, PPM appeared to be digested immediately. All the major pea protein bands, especially convicilin ($M_w = 77.9$ kDa), legumin ($M_w = 22.3, 23.1$ kDa), vicilin ($M_w = 47.3, 35.0, 28.7$ kDa) and minor sub units ($M_w = 37.0, 33.1, 31.8$ kDa) disappeared within 30 min of digestion, except convicilin ($M_w = 72.4$ kDa) and vicilin subunits of $M_w = 20$ and ≤ 14.2 kDa). Both convicilin ($M_w = 72.4$ kDa) and vicilin subunits ($M_w = 20$ and ≤ 14.2 kDa) showed slow digestion and remained in significant proportions after 30 min and faint bands were visible even after 150 min digestion. According to the report by Laguna et al. (2017b) post *in vitro* gastric digestion of pea protein isolate (PPI), only 20% of vicilin major sub units ($M_w = 35.0$ kDa) remained after 30 min in SGF containing pepsin, even with the much higher protein concentration used (*i.e.* 5 wt%). One might attribute the slower digestion in PPM compared to PPI due to the greater difficulty the enzyme has in penetrating into the microgel particles

and accessing all the available substrate sites (Luo et al., 2015). Opazo-Navarrete et al. (2018) compared pea protein concentrate and its gels during gastric digestion and also demonstrated the ability of the gel structure to reduce enzyme diffusion. Similar results have been obtained when comparing whey protein, soy protein and egg white protein and their gel/microgel counterparts (Nyemb et al., 2016, Opazo-Navarrete et al., 2018, Torres et al., 2019).

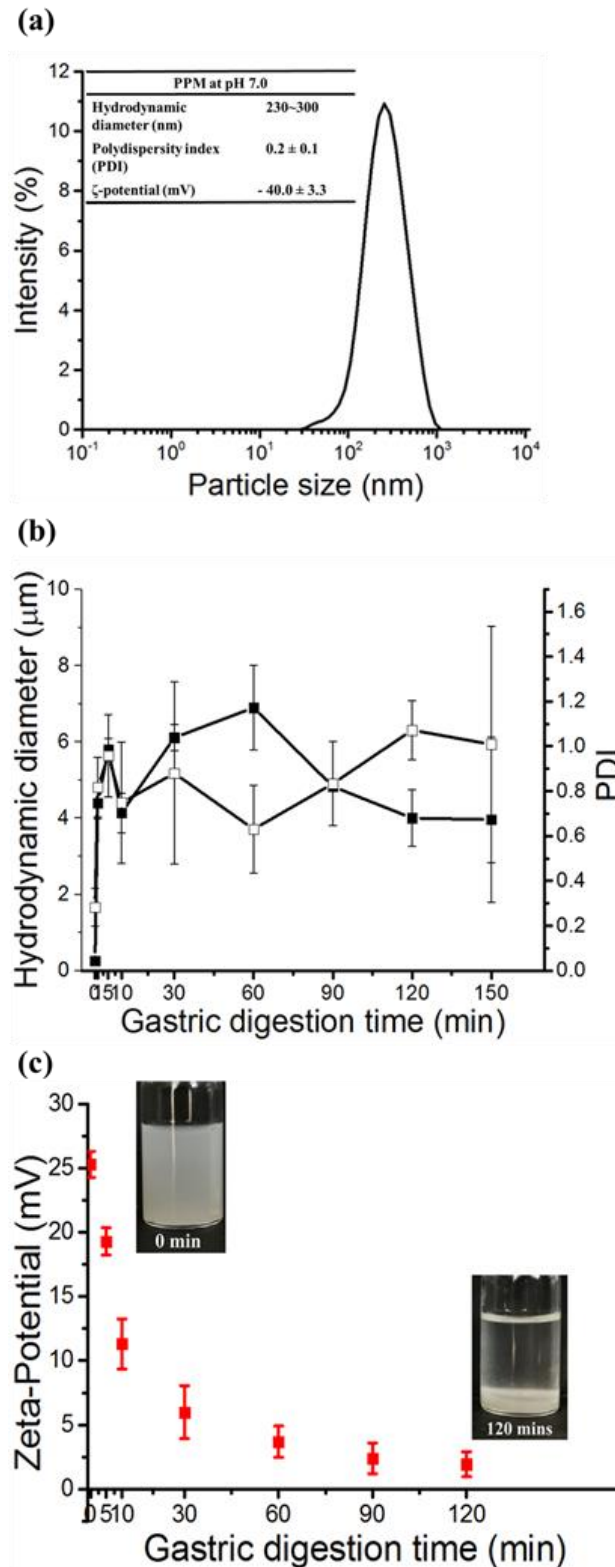


Figure 4.1. (a) PSD of pea protein microgel particles (PPM) at pH 7.0 with inset table showing the hydrodynamic diameter (d_h), polydispersity index (PDI) and zeta-potential. (b) and (c) Evolution of the mean d_H (■), PDI (□) and zeta-potential (■), respectively, of PPM at pH 3.0 after *in vitro* gastric digestion at different time points (0-120 min). The insets in (c) are images of aqueous dispersions of PPM before and after 120 min of gastric digestion, respectively.

Time 0 min represents the PPM + SGF mixture at pH 3.0 without the addition of pepsin. Error bars represent standard deviations.

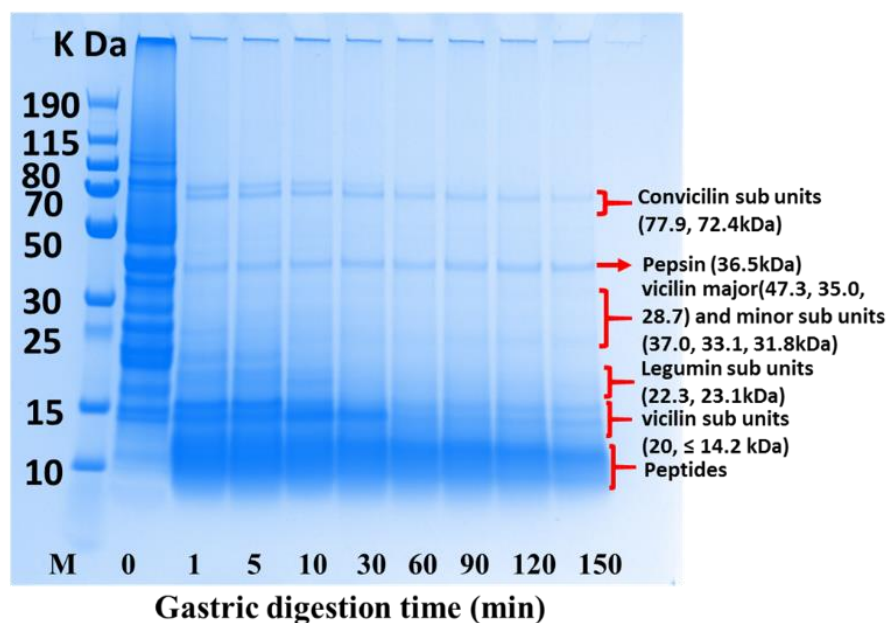


Figure 4.2. SDS-PAGE electrogram of aqueous dispersions of PPM at pH 3.0 after *in vitro* gastric digestion at different times (0-150 min). Lane M represents the protein markers of 10-250 kDa M_w range.

4.3.3 PPM-stabilized Pickering emulsions (PPM-E).

As shown in **Figure 4.3a**, the droplet size distribution of PPM-E at pH 7.0 was bimodal, consisting of a main peak in the size range 10 to 100 μm and a much smaller peak between 0.1 and 1 μm .

Comparison with the microscopy of the emulsions suggests that the large peak represents the emulsion droplets whilst **Figure 4.1** suggests the small peak most likely corresponds to unabsorbed PPM, in line with previous studies (Zhang et al., 2020). Interestingly, there were no particles observed above 100 μm as seen with lactoferrin-stabilized emulsions under similar conditions, which was attributed to flocculation (Sarkar et al., 2018a). This suggests that sharing of PPM between droplets was not so obvious in this study and the amount of PPM was sufficient to cover the droplets.

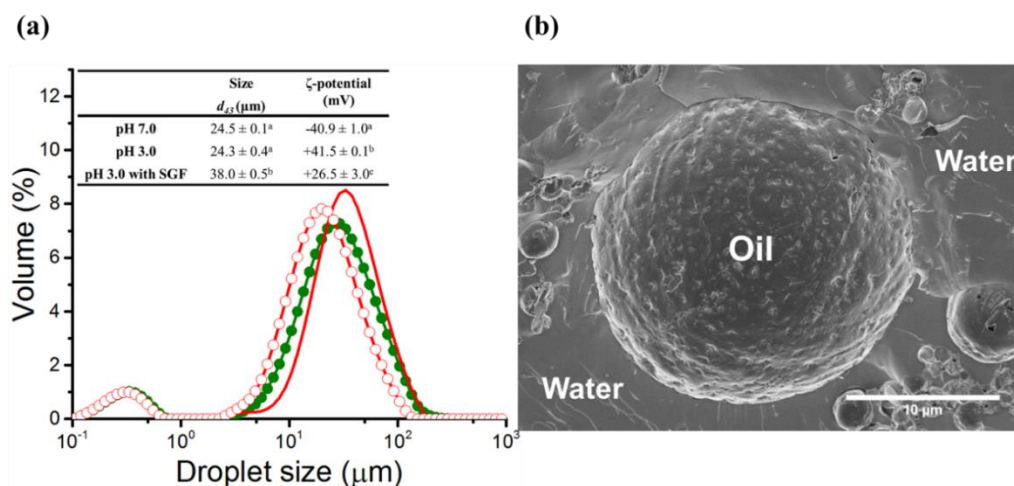


Figure 4.3. (a) Droplet size distribution of 20 wt% oil-in-water emulsions stabilized by PPM (PPM-E) at pH 7.0 (●), pH 3.0 (○) and PPM + SGF mixture at pH 3.0 without the addition of pepsin (-) with insets showing corresponding volume-average mean diameter (d_{43}) and zeta-potential of all the samples. Different superscripts (a-c) in the same columns of the inset of (a) represent significant differences between different samples at $p < 0.05$ level. (b) cryo-SEM micrograph of PPM-E at pH 7.0. Scale bar in (b) represents 10 μm .

The volume-average mean diameter (d_{43}) of PPM-E at pH 7.0 was around 25 μm and the zeta-potential was about -40 mV (**Figure 4.3a**), in agreement with previous work (Zhang et al., 2020). As such, the emulsions would be expected to exhibit long-term stability to coalescence. Efficient adsorption of the PPM particles to the oil-water (O/W) interface can be attributed to an increase in surface hydrophobicity of pea protein, resulting from the heat treatment (Peng et al., 2016) and agree with previous observations that 1% protein microgel particles of this sort of size can provide enough surface coverage to act as efficient Pickering stabilizers of 20 wt% O/W emulsions (Araiza-Calahorra and Sarkar, 2019b, Sarkar et al., 2016c, Zhang et al., 2020). The cryo-SEM images (*e.g.*, **Figure 4.3b**) show that the PPM appeared to cover the droplets effectively. In addition, there were no significant differences ($p > 0.05$) between the d_{43} of PPM-E at pH 7.0 and that at pH 3.0 (**Figure 4.3a**), even though the zeta-potential was reversed and so must have passed through zero on acidification. The reversal of the sign of the zeta-potential (from -40 mV to +42 mV) on acidification from pH 7.0 to pH 3.0 was expected from **Figure 4.1c** and because the isoelectric point of pea protein is between these two pH values (Zhang et al., 2020).

4.3.4 *In vitro* gastric digestion of PPM-E.

As seen in **Figure 4.3a**, in the presence of SGF without pepsin, the mean droplet size of PPM-E (0 min) was comparable to that of the freshly prepared PPM-E at pH 3.0. However, the surface charge of PPM-E at 0 min incubation time (~ 27 mV) reduced slightly as compared to that before gastric digestion (~ 42 mV), presumably due to the presence of the SGF ions. As noted earlier for the PPM alone, (Sarkar et al., 2018a) although the mean droplet size (d_{43}) increased ($p < 0.05$), and the main peak in the size range 10 to 100 μm moved slightly to right (**Figure 4.3a**), this effect was not strong enough to influence the observed stability of the PPM-E, *i.e.*, the PPM-E should be stable under gastric conditions before pepsin starts to act.

With increasing incubation time the main peak (droplets) showed a narrowing and slight increase in height, whereas the smaller peak (unabsorbed PPMs) appeared to decrease in height and move to higher sizes (**Figure 4.4a**). It seems possible that this represents the pepsin preferentially hydrolyzing the PPM-based network between droplets as well as any unabsorbed PPMs, as opposed to the PPM adsorbed at the droplet surface. Interestingly, a similar droplet size distribution was found between PPM-E at 60 min and 90 min (**Figure 4.4a**) suggested that the digestion by pepsin was fairly complete within 1 h of gastric digestion time. In line with the droplet distribution behaviour, mean droplet size (d_{43}) slightly decreased ($p < 0.05$) while the surface mean size (d_{32}) remained steady ($p > 0.05$) within the first 10 min of gastric digestion (**Figure 4.4b**).

At 30 min, d_{43} slightly increased back to ~ 35 μm and d_{32} slightly rose to ~ 10 μm . Beyond this time the smaller peak (unabsorbed PPMs) tended to disappear completely whilst there was with a significant increase in both d_{43} and d_{32} (**Figure 4.4d**), suggesting the attack by pepsin led to droplet flocculation and/or coalescence (Araiza-Calahorra and Sarkar, 2019a, Sarkar et al., 2017c), as discussed later. It should be pointed out that there is no simple way of distinguishing the proportion or interfacial versus bulk microgels that are digested by the pepsin. Both populations are already relatively unfolded protein and therefore probably quite accessible to pepsin as a result of the method of their formation.

As can be seen in **Figure 4.4c**, the zeta-potential of the droplets was also dramatically reduced ($p < 0.05$) after 30 min incubation and was close to zero at the end of digestion time. This indicates, at least, that the composition of the PPM interfacial layer must change and/or the amount adsorbed is reduced, as might be expected from the SDS-PAGE hydrolysis pattern of PPM (**Figure 4.2**). As the PPM becomes hydrolyzed into smaller and smaller peptide chains these are expected to become less surface active and more water soluble, leading to less stable emulsions. **Figure 4.4b** clearly shows extensive creaming of the emulsions after 120 min digestion and there was evidence of some free oil floating on top of the gastric fluid.

The above results were clearly represented in the microstructural changes observed in the CLSM images (**Figure 4.5**). (Tiled images of the samples over larger areas are shown in **Supplementary Figure S4.1**.) With addition of pepsin, a clear sign of larger oil droplets was observed, confirming that droplets underwent coalescence within the first 30 min, in agreement with the changes in PSD, etc., seen in **Figure 4.4**. Similar CLSM observations have been made for a range of protein-based Pickering emulsions in gastric digestion conditions: whey protein microgels and ‘nanoparticles’, (Araiza-Calahorra and Sarkar, 2019a, Sarkar et al., 2016c) lactoferrin ‘nanoparticles’, (Sarkar et al., 2018a, Shimoni et al., 2013) and karifin ‘nanoparticles’ (Xiao et al., 2015b).

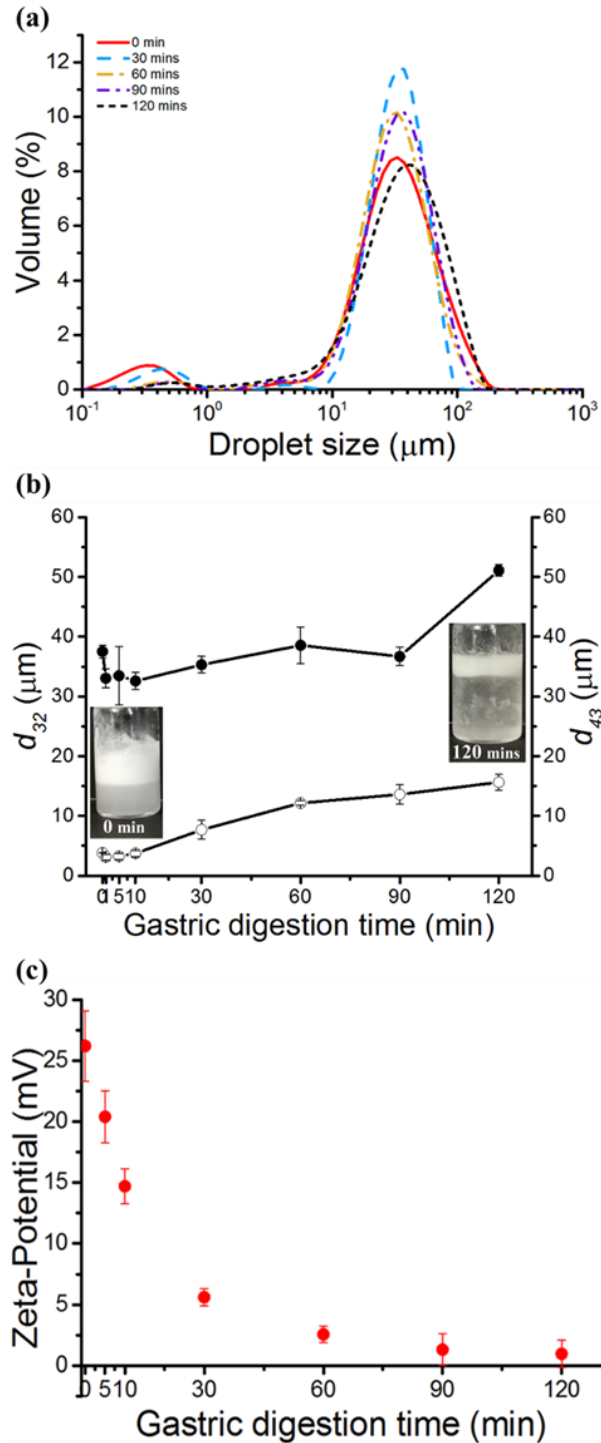


Figure 4.4. (a) Droplet size distribution, (b) d_{32} (\circ) and d_{43} , (\bullet) and (c) zeta-potential (\bullet), of PPM-E as a function of *in vitro* gastric digestion time with SGF containing pepsin. The insets in (b) are images of the emulsions before and after 120 min of gastric digestion. Time 0 min represents the PPM-E + SGF mixture at pH 3.0 without the addition of pepsin. Error bars represent standard deviations.

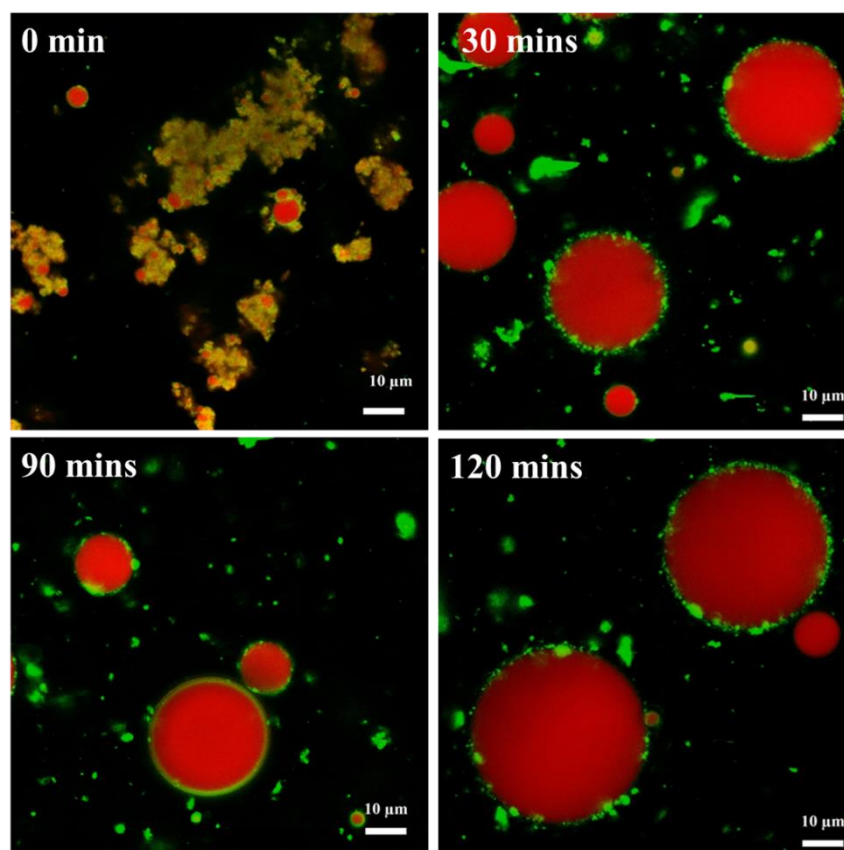


Figure 4.5. Confocal micrographs of 20 wt% oil-in-water emulsions stabilized by PPM (PPM-E) as a function of *in vitro* gastric digestion time (0-120 mins) at pH 3.0 (refer to **Supplementary Figure S4.1** for tiled confocal micrographs covering larger fields of view). Green color represents PPM (stained by Nile Blue); red color represents oil (stained by Nile Red); black color represents air or water. Time 0 min represents the PPM-E + SGF mixture at pH 3.0 without the addition of pepsin. Scale bar represents 10 μm.

4.3.5 Interactions between CNCs and PPM-E at pH 3.0.

The CNCs used in this study were needle-like solid crystals with a diameter of ~100 nm. As reported in previous research, (Sarkar et al., 2018b, Sarkar et al., 2019b, Du Le et al., 2020) and discussed in the introduction, the zeta-potential of CNC is relatively high (and negative) at pH 3.0. (Ehmann et al., 2013, George and Sabapathi, 2015, Scheuble et al., 2014b) Since the oil droplets in PPM-E had an opposite, positive zeta-potential (**Figure 4.3a**) at pH 3.0, adsorption of CNC onto the adsorbed PPM layer is expected with a change in the droplet zeta-potential to smaller +ve and even -ve values. As shown in **Figure 4.6a**, this is indeed the case - as the concentration of CNC was increased from 0.5 to 4.0 wt%, the zeta-potential changed from +40 to -45 mV, mostly between 0.5 and 2.0 wt% CNC. (CNC added to PPM dispersions alone produced very much the

same effect, as shown in **Supplementary Figure S4.2**). The slightly positively charged PPM-E + CNC_{1.0} (+4 mV) suggests that the droplets were not completely coated with CNC at this lower CNC concentration (1 wt%). Beyond 2 wt% CNC the value of zeta-potential was almost stable, suggesting that at ≥ 2 wt% CNC the PPM-E droplets were ‘completely’ covered by CNC, so that excess CNC probably existed in the bulk phase at ≥ 2 wt% CNC. Note, however, the impossibility of complete coverage of a spherical surface, i.e., one with no gaps at all, with solid objects. Similar findings for the protein microgel-stabilized emulsions coated with polysaccharides have been reported elsewhere - where increasing the concentration of the polysaccharide led to full coverage and charge reversal of the droplets. (Araiza-Calahorra and Sarkar, 2019a, Sarkar et al., 2017c) Another important aspect is that at ≥ 2 wt%, the samples showed gel-like characteristics with limited visual flowability (see **Figure 4.6b**). Such behaviour was also seen in case of PPM alone with 3 wt% CNC added. This gel like behaviour has also been seen previously (Du Le et al., 2020) in emulsions with hydrophically-modified CNCs added. So one must also be aware that these CNCs may affect the bulk rheology by forming CNC-CNC network or CNC-PPM network in the continuous phase and consequently may influence stability and digestibility of the emulsions. On the basis of the above results, CNC concentrations of 1, 2 and 3 wt% were selected for investigating the effect of CNCs on the gastric digestions of PPM-E, as described later.

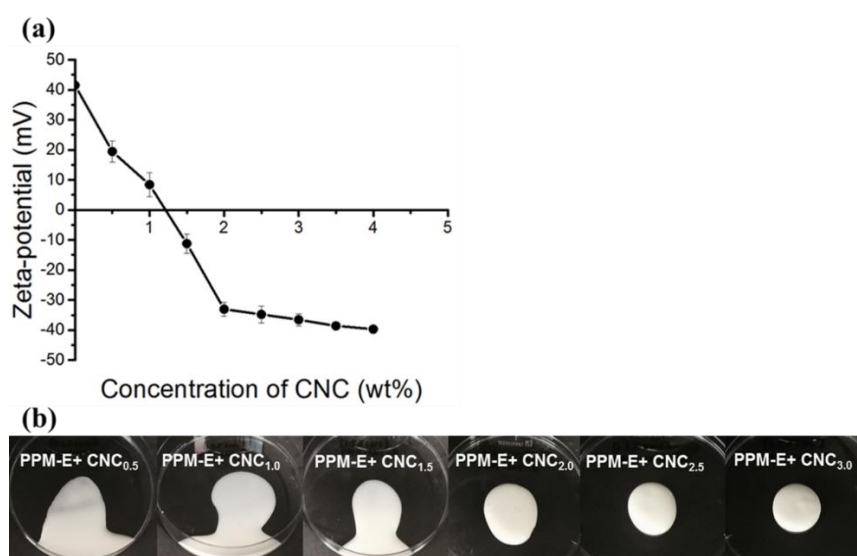


Figure 4.6. (a) Influence of concentration of cellulose nanocrystal (CNC) on zeta-potential (●); (b) corresponding visual images of PPM-E with added CNC. Error bars on (a) represent standard deviations.

4.3.6 Monolayer experiments on PPM and PPM + CNC.

In order to further confirm the nature of the binding of CNC to PPM at the interface and to try and identify whether the PPM and CNC form multilayers or a single composite mixed film, surface pressure (π) versus area isotherms of PPM, CNC and PPM + CNC at air-water (A-W) interface were measured *via* the Langmuir trough-methods described above.

Figure 4.7a shows representative surface pressure (π) – area isotherms for 100 μL of 0.466 wt% PPM spread at the A-W interface at pH 3.0 and pH 7.0. A spherical PPM radius, $r = 125$ nm, according to the DLS data in **Figure 4.1a**, plus an assumed PPM particle density of 1 g cm^{-3} , were used to calculate the number of particles (N_p) spread from the mass of PPM spread. So the x-axis is the trough area (A) per particle, *i.e.*, A/N_p . In each case the film was compressed then expanded to the maximum trough area and compressed again, *i.e.*, compressed at least twice. For all PPM experiments, within experimental error, the repeated compression gave the same isotherm, confirming that the spread material was retained at the interface and/or any compression of the adsorbed microgel particles was reversible up to the π imposed on the film. It should be noted, however, that occasionally some small jumps in π were observed, which may indicate some film instability on compression (see below).

The isotherms for PPM at pH 7.0 appear to be displaced to slightly higher A/N_p than at pH 3.0, which might suggest greater expansion of the PPM at the pH 7.0 interface, due to their greater swelling and/or deformability at the higher pH value. Such effects would obviously be related to the different charges on the PPM at the two pH values. However, the **Supplementary Figure S4.3** shows the average values of π and their standard deviation for 3 separate experiments, compressed 3 times, *i.e.*, 9 isotherms for both pH 7.0 and pH 3.0 and it is seen that within experimental error there is negligible difference between the two, within the error of reproducibility. It is difficult to make more accurate measurements because of the experimental difficulty of ensuring that none of the spreading solution is lost to the sub phase during the spreading, which is a common problem when spreading any proteinaceous material as opposed to completely insoluble surfactants. The inset to **Figure 4.7a** compares the average of the two isotherms for PPM at pH 3.0 in the main Figure with the

average π v. A/N_p isotherm for whey protein microgels (WPM) also spread at pH 3.0, taken from previously published work (Zembyla et al., 2019). In this case the mean r of the WPM was 45 nm. The far more expanded isotherm for the WPM compared to the PPM is well within any experimental error, so that the PPM can be concluded to be far less deformed than WPM on adsorption at the A-W interface. For example, if the linear π - A/N_p region at the highest π is measured are extrapolated to the A/N_p axis, as shown by the straight dashed lines on **Figure 4.7a**, the intercept may be taken as the effective PPM cross-sectional area within the interface at which the PPM start to interact strongly. Assuming the PPM adopt a circular cross-sectional area of radius r' and that the maximum 2-dimensional packing fraction (Zembyla et al., 2019) of these 'circles' is 0.9069, then the intercept of $0.31 \mu\text{m}^2$ translates to $r' = 310$ nm. It is seen that r' is only moderately larger than $r = 125$ nm for the un-deformed PPM, whereas the equivalent r' for WPM is ~ 4 x larger, despite r being smaller for WPM (Destribats et al., 2014c, Andablo-Reyes et al., 2019). Although instructive, such calculations ignore the wide distribution of microgel particle sizes (*e.g.*, see **Figure 4.1a**) and/or their aggregates and a lack of knowledge of the contact angles of such particle at the interface, so that absolute magnitude of these r' values should be treated with caution. The main reason for the conducting the isotherm experiments was to gain more insight into the effect of CNCs when present in addition to PPM particles at the interface.

Figure 4.7b shows isotherms for 100 μl of 0.04 wt% CNC dispersion spread at the A-W interface at pH 3.0. CNC particle dimensions of a cylinder of diameter 6 nm and length 100 nm, plus a particle density of 1.5 g cm^{-3} , were used to calculate N_p spread. (The cylinder volume is equivalent to that of a sphere of radius only 8.8 nm, hence the much lower values of A/N_p , since N_p is so much higher despite the concentration spread being lower). It is seen that $\pi = 0 \pm 0.5 \text{ mN m}^{-1}$ for either the first or second compression. This experiment was repeated many times, sometimes increasing the CNC concentration spread, but the result was always the same. This suggests that the CNCs are not surface active enough to be retained by the A-W interface, but that they disperse into the aqueous subphase. **Figure 4.7c** shows isotherms for PPM spread as in **Figure 4.7a** at pH 3.0, but followed by spreading of 100 μl of 0.04 wt% CNC

dispersion (as in **Figure 4.7b**) at the maximum trough area (*i.e.*, $\pi = 0 \text{ mN m}^{-1}$) on top of the PPM film. In view of the results in **Figure 4.7b**, it is perhaps not surprising that the PPM isotherm is not much affected by the addition of the apparently non-surface active CNC. Therefore, if any CNC particles that are associated with the adsorbed PPM they must be on top of (or below) the PPM layer and not within it.

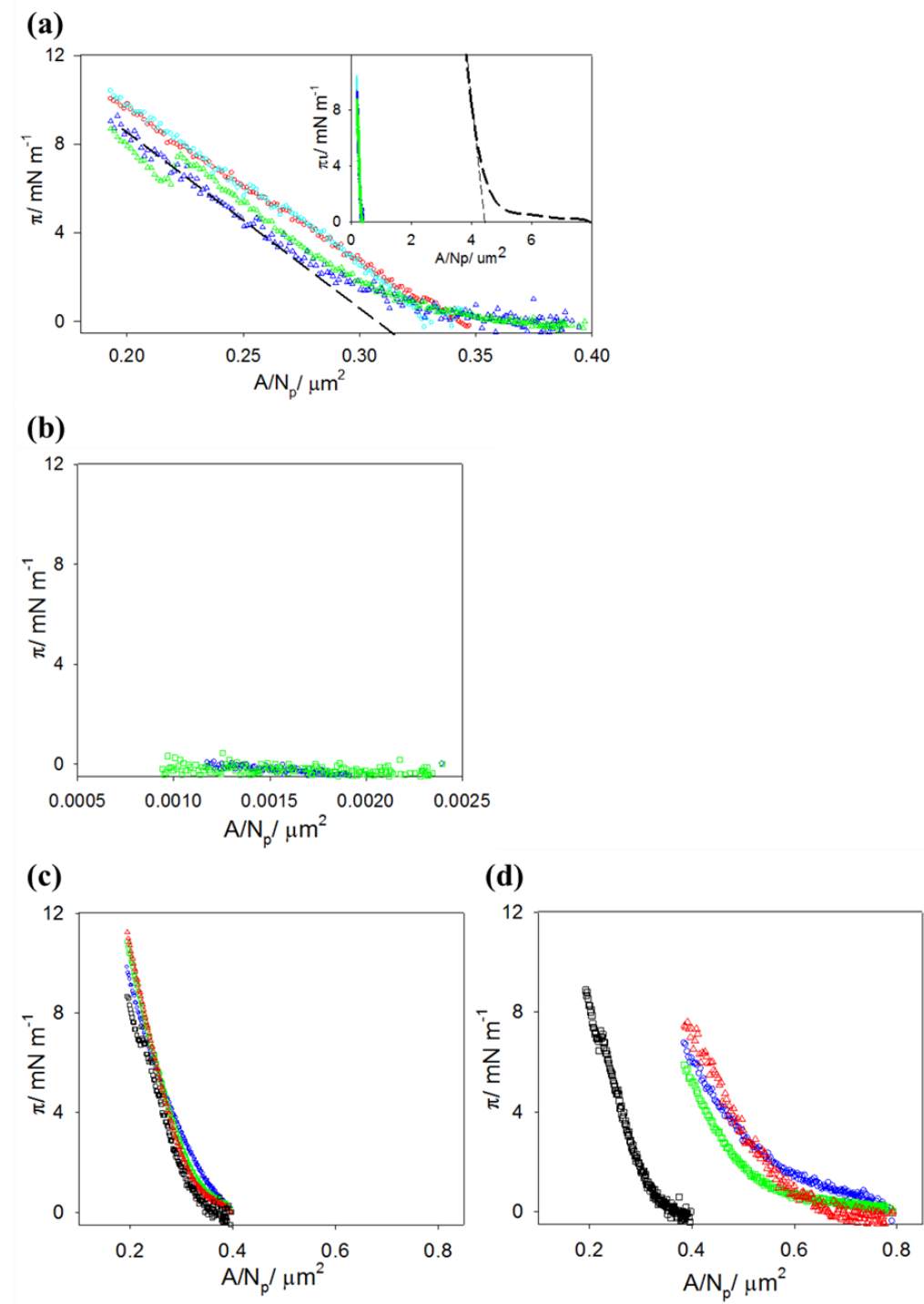


Figure 4.7. Surface pressure (π) versus area per particle (A/N_p) spread at the A-

W interface for various systems. (a) 0.466 wt% PPM at pH 7.0 (■, □) and pH 3.0 (△, ▽): 1st compressions ■, ▽; 2nd compressions □, △. (b) 0.04 wt% CNC alone at pH 3.0: 1st compression △; 2nd compression □. (c) 0.466 wt% PPM spread first at pH 3.0, followed by spreading of 0.04 wt% CNC on top of PPM: 1st compression ■; 2nd compression □; 3rd compression △; average π -A/N_p result for 0.466 wt% PPM alone at pH 3.0 from (a) above □. (d) Mixture of 0.02 wt% CNC + 0.233 wt% PPM at pH 3.0: 1st compression ■; 2nd compression □; 3rd compression △; average π -A/N_p result for 0.466 wt% PPM alone at pH 3.0 from (a) above □. The dashed curve in the inset of Figure (a) shows the isotherm for whey protein microgels (WPM) taken from reference (Zembyla et al., 2019) compared to the pH 3.0 data for PPM in (a). The dashed straight lines in (a) are the extrapolations to estimate the dimensions of the adsorbed microgels (see text).

Figure 4.7d shows the result of spreading 100 μ l of a mixed solution of 0.0233 wt% PPM + 0.02 wt% CNC. Despite these PPM and CNC concentrations being half those in **Figures 4.7a-c**, the isotherm is much more expanded than that for the sequential addition in **Figure 4.7c**. In fact, this is why the concentrations had to be reduced in the spreading solution - to obtain a region where π tends to zero at the start of the compression. Thus, co-adsorbing PPM and CNC apparently leads to a much different film structure, presumably with some CNC embedded within the PPM film in the interfacial region – although we have no direct evidence for this as yet. However, this is not how the emulsion droplet interface is formed: PPM adsorbs first, stabilizing the emulsion and then CNC is added afterwards. Therefore, the adsorbed film structure is more likely to resemble that formed in the sequential adsorption experiment in **Figure 4.7c**, *i.e.*, if any CNC adsorbs it does so to the outside of the primary adsorbed PPM film. However, one should note that eventually the surface layers will approach the same final “equilibrium” composition and structure, irrespective of the sequence of addition of the particulate layers. Possibly the stark differences in the results illustrated in **Figures 4.7c and d** partly explain some of the apparent disagreements between the data in the literature concerning the surface activity (or not) of various CNCs. CNC may appear to be surface active when it is co-adsorbed with proteins but not on its own. Certainly the CNC used in these experiments has been shown elsewhere (Du Le et al., 2020) not to depress the tension at the oil-water interface.

4.3.7 Particle size distributions of PPM-E with different CNC concentrations.

As shown in **Figure 4.8a**, the PSDs of PPM-E + CNC with 1 to 3 wt% CNC at pH 3.0 were bimodal, with the largest peak between 1 and 100 μm . The smaller peak between 0.1 and 1 μm most likely represented free PPM particles (as discussed earlier for the PPM-E emulsions) and/or free CNC particles and/or free PPM + CNC electrostatic complexes. The PSD in all of PPM-E + CNC systems was noticeably shifted to lower sizes compared to that of PPM-E at pH 3.0, in particular the main peak. This is consistent with significantly ($p < 0.05$) lower d_{43} : 16, 12 and 14 μm for 1, 2 and 3 wt% CNC respectively, suggesting that the CNCs reduce droplet flocculation. (Sarkar et al., 2018a)

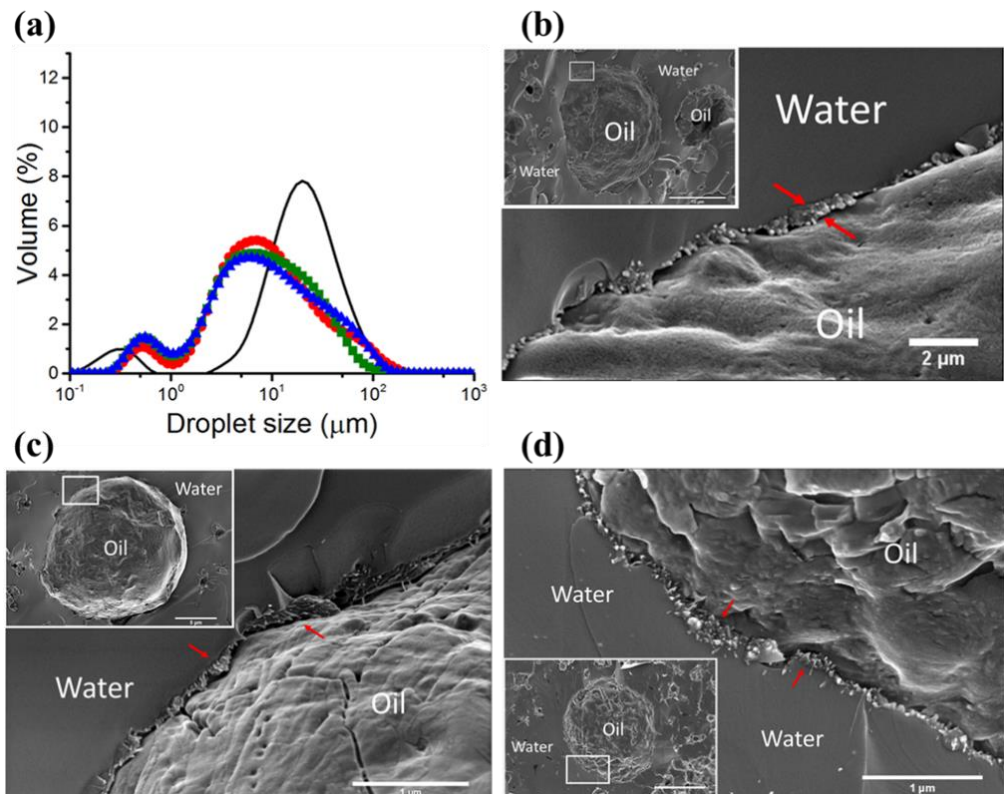


Figure 4.8. (a) PSDs of freshly prepared 20 wt% O/W emulsions at pH 3.0: stabilized by PPM only (PPM-E) (-); PPM-E with 1 wt% CNC (●), PPM-E with 2 wt% CNC (■); PPM-E with 3 wt% CNC (▲). Cryo-SEM micrograph and partial enlarged detail of PPM-E with: (b) 1 wt% CNC (c) 2 wt% CNC, (d) 3 wt% CNC (d). Scale bars represent in (b) 10 μm , in (c) and (d) 5 μm . The red arrows indicate what are thought to be CNC particles.

Interestingly, there was a slight increase of d_{43} when the CNC

concentration was increased 2 wt% to 3 wt%, possibly due to depletion flocculation *via* excess CNC. (Sarkar et al., 2017c) Cryo-SEM images in **Figure 4.8b-d** clearly show CNCs adsorbed on the surface of the PPM-stabilized emulsion droplets, which appeared to have incomplete CNC surface coverage in case of PPM-E + CNC_{1.0}, and near full coverage in case of PPM-E + CNC_{3.0}.

4.3.8 Rheological properties of PPM-E + CNC emulsions.

More detailed measurements were made on the influence of the CNCs on the viscoelasticity of the PPM-E + CNC emulsions (**Figure 4.9**). All emulsions with 1 to 3 wt% CNC were shear thinning over the shear rate ranging 0.1 to 1000 s⁻¹ (**Figure 4.9a**), with the flow index (n) < 1 (**Table 4.1**). As the CNC concentration increased the consistency index (K) increased significantly ($p < 0.01$) (**Table 4.1**), suggesting a stronger attractive inter particle interaction between CNC-CNC and/or CNC-PPM. This was also supported by the optical images in **Figure 4.6b** based on the reduced flowability of PPM- E + CNCs at higher CNC concentration. At the same time, strain amplitude sweeps.

Figure 4.9b suggested that PPM-E with 2 wt% or 3 wt% CNC required a higher shear strain to break some sort of the network structure compared to 1 wt% CNC, as evidenced by the strain at which G' and G'' suddenly started to decrease. **Figure 4.9c** shows the frequency sweep curves of G' and G'' versus with frequency (Hz) $G' > G''$ for all emulsions between 0.01 and 10 Hz, further suggesting a gel-like viscoelastic network in the presence of CNC, (Zhang et al., 2019) particularly at the higher CNC concentrations (Hu et al., 2016a, Wei et al., 2020a, Bertsch et al., 2018). Note that both G' and G'' for PPM-E + CNC_{1.0} were higher than for PPM-E (**Figure 4.9c and Supplementary Figure S4.4**), *i.e.*, without CNC, confirming the essential nature of CNC to the network formation process (Hu et al., 2016a, Wei et al., 2020a). It is worth noting that both the shear thinning behaviour (**Supplementary Figure S4.5a**) and the gel-like behaviour (**Supplementary Figure S4.5b**) were also observed in PPM + CNC dispersions without oil, highlighting the influence of CNC in network formation in the bulk phase.

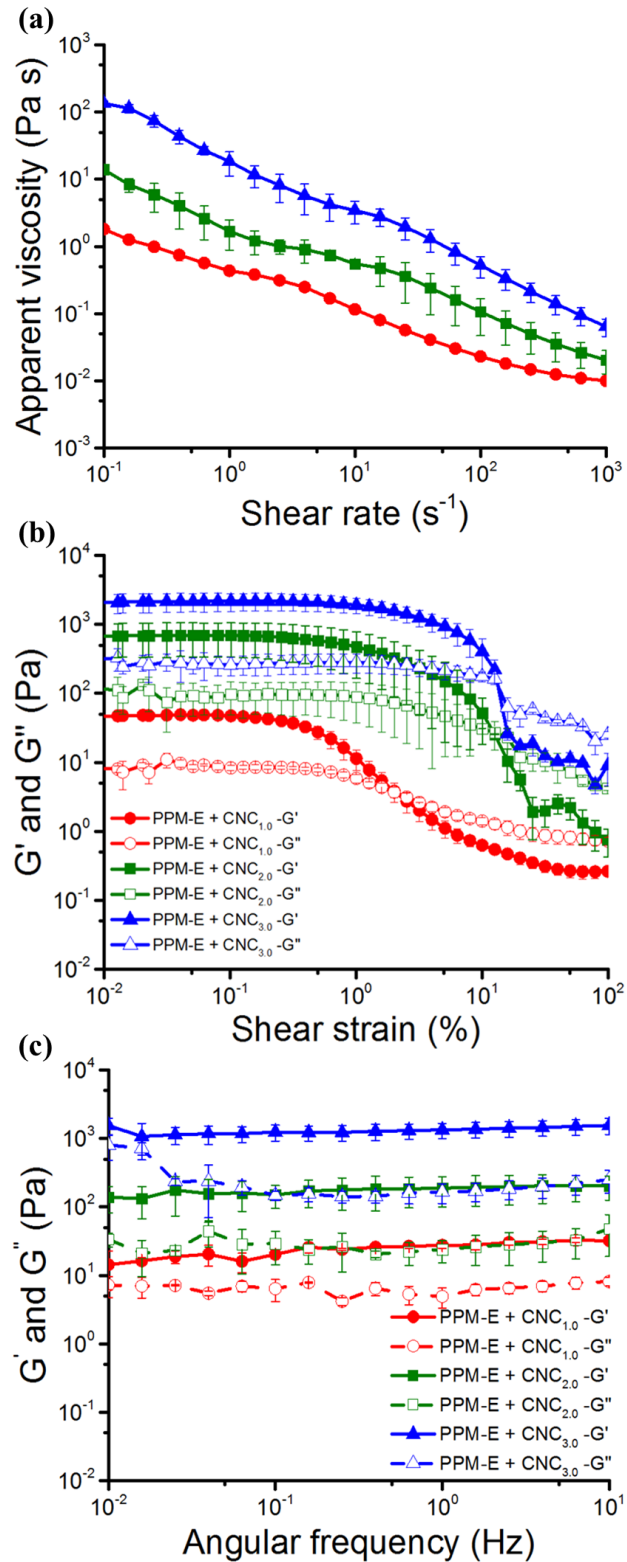


Figure 4.9. (a) Flow curves, (b) strain amplitude sweep curves, (c) frequency sweep curves of freshly prepared 20 wt% oil-in-water emulsions at pH 3 stabilized by PPM (PPM-E) with 1 wt% CNC (PPM-E + CNC_{1.0}) (●), 2 wt% CNC (PPM-E + CNC_{2.0}) (■) and 3 wt% CNC (PPM-E + CNC_{3.0}) (▲). Error bars represent standard deviations.

Table 4.1. Consistency index (K) and flow behaviour index (n) of PPM-E + 1, 2 or 3 wt% CNC.

Power-Law Model	<i>Ostwald de Waele fit for the</i>		R ²
	<i>apparent viscosity (η_a)</i>		
	$\eta_a(\dot{\gamma}) = K(\dot{\gamma})^{n-1}$		
	<i>n</i>	<i>K (Pa sⁿ)</i>	
PPM-E + CNC _{1.0}	0.3 ± 0.1	0.5 ± 0.1 ^a	0.95
PPM-E + CNC _{2.0}	0.3 ± 0.1	1.0 ± 0.3 ^b	0.99
PPM-E + CNC _{3.0}	0.2 ± 0.1	18.1 ± 6.6 ^c	0.93

Note: Different superscripts (a-c) in the same column represent significant differences between different samples at $p < 0.05$ level. The superscript n in units for K is the flow behaviour index.

4.3.9 *In vitro* gastric digestion of PPM-E + CNC.

As hypothesized, the presence of SGF without pepsin had only a slight effect on PPM-E + CNC (see **Figure 4.10**, **Supplementary Table S4.1** and **Table 4.2**). All the PPM-E + CNC emulsions at 0 min had no significant differences in the mean droplet size as compared to those of freshly prepared emulsions at pH 3.0. The zeta-potential of PPM-E + CNC_{1.0} at 0 min was also the same as the freshly prepared emulsion ($p > 0.05$) (see **Supplementary Table S4.1** and **Table 4.2**), but the zeta-potential of both PPM-E + CNC_{2.0} and PPM-E + CNC_{3.0} at 0 min were slightly less negative compared to the fresh emulsions. These results suggested that the droplets did not initially aggregate and so all the PPM-E + CNC were stable in the absence of pepsin action, similar to the behaviour of the PPM-E noted earlier.

After being incubated in SGF with pepsin, the mean droplet size (d_{43}) of PPM-E + CNC_{1.0} showed no significant change during gastric digestion for 2 h (**Figure 4.10d** and **Supplementary Table S4.1**) whilst there was an increase in the vol% of the minor peak between 0.1 and 1 μm in the first 30 min (**Figure 4.10a**) and a significant decrease in the d_{32} , as summarised in **Figure 4.10d** and **Supplementary Table S4.1**. This suggests the pepsin digested the aggregated network of unabsorbed PPM particles in the first 30 min, freeing up more primary emulsion droplets. Both PPM-E + CNC_{2.0} and PPM-E + CNC_{3.0} showed

similar changes: d_{32} and d_{43} remained constant ($p > 0.05$) within the first 30 min (**Figure 4.10d** and **Supplementary Table S4.1**), whilst there was a similar increase in the vol% of the minor peak (**Figure 4.10b, c**) but the mean particle sizes had decreased considerably ($p < 0.05$) after 120 min digestion (**Figure 4.10d** and **Supplementary Table S4.1**). A possible explanation for these reduced mean particle sizes might be that pepsinolysis of the aggregated network of PPM. It was also thought the CNCs might reduce pepsin activity by either binding or trapping the enzyme in the CNC network in the continuous phase. This was confirmed *via* the pepsin activity assay with 2% w/v protein (haemoglobin) mixed with CNC, as showed in **Table 4.3**. The pepsin activity reduced from ~ 655 U/mg to 100-160 U/mg after adding CNCs to the protein dispersion. Consequently, the CNC can reduce pepsinolysis and breakdown of the PPM-stabilized emulsions in two ways: (i) binding to the PPM-laden interface and (ii) bonding or trapping the enzyme.

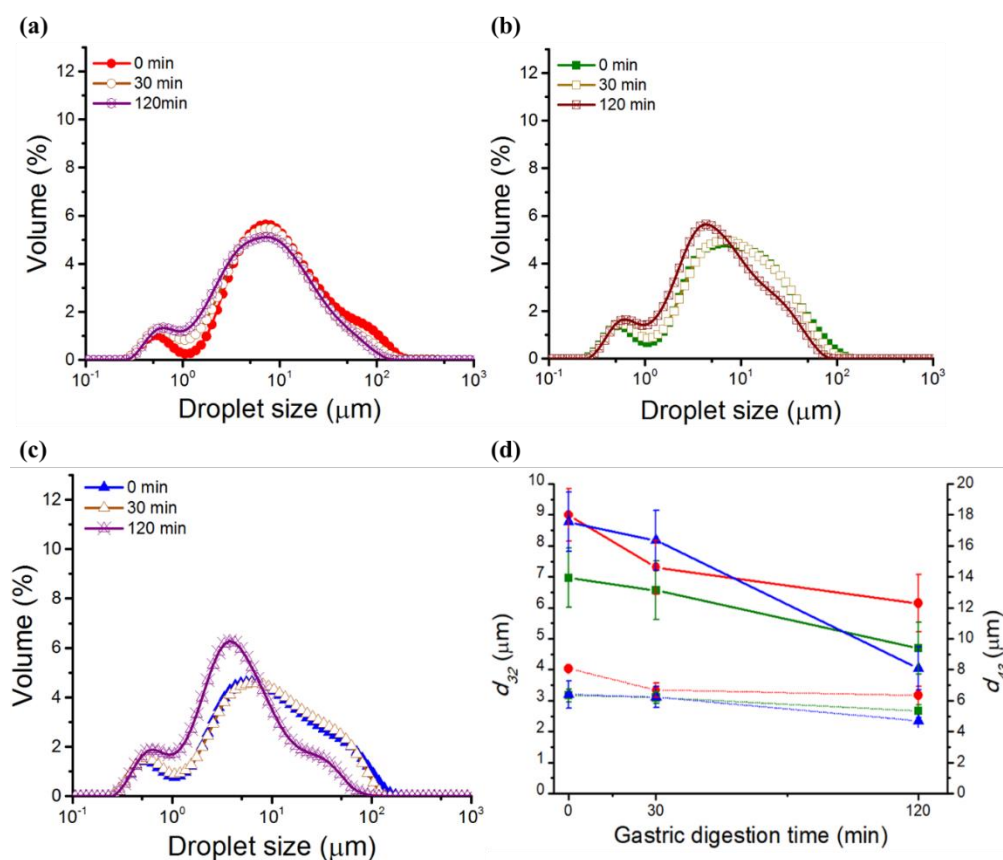


Figure 4.10. PSDs of PPM-E with: (a) 1 wt%, (b) 2 wt%, (c) 3 wt% CNC after different *in vitro* gastric digestion times. Time 0 min represents the emulsion + SGF mixture at pH 3.0 without the addition of pepsin. (d) Shows d_{32} (···) and

d_{43} (-) at 0, 30 and 120 min for 1 (●), 2 (■) and 3 wt% CNC (▲). Error bars represent standard deviations.

Table 4.2. Mean zeta-potential of PPM-E with 1, 2 and 3 wt% CNC after 0, 30 and 120 min *in vitro* gastric digestion. Time 0 min represents the emulsion + SGF mixture at pH 3.0 without the addition of pepsin.

Mean zeta-potential (mV)	Digestion time (min)		
	0	30	120
PPM-E + CNC _{1.0}	5.9 ± 1.3 ^a	-5.5 ± 2.5 ^b	-8.8 ± 1.4 ^b
PPM-E + CNC _{2.0}	-29.7 ± 3.2 ^a	-18.5 ± 1.5 ^b	-20.5 ± 2.7 ^b
PPM-E + CNC _{3.0}	-34.3 ± 2.5 ^a	-26.1 ± 2.5 ^b	-26.0 ± 2.5 ^b

Note: Different superscripts (a-b) in the same column indicate significant differences between different samples at $p < 0.05$ level.

PPM-E + CNC_{1.0} droplets showed a significant change in zeta-potential ($p < 0.05$) after simulated gastric digestion (see **Table 4.2**). The zeta-potential changed from ~ +6 mV to -6 mV within 30 min, followed by a more gradual change to -9 mV by the end of the digestion time. This seems to indicate a loss of PPM from the interface. However, there was no increase in mean droplet size, as mentioned before. Since a negative value of zeta would seem to indicate the predominance of CNC at the interface, the peptide fragments produced by hydrolysis combined with the CNC must form a new type of protective shell surrounding oil droplets, preventing coalescence. Both PPM-E + CNC_{2.0} and PPM-E + CNC_{3.0} showed a significant change in zeta-potential ($p < 0.05$) after 30 min, zeta-potential changing from -30 mV to -20 mV and from -35 mV to -26 mV, respectively. In the case of PPM-E + CNC_{3.0}, this was followed by a stable zeta-potential until the end of the digestion time.

Table 4.3. Pepsin activity assay with 2 % w/v hemoglobin mixed with 1 wt% or 2 wt% CNC.

Substrate	Pepsin activity (U/mg)
Haemoglobin	654.7 ± 53.4 ^a
Haemoglobin+ CNC _{1.0}	133.8 ± 109.3 ^b
Haemoglobin + CNC _{2.0}	158.8 ± 97.8 ^b

Note: Different superscripts (a-b) in the same column represent results with significant differences between different samples at $p < 0.05$ level.

Confocal micrographs of PPM-E + CNC emulsions before and after digestion, shown in **Figure 4.11**, also provide evidence that no large coalesced oil droplets were formed after 2 h incubation, except PPM-E + CNC_{1.0}. Interestingly, the blue color, *i.e.*, the stain for cellulose in the micrographs before digestion with increasing CNC concentration is enhanced, *i.e.*, darker blue, suggesting concentration of the CNC into specific regions. These regions probably represent the gel-like network in bulk that get stronger with increasing CNC concentration, as discussed above. The inset to the micrographs are photographs of the emulsions and show that no phase separation was observed, emphasizing again the greater stability of the emulsions to gastric digestion when CNC was added.

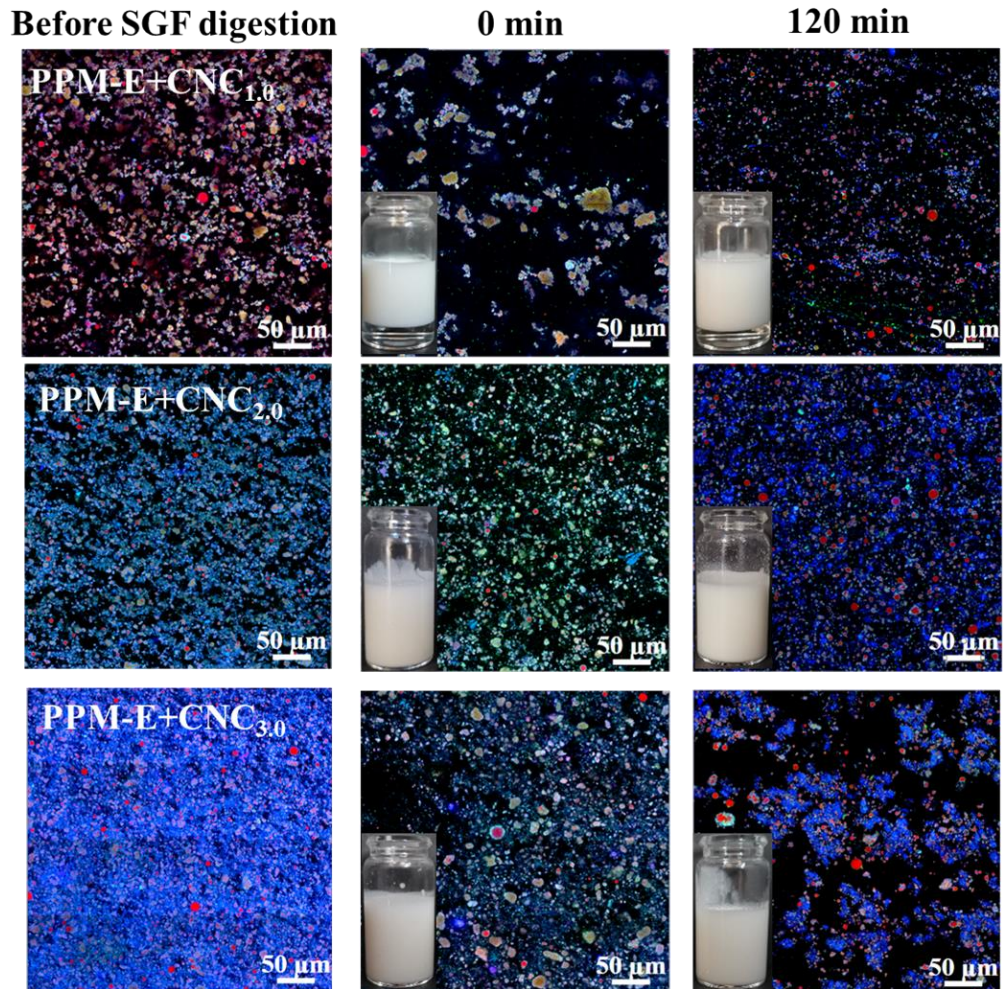


Figure 4.11. Confocal micrographs of 20 wt% oil-in-water emulsions stabilized by PPM (PPM-E) and 1 wt% CNC (PPM-E + CNC_{1.0}), 2 wt% CNC (PPM-E + CNC_{2.0}), and 3 wt% CNC (PPM-E + CNC_{3.0}) as a function of *in vitro* gastric digestion time (0, 120 min) at pH 3.0. The green color represents PPM (stained by Nile Blue); the red color represents the oil phase (stained by Nile Red); the blue color represents the CNC (stained by Calcofluor White); the black color represents air or water. Time 0 min represents the PPM-E + SGF mixture at pH 3.0 without the addition of pepsin. Scale bar represents 50 μm .

4.4 Conclusions

This study set out to understand the *in vitro* gastric digestion fate of Pickering O/W emulsions stabilized by pea protein microgels (PPM) with and without added cellulose nanocrystals (CNC). The study confirms that emulsion droplets stabilized by pea protein microgels alone break down completely when subjected to *in vitro* gastric digestion conditions, which causes droplet coalescence and phase separation. Addition of CNC stabilizes the emulsions

against these effects. The added stability may be the result of the CNCs binding electrostatically to the outside of the adsorbed PPM layer at low pH, for which there is good evidence from zeta-potential and Langmuir trough experiments. On the other hand, rheological measurements indicate that the CNCs also induce the formation of a strong gel-like structure in the emulsions and it has also been shown that this CNC network can bind or trap the pepsin enzyme responsible for the digestion. This CNC-induced gelation and/or binding of the enzyme to the CNCs may restrict the access of the pepsin to the substrate sites available in the PPM and so contribute to the greater gastric stability of the emulsions. Such emulsions, based on complex plant-based particulate interfaces might be used to deliver bioactive molecules that require protection in the gastric regime. Pickering emulsions formed by PPM or the complex PPM + CNC interfaces were compared on their stability during *in vitro* gastrointestinal digestion in the next chapter (**Chapter 5**).

4.5 References

- ANDABLO-REYES, E., YERANI, D., FU, M., LIAMAS, E., CONNELL, S., TORRES, O. & SARKAR, A. 2019. Microgels as viscosity modifiers influence lubrication performance of continuum. *Soft Matter*, 15, 9614-9624.
- ANSON, M. L. & MIRSKY, A. E. 1932. The estimation of pepsin with hemoglobin. *The Journal of general physiology*, 16, 59-63.
- ARAIZA-CALAHORRA, A. & SARKAR, A. 2019a. Designing biopolymer-coated Pickering emulsions to modulate in vitro gastric digestion: a static model study. *Food Funct*, 10, 5498-5509.
- ARAIZA-CALAHORRA, A. & SARKAR, A. 2019b. Pickering emulsion stabilized by protein nanogel particles for delivery of curcumin: Effects of pH and ionic strength on curcumin retention. *Food Structure*, 21, 100113.
- BERTSCH, P., DIENER, M., ADAMCIK, J., SCHEUBLE, N., GEUE, T., MEZZENGA, R. & FISCHER, P. 2018. Adsorption and Interfacial Layer Structure of Unmodified Nanocrystalline Cellulose at Air/Water Interfaces. *Langmuir*, 34, 15195-15202.
- DAVID-BIRMAN, T., MACKIE, A. & LESMES, U. 2013. Impact of dietary fibers on the properties and proteolytic digestibility of lactoferrin nanoparticles. *Food Hydrocolloids*, 31, 33-41.
- DESTREBATS, M., ROUVET, M., GEHIN-DELVAL, C., SCHMITT, C. & BINKS, B. P. 2014. Emulsions stabilized by whey protein microgel particles: towards food-grade Pickering emulsions. *Soft Matter*, 10, 6941-54.
- DESTREBATS, M., WOLFS, M., PINAUD, F., LAPEYRE, V., SELLIER, E., SCHMITT, V. & RAVAINÉ, V. 2013. Pickering emulsions stabilized by soft microgels: influence of the emulsification process on particle interfacial organization and emulsion properties. *Langmuir*, 29, 12367-

74.

- DICKINSON, E. 2012. Use of nanoparticles and microparticles in the formation and stabilization of food emulsions. *Trends in Food Science & Technology*, 24, 4-12.
- DICKINSON, E. 2015. Microgels — An alternative colloidal ingredient for stabilization of food emulsions. *Trends in Food Science & Technology*, 43, 178-188.
- DU LE, H., LOVEDAY, S. M., SINGH, H. & SARKAR, A. 2020. Pickering emulsions stabilized by hydrophobically modified cellulose nanocrystals: Responsiveness to pH and ionic strength. *Food Hydrocolloids*, 99, 105344.
- EHMANN, H. M., SPIRK, S., DOLISKA, A., MOHAN, T., GOSSLER, W., RIBITSCH, V., SFILIGOJ-SMOLE, M. & STANA-KLEINSCHEK, K. 2013. Generalized indirect fourier transformation as a valuable tool for the structural characterization of aqueous nanocrystalline cellulose suspensions by small angle X-ray scattering. *Langmuir*, 29, 3740-8.
- FILIPPIDI, E., PATEL, A. R., BOUWENS, E. C. M., VOUDOURIS, P. & VELIKOV, K. P. 2014. All-natural oil-filled microcapsules from water-insoluble proteins. *Advanced Functional Materials*, 24, 5962-5968.
- FRENCH, D. J., BROWN, A. T., SCHOFIELD, A. B., FOWLER, J., TAYLOR, P. & CLEGG, P. S. 2016. The secret life of Pickering emulsions: particle exchange revealed using two colours of particle. *Sci Rep*, 6, 31401.
- GEORGE, J. & SABAPATHI, S. N. 2015. Cellulose nanocrystals: synthesis, functional properties, and applications. *Nanotechnol Sci Appl*, 8, 45-54.
- GONG, Y., WANG, M. & HE, J. 2016. The behaviour of hydrophobic-core/hydrophilic-shell structured microgels at an interface: from Pickering emulsion to colloidosomes with dual-level controlled permeability. *RSC Advances*, 6, 95067-95072.
- HU, H.-Y., XING, L.-J., HU, Y.-Y., QIAO, C.-L., WU, T., ZHOU, G.-H. & ZHANG, W.-G. 2016. Effects of regenerated cellulose on oil-in-water

- emulsions stabilized by sodium caseinate. *Food Hydrocolloids*, 52, 38-46.
- LAGUNA, L., PICOUET, P., GUÀRDIA, M. D., RENARD, C. M. G. C. & SARKAR, A. 2017. In vitro gastrointestinal digestion of pea protein isolate as a function of pH, food matrices, autoclaving, high-pressure and re-heat treatments. *Lwt*, 84, 511-519.
- LI, X. & DE VRIES, R. 2018. Interfacial stabilization using complexes of plant proteins and polysaccharides. *Current Opinion in Food Science*, 21, 51-56.
- LIU, F. & TANG, C.-H. 2016. Soy glycinin as food-grade Pickering stabilizers: Part. III. Fabrication of gel-like emulsions and their potential as sustained-release delivery systems for β -carotene. *Food Hydrocolloids*, 56, 434-444.
- LUO, Q., BOOM, R. M. & JANSSEN, A. E. M. 2015. Digestion of protein and protein gels in simulated gastric environment. *LWT - Food Science and Technology*, 63, 161-168.
- MESHULAM, D. & LESMES, U. 2014. Responsiveness of emulsions stabilized by lactoferrin nano-particles to simulated intestinal conditions. *Food & function*, 5, 65-73.
- MINEKUS, M., ALMINGER, M., ALVITO, P., BALLANCE, S., BOHN, T., BOURLIEU, C., CARRIERE, F., BOUTROU, R., CORREDIG, M., DUPONT, D., DUFOUR, C., EGGER, L., GOLDING, M., KARAKAYA, S., KIRKHUS, B., LE FEUNTEUN, S., LESMES, U., MACIERZANKA, A., MACKIE, A., MARZE, S., MCCLEMENTS, D. J., MENARD, O., RECIO, I., SANTOS, C. N., SINGH, R. P., VEGARUD, G. E., WICKHAM, M. S., WEITSCHIES, W. & BRODKORB, A. 2014. A standardised static in vitro digestion method suitable for food - an international consensus. *Food Funct*, 5, 1113-24.
- MURRAY, B. S. 1997. Equilibrium and dynamic surface pressure-area measurements on protein films at air-water and oil-water interfaces.

Colloids and Surfaces A: Physicochemical and Engineering Aspects,
125, 73-83.

MURRAY, B. S. 2019a. Microgels at fluid-fluid interfaces for food and drinks.
Advances in Colloid and Interface Science, 271, 101990.

MURRAY, B. S. 2019b. Pickering emulsions for food and drinks. *Current
Opinion in Food Science*, 27, 57-63.

MURRAY, B. S., CATTIN, B., SCHÜLER, E. & SONMEZ, Z. O. 2002.
Response of adsorbed protein films to rapid expansion. *Langmuir*, 18,
9476-9484.

MURRAY, B. S. & NELSON, P. V. 1996. A novel Langmuir trough for
equilibrium and dynamic measurements on air-water and oil-water
monolayers. *Langmuir*, 12, 5973-5976.

NGUYEN, T. T. P., BHANDARI, B., CICHERO, J. & PRAKASH, S. 2015.
Gastrointestinal digestion of dairy and soy proteins in infant formulas:
An in vitro study. *Food Research International*, 76, 348-358.

NYEMB, K., GUÉRIN-DUBIARD, C., PÉZENNEC, S., JARDIN, J.,
BRIARD-BION, V., CAUTY, C., RUTHERFURD, S. M., DUPONT, D.
& NAU, F. 2016. The structural properties of egg white gels impact the
extent of in vitro protein digestion and the nature of peptides generated.
Food Hydrocolloids, 54, 315-327.

OPAZO-NAVARRETE, M., ALTENBURG, M. D., BOOM, R. M. & JANSSEN,
A. E. M. 2018. The effect of gel microstructure on simulated gastric
digestion of protein gels. *Food Biophys*, 13, 124-138.

PEINADO, I., LESMES, U., ANDRES, A. & MCCLEMENTS, J. D. 2010.
Fabrication and morphological characterization of biopolymer particles
formed by electrostatic complexation of heat treated lactoferrin and
anionic polysaccharides. *Langmuir*, 26, 9827-34.

PENG, W., KONG, X., CHEN, Y., ZHANG, C., YANG, Y. & HUA, Y. 2016.
Effects of heat treatment on the emulsifying properties of pea proteins.
Food Hydrocolloids, 52, 301-310.

- SARKAR, A., ADEMUYIWA, V., STUBLEY, S., ESA, N. H., GOYCOOLEA, F. M., QIN, X., GONZALEZ, F. & OLVERA, C. 2018a. Pickering emulsions co-stabilized by composite protein/ polysaccharide particle-particle interfaces: Impact on in vitro gastric stability. *Food Hydrocolloids*, 84, 282-291.
- SARKAR, A. & DICKINSON, E. 2020. Sustainable food-grade Pickering emulsions stabilized by plant-based particles. *Current Opinion in Colloid & Interface Science*, 49, 69-81.
- SARKAR, A., LI, H., CRAY, D. & BOXALL, S. 2018b. Composite whey protein–cellulose nanocrystals at oil-water interface: Towards delaying lipid digestion. *Food Hydrocolloids*, 77, 436-444.
- SARKAR, A., MURRAY, B., HOLMES, M., ETTELAIE, R., ABDALLA, A. & YANG, X. 2016. In vitro digestion of Pickering emulsions stabilized by soft whey protein microgel particles: influence of thermal treatment. *Soft Matter*, 12, 3558-69.
- SARKAR, A., ZHANG, S., HOLMES, M. & ETTELAIE, R. 2019. Colloidal aspects of digestion of Pickering emulsions: Experiments and theoretical models of lipid digestion kinetics. *Adv Colloid Interface Sci*, 263, 195-211.
- SARKAR, A., ZHANG, S., MURRAY, B., RUSSELL, J. A. & BOXAL, S. 2017. Modulating in vitro gastric digestion of emulsions using composite whey protein-cellulose nanocrystal interfaces. *Colloids Surf B Biointerfaces*, 158, 137-146.
- SCHEUBLE, N., GEUE, T., WINDHAB, E. J. & FISCHER, P. 2014. Tailored interfacial rheology for gastric stable adsorption layers. *Biomacromolecules*, 15, 3139-45.
- SHAO, Y. & TANG, C.-H. 2016. Gel-like pea protein Pickering emulsions at pH 3.0 as a potential intestine-targeted and sustained-release delivery system for β -carotene. *Food Research International*, 79, 64-72.
- SHIMONI, G., SHANI LEVI, C., LEVI TAL, S. & LESMES, U. 2013.

- Emulsions stabilization by lactoferrin nano-particles under in vitro digestion conditions. *Food Hydrocolloids*, 33, 264-272.
- TORRES, O., MURRAY, B. S. & SARKAR, A. 2019. Overcoming in vitro gastric destabilisation of emulsion droplets using emulsion microgel particles for targeted intestinal release of fatty acids. *Food Hydrocolloids*, 89, 523-533.
- TZOUMAKI, M. V., MOSCHAKIS, T., SCHOLTEN, E. & BILIADERIS, C. G. 2013. In vitro lipid digestion of chitin nanocrystal stabilized o/w emulsions. *Food Funct*, 4, 121-9.
- WEI, Y., CAI, Z., WU, M., GUO, Y., TAO, R., LI, R., WANG, P., MA, A. & ZHANG, H. 2020. Comparative studies on the stabilization of pea protein dispersions by using various polysaccharides. *Food Hydrocolloids*, 98, 105233.
- XIAO, J., LI, C. & HUANG, Q. 2015. Kafirin nanoparticle-stabilized Pickering emulsions as oral delivery vehicles: Physicochemical stability and *in vitro* digestion profile. *J Agric Food Chem*, 63, 10263-70.
- YOUNAS, M., NOREEN, A., SHARIF, A., MAJEED, A., HASSAN, A., TABASUM, S., MOHAMMADI, A. & ZIA, K. M. 2019. A review on versatile applications of blends and composites of CNC with natural and synthetic polymers with mathematical modeling. *Int J Biol Macromol*, 124, 591-626.
- ZEMBYLA, M., LAZIDIS, A., MURRAY, B. S. & SARKAR, A. 2019. Water-in-oil Pickering emulsions stabilized by synergistic particle-particle interactions. *Langmuir*, 35, 13078-13089.
- ZHANG, S., HOLMES, M., ETTOLAIE, R. & SARKAR, A. 2020. Pea protein microgel particles as Pickering stabilizers of oil-in-water emulsions: Responsiveness to pH and ionic strength. *Food Hydrocolloids*, 102, 105583.
- ZHANG, X., LIU, Y., WANG, Y., LUO, X., LI, Y., LI, B., WANG, J. & LIU, S. 2019. Surface modification of cellulose nanofibrils with protein

nanoparticles for enhancing the stabilization of O/W pickering emulsions. *Food Hydrocolloids*, 97, 105180.

ZHOU, F. Z., YAN, L., YIN, S. W., TANG, C. H. & YANG, X. Q. 2018. Development of Pickering emulsions stabilized by gliadin/proanthocyanidins hybrid particles (GPHPs) and the fate of lipid oxidation and digestion. *J Agric Food Chem*, 66, 1461-1471.

Chapter 5^d

Gastrointestinal fate and fatty acid release of Pickering emulsions stabilized by mixtures of plant protein microgels + cellulose particles: an *in vitro* static digestion study

Abstract

The present study aims to investigate the *in vitro* intestinal digestion fate of Pickering emulsions with complex dual particle interfaces. Pickering oil-in-water emulsions (PPM-E) stabilized by plant (pea) protein-based microgels (PPM), as well as PPM-E where the interface was additionally covered by cellulose nanocrystals (CNC), were designed at acidic pH (pH 3.0). The gastrointestinal fate of the PPM-E and free fatty acid (FFA) release, was tested *via* the INFOGEST static *in vitro* digestion model and data was fitted using theoretical models. Lipid digestion was also monitored using lipase alone bypassing the gastric phase to understand the impact of proteolysis on FFA release. Coalescence was observed in the PPM-stabilized emulsions in the gastric phase, but not in the ones co-stabilized by CNC. However, coalescence occurred during the intestinal digestion stage, irrespective of the CNC concentration added (1-3 wt % CNC). The presence of CNC lowered the lipolysis kinetics but raised the extent of FFA release as compared to its absence ($p < 0.05$), due to lower levels of gastric coalescence, *i.e.*, a higher interfacial area. The trends were similar when just lipase was added with no prior gastric phase, although the extent and rate of FFA release was reduced in all emulsions, highlighting the importance of prior proteolysis in lipolysis of such systems. In summary, an electrostatically self-assembled interfacial structure of two types of oppositely-charged particles (at gastric pH) might be a useful strategy to enable enhanced delivery of lipophilic compounds that require protection in the stomach but release in the intestines.

^d Submitted for peer-reviewing in Zhang, S., Murray B S., Holmes, M., Ettelaie, R., Sarkar, A. (2022) Gastrointestinal fate and fatty acid release of Pickering emulsions stabilized by mixtures of plant protein microgels + cellulose particles: an *in vitro* static digestion study. *Food Biophysics*

5.1 Introduction

Oil-in-water emulsions are omnipresent in foods such as milk alternatives, cream, sauces, butter and functional beverages. Colloidal dispersions can be considered as an extremely efficient delivery system for macronutrients, micronutrients and nutraceuticals— including lipids, fat-soluble vitamins, omega-3 fatty acids, proteins and minerals (McClements et al., 2007, Singh et al., 2009, McClements, 2010, Benschitrit et al., 2012, Velikov and Pelan, 2008). However, many conventional emulsions suffer from physicochemical instability and concomitant variations in texture, appearance and bioavailability of the intrinsic components due to changes in temperature, pH extremes and high salt concentrations. Consequently, there has been an increasing interest in designing emulsions with enhanced and/or more controlled stability. Paramount amongst these developments has been the expansion of the range of particle-stabilized emulsions (Pickering emulsions), due to their higher resistance to coalescence and Ostwald ripening (Binks, 2002a, Binks and Horozov, 2006, Dickinson, 2010a, Sarkar et al., 2019b) plus additional opportunities for using such emulsions to develop novel ways of protecting and delivering bioactive species (Guo et al., 2017b, Sarkar et al., 2019b, Sarkar and Dickinson, 2020).

Sarkar et al. (2016c) designed whey protein microgel particles-laden Pickering oil-in-water (O/W) emulsions and determined their ability to control the extent and rate of lipolysis using INFOGEST *in vitro* gastrointestinal digestion models. Shimoni et al. (2013) and Meshulam and Lesmes (2014b) focused on lactoferrin nanoparticles (LFnp) as stabilizer and showed the influence of LFnp on O/W droplet stability during *in vitro* oral, gastric and intestinal conditions. These studies show promise of animal protein-based Pickering particles not only to design coalescence-resilient emulsions but also to control and mostly reduce the rate and degree of free fatty acid release during intestinal digestion.

With growing consumer demand for more plant-based food products, there has been an increasing attention on plant protein-based particles, such as soy glycinin (Liu and Tang, 2016a), soy protein nanoparticles (Zhao et al., 2021), kafirin nanoparticles (Xiao et al., 2015b), zein colloidal particles (ZCPs)

(Wei et al., 2021b, Wei et al., 2021d), peanut protein nanoparticles (Ning et al., 2019), and pea protein particles (Shao and Tang, 2016a, Zhang et al., 2021) as Pickering emulsion stabilizers. Although Pickering emulsions, in general, have proved to be more resistant to lipolysis due to the high energy barrier to their displacement from the interface by bile salts, studies using plant protein-based microgel particles are relatively scarce (Bellesi et al., 2016). Any emulsions stabilized by protein particles tend to destabilize under gastric conditions, due to the low pH, mucins and/or pepsin action, making them unsuitable for site-dependent release of hydrophobic bioactives to the intestines. For this reason, combinations of stabilizers have been tested to try and improve the stimuli-responsiveness of the Pickering emulsions to enable the release of lipid-soluble nutrients like β -carotene and curcumin (Wei et al., 2021d, Shimoni et al., 2013, Wei et al., 2020b, Surjit Singh et al., 2021, Araiza-Calahorra et al., 2020, Wei et al., 2021b, Meshulam and Lesmes, 2014b).

Meshulam and Lesmes (2014b) found that the combining of LFnp-stabilized emulsions with alginate reduced the extent and reaction rate of lipolysis, while free fatty acids (FFAs) release was enhanced in the case of the emulsions mixed with iota-carrageenan. Wei et al. (2021b) reported that the bioaccessibility of β -carotene ranged from 9.1 to 27.2% while the extent of FFA release ranged from 19.5 to 12.9% on adjusting the mass ratio of hydrophilic cellulose nanocrystals (CNC) to ZCP-stabilized Pickering emulsions. Apart from the above mentioned examples, it seems that there have been a limited number of studies of the digestion of Pickering O/W emulsions stabilized by combinations of different particles. Such combination of particles offer complex interfaces might provide an improved route to create O/W emulsion based encapsulation systems for bioactive compounds based on plant biopolymers, since many plant storage proteins and polysaccharides are relatively insoluble in the first place.

Consequently, the aim of this study was to investigate the stability of an O/W emulsion stabilized by plant-based pea protein microgels + CNC and understand the influence that this dual particle system has on FFA release from the emulsion when passing through in vitro intestinal digestion conditions without/ with a prior gastric digestion step. The thermally-cross-linked-sheared

pea protein microgel particles (PPM), produced *via* a top down approach, have already proven their ability to serve as soft Pickering-like stabilizers of O/W emulsions (Zhang et al., 2020). These Pickering emulsions (PPM-E) showed high stability to varying temperature, pH and ionic strength. However, not surprisingly, destabilization occurred in the presence of pepsin at low pH, *i.e.*, simulated gastric conditions (Zhang et al., 2021). It was demonstrated that the addition of unmodified CNC at pH 3.0 led to the formation of a stronger and more coherent interfacial layer, proven *via* Langmuir trough experiments (Zhang et al., 2021). This strengthening was based on electrostatic attraction between the positively charged PPM and the negatively charged CNC at this pH. The negative charge on the CNC is a result of their production *via* sulfuric acid hydrolysis of cellulose and subsequent grafting of sulfate groups to the crystals (Beck-Candanedo et al., 2005, George and Sabapathi, 2015, Younas et al., 2019, Moon et al., 2013).

Our hypothesis is that such particle–particle interactions at the interface should be broken during the following intestinal digestion stage, since this occurs at around pH 7.0, when both types of particle are negatively charged. Whether such break down of the electrostatic complexation between the particles at the interface leads to greater or lesser extent of lipolysis and consequently FFA release compared to in the absence of CNC remains to be revealed and this is the key novelty of this work. The size distributions and zeta-potentials of microgels and emulsions were measured *via* static light scattering techniques. Confocal laser scanning microscopy (CLSM) was employed to observe the evolution of microstructure during *in vitro* gastrointestinal digestion and a pH–stat-based titrimetric method was used to measure the kinetics of FFA release. In some cases, thermal treatment of the emulsions prior to gastrointestinal digestion was monitored to see if fusion of microgel particles at the interface had any influence, since this is of relevance to real food processing.

5.2 Material and Methods

5.2.1 Materials

Pea protein concentrate (Nutralys S85X, 85 wt% protein) was a gift from Roquette, Lestrem, France. Commercially available cellulose nanocrystals (CNC) were purchased from Cellulforce™ (Quebec, Canada), this was sulfated

during the processing by the manufacturer and was used without any modification. Whey protein isolate (WPI, 90 wt% protein) was gifted by Fonterra Co-operative Group Limited, Auckland, New Zealand. For the oil phase, sunflower oil was purchased from a local supermarket (Tesco, UK) and used without any additional purification. Porcine pepsin (product number: P7000, activity 650 U/mg (Zhang et al., 2021)); porcine pancreatin (product number: P7545, 8 × USP, pancreatin (lipase activity of 82.62 U mg⁻¹ as a substrate (Brodkorb et al., 2019, Minekus et al., 2014); lipase from porcine pancreas Type II (activity 68 U/mg containing amylase and protease activity) and porcine bile extract (product number: B8631 (total bile salt content ~50 wt% containing glycodeoxycholic acid (10-15 wt%), taurodeoxycholic acid (3-9 wt%), deoxycholic acid (0.5–7 wt%) and phospholipids (5 wt%)) were purchased from Sigma-Aldrich Company Ltd, Dorset, UK. Analytical grade chemicals were purchased from Sigma-Aldrich (Dorset, UK), unless otherwise specified. Milli-Q water (purified by a Milli-Q apparatus, Millipore Corp., Bedford, MA, USA) was used to prepare solvents such as buffer, gastric and intestinal fluids.

5.2.2 Fabrication of pea protein microgel particles (PPM)

The fabrication of pea protein microgels (PPM) was carried out using a top-down method as reported previously by Zhang and coworkers (Zhang et al., 2020, Zhang et al., 2021). Briefly, heat-set hydrogels were prepared by dispersing pea protein concentrate (12.54 wt% protein) in 20 mM phosphate buffer at pH 7.0 for 2 h and heating the protein dispersion at 90 °C for 60 min. After cooling the hydrogels to room temperature to stop the crosslinking reaction, they were stored overnight at 4 °C. The protein hydrogels were mixed with phosphate buffer (1:1 w/w) and homogenized using a kitchen blender (HB711M, Kenwood, UK) for 5 min at speed 3. A vacuum oven was used to defoam the aqueous dispersion. Subsequently, the macroscopic dispersion of hydrogel particles was passed through a two-stage valve homogenizer (Panda, GEA Niro Soavi Homogeneizador Parma, Italy) two times at a pressure of 250/50 bar. The resulting aqueous dispersion of PPM contained 6.28 wt% pea protein. Sodium azide (0.02 wt%) was added as a bactericide. The PPM dispersion was further diluted to 1.25 or 3.33 wt% protein levels before its use

in emulsion preparation.

5.2.3 Preparation of O/W Pickering emulsions (PPM-E)

Pea protein microgel-stabilized Pickering emulsions (PPM-E) were fabricated by mixing sunflower oil and an aqueous dispersion of PPM (20: 80 w/w), where the PPM dispersion contained 1.25 wt% protein, at pH 7.0. The oil phase and the aqueous dispersion containing PPM were pre-sheared at 8,000 rpm using a rotor–stator type mixer (Silverson Shear Mixer, L5M-A, UK) for 5 min. To create fine emulsions, these pre-homogenized coarse emulsions were then passed through the Panda homogenizer at 250/ 50 bar pressure two times. For preparation of particle–particle-stabilized emulsions containing CNC, the CNC dispersions were prepared in Milli-Q water at pH 3.0 and stirred overnight. PPM-E+CNC were prepared in a similar way but oil: aqueous phase (40:60 w/w) was altered with the PPM dispersion containing 3.33 wt% protein. Subsequently, the 40.0 wt% O/W emulsion was adjusted to pH 3.0 and diluted with a dispersion of 2.0 or 6.0 wt% CNC particles and stirred for 3 h. In this way, all the emulsions prepared had the same 20.0 wt% oil and 1.0 wt% PPM as above but with +1.0 wt% CNC (referred to as PPM-E+ CNC_{1.0}) or 3.0 wt% CNC (referred to as PPM-E+ CNC_{3.0}).

For the measurement of free fatty acid (FFA) release using the pH stat-based titrimetric method, a whey protein isolate (WPI)-stabilized emulsion was prepared, using same methodology as for the PPM-E but using 1.0 wt% WPI at pH 7.0. In addition, heat treated emulsions *i.e.* PPM-E and PPM-E + CNC_{1.0} were heated at 90 °C for 30 min for FFA release measurements but without a prior gastric digestion step.

5.2.4 *In vitro* gastrointestinal digestion

In vitro gastrointestinal digestion based on the static INFOGEST model developed by Minekus and coworkers (Minekus et al., 2014) was employed, but without the oral step since the emulsions did not contain any starch. Emulsion samples were incubated in simulated gastric fluid as previously reported Zhang et al. (2021). Briefly, 10 mL of emulsion sample at pH 3.0 was mixed with 10 mL of simulated gastric fluid (SGF) containing 2000 U mL⁻¹ pepsin at pH 3.0

(Minekus et al., 2014). The mixture was incubated for 2 h at 37 °C using a shaking water bath (100 rpm, Grant Instruments Ltd, Cambridge, UK). For sequential intestinal digestion, the sample + SGF mixture was adjusted to the intestinal pH (pH 6.8) with 1.0 M NaOH and mixed with 3.18 mL simulated intestinal fluid (SIF), the recipe contained 3.570 g L⁻¹ of NaHCO₃, 1.123 g L⁻¹ of NaCl, 0.335 g L⁻¹ of MgCl₂(H₂O)₆, 0.254 g L⁻¹ of KCl, 0.054 g L⁻¹ of KH₂PO₄, and freshly prepared bile acid solution (10 mM in the final digestion mixture), 0.02 mL of 0.3 M CaCl₂, and pancreatin solution (2000 U/mL based on lipase activity in the final volume). The emulsion + SGF + SIF mixture was further incubated at 37 °C for 2 h using a shaking water bath (100 rpm, Grant Instruments Ltd, Cambridge, UK).

To separate out the effects of lipolysis alone on the emulsions, in some experiments the gastric phase was bypassed and lipase from porcine pancreas Type II (activity 68 U mg⁻¹) was added in SIF buffer instead of pancreatin. Aliquots were collected at 0, 30 and 120 min and droplet size and zeta-potential measured immediately. Data described as being collected at “0 min SIF” refer to the aliquot at 0 min, *i.e.*, gastric-digested sample + SIF buffer *without* any pancreatic enzymes or bile salts being added. At the same time, to try to separate out the effects of the bile salts, a mixture of post-gastric digested sample and SIF buffer without any added pancreatic enzymes was formed and named as “0 min SIF + bile”.

5.2.5 Sizing of PPM and emulsion droplets

The mean hydrodynamic diameters (d_H) of the PPM dispersions as a function of intestinal digestion time were measured using dynamic light scattering (DLS) at 25 °C using a Zetasizer Nano-ZS (Malvern Instruments, Malvern UK). The aliquots were diluted 100-times in SIF buffer. Refractive index and absorbance value of 1.52 and 0.001 was used for PPM, respectively, as mentioned by Zhang et al. (2021)

To measure the droplet size distributions of the Pickering emulsions before and after gastrointestinal digestion, static light scattering (SLS) was used employing a Mastersizer 3000 (Malvern Instruments Ltd, Malvern,

Worcestershire, UK). The mean droplet size was reported as d_{32} (surface mean diameter, $\frac{\sum n_i d_i^3}{\sum n_i d_i^2}$) and d_{43} (the volume mean diameter, $\frac{\sum n_i d_i^4}{\sum n_i d_i^3}$) where, n_i is the number of droplets with a diameter, d_i . In some cases, $d_{(90)}$ is reported meaning that 90% of the total droplets are smaller than this size. Refractive indices of 1.46 and 1.33 were used for sunflower oil and the aqueous phase, respectively.

5.2.6 Zeta-potential

A Zetasizer Nano ZS (Malvern Instruments, Worcestershire, UK) was used to measure zeta-potentials (ζ -potentials) of the particles and the emulsions. The samples were diluted to 0.01 wt% particle concentration (or 0.008 wt% droplet concentration) using the appropriate buffer (phosphate buffer, SGF or SIF), and then added into a folded capillary cell (DTS1070 cell, Malvern Instruments Ltd., Worcestershire, UK) for measurement of the electrophoretic mobilities and calculation of the ζ -potentials.

5.2.7 Confocal laser scanning microscopy and visual imaging

Evolution of microstructures of PPM-E and PPM-E + CNC_{1.0} or PPM-E + CNC_{3.0} as a function of *in vitro* gastrointestinal digestion was probed using a confocal microscope (Zeiss LSM 880, Carl Zeiss MicroImaging GmbH, Jena, Germany). Approximately, 5 mL of sample was stained using Nile Red (2% w/v dispersion in dimethyl sulfoxide) for the oil phase, Nile Blue (10% w/v dispersion in Milli-Q water) for the PPM and Calcofluor White (1 mg/mL dispersion in Milli-Q water) for CNC. Multiple channels *i.e.* 410, 514, 633 nm were used simultaneously to excite Calcofluor White, Nile Red and Nile Blue, respectively. In order to reduce Brownian motion of the droplets, few drops of a thickener *i.e.* xanthan gum solution (1.0 wt%) was added to the stained samples. The samples were imaged using 63 \times (oil immersion) objective lens.

Samples were also stored glass tubes or Petri dishes and photographed with a digital camera in order to record any oiling off, creaming, aggregation or sedimentation.

5.2.8 Kinetics of free fatty acids (FFAs) release

An automated pH-stat-based titration unit (TIM 856 titration manager, Titralab, Radiometer analytical, UK) was used to monitor the kinetics of release of free fatty acids (FFAs) from the emulsions during *in vitro* intestinal digestion with or without bypassing the gastric digestion stage. The pH of the emulsion was maintained at pH 6.8 for 2 h and any FFAs released was neutralized using NaOH (0.05 M). The volumes of NaOH utilized allowed to calculate the quantity of FFAs generated from the emulsions, assuming 2 moles of FFAs were released per mole of triacylglycerol (5.1) (Sarkar et al., 2016c):

$$\%FFA = 100 \times \left(\frac{v_{NaOH} \times M_{NaOH} \times M_{W_{Lipid}}}{2 \times W_{Lipid}} \right) \quad (5.1)$$

where, V_{NaOH} is the required volume (mL) of NaOH added to neutralize the FFAs, M_{NaOH} is the molarity of sodium hydroxide (0.05 M for PPM-E and PPM-E + CNC_{1.0} and PPM-E + CNC_{3.0}, and 0.1 M for the WPI-stabilized emulsion), $M_{W_{Lipid}}$ is the molar mass of sunflower oil (0.880 kg mol⁻¹) and W_{Lipid} is the mass of the lipid in the initial emulsion (2g). The FFA release from the emulsions was analyzed using a nonlinear regression model equations (5.2) and (5.3), as described by Sarkar and coworkers (Sarkar et al., 2016c, Sarkar et al., 2019b):

$$\Phi_t = \Phi_{max} \left[1 - \exp \left(\frac{-6kM_{W_{Lipid}}Dnt^2}{\rho_0 d_0^2 \Gamma^{max}} \right) \right] \quad (5.2)$$

where, Φ_t (%) is the total quantity of FFAs released at time (t) during the simulated intestinal digestion; Φ_{max} (%) is the maximum quantity of FFA released; k (mol s⁻¹ m⁻²) is the lipid-FFA conversion rate per unit surface area of the emulsion droplet; D is the diffusion coefficient of the enzyme (lipase); n is the molar concentration of the lipase in the SIF; ρ_0 is the density of the sunflower oil (910 kg m⁻³); d_0 is the initial volume mean diameter of the emulsions and Γ^{max} is the maximum coverage of the droplet surface by the lipase. Meanwhile,

$t_{1/2}$ is the time required to achieve 50% of the Φ_{max} (%), calculated from equation (5.3):

$$t_{1/2} = \ln(2) \frac{d_0 \rho_0}{6kM_W} \quad (5.3)$$

Thus, the FFA *versus* digestion time curve was characterized *via* the following quantitative terms with Φ_{10} (the quantity of FFA released in the first 10 min), Φ_{max} , k and $t_{1/2}$, by fitting the experimental data to equation (5.3).

5.2.9 Statistical analyses

All measurements were repeated three times on samples prepared on three separate days. Results are reported as the means and standard deviations ($n = 3 \times 3$). The statistical analyses were determined using one-way (ANOVA) and the significant difference between samples were considered when $p < 0.05$ using Tukey's adjustment. Model parameters for the release of FFAs were determined by minimisation of summed residuals.

5.3 Results and discussion

5.3.1 Colloidal stability of PPM dispersions during simulated gastrointestinal digestion

The PPMs used in this study were soft spherical particles with d_H ranging from 230 to 300 nm at pH 7.0. As reported previously (Zhang et al., 2021, Zhang et al., 2020), the PPM particles had a negative charge at pH 7.0 (~ -40 mV) and served as Pickering stabilizer of O/W emulsions irrespective of the pH. Before analyzing the effects of gastrointestinal treatments on the behaviour of PPM-E, the effects of exposure to SIF, with or without prior exposure to SGF, was first studied for the PPM dispersions alone.

Fig. 5.1a shows that the d_H of PPM was essentially unchanged at time 0 on adding SIF + bile salts at pH 7.0 but without pancreatin ($p > 0.1$). This agrees with previous results, illustrating the high electrostatic and steric repulsion

between the microgel particles (Zhang et al., 2020). However, since pancreatin contains various proteases (Mun et al., 2007, Minekus et al., 2014, Brodkorb et al., 2019), not surprisingly d_H was affected on adding pancreatin along with SIF. **Fig. 5.1a** shows that d_H significantly increased from 0.27 to 1.7 μm after 30 min of incubation, and further increased to $\sim 3 \mu\text{m}$ after 2 h digestion time ($p < 0.05$). The increase in d_H was accompanied with increased polydispersity index (PDI), indicating PPM aggregation, which also agreed with visual appearance of aggregates and sediments (see in **Fig. 5.1b**). Presumably hydrolysis of the chains on the surface of the PPMs occurs first and this could lead to reduced steric stability. However, the ζ -potential of PPM (-36 mV at 0 min) also slightly decreased in the first 30 min of digestion time ($p < 0.05$) but then remained steady for longer times ($p > 0.1$), even though d_H continued to increase. These changes in ζ -potential were probably due to the adsorption of anionic bile salts to the PPM (Mun et al., 2007, Sarkar et al., 2016c, Sarkar et al., 2016e), in addition to changes due to proteolysis of the surface chains of protein in the PPMs. The variation of d_H on exposure to SGF then SIF is shown in **Fig. 5.1c**. It is known that protein is “completely” digested by pepsin after 2 h (Zhang et al., 2021), so the initial spherical structure is expected to be partly disintegrated early on, though again the initial result seemed to be the formation of larger ($> 1 \mu\text{m}$) aggregates with a high PDI. Proteolysis of protein-based fragments produced by gastric treatment can be enhanced in the intestinal phase depending on what kinds of bile salts are present (Gass et al., 2007, Martos et al., 2010). It is worth noting that the increase of d_H in **Fig. 5.1c** (SGF then SIF) was similar to that in **Fig. 5.1a** (SIF only) ($p > 0.1$), suggesting that further addition of intestinal proteases did not influence the PPM size and structure (Bokkhim et al., 2016, Zhang et al., 2017). This might be expected owing to the significantly smaller size of the digestive enzymes compared to the typical mesh size in the PPM network, which may hydrolyze the PPM already in the gastric phase and thus the intestinal enzymes might not further alter the size of the PPM (Sarkar et al., 2015b).

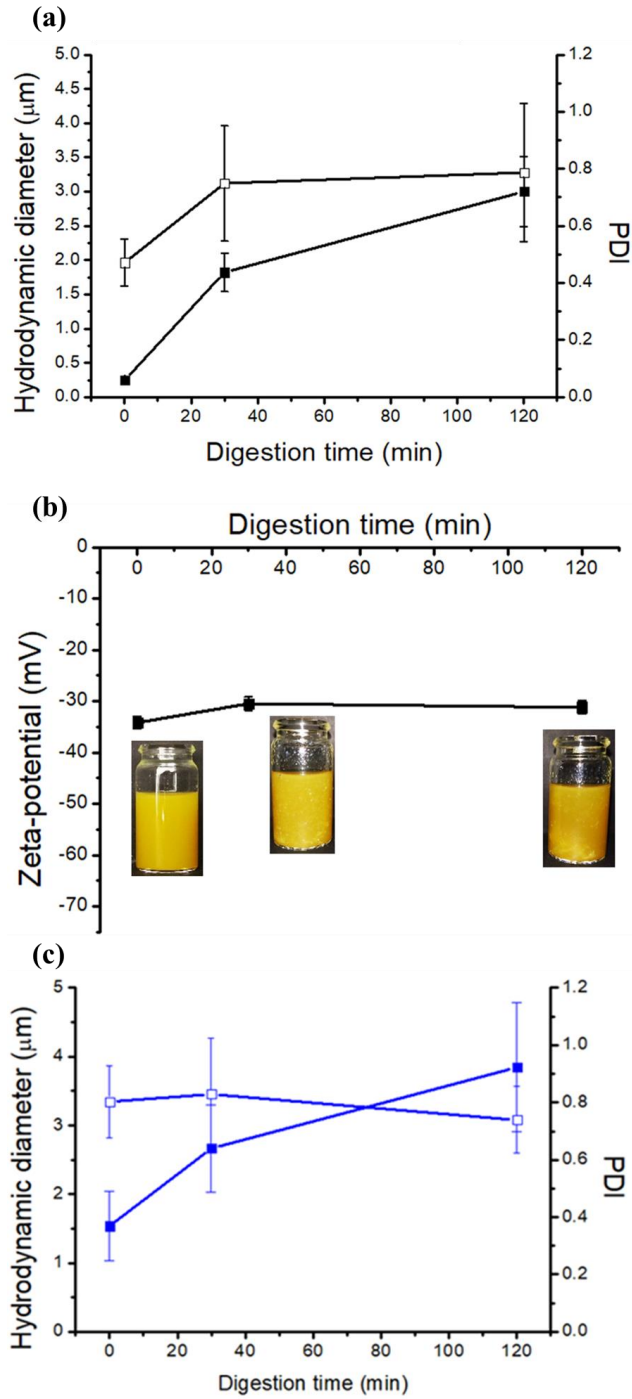


Figure 5.1. Evolution of mean hydrodynamic diameter (■), polydispersity index (PDI) (□) after intestinal digestion without gastric step (a), ζ -potential (■) of PPM after *in vitro* intestinal digestion as a function of time (0, 30 and 120 mins) (b) or evolution of mean hydrodynamic diameter (■), polydispersity index (PDI) (□) after intestinal digestion with gastric step (c). Insets in (b) represent the visual images of aqueous dispersion of PPM during intestinal digestion at different time points, respectively. Digestion time 0 min in (a) shows the original PPM+ SIF+ bile salt mixture at pH 7.0 without the addition of pancreatin. Digestion time of 0 min in (c) represents the gastric-digested PPM+ SIF+ bile salt mixture at pH 7.0 without the addition of pancreatin at pH 6.8. Standard deviations are shown by error bars.

5.3.2 Behaviour of Pickering emulsions during simulated gastrointestinal digestion

5.3.2.1 Evolution of size of droplets

Fig. 5.2 shows the gradual evolution in the particle size distribution (PSD) of the PPM-E during *in vitro* gastrointestinal digestion. **Table 5.1** shows the d_{43} , d_{32} and $d_{(90)}$ values for the PPM-E \pm CNC. For the PPM-E without CNC, the PSD initially had two peaks with the smaller one ranging between 0.1 and 1.0 μm , as reported in previous papers (Zhang et al., 2021, Minekus et al., 2014). We assume that this smaller peak represents free PPM in the continuous phase since it completely disappeared after 2 h gastric digestion. After the gastric phase and adjusting the pH of the PPM-E to 7.0 and diluting with SIF buffer (0 min SIF, **Fig. 5.2a**), there was no noticeable change in the PSD: d_{43} reduced from 50 to 40 μm ($p < 0.05$) (Zhang et al., 2021) whilst d_{32} was unaffected ($p > 0.05$). On addition of bile salts (**Fig. 5.2a**), the main peak moved to lower particle sizes, with a significant decrease in d_{32} but a steady value of d_{43} . Adsorption of the bile salts to the PPM-E and remaining PPM obviously leads to some rearrangement of the aggregates of PPM-E and PPM, no doubt due to the negative charge on some bile salt molecules.

When pancreatin was added the PSD became multi-modal, with a second peak appearing in the range 500–5000 μm , whilst the main peak moved to a larger size range and decreased in height. In line with these changes, d_{43} significantly increased, by nearly five times, ($p < 0.05$) whilst d_{32} nearly halved in the first half-an-hour of the intestinal digestion (see **Table 5.1**). With increasing incubation time, the height of first peak in the size range 1 to 100 μm significantly reduced whilst the area of the second peak in the larger size range increased, in agreement with the 4 x increase in both d_{43} and d_{32} (**Table 5.1**). These changes suggested extensive droplet coalescence as well as aggregation, due to the pancreatic lipases accessing the oil droplet as the PPM particles become increasingly degraded by the protease action. At this stage the PPM fragments are obviously too small to provide effective Pickering stabilization and/or their surface activity is significantly reduced such that they are completely displaced by other surface active species that allow lipase adsorption. Of course, even when the PPM remain at the interface at their maximum

packing density, if they remain spherical then there will still be gaps between the particles far larger than the size of a lipase molecule. For a contact angle of 90° the maximum width of the gap is $(\frac{\sqrt{3}-1}{2}d_o) \approx 85$ to 110 nm (where d_o is the particle diameter, *i.e.*, 230 to 300 nm), whereas the radius of gyration of the pancreatic lipase/co-lipase complex is approximately 2.5 nm (Sarkar et al., 2016c). Thus, lipase molecules can easily diffuse through the gaps between non-digested PPM at the interface, unless they flatten and/or fuse together.

The initial behaviour of the PPM-E + CNC_{1.0} emulsions is quite different to in the absence of CNC (see **(Fig. 5.2b)**) but addition of 3.0 wt% CNC does not change the PSD markedly (**(Fig. 5.2c)**). There is no significant change in PSD after incubation in SGF with pepsin for 2 h. It is known that CNC protects PPM-E from complete peptic digestion (Zhang et al., 2021). The partial PPM fragments therefore seem to cooperate with the CNC to form an effective stabilizing layer around the oil droplets, no doubt due to the opposite charges on CNC and PPM at pH 3.0 . The PSD of the gastric-digested PPM-E + CNC_{1.0} or PPM-E + CNC_{3.0} shows the prominent peak with 1 to 100 μm -sized emulsion droplets that moves to larger sizes when diluted with SIF at pH 7.0 but before addition of pancreatin: d_{43} increased from 12 to 13 μm ($p < 0.05$) (see **Table 5.1**). This suggests some droplet flocculation and/or coalescence. In presence of bile salts, the PSD shows a third peak in a smaller size range whilst the height of main peak is slightly reduced and both d_{43} and d_{32} values are slightly decreased ($p < 0.05$) (see **Table 5.1**). This implies that the bile salts cause some re-dispersal of the flocs to smaller sizes. On addition of pancreatin d_{43} significantly increased to nearly 30 folds at 30 min, reflecting the shift in the main peak to high droplet sizes in the PSD. With increased incubation time, the smaller peak in the PSD moved to a slightly higher size range with negligible change in the larger peak in both PPM-E + CNC_{1.0} and PPM-E + CNC_{3.0}, and the overall d_{43} and d_{32} remained unaltered.

The variations in PSD of PPM-E + CNC_{3.0} were similar to that of PPM-E + CNC_{1.0}. As shown in **Table 5.1**, there was a marked increase in d_{43} of gastric-digested PPM-E + CNC_{3.0} after pH adjustment from pH 3.0 to pH 7.0 with SIF ions, whilst addition of bile salts reduced d_{43} . After addition of pancreatin d_{43} significantly increased to more than 350 μm . The similarity in

these trends indicates that the concentration of CNC (at least between 1 and 3 wt%) has little influence on droplet stability in the intestinal phase. In other words, although CNC is efficacious in aiding the stability of droplets in gastric phase, CNC does not offer promising protection against intestinal destabilization.

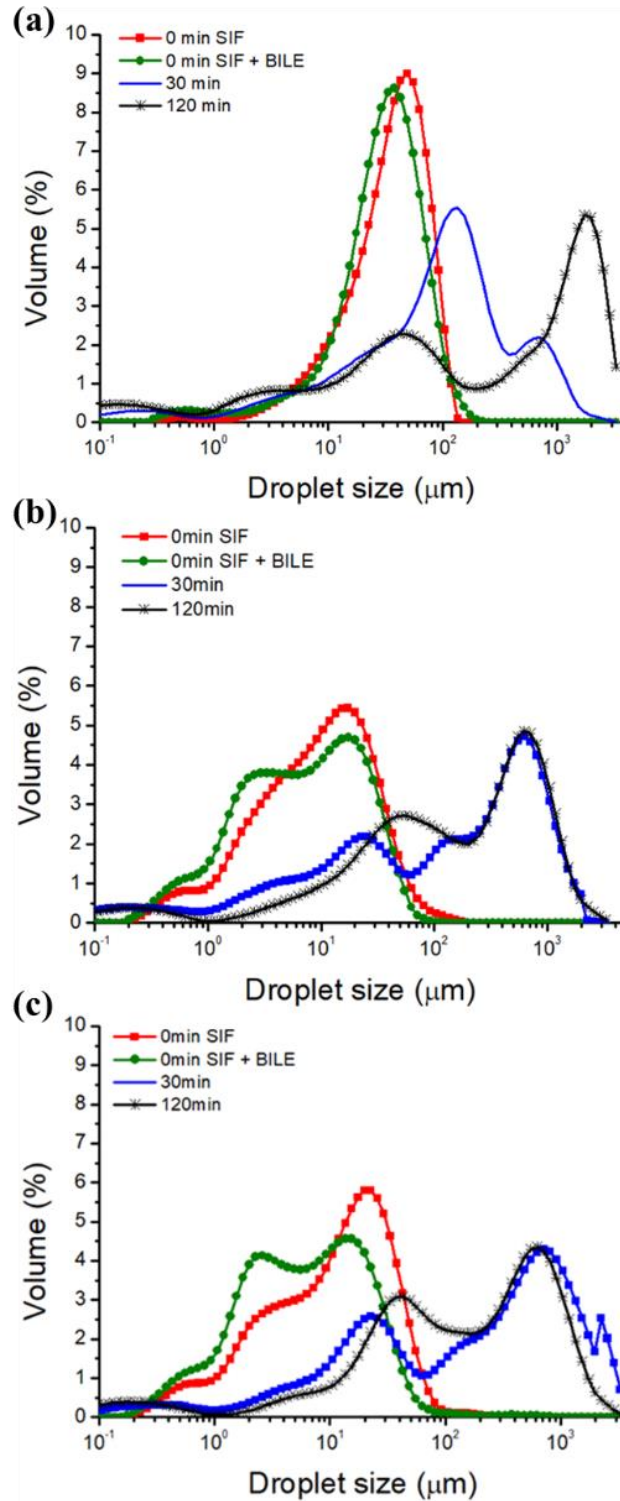


Figure 5.2. Mean size distribution of gastric-digested Pickering oil-in-water emulsions stabilized by PPM containing 20 wt% oil (PPM-E) (a), PPM-E further coated by 1.0 wt% CNC (PPM-E+ CNC_{1.0}) or (b) 3.0 wt% CNC (PPM-E+ CNC_{3.0}) (c) during *in vitro* intestinal digestion. Digestion time of 0 min SIF shows the gastric-digested emulsion + SIF mixture without the addition of pancreatin and bile salts at pH 7.0. Time 0 min SIF + bile represents the gastric-digested emulsion+ SIF+ bile salt mixture without the addition of pancreatin at pH 7.

Table 5.1. Average droplet size of PPM-stabilized Pickering emulsion (PPM-E), PPM-E coated with 1.0 wt% CNC (PPM-E + CNC_{1.0}) and PPM-E coated with 3.0 wt% CNC (PPM-E + CNC_{3.0}) during *in vitro* during intestinal digestion.

Digestion time	PPM-E			PPM-E+ CNC _{1.0}			PPM-E+ CNC _{3.0}		
	d_{32} (μm)	d_{43} (μm)	$dx_{(90)}$ (μm)	d_{32} (μm)	d_{43} (μm)	$dx_{(90)}$ (μm)	d_{32} (μm)	d_{43} (μm)	$dx_{(90)}$ (μm)
0min SIF	16.8±3.9 ^a	40.7±1.6 ^a	77.4±1.8 ^a	3.8± 0.5 ^a	15.0±1.7 ^a	34.0±2.3 ^a	3.7±0.2 ^a	17.3±2.4 ^a	37.9±3.5 ^a
0min SIF + bile	10.8±0.2 ^b	37.3±4.5 ^a	72.9±11.5 ^a	2.9±0.4 ^b	12.0±1.9 ^a	29.2±2.7 ^b	2.6±0.3 ^a	12.5±5.9 ^a	26.1±3.4 ^b
30min	4.5±0.7 ^c	203.3±24.7 ^c	71.5±23.7 ^a	2.4±0.6 ^b	338.6±96.1 ^b	938.4±257.7 ^c	4.4±1.8 ^a	446.9±90.4 ^b	1277.9±313.3 ^c
120min	1.2±0.5 ^d	735.0±245.3 ^d	1987.5±481.6 ^b	3.2±1.3 ^b	373.4±85.9 ^b	992.9±197.4 ^c	2.6±0.3 ^a	355.9±64.8 ^b	980.6±179.7 ^c

Different superscripts in the same column show significant differences between different samples at $p < 0.05$ level.

5.3.2.2 Microstructural changes

CLSM images of PPM-E \pm CNC after sequential *in vitro* gastrointestinal digestion are shown in **Figs. 5.3-5.5**. The PPM and their fragments (labeled with Nile blue) are represented in green, the oil (labeled by Nile red) is represented in red and the CNC (labeled by Calcofluor white) is represented by blue colour. At 0 min SIF, PPM-E droplets are clearly seen to be surrounded by a proteinaceous layer, suggesting a residue of gastric-digested PPM fragments still remains at the interface. On addition of bile salts, this proteinaceous layer appears to disappear from around most oil droplets, especially the larger ones (**Fig. 5.3**). This qualitative observation, coupled with an increased green (protein) signal in the continuous phase, is good evidence of displacement of the adsorbed PPM fragments by more surface active bile salts. Furthermore, the emulsion droplets appeared to be slightly deflocculated, in agreement with the reduction in d_{43} and discussed above (**Table 5.1**).

After addition of pancreatin, the separated cream phase was replaced by a clear oil layer, clearly indicating significant coalescence. This is consistent with the dramatic increase in d_{43} (**Table 5.1**) and illustrates the dramatic effect of the combined digestive action of pancreatic lipases plus proteases (Haque and Morris, 1993, Mun et al., 2007, Maldonado-Valderrama et al., 2008, Sarkar et al., 2010c, Wilde and Chu, 2011a, Sarkar et al., 2016e). The FFAs and monoacylglycerols (MAG) generated at the surfaces of the emulsion droplets *via* the action of lipases (Sarkar et al., 2010c, Sarkar et al., 2018b) whilst surface active and present in sufficient quantities to displace the bile salts, are less effective in preventing droplet coalescence.

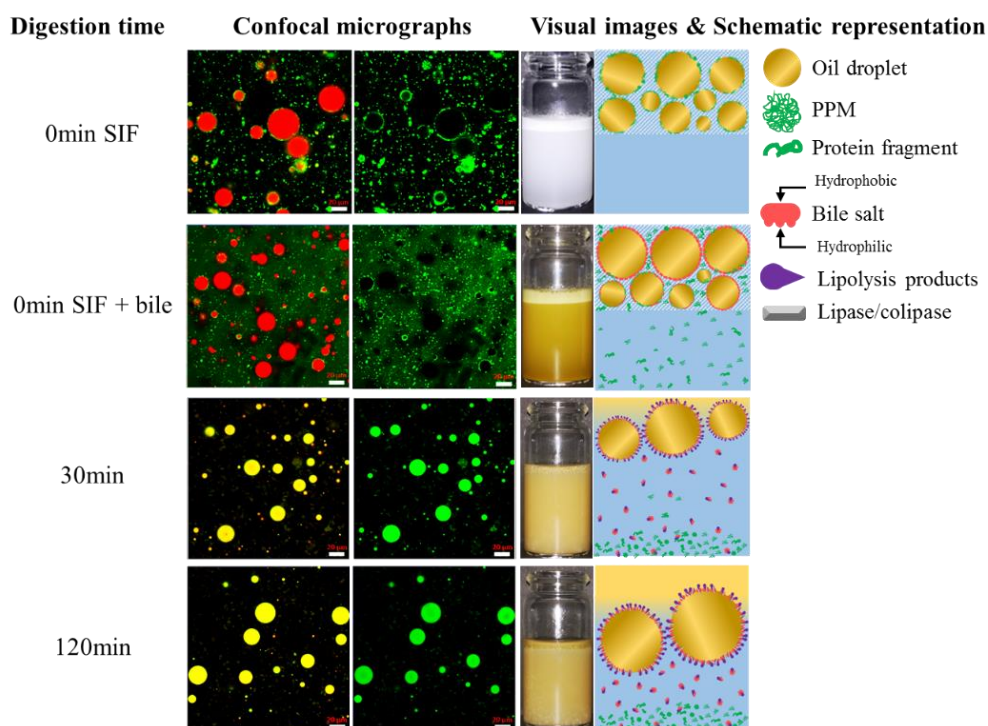


Figure 5.3. Confocal micrographs, visual images and schematic representations of PPM-stabilized emulsion (PPM-E) after sequential *in vitro* gastrointestinal digestion. Green colour (Nile Blue stain) represents PPM; the red colour (Nile Red stain) represents the oil phase and the black background is air or water. Digestion time of 0 min SIF represents the gastric- digested emulsion + SIF mixture without the addition of pancreatin and bile salts at pH 7.0. Digestion time of 0 min SIF+ bile represents the gastric- digested emulsion + SIF + bile salt mixture without the addition of pancreatin at pH 7.0. Scale bar in the micrographs correspond to 20 μm .

The CLSM observations of PPM-E + CNC_{1.0} (**Fig. 5.4**) were quite similar to those recorded with PPM-E in the absence of CNC – significant coalescence was the end result. Since the enhanced stabilization with PPM and CNC in the gastric phase is dependent on their opposite charges at low pH, this mechanism cannot operate when the pH is raised to 7.0, in the intestinal phase, because the two types of particle are both negative and will repel one another. The CNC particles are most likely released into the bulk continuous phase, as **Fig. 5.4** suggests, and this CNC now in the bulks would appear to have little effect on the course of the emulsion digestion. Interestingly, although the measured d_{43} still increased dramatically (**Table 5.1**), a CNC network appeared to form in the bulk phase as shown in the confocal micrograph and in non-diluted samples stored in test tubes. This inhibited the formation of a cream layer,

unlike with PPM-E in the absence of CNC.

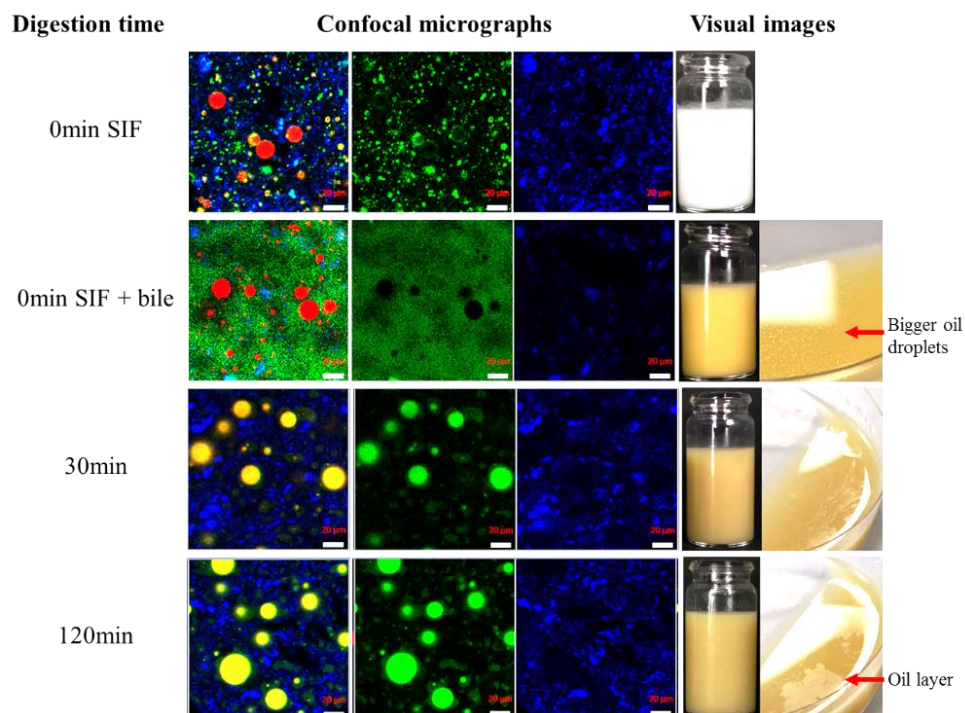


Figure 5.4. Confocal micrographs and visual images of PPM stabilized emulsion coated with 1.0 wt% CNC after sequential *in vitro* gastrointestinal digestion. Green colour (Nile Blue stain) represents PPM; the red colour (Nile Red stain) represents the oil phase; the blue colour (Calcufluor White stain) represents the CNC and the black background represents air or water. Digestion time of 0 min SIF represents the gastric-digested emulsion + SIF mixture without the addition of pancreatin and bile salts at pH 7.0. Digestion time of 0 min SIF + bile represents the gastric-digested emulsion + SIF + bile salt mixture without the addition of pancreatin at pH 7.0. Scale bar in the micrographs correspond to 20 μm .

For PPM-E + CNC_{3.0} (**Fig. 5.5**), the CLSM images were essentially no different from those with PPM-E + CNC_{1.0}, except that there was a stronger blue signal due to the higher concentration of CNC. Addition of cellulose has been shown to significantly inhibit lipase action on emulsions (Espinal-Ruiz et al., 2014, Sarkar et al., 2018b, Bai et al., 2019, Meng et al., 2020, Ding et al., 2021, Surjit Singh et al., 2021, Wei et al., 2021b, Wei et al., 2021d). Sarkar, Li, Cray and Boxall (Sarkar et al., 2018b) studied an O/W emulsion stabilized by a complex of whey protein isolate (WPI) and CNC. They found that the emulsion droplets became encapsulated in a strong, gel-like CNC network and formed “raspberry-like” flocs. resulting in emulsion microgel-like particle. Such

encapsulation could inhibit direct access of bile salts or digestive enzymes to the droplets. On the other hand, Surjit Singh, Lim, Tey and Chan (Surjit Singh et al., 2021) stabilized Pickering emulsion using chitosan particles as the emulsifier and alginate as a coating and showed significant inhibition of lipid digestion of the oil droplets. However, excess alginate in the continuous phase significantly enhanced the viscosity of emulsions, and this was one of the reasons for the inhibition of the lipid digestion. Although such network-like structure was also observed in this study in the confocal images, the strength of the network in the bulk phase might not be sufficient to prevent the access of bile salts and lipase due to the limited concentration of CNC used.

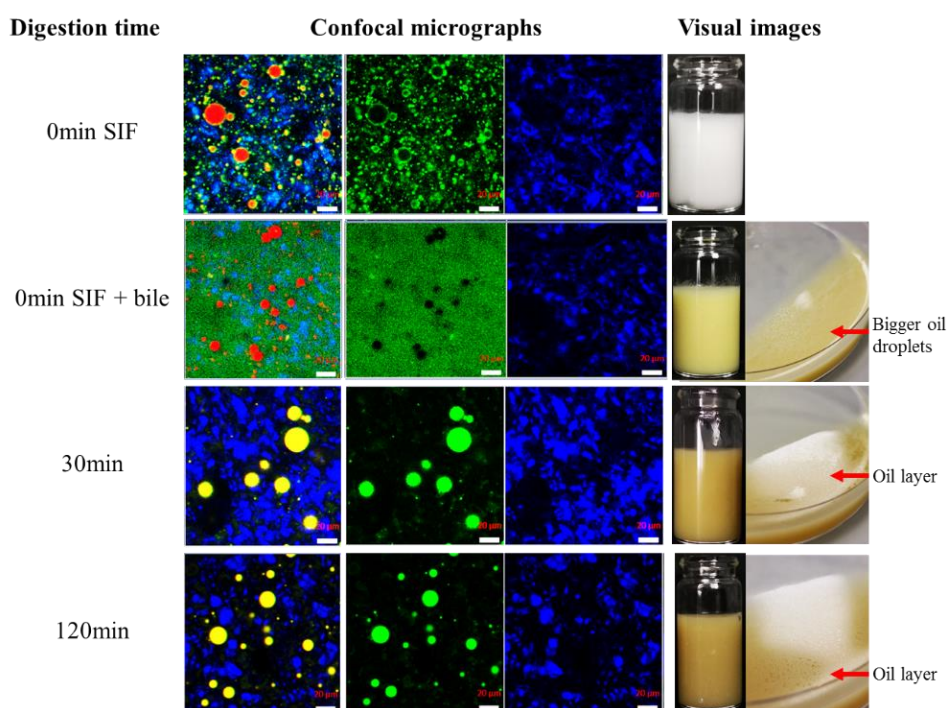


Figure 5.5. Confocal micrographs and visual images of PPM stabilized emulsion coated with 3.0 wt% CNC after sequential *in vitro* gastrointestinal digestion. Green colour (Nile Blue stain) represents PPM; the red colour (Nile Red stain) represents the oil phase; the blue colour (Calcufluor White stain) represents the CNC and the black background represents air or water. Digestion time of 0 min SIF represents the gastric-digested emulsion + SIF mixture without the addition of pancreatin and bile salts at pH 7.0. Digestion time of 0 min SIF + bile represents the gastric-digested emulsion + SIF + bile salt mixture without the addition of pancreatin at pH 7.0. Scale bar in the micrographs correspond to 20 μm .

5.3.2.3 ζ - potential

The ζ -potential values of emulsions at pH 7.0 and in presence of SIF without/with the addition of bile salts and/or pancreatin are shown in **Fig. 5.6**. The ζ -potential of PPM-E was nearly zero at pH 3.0 after gastric digestion (Zhang et al., 2021). After adjust the pH to pH 7.0 but without SIF, the gastric digested PPM-E showed a rapid increase of negative charge, with $\zeta \sim -45$ mV. The magnitude of ζ -potential value reduced slightly (~ -33 mV) on addition of pancreatin only ($p < 0.05$) whilst the inclusion of bile salts enhanced the negative surface charge (~ -50 mV), as expected if the anionic surfactant components of bile become strongly adsorbed. In this respect, this agrees with the CLSM images (**Fig. 5.3**), where it seemed that the adsorbed protein material was displaced. Bile salts are known to be efficient displacers of a range of proteinaceous emulsifiers, for example, soy, caseins and whey protein (Nguyen et al., 2015a, Sarkar et al., 2016e, Sarkar et al., 2018b), whilst particles are supposed to be harder to displace due to their high desorption energies (Sarkar et al., 2019b). However, as already discussed above, by the time the PPM-E reach the intestinal digestion stage, the adsorbed protein material will have already been degraded to some extent by the gastric pepsin-induced proteolysis, *i.e.* it is unlikely that intact PPM remain at the interface anyway. After the initial addition of both bile salts and pancreatin, the ζ -potential of the PPM-E droplets showed no significant change over the next 30 min, but by the end (2 h) of the SIF digestion stage ζ had increased in magnitude to -70 mV, presumably due to adsorption of lipolysis products including FFAs.

PPM-E + CNC_{1.0} droplets after gastric digestion at pH 3 had $\zeta \sim -9$ mV but after neutralization to pH 7.0 with SIF buffer $\zeta \sim -60$ mV. In other words, the inclusion of 1% CNC seemed to have little effect on ζ . However, this was to be expected if the two adsorbing species are both negative at pH 7, in which case there is no reason why the CNC should remain at the interface. The magnitude of ζ reduced slightly to ~ -50 mV on the addition of pancreatin ($p > 0.05$) and slightly further increased to ~ -65 mV on addition of bile salts, again suggesting that bile salts displaced any other interfacial material. By 30 min, ζ -potential changed to -70 mV but then remained constant for the next 90 min, again agreeing with the suggestion from the PSDs (**Fig. 5.2b**) that droplet

destabilisation of emulsion was completed within the first 30 min. The values of ζ -potential observed throughout the various digestion stages for PPM-E + CNC_{3.0} were very similar to those for PPM-E + CNC_{1.0} (Fig. 5.6), further emphasizing that CNC has little influence on the intestinal digestion of PPM-E after the gastric digestion step.

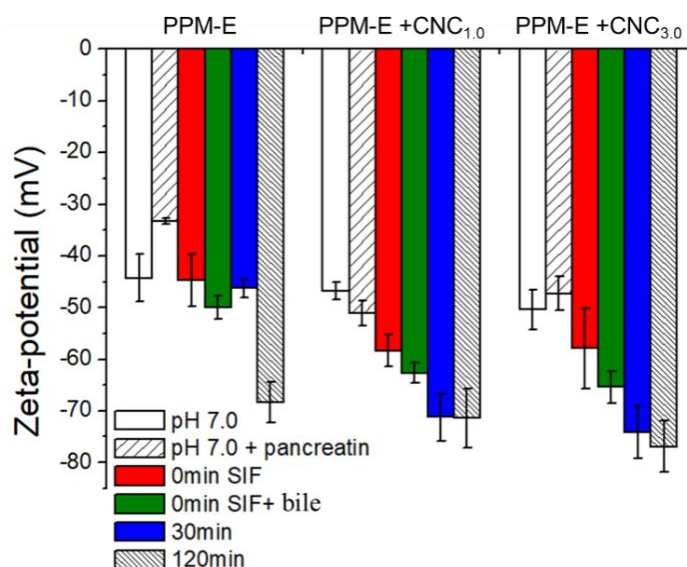


Figure 5.6. Mean ζ -potential of gastric-digested PPM-E, PPM-E+CNC_{1.0} and PPM-E+CNC_{3.0} at pH 7.0. Digestion time of 0 min SIF represents the gastric-digested emulsion + SIF mixture without the addition of pancreatin or bile salts at pH 7.0. Digestion time of SIF + bile represents the gastric- digested emulsion + SIF + bile salt mixture without the addition of pancreatin at pH 7.0. Standard deviations are represented by error bars.

5.3.3 Lipid digestion kinetics

The release of FFAs from the emulsions was determined *via* the INFOGEST static model (Brodkorb et al., 2019), shown in Fig.5.7. The corresponding parameters (FFA release at 10 min, Φ_{10} , maximum quantity of FFA release, Φ_{max} , lipid-FFA conversion, k and the time to achieve half of the Φ_{max} , $t_{1/2}$) are reported in Table 5.2. Since the pea protein isolate used in this study to create the PPM had low solubility and was unsuitable as an emulsion stabilizer on its own (Zhang et al., 2020), for comparison a conventional (*i.e.*, non- microgel stabilized) emulsion was created using whey protein isolate (WPI) as the stabilizer. With the latter, the oil droplets are usually rapidly digested and FFAs and MAGs released due to the ease of access of the lipase to the interface

(Sarkar et al., 2018b, Sarkar et al., 2016c). Thus, the WPI-stabilized emulsions generated $\Phi_{\max} \sim 69\%$ (data not shown), consistent with the results of previous studies (Sandoval-Cuellar et al., 2020, Ye et al., 2020, Zhang et al., 2015).

In the case of PPM-E, the maximum FFA release of lipid digestion was significantly lower, as expected for Pickering emulsions, since the size of the droplets was two orders of magnitude higher ($d_{43} \sim 25$ to $40 \mu\text{m}$) compared to the WPI-stabilized emulsions ($d_{43} \sim 0.2$ to $0.5 \mu\text{m}$), hence the interfacial area much lower. The PPM-E stabilized emulsions after the gastric digestion step were rapidly hydrolysed in the first 10 min, generating $\Phi_{10} \sim 15\%$, followed by a slower release of FFA, reaching $\sim 20\%$ at the end of digestion (2 h). This ‘self-inhibition’ might be due to long-chain FFAs produced from the sunflower oil accumulating at the interface and inhibiting of further lipase activity (Tzoumaki et al., 2013a, Sarkar et al., 2016c, Li and McClements, 2010b). Similar results were reported in previously. For example Zhao et al. (2021) reported 15 to 20% of FFA release in the soy protein nanoparticles-stabilized Pickering emulsions (SPHE). These Pickering emulsions were produced *via* enzymatic hydrolyzed soy protein and gave a significant lower extent and rate of FFA release than the non-hydrolysed soy protein as stabilizer. The maximum FFA release of lipolysis of Pickering emulsions stabilized by zein colloidal particles also had a similar value ($\phi_{\max} = 19.5\%$) (Wei et al., 2021b) and the extent of FFA release from Pickering emulsions stabilized by WPI microgels and kafirin nanoparticle-stabilized emulsions was 40% after the gastrointestinal digestion (Sarkar et al., 2016c, Xiao et al., 2015b). Conversely, Meshulam and Lesmes (2014b) concluded that the FFA release from Pickering emulsions stabilized by lactoferrin nanoparticles or native lactoferrin was essentially the same, giving a ‘final’ release values of 65%. In all these different digestion studies one should remember that different digestion protocols and conditions have been used, so that it may be misleading to compare absolute values of FFA release.

For PPM-E + CNC_{1.0}, Φ_{10} was $\sim 22\%$, significantly higher than that of PPM-E. Meanwhile, the *rate* of lipolysis was slightly lower, and $t_{1/2}$ in PPM-E + CNC_{1.0} shorter (approximately half) compared to that required for PPM-E, as shown by the data in **Table 5.2**. The behaviour of PPM-E + CNC_{3.0} and PPM-E + CNC_{1.0} in terms of k and $t_{1/2}$ were not significantly different ($p > 0.05$) but

the Φ_{\max} of PPM-E + CNC_{3.0} was slightly higher and Φ_{10} was highest for PPM-E + CNC_{3.0}. The increase in FFA release in PPM-E + CNC_{1.0-3.0} might be related to the larger surface area of the oil droplets generated after gastric digestion in presence of cellulose, due to secondary surface coverage (Zhang et al., 2021) as compared with the coalesced PPM-E droplets after gastric digestion in the absence of CNC. However, it seems that there may still be some coverage of the droplets by CNC in the PPM-E + CNC_{1.0-3.0} samples, which reduces the rate of lipid digestion compared to in the absence of CNC ($p < 0.05$) (Table 5.2).

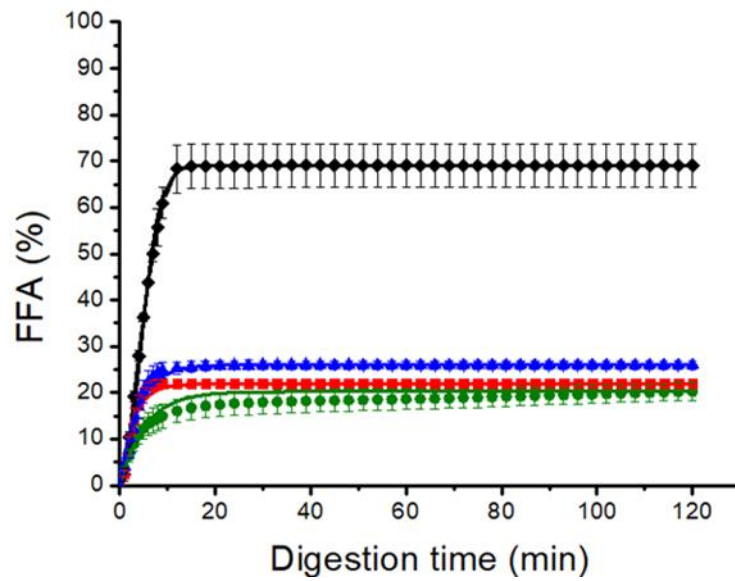


Figure 5.7. Release of free fatty acid during intestinal digestion (after prior-gastric digestion) of WPI-stabilized emulsion (black diamond), PPM-E (green circle), PPM-E + CNC_{1.0} (red square), and PPM-E + CNC_{3.0} (blue triangle). Error bars represent the standard deviations. The solid lines in each of the %FFA curves connecting the symbols (data points) are the best theoretical fits to the experimental data predicted using the mathematical model (Eq. (5.1)).

Table 5.2. Kinetic data from free fatty acid release *i.e.* FFA release at 10 min (Φ_{10} , %), maximum quantity of FFA release (Φ_{max} , %), lipid-FFA conversion rate constant (k , $\mu\text{mol s}^{-1} \text{m}^{-2}$) and the time to achieve 50% Φ_{max} ($t_{1/2}$, min) during *in vitro* gastrointestinal digestion of PPM-E and PPM-E+ CNC_{1.0-3.0}.

Sample	Φ_{10} (%)	Φ_{max} (%)	k ($\mu\text{mol s}^{-1} \text{m}^{-2}$)	$t_{1/2}$ (min)
PPM-E	15.4 ± 2.6 ^a	20.2 ± 1.9 ^a	1.18 ^a	4.36 ^a
PPM-E+ CNC _{1.0}	21.9 ± 0.8 ^b	22.0 ± 0.9 ^a	0.73 ^b	2.39 ^b
PPM-E+ CNC _{3.0}	25.0 ± 1.5 ^c	25.9 ± 1.0 ^b	0.57 ^b	3.18 ^b

Different alphabets superscripts (a-c) in the same column represent significant differences between different samples at $p < 0.05$ level.

5.3.4 Lipid digestion kinetics bypassing the gastric phase and using pure lipase

Fig. 5.8 showed the variation of the FFA release from PPM-E and PPM-E +CNC_{1.0-3.0} with and without the prior gastric digestion stage and without any intestinal proteolytic enzyme (trypsin). These experiments were also performed using the pure lipase from porcine pancreas Type II and bile salts. For PPM-E, Φ_{10} was significantly lower (almost half - 7.4% - see **Table 5.3**) compared to Φ_{10} with gastric proteolysis (15% - see **Table 5.2**), whilst $\Phi_{max} \sim 13\%$ and $k \sim 0.63 \mu\text{mol s}^{-1}\text{m}^{-2}$. The value of $t_{1/2}$ (8.4 min) was nearly 2 times longer when the prior gastric stage was excluded, suggesting that the bile salts have more difficulty in displacing the intact PPM from the interface compared to when they have undergone some proteolysis on the gastric stage. In the case of PPM-E + CNC_{1.0}, Φ_{max} was slightly lower (8%) compared to that of PPM-E, while k was similar ($0.72 \mu\text{mol s}^{-1}\text{m}^{-2}$ - see **Table 5.3**). Similar results were reported in previous work, *i.e.*, a slight reduction in Φ_{max} with addition of soluble polysaccharides, such as chitosan, pectin, methyl-cellulose, propylene glycol alginate or insoluble chitin nanocrystals (Jo et al., 2019, Wei et al., 2021d, Zhou et al., 2021, Espinal-Ruiz et al., 2014).

The $t_{1/2}$ of PPM-E + CNC₁ was almost three times shorter than that of PPM-E, also suggesting more rapid accumulation lipid hydrolysis products at the O/W interface that inhibit further lipase activity. It is interesting to note that the post-gastric digestion step had no influence on the rate constant k or $t_{1/2}$, whilst Φ_{max} was $3\times$ lower than when the gastric phase was excluded, again

highlighting the importance of proteolysis in the overall lipid digestion process (compare **Table 5.2** and **5.3**). At the higher concentration of CNC, *i.e.*, PPM-E + CNC_{3.0}, **Table 5.3** shows that k was lower ($0.31 \mu\text{mol s}^{-1}\text{m}^{-2}$) compared to PPM-E + CNC_{1.0}, whilst $t_{1/2}$ was nearly 2x longer and Φ_{max} was similar. The reason for the similar extent but reduced rate of lipolysis of PPM-E + CNC_{1.0} and PPM-E + CNC_{3.0} might be a difference in the viscosities of the emulsions – higher viscosity would be expected to slow down the rate of mass transport of enzyme to the interface and the products from the interface (Espinal-Ruiz et al., 2014). PPM-E + CNC_{3.0} has a viscosity 100 x higher than PPM-E + CNC_{1.0} (Zhang et al., 2021), although in this work the emulsions were diluted by a factor of 2 into the SIF buffer (as described in the methods section) and small molecules like bile salts and lipase would be expected to easily pass through the pores in the network of CNC crystals (Espinal-Ruiz et al., 2014).

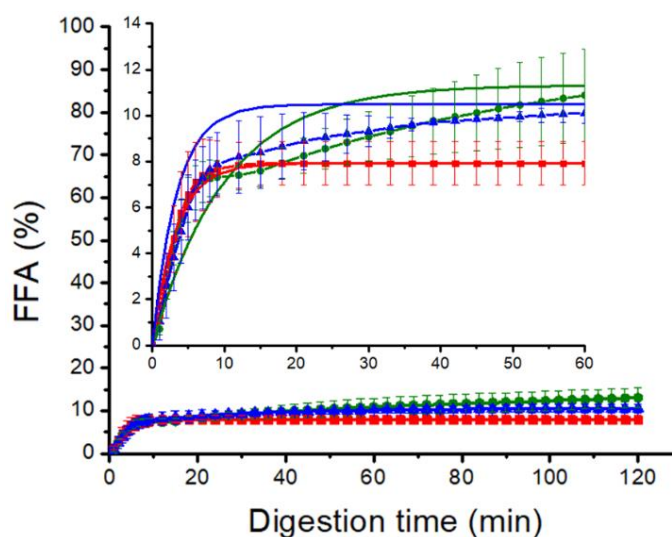


Figure 5.8. Release of free fatty acids (FFA%) during *in vitro* intestinal digestion bypassing the gastric phase (using pure lipase) with inset showing the zoomed image over time of PPM-E (green circle), PPM-E+CNC_{1.0} (red square), and PPM-E+CNC_{3.0} (blue triangle). Error bars represent standard deviations. Solid lines connecting the symbols (data points) in each of the %FFA curves are the best theoretical fits to the experimental data predicted using the mathematical model (Eq. 5.1).

Table 5.3. Kinetic data from free fatty acid release *i.e.* FFA release at 10 min (Φ_{10} , %), maximum quantity of FFA release (Φ_{max} , %), lipid-FFA conversion rate constant (k , $\mu\text{mol s}^{-1} \text{m}^{-2}$) and the time to achieve 50% Φ_{max} ($t_{1/2}$, min) during *in vitro* intestinal digestion *i.e.* by passing the gastric phase of PPM-E and PPM-E+CNC_{1.0-3.0}, using pure lipase from porcine pancreas Type II.

Sample	Φ_{10} (%)	Φ_{\max} (%)	k ($\mu\text{mol s}^{-1} \text{m}^{-2}$)	$t_{1/2}$ (min)
PPM-E	7.4 ± 0.7^a	13.0 ± 2.3^a	0.63^a	8.39^a
PPM-E+ CNC _{1.0}	7.7 ± 1.1^a	7.9 ± 0.9^b	0.72^a	2.83^b
PPM-E+ CNC _{3.0}	8.0 ± 1.4^a	10.5 ± 1.0^b	0.31^b	5.73^c

Different alphabets in the superscripts (a-c) in the same column represent significant differences between different samples at $p < 0.05$ level.

5.3.5 Lipid digestion kinetics of heat-treated emulsions

One way of possibly improving the barrier properties of an adsorbed microgel layer is to heat the system above the melting point of the gel network, so that the individual particles might fuse to form a more coherent layer. At the same time, heating is relevant to practical applications, since most emulsions for consumer use would probably also undergo a pasteurization step. Therefore, samples of PPM-E and PPM-E+CNC_{1.0} (without a prior gastric stage) were heat treated at 90 °C at pH 7.0 for 30 min and their subsequent *in vitro* intestinal stage digestion was measured as previously. The results are shown in **Figure 5.9**. It is interesting to note that HT-PPM-E had a significant lower Φ_{\max} than the unheated PPM-E (**Fig. 5.9a**). Possibly this indicates that some PPM fusion had occurred as hypothesized (Sarkar et al., 2016c). In contrast, there was no significant difference between PPM-E + CNC_{1.0} and HT-PPM-E + CNC_{1.0} in the overall kinetics of FFA (**Fig. 5.9b**), suggesting that the heat treatment did not improve barrier properties of the mixed PPM + CNC adsorbed film, although it is again noted that at pH 7.0 the two types of particle will repel each other electrostatically.

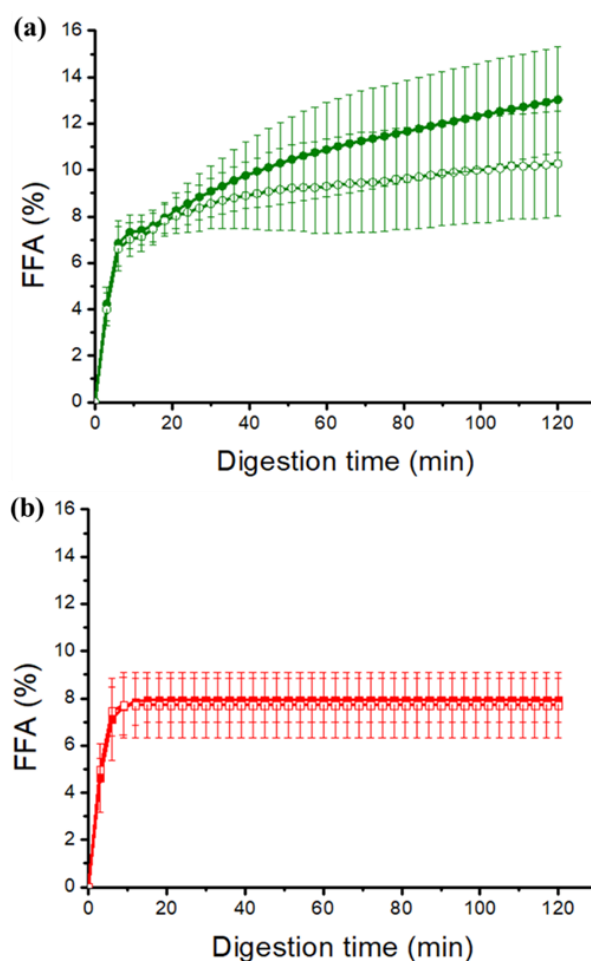


Figure 5.9. Release of free fatty acids (%FFA) during *in vitro* intestinal digestion bypassing the gastric phase (using pure lipase with no added proteases) over time of (a) PPM-E and (b) PPM-E+CNC_{1.0} with (open circle) or without heat treatment (solid circle). Error bars represent standard deviations.

5.4 Conclusion

Pickering emulsions stabilized by pea protein microgel (PPM) particles with the addition of cellulose nanocrystals (CNC) were tested to understand the influence of complex particle systems in modulating lipid digestion. The CNC were shown to inhibit the coalescence of oil droplets in the *in vitro* gastric stage, probably due to electrostatic attraction between the anionic CNC and the cationic PPM at the interface at low pH. Even though this attractive charge interaction should not be present during the intestinal digestion stage at pH 7.0 (where the particles are both negatively-charged), unprecedented results from this study reveal that in the presence of CNC lipolysis was slightly delayed, but the overall extent (at least after 2 h) of lipid digestion increased. To our knowledge, such increase in FFA release is not observed in any other particle-

particle interface study to date. These novel results suggests that such 'dual particle' Pickering emulsions, *i.e.*, with a mixed interfacial particle layer, could be used to protect lipophilic bioactive compounds in the stomach by creating more stable droplets under gastric conditions, without inhibiting their release them in the intestines.

5.5 References

- ARAIZA-CALAHORRA, A., WANG, Y., BOESCH, C., ZHAO, Y. & SARKAR, A. 2020. Pickering emulsions stabilized by colloidal gel particles complexed or conjugated with biopolymers to enhance bioaccessibility and cellular uptake of curcumin. *Curr Res Food Sci*, 3, 178-188.
- BAI, L., HUAN, S., XIANG, W., LIU, L., YANG, Y., NUGROHO, R. W. N., FAN, Y. & ROJAS, O. J. 2019. Self-Assembled Networks of Short and Long Chitin Nanoparticles for Oil/Water Interfacial Superstabilization. *ACS Sustain Chem Eng*, 7, 6497-6511.
- BECK-CANDANEDO, S., ROMAN, M. & GRAY, D. G. 2005. Effect of Reaction Conditions on the Properties and Behavior of Wood Cellulose Nanocrystal Suspensions. *Biomacromolecules*, 6, 1048-1054.
- BELLESI, F. A., MARTINEZ, M. J., PIZONES RUIZ-HENESTROSA, V. M. & PILOSO, A. M. R. 2016. Comparative behavior of protein or polysaccharide stabilized emulsion under in vitro gastrointestinal conditions. *Food Hydrocolloids*, 52, 47-56.
- BENSHITRIT, R. C., LEVI, C. S., TAL, S. L., SHIMONI, E. & LESMES, U. 2012. Development of oral food-grade delivery systems: current knowledge and future challenges. *Food Funct*, 3, 10-21.
- BINKS, B. P. 2002. Particles as surfactants—similarities and differences. *Current Opinion in Colloid & Interface Science*, 7, 21-41.
- BINKS, B. P. & HOROZOV, T. S. 2006. Colloidal Particles at Liquid Interfaces: An Introduction. In: BINKS, B. P. & HOROZOV, T. S. (eds.) *Colloidal Particles at Liquid Interfaces*. Cambridge: Cambridge University Press.
- BOKKHIM, H., BANSAL, N., GRØNDAHL, L. & BHANDARI, B. 2016. In-vitro digestion of different forms of bovine lactoferrin encapsulated in alginate micro-gel particles. *Food Hydrocolloids*, 52, 231-242.
- BRODKORB, A., EGGER, L., ALMINGER, M., ALVITO, P., ASSUNCAO, R., BALLANCE, S., BOHN, T., BOURLIEU-LACANAL, C., BOUTROU, R., CARRIERE, F., CLEMENTE, A., CORREDIG, M., DUPONT, D., DUFOUR, C., EDWARDS, C., GOLDING, M., KARAKAYA, S.,

- KIRKHUS, B., LE FEUNTEUN, S., LESMES, U., MACIERZANKA, A., MACKIE, A. R., MARTINS, C., MARZE, S., MCCLEMENTS, D. J., MENARD, O., MINEKUS, M., PORTMANN, R., SANTOS, C. N., SOUCHON, I., SINGH, R. P., VEGARUD, G. E., WICKHAM, M. S. J., WEITSCHIES, W. & RECIO, I. 2019. INFOGEST static in vitro simulation of gastrointestinal food digestion. *Nat Protoc*, 14, 991-1014.
- DICKINSON, E. 2010. Food emulsions and foams: Stabilization by particles. *Current Opinion in Colloid & Interface Science*, 15, 40-49.
- DING, M., LIU, L., ZHANG, T., TAO, N., WANG, X. & ZHONG, J. 2021. Effect of interfacial layer number on the storage stability and in vitro digestion of fish oil-loaded multilayer emulsions consisting of gelatin particle and polysaccharides. *Food Chem*, 336, 127686.
- ESPINAL-RUIZ, M., PARADA-ALFONSO, F., RESTREPO-SANCHEZ, L. P., NARVAEZ-CUENCA, C. E. & MCCLEMENTS, D. J. 2014. Impact of dietary fibers [methyl cellulose, chitosan, and pectin] on digestion of lipids under simulated gastrointestinal conditions. *Food Funct*, 5, 3083-95.
- GASS, J., VORA, H., HOFMANN, A. F., GRAY, G. M. & KHOSLA, C. 2007. Enhancement of dietary protein digestion by conjugated bile acids. *Gastroenterology*, 133, 16-23.
- GEORGE, J. & SABAPATHI, S. N. 2015. Cellulose nanocrystals: synthesis, functional properties, and applications. *Nanotechnol Sci Appl*, 8, 45-54.
- GUO, Q., YE, A., BELLISSIMO, N., SINGH, H. & ROUSSEAU, D. 2017. Modulating fat digestion through food structure design. *Prog Lipid Res*, 68, 109-118.
- HAQUE, A. & MORRIS, E. R. 1993. Thermogelation of methylcellulose. Part I: molecular structures and processes. *Carbohydrate Polymers*, 22, 161-173.
- JO, M., BAN, C., GOH, K. K. T. & CHOI, Y. J. 2019. Influence of chitosan-coating on the stability and digestion of emulsions stabilized by waxy maize starch crystals. *Food Hydrocolloids*, 94, 603-612.

- LI, Y. & MCCLEMENTS, D. J. 2010. New mathematical model for interpreting pH-stat digestion profiles: impact of lipid droplet characteristics on in vitro digestibility. *J Agric Food Chem*, 58, 8085-92.
- LIU, F. & TANG, C.-H. 2016. Reprint of “Soy glycinin as food-grade Pickering stabilizers: Part. III. Fabrication of gel-like emulsions and their potential as sustained-release delivery systems for β -carotene”. *Food Hydrocolloids*, 60, 631-640.
- MALDONADO-VALDERRAMA, J., WOODWARD, N. C., GUNNING, A. P., RIDOUT, M. J., HUSBAND, F. A., MACKIE, A. R., MORRIS, V. J. & WILDE, P. J. 2008. Interfacial characterization of β -lactoglobulin networks: Displacement by bile salts. *Langmuir*, 24, 6759-6767.
- MARTOS, G., CONTRERAS, P., MOLINA, E. & LOPEZ-FANDINO, R. 2010. Egg white ovalbumin digestion mimicking physiological conditions. *J Agric Food Chem*, 58, 5640-8.
- MCCLEMENTS, D. J. 2010. Emulsion design to improve the delivery of functional lipophilic components. *Annu Rev Food Sci Technol*, 1, 241-69.
- MCCLEMENTS, D. J., DECKER, E. A. & WEISS, J. 2007. Emulsion-based delivery systems for lipophilic bioactive components. *J Food Sci*, 72, R109-24.
- MENG, R., WU, Z., XIE, Q.-T., ZHANG, B., LI, X.-L., LIU, W.-J., TAO, H. & LI, P.-J. 2020. Zein/carboxymethyl dextrin nanoparticles stabilized pickering emulsions as delivery vehicles: Effect of interfacial composition on lipid oxidation and in vitro digestion. *Food Hydrocolloids*, 108, 106020.
- MESHULAM, D. & LESMES, U. 2014. Responsiveness of emulsions stabilized by lactoferrin nano-particles to simulated intestinal conditions. *Food Funct*, 5, 65-73.
- MINEKUS, M., ALMINGER, M., ALVITO, P., BALLANCE, S., BOHN, T., BOURLIEU, C., CARRIERE, F., BOUTROU, R., CORREDIG, M., DUPONT, D., DUFOUR, C., EGGER, L., GOLDING, M., KARAKAYA, S., KIRKHUS, B., LE FEUNTEUN, S., LESMES, U., MACIERZANKA, A., MACKIE, A., MARZE, S., MCCLEMENTS, D. J., MENARD, O.,

- RECIO, I., SANTOS, C. N., SINGH, R. P., VEGARUD, G. E., WICKHAM, M. S., WEITSCHIES, W. & BRODKORB, A. 2014. A standardised static in vitro digestion method suitable for food - an international consensus. *Food Funct*, 5, 1113-24.
- MOON, R., BECK, S. & RUDIE, A. 2013. Cellulose nanocrystals—A material with unique properties and many potential applications. *Production and applications of cellulose nanomaterials*, 9.
- MUN, S., DECKER, E. A. & MCCLEMENTS, D. J. 2007. Influence of emulsifier type on in vitro digestibility of lipid droplets by pancreatic lipase. *Food Research International*, 40, 770-781.
- NGUYEN, T. T. P., BHANDARI, B., CICHERO, J. & PRAKASH, S. 2015. Gastrointestinal digestion of dairy and soy proteins in infant formulas: An in vitro study. *Food Res Int*, 76, 348-358.
- NING, F., WANG, X., ZHENG, H., ZHANG, K., BAI, C., PENG, H., HUANG, Q. & XIONG, H. 2019. Improving the bioaccessibility and in vitro absorption of 5-demethylnobiletin from chenpi by se-enriched peanut protein nanoparticles-stabilized pickering emulsion. *Journal of Functional Foods*, 55, 76-85.
- SANDOVAL-CUELLAR, C. E., DE JESUS PEREA-FLORES, M. & QUINTANILLA-CARVAJAL, M. X. 2020. In-vitro digestion of whey protein- and soy lecithin-stabilized High Oleic Palm Oil emulsions. *Journal of Food Engineering*, 278.
- SARKAR, A. & DICKINSON, E. 2020. Sustainable food-grade Pickering emulsions stabilized by plant-based particles. *Current Opinion in Colloid & Interface Science*, 49, 69-81.
- SARKAR, A., HORNE, D. S. & SINGH, H. 2010. Pancreatin-induced coalescence of oil-in-water emulsions in an in vitro duodenal model. *International Dairy Journal*, 20, 589-597.
- SARKAR, A., JUAN, J. M., KOLODZIEJCZYK, E., ACQUISTAPACE, S., DONATO-CAPEL, L. & WOOSTER, T. J. 2015. Impact of Protein Gel

- Porosity on the Digestion of Lipid Emulsions. *J Agric Food Chem*, 63, 8829-37.
- SARKAR, A., LI, H., CRAY, D. & BOXALL, S. 2018. Composite whey protein–cellulose nanocrystals at oil-water interface: Towards delaying lipid digestion. *Food Hydrocolloids*, 77, 436-444.
- SARKAR, A., MURRAY, B., HOLMES, M., ETTELAIE, R., ABDALLA, A. & YANG, X. 2016a. In vitro digestion of Pickering emulsions stabilized by soft whey protein microgel particles: influence of thermal treatment. *Soft Matter*, 12, 3558-69.
- SARKAR, A., YE, A. & SINGH, H. 2016b. On the role of bile salts in the digestion of emulsified lipids. *Food Hydrocolloids*, 60, 77-84.
- SARKAR, A., ZHANG, S., HOLMES, M. & ETTELAIE, R. 2019. Colloidal aspects of digestion of Pickering emulsions: Experiments and theoretical models of lipid digestion kinetics. *Adv Colloid Interface Sci*, 263, 195-211.
- SHAO, Y. & TANG, C.-H. 2016. Gel-like pea protein Pickering emulsions at pH3.0 as a potential intestine-targeted and sustained-release delivery system for β -carotene. *Food Research International*, 79, 64-72.
- SHIMONI, G., SHANI LEVI, C., LEVI TAL, S. & LESMES, U. 2013. Emulsions stabilization by lactoferrin nano-particles under in vitro digestion conditions. *Food Hydrocolloids*, 33, 264-272.
- SINGH, H., YE, A. & HORNE, D. 2009. Structuring food emulsions in the gastrointestinal tract to modify lipid digestion. *Prog Lipid Res*, 48, 92-100.
- SURJIT SINGH, C. K., LIM, H. P., TEY, B. T. & CHAN, E. S. 2021. Spray-dried alginate-coated Pickering emulsion stabilized by chitosan for improved oxidative stability and in vitro release profile. *Carbohydr Polym*, 251, 117110.
- TZOUMAKI, M. V., MOSCHAKIS, T., SCHOLTEN, E. & BILIADERIS, C. G. 2013. In vitro lipid digestion of chitin nanocrystal stabilized o/w emulsions. *Food Funct*, 4, 121-9.
- VELIKOV, K. P. & PELAN, E. 2008. Colloidal delivery systems for micronutrients and nutraceuticals. *Soft matter*, 4, 1964-1980.

- WEI, Y., LIU, Z., GUO, A., MACKIE, A., ZHANG, L., LIAO, W., MAO, L., YUAN, F. & GAO, Y. 2021a. Zein Colloidal Particles and Cellulose Nanocrystals Synergistic Stabilization of Pickering Emulsions for Delivery of beta-Carotene. *J Agric Food Chem*, 69, 12278-12294.
- WEI, Y., TONG, Z., DAI, L., WANG, D., LV, P., LIU, J., MAO, L., YUAN, F. & GAO, Y. 2020. Influence of interfacial compositions on the microstructure, physiochemical stability, lipid digestion and β -carotene bioaccessibility of Pickering emulsions. *Food Hydrocolloids*, 104.
- WEI, Y., ZHOU, D., MACKIE, A., YANG, S., DAI, L., ZHANG, L., MAO, L. & GAO, Y. 2021b. Stability, Interfacial Structure, and Gastrointestinal Digestion of beta-Carotene-Loaded Pickering Emulsions Co-stabilized by Particles, a Biopolymer, and a Surfactant. *J Agric Food Chem*, 69, 1619-1636.
- WILDE, P. & CHU, B. 2011. Interfacial & colloidal aspects of lipid digestion. *Advances in Colloid and Interface Science*, 165, 14-22.
- XIAO, J., LI, C. & HUANG, Q. 2015. Kafirin Nanoparticle-Stabilized Pickering Emulsions as Oral Delivery Vehicles: Physicochemical Stability and in Vitro Digestion Profile. *J Agric Food Chem*, 63, 10263-70.
- YE, A., WANG, X., LIN, Q., HAN, J. & SINGH, H. 2020. Dynamic gastric stability and in vitro lipid digestion of whey-protein-stabilised emulsions: Effect of heat treatment. *Food Chem*, 318, 126463.
- YOUNAS, M., NOREEN, A., SHARIF, A., MAJEED, A., HASSAN, A., TABASUM, S., MOHAMMADI, A. & ZIA, K. M. 2019. A review on versatile applications of blends and composites of CNC with natural and synthetic polymers with mathematical modeling. *Int J Biol Macromol*, 124, 591-626.
- ZHANG, MURRAY, B. S., SURIYACHAY, N., HOLMES, M., ETTALAIE, R. & SARKAR, A. 2021. Synergistic Interactions of Plant Protein Microgels and Cellulose Nanocrystals at the Interface and Their Inhibition of the Gastric Digestion of Pickering Emulsions. *Langmuir*, 37, 827-840.

- ZHANG, R., ZHANG, Z., ZHANG, H., DECKER, E. A. & MCCLEMENTS, D. J. 2015. Influence of lipid type on gastrointestinal fate of oil-in-water emulsions: In vitro digestion study. *Food Res Int*, 75, 71-78.
- ZHANG, S., HOLMES, M., ETTALAIE, R. & SARKAR, A. 2020. Pea protein microgel particles as Pickering stabilisers of oil-in-water emulsions: Responsiveness to pH and ionic strength. *Food Hydrocolloids*, 102, 105583.
- ZHANG, Z., ZHANG, R. & MCCLEMENTS, D. J. 2017. Control of protein digestion under simulated gastrointestinal conditions using biopolymer microgels. *Food Res Int*, 100, 86-94.
- ZHAO, M., SHEN, P., ZHANG, Y., ZHONG, M., ZHAO, Q. & ZHOU, F. 2021. Fabrication of Soy Protein Nanoparticles via Partial Enzymatic Hydrolysis and Their Role in Controlling Lipid Digestion of Oil-in-Water Emulsions. *ACS Food Science & Technology*, 1, 193-204.
- ZHOU, H., DAI, T., LIU, J., TAN, Y., BAI, L., ROJAS, O. J. & MCCLEMENTS, D. J. 2021. Chitin nanocrystals reduce lipid digestion and β -carotene bioaccessibility: An in-vitro INFOGEST gastrointestinal study. *Food Hydrocolloids*, 113, 106494.

Chapter 6

General discussion

6.1 Introduction

The overall aim of this thesis is to design sustainable Pickering emulsions with tailored digestion properties. Figure 6.1 shows the overall illustration of the results obtained in the entire thesis using a range of light scattering, microscopy, rheology, interfacial techniques and digestion experiments. In this thesis, pea protein microgels (PPM) were designed for the first time to fabricate sustainable Pickering emulsions. These emulsions were stable for prolonged period and showed various degree of flocculation as a function of pH and ionic strength. When these emulsions were subjected to gastric digestion it was clear that the emulsions were destabilized owing to pepsin-induced rupture of the interfacial PPM-laden interface leading to droplet coalescence. However, on using a secondary layer of cellulose nanocrystals (CNC) at the interface by electrostatically complexing PPM with CNC at gastric pH (pH 3.0), such coalescence was hindered. Thus, this thesis shows a novel way of making particle-particle-complex as interfaces to make gastric stable emulsions. When further gastrointestinal digestion was probed, it was found that indeed the PPM+CNC emulsions that allowed generating gastric stable emulsions were better in releasing higher degree of fatty acids at a lower rate as compared to the ones containing only PPM. Of course the electrostatic complex was not strong enough at intestinal pH (pH 7.0), so the destabilization and coalescence was expected. Overall, this shows that using complex particulate system may allow making stable droplets that can have higher release in intestinal phase allowing an opportunity to have a pH-based controlled release. Briefly, all the chapter-wise results are summarized in this chapter using corresponding graphical abstracts for each chapter and comparing any new literature that has appeared in the field, followed by highlighting some key results obtained in this PhD that were not included in individual published chapters. Finally the future directions that can be carried further from this thesis are elaborate.

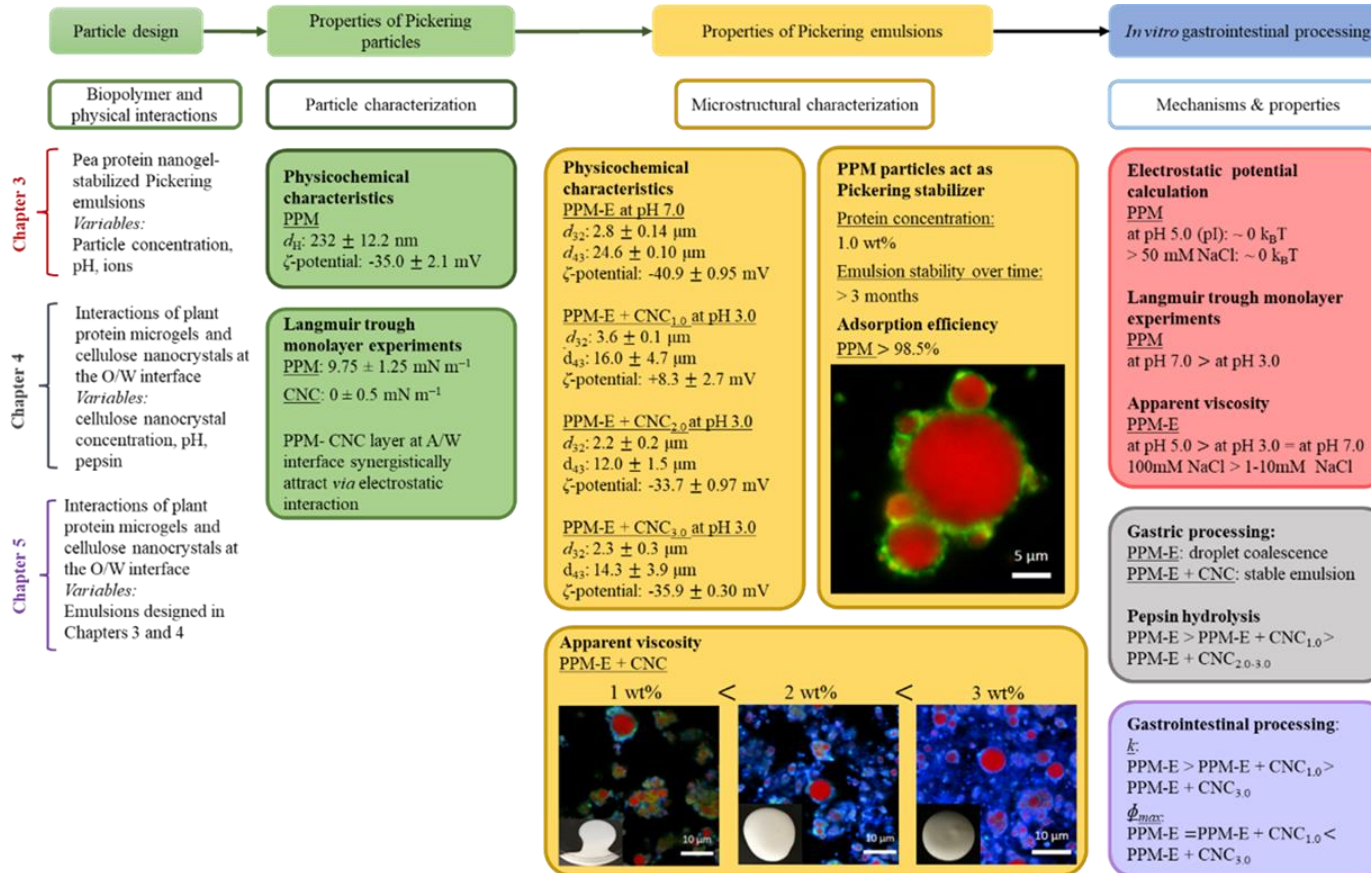


Figure 6.1. Schematic framework of the thesis.

6.2 Summary of main results obtained in this thesis.

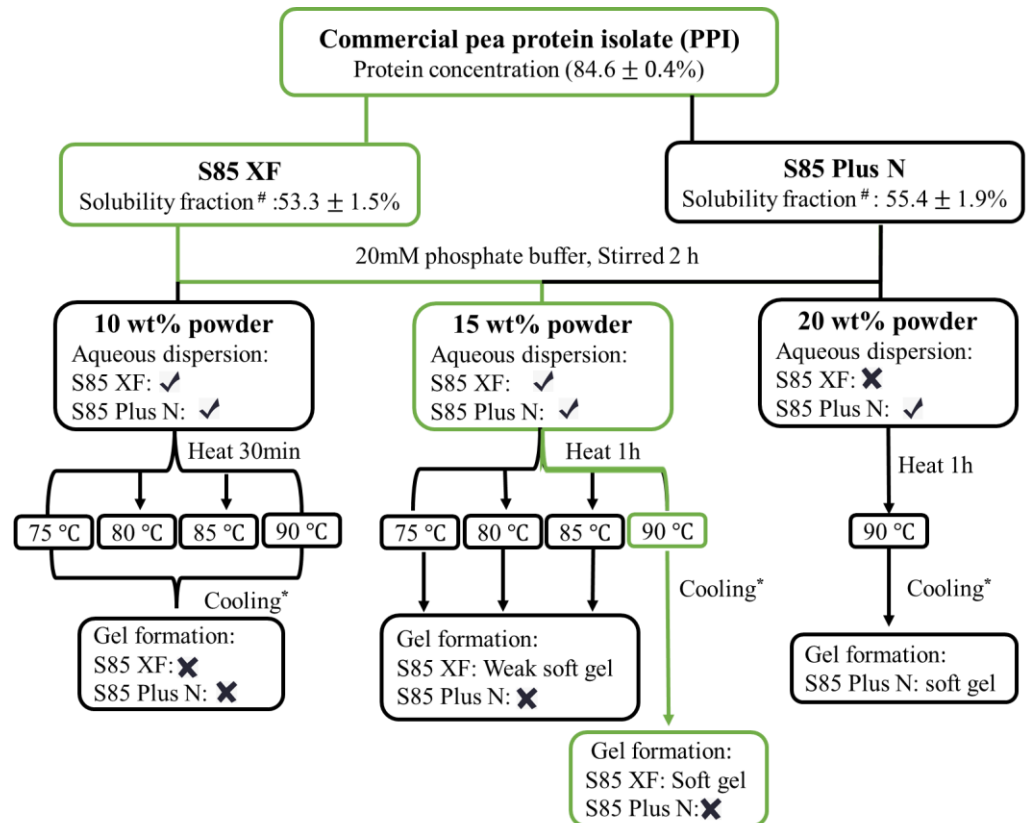


Figure 6.2. Flow chart of producing protein hydrogel using commercial pea protein isolate. . *: Cooling: Heated gel was cooled to room temperature *via* flowing water, and stored at 4 °C for 24 h. # Solubility fraction was determined by Lowry assay *via* DC protein assay, absorbance measured at 750 nm.

Before the novel pea protein microgel particles was designed, two different commercial pea protein isolate (PPI) (S85 XF and S85 Plus N) were compared based on several measurements, as shown in **Figure 6.2**. Both PPIs had protein concentration was at near 85%, which is consistent with the concentration provided by the company. However, S85 Plus N has a higher solubility fraction as compared with S85 XF. Following the studies by Mession et al. (2015, 2017a) and Ben-Harb et al. (2018a), heat-induced gelation was investigated at 75, 80, 85 and 90 °C for 30 min in this thesis to denature the pea protein. As shown in **Figure 6.2**, three different concentrations of PPIs were tried to form heat-induced gel, *i.e.* 10 wt% PPI powder as 8.5 wt% protein, 15 wt% PPI powder as 12.75 wt% protein, and 20

wt% PPI powder as 17 wt% protein. For 10 wt% PPI (powder), none of the protein isolate formed heat-set gel after cooling overnight. In contrast, the 15 wt% S85 XF(powder) formed soft hydrogel, especially in the case which was heated at 90 °C. In addition, S85 Plus N only formed heat-set gel when the powder concentration was raised to 20 wt%. However, 20 wt% of S85 XF was difficult to disperse in phosphate buffer. Therefore, S85 XF with the concentration of 15 wt% (powder) and S85 Plus N with the concentration of 20 wt% (powder) was used to form the heat-set gel, after heating the protein dispersion at 90 °C and cooling at 4 °C overnight. In order to increase the gel strength of the pea protein gel, heating time of PPI (powder) dispersion was extended to 1 hour, producing a moderately firm gel, which was suitable to produce microgel particle dispersion.

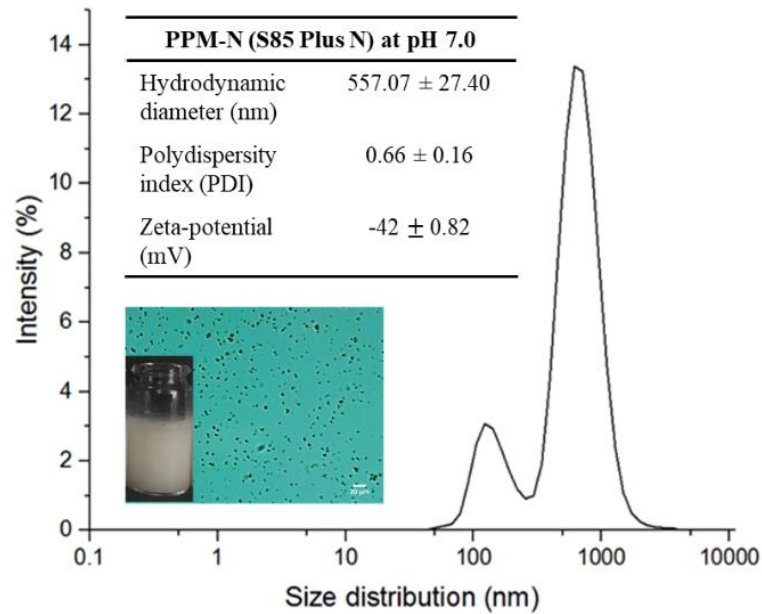


Figure 6.3. Particle size distribution (PSD) of pea protein microgel particles (PPM-N) formed by S85 Plus N at pH 7.0 with inset table showing the hydrodynamic diameter (d_h), polydispersity index (PDI) and zeta-potential. The insets are visual and optical images of aqueous dispersions of PPM-N (S85 Plus N). Scale bar represents 20 μm .

In this thesis, PPI of S85 XF was chosen to form pea protein microgels particle (PPM) by controlled shearing of heat-set gel in this thesis (**Chapter 3-5**) rather than of S85 Plus N, because of several reasons. Firstly, the PPM-N particles had a higher

value of hydrodynamic diameter (d_h) of about 560 nm with high polydispersity index ($PDI > 0.6$) (**Figure 6.3**), as compared with the d_h of PPM *i.e.* 232 nm (**Figure 6.1**). As shown in **Figure 6.3**, the aqueous dispersion of PPM formed by S85 Plus N (PPM-N) in phosphate buffer at pH 7.0 had two peaks in size distribution, which means that the particle size of PPM-N was not monomodal. These two population of particles led to separation and sedimentation of particle dispersion after one week of storage under refrigerated conditions (data not shown).

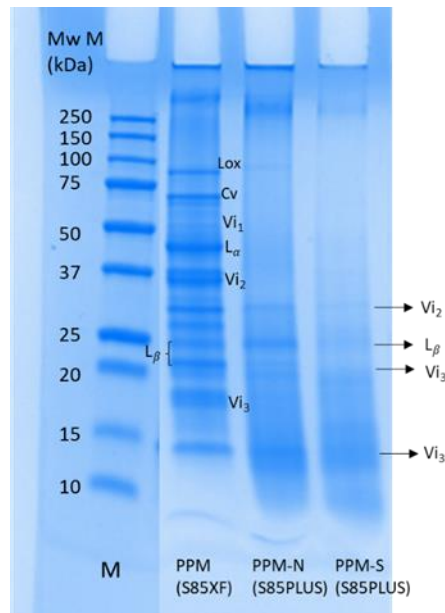


Figure 6.4. SDS-PAGE electrogram of aqueous dispersions of PPM (S85 XF), PPM-N (S85 Plus N) and the supernatant of aqueous dispersions of PPM-N (PPM-S) at pH 7.0. Lane M represents the protein markers of 10-250 kDa M_w range.

Of more importance, the laboratory-synthesized PPM formed using S85 XF had more than ten polypeptides, which has been discussed in the previous chapters (**Chapter 3** and **4**), however, PPM-N created from S85 Plus N just contains basic subunit (L_β) at 18- 24 kDa and two vicilin subunits (Vi_{2-3}), which are respectively observed in fractions of around 36-30 kDa , 20 kDa and 15 kDa.. The proportions of these bands were further reduce in the supernatant of aqueous dispersions of PPM-N (**Figure 6.4**)

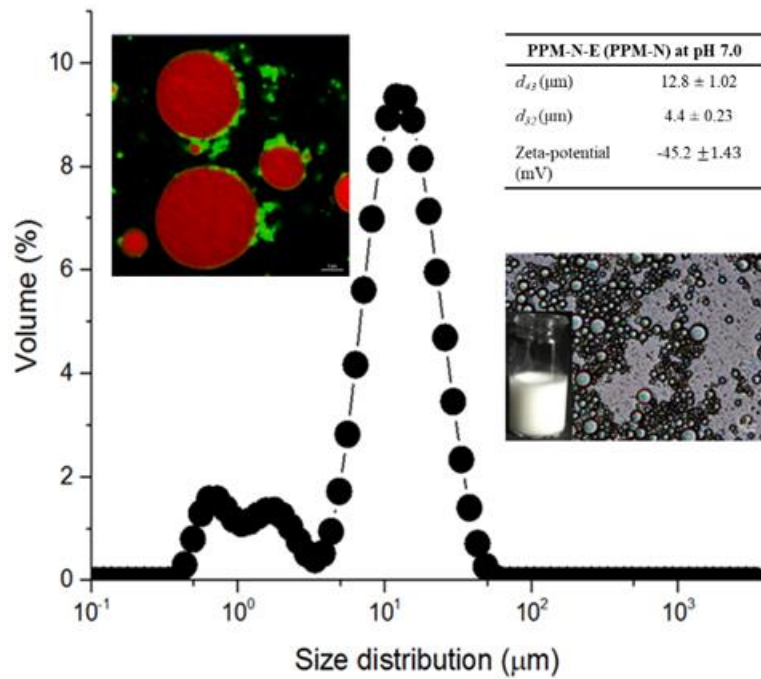


Figure 6.5. Droplet size distribution of 20 wt% oil-in-water emulsions stabilized by PPM-N (S 85 Plus N) at pH 7.0 (●) with insets showing corresponding surface-average mean diameter (d_{32}), volume-average mean diameter (d_{43}) and zeta-potential. The insets are confocal visual and optical images of emulsion stabilized by PPM-N (S85 Plus N). Scale bar of confocal image represents 5 μm , Scale bar of optical image represents 20 μm .

Last but not least, the Pickering emulsion stabilized using the polydisperse PPM-N (PPM-N-E) had three peaks in the droplet size distribution of Pickering emulsions (**Figure 6.5**). Although oil droplets in PPM-N-E were small-sized ($d_{43} \sim 12 \mu\text{m}$), the unexpected phase separation was discernible in such Pickering emulsion macroscopically under refrigerated conditions for a week (data not shown). Even, the confocal image of Pickering emulsion stabilized by PPM-N suggests that although adsorbed layer of PPM-N was present in some areas, there was droplet coalescence and thus PPM-N was not used in this thesis.

In **Chapter 3**, pea protein microgels (PPM) prepared by controlled shearing of heat-set gel using S85 XF isolate had a great colloidal stability against aggregation for long time. Pickering oil-in-water emulsions (PPM-E) which was stabilized by the submicron-sized PPM presented an excellent stability against

coalescence over few months. As summarized in **Figure 6.6**, it is worth emphasizing that the adsorbed PPM aggregated their neighbours at droplet surface while the value of pH switched from pH 7.0 to pH 5.0, which was also theoretically proven. Overall, this thesis shows for the first time the role of PPM prepared using top down approach to create Pickering emulsions. As compared with the approach using in literature suggesting pea protein particles being formed through self-assembly by potassium metabisulfite or Ca^{2+} ions (Fan et al., 2020, Li et al., 2021b), the top-down approach used in this thesis is facile and offer significant level of control over the microgel particle properties (Lefroy et al., 2021). Another common approach to produce pea protein submicrometer-sized particles in literature is using acidic precipitation (Liang and Tang, 2014b, Shao and Tang, 2016b, Sridharan et al., 2020). However, these gel-like pea protein stabilized Pickering emulsions were sensitive to environmental changes, especially to the pH that self-assemble pea protein would disintegrate at interface at neutral condition. Pickering emulsion stabilized by PPMs in this thesis which were formed by the top-down approach showed excellent stability against the variation of pH and ionic strength as evidenced experimentally and theoretically in **Chapter 3**.

There is no surprise that the protein particles produced from plant sources are receiving a huge attention for their potential to act as Pickering stabilizers over the past three years. A range of novel hydrogel particles from plant-based proteins have been designed with the cooperation of heat-induced protein denaturation. For instance, Wang et al. (2020) created self-assembled rapeseed nanogel particles by chemical acylation and heat-induced denaturation, which has the potential ability for hydrophobic drug delivery such as curcumin. Zhang *et al.* (2022a, 2022b) created bamboo fungus protein microgel particles *via* enzymatic method using transglutaminase. Such microgel particles could stabilize high internal phase Pickering emulsions (80 wt% of antarctic krill oil fraction) with anti-inflammatory activity. Liu et al. (2020) created self-assembled potato protein microgel particles *via* adjusting pH conditions. In addition, other forms of pea protein-based microparticles have also received a great deal of attention, such as pea protein microparticles that have been produced by using high moisture extrusion cooking,

for Pickering emulsification (Tanger et al., 2021a), and heat-induced pea protein amyloid fibrils for high internal phase emulsification (Wu et al., 2022).

According to the findings in **Chapter 3**, main advantages of microgels used as Pickering stabilizers have been emphasized again, which are ultrastability against coalescence, biocompatibility, and clean-label being “surfactant free” (Frelichowska et al., 2009, Leal-Calderon and Schmitt, 2008). Microgels usually aggregate in the system with high internal phase and generate high viscosity, which also provides benefits in some cases such as fat replacement (Linke and Drusch, 2018). Pea protein-based microparticles proved as a fat replacer to create a same creamy mouthfeel product compared to the full-fat food, such as milk dessert or commercial mayonnaise (Li et al., 2021a, Tanger et al., 2021a, Tanger et al., 2021b). However, a kind of especial beany flavour with pea protein-based microparticles would have disadvantageous impact on taste and smell in fat-reduced product.

Although the benefits of microgel as Pickering stabilizers are significant, their limitations cannot be ignored. Microgel, as a “soft” colloidal particle, would swell, deform, even disintegration at interface depending on the particle properties including size and crosslink density, as well as the surrounding environment such as the balance of solvation between the dispersion and bulk phases, pH and temperature (Lefroy et al., 2020, Berton-Carabin and Schroen, 2015) may also affect their properties and consequently the performance of the emulsion.

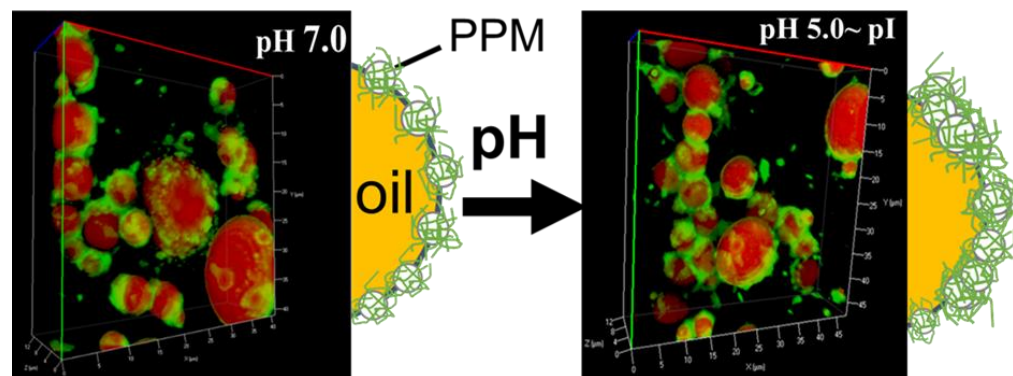


Figure 6.6. Graphical summary for **Chapter 3** showing how Pickering emulsion droplets stabilized by PPM show a pH dependent transition from being intact particles to aggregated network at the oil-water (O/W) interface.

In **Chapter 4**, it was further investigated that PPM as soft particles could swell and stretch two-fold due to the deformable hydrogel structure, as well as could effectively adsorb at the droplets surface to form a monolayer. As shown in **Figure 6.7**, such monolayer formed by PPM was hydrolysed when subjected to *in vitro* gastric digestion conditions, resulting in droplet coalescence and phase separation in PPM-E. However, addition of CNC stabilized the emulsions against these gastric coalescence. The Pickering emulsions co-stabilized *via* the particle-particle electrostatic interaction had a high physicochemical stability under *in vitro* gastric digestion conditions. Although the gaps between CNCs were much larger as compared to the size of enzyme, a strong gel-like structure formed by CNCs in the emulsions could bind or trap the pepsin enzyme responsible for the digestion, and then may restrict the access of the pepsin to the substrate sites available in the PPM. On the other hand, this CNC-induced gelation also inhibited any tendency of oil droplets to coalesce due to the steric resistance.

Next, the studies in the **Chapter 5** focused on the intestinal digestion of droplets in emulsion based on such complex plant-based particulate interfaces. Although the electrostatic interaction between PPM and CNCs should be limited when subjected to *in vitro* intestinal digestion conditions because of the negatively-charge of both particles at neutral pH, the lipolysis was slightly delayed with in the presence of CNCs, when compared with the rate of lipolysis of PPM-E. Meanwhile, the overall extent of lipid digestion of PPM-E + CNC increased after 2 h digestion when compared with that of PPM-E. These results suggests that such Pickering emulsions co-stabilized by particle-particle interface, could be used to protect lipophilic bioactive compounds in the stomach without inhibiting their release in the intestines.

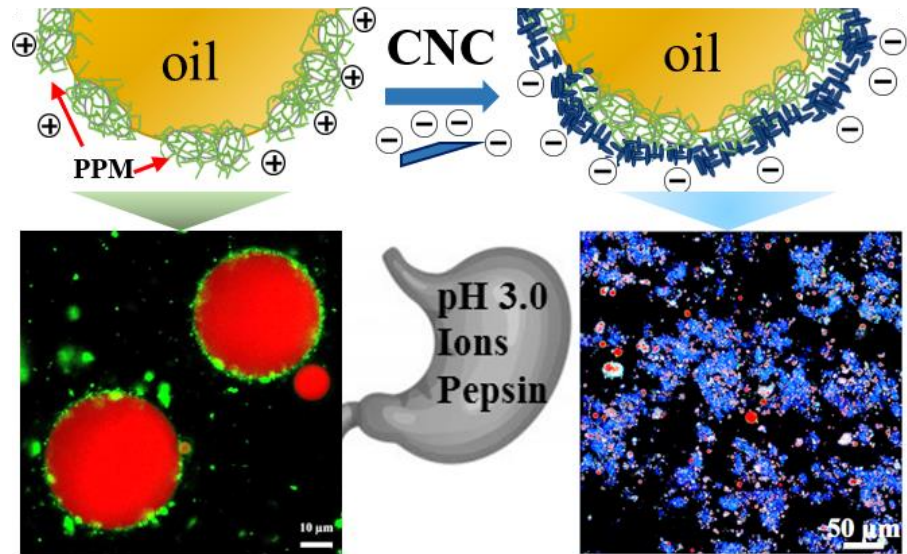


Figure 6.7. Graphical abstract for **Chapter 4** showing how Pickering emulsion droplets stabilized by PPM resulted in gastric coalescence whereas addition of CNC as a second layer *via* electrostatic complexation with PPM at the interface protects against such destabilization.

Such colloidal Pickering system with particle-particle complex interface is essential in food, cosmetics, and pharmaceuticals, and has attracted some attention, *e.g.*, the combination of waxy maize starch nanocrystals and zein nanoparticles (Tao et al., 2021), CNC and zein colloidal particles (ZCPs) (Wei et al., 2021b), as well as zein-propylene glycol alginate composite particles (ZPCPs) and whey protein microgel particles (WPM) (Wei et al., 2021c). In order to achieve the purpose of enhanced stability and controlled delivery of β -carotene, Wei and his co-workers firstly considered the cooperation between the hydrophobic ZCPs and hydrophilic CNCs (Wei et al., 2021b). The Pickering emulsion had high physical-, thermal-, storage-, pH-, ionic strength- as well as photo-stability, when the mass ratio of ZCP to CNC was 1: 4. They believed that if the emulsion was stabilized by CNC and covered with ZCP as an outer layer, the free fatty acid release rate of Pickering emulsions was reduced whilst the bioaccessibility of β -carotene was increased. However, such complex interfacial structure formed by CNC (an inner layer) and ZCP (an outer layer) is unclear. Unmodified CNCs alone are not suitable to stabilize emulsion since they are highly hydrophilic without much surface

activity, which is also proven in **Chapter 4**. The formation of CNC – ZCP interface in stable Pickering emulsion should depend on the presence of ZCP rather than CNC at the droplet surface. Therefore, Pickering emulsion designed by Wei et al. (2021b) could be stabilized by a mixed CNC-ZCP layer, rather than a layer-by-layer interfacial structure. Next, Wei et al. (2021c) tried the combination of ZPCPs and WPM. The Pickering emulsion stabilized by ZPCPs with WPM as the outer layer also showed the high stability and β -carotene bioaccessibility, especially when the mass ratio of ZPCPs to WPM was 4 : 1. This type of Pickering emulsion with protein-based particle-particle complex interface serves a promising tool to enhance stability, delay lipid digestion or protect and deliver liposoluble bioactive components, which highlights the importance and growing literature in the field of particle-particle interfaces.

6.3 Future directions

This thesis has demonstrated the potential of pea protein microgel particles to act as Pickering stabilizers and create an interfacial combination with cellulose nanocrystals, which has potential to enhance the stability of Pickering emulsion, also on controlling the digestion behaviour during *in vitro* gastrointestinal regimes. Based on these findings, the main recommendations on further research that could be undertaken are summarized.

A. Materials

a. Materials for fabricating the Pickering emulsion stabilizers

- In this thesis, pea protein isolate was used to form plant-based protein microgel particle. However, the behaviour of these protein microgel particles cannot represent the properties of any plant-based protein microgels. The reason is that proteins produced from different plant sources have great differences in structure, type of amino acids as well as subunits of proteins. For instance, Xu et al. (2015) created soy protein microgel particle (SPM) using the same technology as used in this thesis. This SPM acted as a great Pickering stabilizer similar to PPM, but SPM was unstable

under different salt concentrations whilst PPM in our thesis showed high colloidal stability. Thus, future work should investigate various kinds of plant proteins, *e.g.* other leguminous proteins from broad beans, lotus, cow peas, chickpeas, pigeon peas, lentils, lupins, green beans, or peanuts (Maphosa and Jideani, 2017), the oilseed proteins from rapeseed, sunflower seeds, coconut, olive, flax, cotton seeds, sesame seeds, chia, or pumpkin seeds (Kotecka-Majchrzak et al., 2020), and the cereal proteins from maize, rice, wheat, barley, sorghum, millet, oats or rye (Scherf et al., 2016, Zou et al., 2019).

b. Materials of interest for the secondary polysaccharide-based particles

- In this thesis, Pickering emulsion was designed with a complex PPM-CNC interface to achieve enhanced stability under *in vitro* gastrointestinal digestion. As discussed in **Chapter 4** and **5**, the mechanism by which PPM and CNC associate at the interface depends only on electrostatic interaction due to the oppositely charged particles at low pH (pH 3.0). And the interfacial combination of CNC and PPM was limited in emulsions under *in vitro* intestinal digestion where both the particles were negatively-charged (pH 7.0). Although the presence of CNC could slightly reduce the rate of lipolysis, coalescence of oil droplets was not inhibited in the intestinal regime. Thus, additional third type of particles could be considered to be added onto the PPM-CNC interface in Pickering emulsion, in order to enhance the intestinal stability as well as to possibly delay the lipolysis. For instance, chitosan nanocrystal (ChN) is the potential choice to play as the third particle. On the one hand, ChN particle is well documented in literature to successfully stabilize Pickering emulsions with long-term stability (Deng et al., 2022, Sharkawy et al., 2020, Ribeiro et al., 2020). On the other hand, this polysaccharide nanocrystal shows positive zeta potential at a range of pH value from pH 3.0 to pH 6.9 due to amino groups at surface (Costa et al., 2020, Qi et al., 2004, Sharkawy et al., 2020). Therefore, it

could be assumed that the presence of ChN could form a new interfacial structure with CNC to continue providing stability to the oil droplet, even if the adsorbed PPM particles are fully hydrolyzed by proteases under *in vitro* gastrointestinal digestion condition. Thus, PPM-CNC-ChN is a potential system to investigate in future to allow more controllable release in the intestinal phase.

c. Materials for preparation of simulated digestion fluids

- Although majority of lipolysis occurs in the intestinal phase, gastric lipase can contribute to nearly 10–30% of lipid digestion resulting in generation of FFAs in the stomach (Armand et al., 1996). In this thesis, gastric lipase was not used because of the unavailability of reliable sources. Therefore, it should be determined that whether Pickering emulsion with a complex particle-particle interface such as PPM-CNC still show gastric stability, once gastric lipases are added in the simulated gastric digestion fluids in future research.
- In this thesis, porcine pancreatin was used in *in vitro* gastrointestinal digestion fluids, which is a complex mixture of several digestive enzymes including amylase, trypsin, lipase, colipase, ribonuclease and protease. In order to understand how interfacial structure effect the behaviour of lipase/co-lipase on lipolysis, pure lipase from porcine pancreas Type II was used to determine lipid digestion kinetics of emulsion bypassing the gastric phase. However, this lipase still showed protease activity. Therefore, lab-purified lipase and co-lipase with limited protease activity should be used in designing simulated intestinal digestion fluids in future research to gain mechanistic understanding on role of digestion metabolites on emulsion destabilization.
- Some research has demonstrated that soluble cellulose/ cellulose nanocrystal could significantly bind bile acids under *in vitro* intestinal environment (Mackie et al., 2019, Torcello-Gomez and Foster, 2014), resulting in controlled lipid digestion. The porcine bile extract used in this

thesis is a mixture of several free bile acids, containing glycodeoxycholic acid, taurodeoxycholic acid, deoxycholic acid, chenodeoxycholic acids and lithocholic acids. Therefore, in future research, interactions between cellulose nanocrystals and each of individual bile acids *in vitro* is a necessary undertaking.

B. Advanced characterization techniques

a. Atomic force microscopy (AFM)

- In this thesis, we have used a range of structural and rheological techniques to characterize pea protein microgel particles. In future research, AFM might be used to visually observe the size, shape and nanomechanical properties (*e.g.* modulus) of such particle.

b. Small Angle X-ray Scattering

- Small angle X-ray scattering is a unique tool to determine structural characterization of particles in real time and under realistic environments. In the next studies, small angle X-ray scattering may be used to understand the organization and ordering of CNCs at the PPM-stabilized interfaces. Such technique can also shed light on samples during *in vitro* digestion on how bile salts, lipase and intact/ hydrolyzed particles order at the O/W interface.

c. In vitro semi-dynamic digestion method

- In this thesis, *in vitro* static model (Minekus et al., 2014) was used to understand gastrointestinal digestion of these emulsions. However, this proposal just can provide end-point assessment without considering the possible kinetic aspects, such as gradual acidification, fluid and enzyme secretion, as well as emptying in gastric regime of digestion. Therefore, the novel *in vitro* semi-dynamic digestion method developed by Mulet-Cabero et al. (2020) should be used in future research.

d. Interfacial shear viscosity

- As mentioned in **Chapters 1, 3 and 4**, sodium dodecyl sulphate polyacrylamide gel electrophoresis (SDS-PAGE) method could not be applied to analyse the extent of protein hydrolysis in our emulsion system in *in vitro* gastric digestion, due to the limitation that some protein within the gel particles were covered by CNC, which were not influenced by SDS or DTT to a great extent. In order to understand the adsorption behaviour and proteolysis of PPM at O/W interface, the interfacial shear viscosity of PPM at pH 7.0 and at pH 3.0 with SGF under *in vitro* gastric digestion condition were measured in this thesis (**Figure 6.8**). At 25 °C, 1 wt% PPM particles at pH 7.0 in phosphate buffer were adsorbed onto O/W interface after 5 h adsorption. Over the next 15 h, increasing value of interfacial viscosity showed that more and more PPM particles continued to adsorb toward the interface. In addition, interfacial shear viscosity of PPM at pH 3.0 in SGF at 25 °C also continue increased to around 0.2 mM s m⁻¹ in the 24 h. As demonstrated in **Figure 6.8(A)**, as the temperature of PPM + SGF dispersion was changed, the value of interfacial shear viscosity increased to about 0.25 mM s m⁻¹ after the temperature reaching at 37 °C (**Figure 6.8(B)**). Next, at point C in **Figure 6.8**, 1 mL of pepsin + SGF mixture was added gently into PPM dispersion using a syringe as shown in **Figure 6.9**. Once the pepsin dispersion was added, the value of interfacial viscosity immediately decreased to zero until gastric digestion finished. After 2 h gastric digestion, the value of interfacial viscosity rapid increased again to 0.3 mM s m⁻¹ in 3 h, but slowly reducing back to zero in the next 12 h. The change in interfacial viscosity plot could prove that some surfactants, *i.e.* peptides produced from protein hydrolysis, moved and adsorbed onto the interface, and releasing from interface in the longer adsorption time due to lower desorption energy.

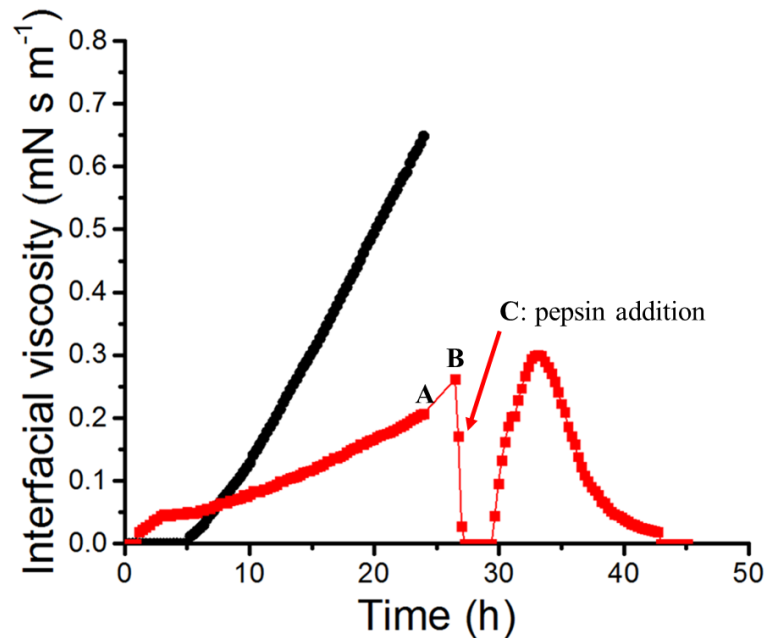


Figure 6.8. Interfacial shear viscosity of 1.0 wt % PPM at pH 7.0(●) with phosphate buffer at 25°C, and the 1.0 wt% PPM at pH 3.0 (■) with SGF in *in vitro* gastric digestion regime. A: changing temperature of PPM dispersion from 25°C to 37°C. B: temperature reaches at 37°C. C: Pepsin + SGF mixture was added into PPM dispersion.

Results as showed in **Figure 6.8** are not enough to clear describe the adsorption behaviour of PPM onto the interface or the deformation of PPM-stabilized interface in *in vitro* gastric digestion regime. In future researches, more samples should be measured: I) interfacial viscosity of whey protein microgel (WPM) in phosphate buffer at pH 7.0 should be measured as a function of 24 h adsorption time, which could play as control sample; II) PPM dispersion at pH 3.0 without SGF should also be investigated to understand how ionic strength in SGF buffer influences the formation of PPM-stabilized interface. In addition, as presented in **Figure 6.9**, 1 mL of the pepsin + SGF mixture was injected into the bottom of the container through an extremely thin needle, in order to minimize damage to the PPM-stabilized interface. At the same time, another 1 mL of PPM dispersion was drawn from the other side of container at the same speed to maintain the interfacial level. However, it is unclear that the dramatically decreased value of interfacial viscosity after addition of pepsin dispersion was due to the presence of enzyme or the

interface was damaged, caused by the needles. Therefore, the interfacial viscosity of PPM under *in vitro* gastric digestion condition without addition of pepsin should be measured as function of time, where 1 mL of SGF buffer would be injected into container rather than the pepsin + SGF mixture.

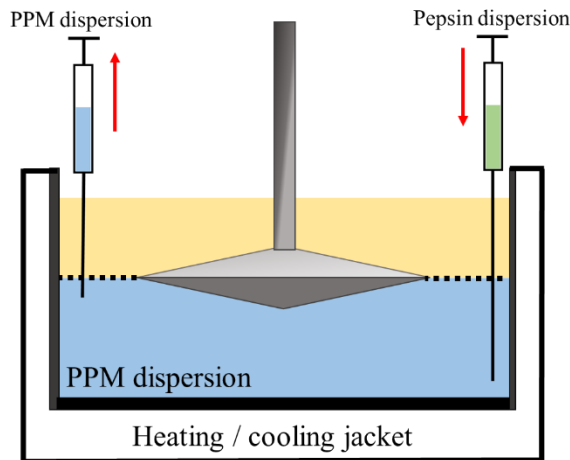


Figure 6.9. Schematic representation of adding pepsin dispersion during the measurement of interfacial shear viscosity.

C. Modelling of digestion

Although in **Chapter 2**, a range of models have been proposed to fit digestion data, the models are developed for Pickering emulsions stabilized by one type of particle. It is important to extend such models to other possibilities such as when the lipase is itself bound to polysaccharide particles and not available for digestion of the lipidic substrate as shown in **Figure 6.10**. Also the polysaccharide can form network at the bulk phase / interface which can significantly affect the droplet size, the surface where lipase can bind and thus can influence the kinetics of free fatty acid release. Therefore, new models are needed to reflect these scenarios – such models will help to fit the data and to get clearer understanding on how lipase activity can be manipulated by various colloidal strategies in Pickering emulsions.

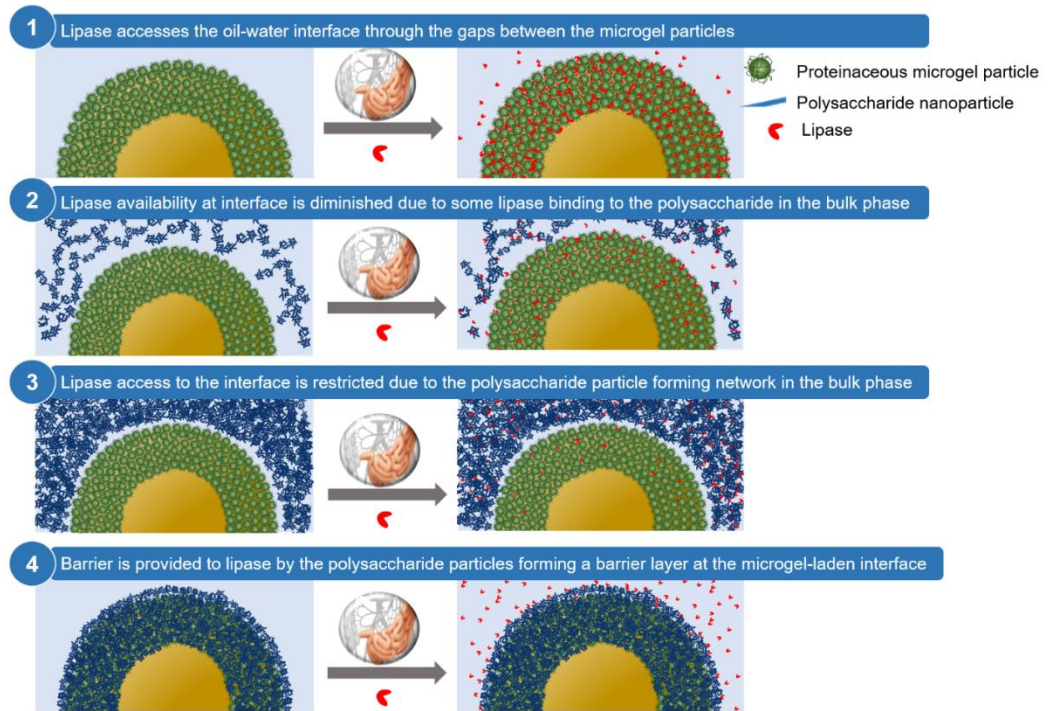


Figure 6.10. Schematic representation of various strategies to influence gastrointestinal digestion kinetics of Pickering emulsion where 1) no barrier *i.e.* lipase gets access to the lipid core through gasps in the microgel layer, 2) lipase binds to polysaccharide in bulk phase reducing overall available activity, 3) lipase activity is affected as the polysaccharide forms network in the bulk phase and 4) lipase activity is affected as the polysaccharide forms a barrier layer at the interface.

6.4 Reference

- ARMAND, M., BOREL, P., PASQUIER, B., DUBOIS, C., SENFT, M., ANDRE, M., PEYROT, J., SALDUCCI, J. & LAIRON, D. 1996. Physicochemical characteristics of emulsions during fat digestion in human stomach and duodenum. *American Journal of Physiology-Gastrointestinal and Liver Physiology*, 271, G172-G183.
- BEN-HARB, S., PANOUILLE, M., HUC-MATHIS, D., MOULIN, G., SAINT-EVE, A., IRLINGER, F., BONNARME, P., MICHON, C. & SOUCHON, I. 2018. The rheological and microstructural properties of pea, milk, mixed pea/milk gels and gelled emulsions designed by thermal, acid, and enzyme treatments. *Food Hydrocolloids*, 77, 75-84.
- BERTON-CARABIN, C. C. & SCHROEN, K. 2015. Pickering emulsions for food applications: background, trends, and challenges. *Annu Rev Food Sci Technol*, 6, 263-97.
- COSTA, A. L. R., GOMES, A., FURTADO, G. D. F., TIBOLLA, H., MENEGALLI, F. C. & CUNHA, R. L. 2020. Modulating in vitro digestibility of Pickering emulsions stabilized by food-grade polysaccharides particles. *Carbohydrate Polymers*, 227.
- DENG, W., LI, Y., WU, L. & CHEN, S. 2022. Pickering emulsions stabilized by polysaccharides particles and their applications: a review. *Food Science and Technology*, 42.
- FAN, Y., ZENG, X., YI, J. & ZHANG, Y. 2020. Fabrication of pea protein nanoparticles with calcium-induced cross-linking for the stabilization and delivery of antioxidative resveratrol. *International journal of biological macromolecules*, 152, 189-198.
- KOTECKA-MAJCHRZAK, K., SUMARA, A., FORNAL, E. & MONTOWSKA, M. 2020. Oilseed proteins – Properties and application as a food ingredient. *Trends in Food Science & Technology*, 106, 160-170.
- LEFROY, K. S., MURRAY, B. S. & RIES, M. E. 2020. Advances in the use of microgels as emulsion stabilisers and as a strategy for cellulose functionalisation. *Cellulose*, 28, 647-670.

- LEFROY, K. S., MURRAY, B. S. & RIES, M. E. 2021. Advances in the use of microgels as emulsion stabilisers and as a strategy for cellulose functionalisation. *Cellulose*, 28, 647-670.
- LI, S., JIAO, B., MENG, S., FU, W., FAISAL, S., LI, X., LIU, H. & WANG, Q. 2021a. Edible mayonnaise-like Pickering emulsion stabilized by pea protein isolate microgels: Effect of food ingredients in commercial mayonnaise recipe. *Food Chem*, 376, 131866.
- LI, X.-L., XIE, Q.-T., LIU, W.-J., XU, B.-C. & ZHANG, B. 2021b. Self-Assembled Pea Protein Isolate Nanoparticles with Various Sizes: Explore the Formation Mechanism. *Journal of agricultural and food chemistry*, 69, 9905-9914.
- LIANG, H.-N. & TANG, C.-H. 2014. Pea protein exhibits a novel Pickering stabilization for oil-in-water emulsions at pH 3.0. *LWT - Food Science and Technology*, 58, 463-469.
- LINKE, C. & DRUSCH, S. 2018. Pickering emulsions in foods - opportunities and limitations. *Crit Rev Food Sci Nutr*, 58, 1971-1985.
- LIU, X., SHEN, L., ZHAO, S. & ZHANG, H. 2020. Formation and emulsification properties of self-assembled potato protein microgel particles under different pH conditions. *International Journal of Food Science & Technology*, 56, 2864-2875.
- MACKIE, A., GOURCY, S., RIGBY, N., MOFFAT, J., CAPRON, I. & BAJKA, B. 2019. The fate of cellulose nanocrystal stabilised emulsions after simulated gastrointestinal digestion and exposure to intestinal mucosa. *Nanoscale*, 11, 2991-2998.
- MAPHOSA, Y. & JIDEANI, V. A. 2017. The Role of Legumes in Human Nutrition. *Functional Food - Improve Health through Adequate Food*.
- MESSIEN, J.-L., CHIHI, M. L., SOK, N. & SAUREL, R. 2015. Effect of globular pea proteins fractionation on their heat-induced aggregation and acid cold-set gelation. *Food Hydrocolloids*, 46, 233-243.

- MESSION, J.-L., ROUSTEL, S. & SAUREL, R. 2017. Interactions in casein micelle–Pea protein system (part D): Heat-induced denaturation and aggregation. *Food Hydrocolloids*, 67, 229-242.
- MINEKUS, M., ALMINGER, M., ALVITO, P., BALLANCE, S., BOHN, T., BOURLIEU, C., CARRIÈRE, F., BOUTROU, R., CORREDIG, M., DUPONT, D., DUFOUR, C., EGGER, L., GOLDING, M., KARAKAYA, S., KIRKHUS, B., LE FEUNTEUN, S., LESMES, U., MACIERZANKA, A., MACKIE, A., MARZE, S., MCCLEMENTS, D. J., MÉNARD, O., RECIO, I., SANTOS, C. N., SINGH, R. P., VEGARUD, G. E., WICKHAM, M. S., WEITSCHIES, W. & BRODKORB, A. 2014. A standardised static in vitro digestion method suitable for food - an international consensus. *Food Funct*, 5, 1113-24.
- MULET-CABERO, A. I., EGGER, L., PORTMANN, R., MENARD, O., MARZE, S., MINEKUS, M., LE FEUNTEUN, S., SARKAR, A., GRUNDY, M. M., CARRIERE, F., GOLDING, M., DUPONT, D., RECIO, I., BRODKORB, A. & MACKIE, A. 2020. A standardised semi-dynamic in vitro digestion method suitable for food - an international consensus. *Food Funct*, 11, 1702-1720.
- QI, L., XU, Z., JIANG, X., HU, C. & ZOU, X. 2004. Preparation and antibacterial activity of chitosan nanoparticles. *Carbohydrate Research*, 339, 2693-2700.
- RIBEIRO, E. F., DE BARROS-ALEXANDRINO, T. T., ASSIS, O. B. G., JUNIOR, A. C., QUILES, A., HERNANDO, I. & NICOLETTI, V. R. 2020. Chitosan and crosslinked chitosan nanoparticles: Synthesis, characterization and their role as Pickering emulsifiers. *Carbohydr Polym*, 250, 116878.
- SCHERF, K. A., KOEHLER, P. & WIESER, H. 2016. Gluten and wheat sensitivities – An overview. *Journal of Cereal Science*, 67, 2-11.
- SHAO, Y. & TANG, C.-H. 2016. Gel-like pea protein Pickering emulsions at pH 3.0 as a potential intestine-targeted and sustained-release delivery system for β -carotene. *Food Research International*, 79, 64-72.

- SHARKAWY, A., BARREIRO, M. F. & RODRIGUES, A. E. 2020. Chitosan-based Pickering emulsions and their applications: A review. *Carbohydrate Polymers*, 250.
- SRIDHARAN, S., MEINDERS, M. B. J., BITTER, J. H. & NIKIFORIDIS, C. V. 2020. On the Emulsifying Properties of Self-Assembled Pea Protein Particles. *Langmuir*, 36, 12221-12229.
- TANGER, C., SCHMIDT, F., UTZ, F., KREISSL, J., DAWID, C. & KULOZIK, U. 2021a. Pea protein microparticulation using extrusion cooking: Influence of extrusion parameters and drying on microparticle characteristics and sensory by application in a model milk dessert. *Innovative Food Science & Emerging Technologies*, 74.
- TANGER, C., UTZ, F., SPACCASASSI, A., KREISSL, J., DOMBROWSKI, J., DAWID, C. & KULOZIK, U. 2021b. Influence of Pea and Potato Protein Microparticles on Texture and Sensory Properties in a Fat-Reduced Model Milk Dessert. *ACS Food Science & Technology*, 2, 169-179.
- TAO, S., JIANG, H., GONG, S., YIN, S., LI, Y. & NGAI, T. 2021. Pickering Emulsions Simultaneously Stabilized by Starch Nanocrystals and Zein Nanoparticles: Fabrication, Characterization, and Application. *Langmuir*, 37, 8577-8584.
- TORCELLO-GOMEZ, A. & FOSTER, T. J. 2014. Interactions between cellulose ethers and a bile salt in the control of lipid digestion of lipid-based systems. *Carbohydr Polym*, 113, 53-61.
- WANG, Z., ZHANG, N., CHEN, C., HE, R. & JU, X. 2020. Rapeseed Protein Nanogels As Novel Pickering Stabilizers for Oil-in-Water Emulsions. *J Agric Food Chem*, 68, 3607-3614.
- WEI, Y., LIU, Z., GUO, A., MACKIE, A., ZHANG, L., LIAO, W., MAO, L., YUAN, F. & GAO, Y. 2021a. Zein Colloidal Particles and Cellulose Nanocrystals Synergistic Stabilization of Pickering Emulsions for Delivery of beta-Carotene. *J Agric Food Chem*, 69, 12278-12294.
- WEI, Y., ZHANG, L., LIAO, W., MAO, L., ZHANG, M., GUO, X., HUANG, C., HAN, H., MACKIE, A. & GAO, Y. 2021b. Enhanced stability and

controlled gastrointestinal digestion of beta-carotene loaded Pickering emulsions with particle-particle complex interfaces. *Food Funct*, 12, 10842-10861.

WU, H., NIAN, Y., LIU, Y., ZHANG, Y. & HU, B. 2022. Formation of pea protein amyloid fibrils to stabilize high internal phase emulsions for encapsulation of lutein. *Journal of Functional Foods*, 94.

XU, H. N., LIU, Y. & ZHANG, L. 2015. Salting-out and salting-in: competitive effects of salt on the aggregation behavior of soy protein particles and their emulsifying properties. *Soft Matter*, 11, 5926-32.

ZHANG, M., ZHOU, L., YANG, F., YAO, J., MA, Y. & LIU, J. 2022a. Construction of high internal phase Pickering emulsions stabilized by bamboo fungus protein gels with the effect of pH. *Food Chem*, 369, 130954.

ZHANG, M., ZHU, J., ZHOU, L., KAN, J., ZHAO, M., HUANG, R., LIU, J. & MARCHIONI, E. 2022b. Antarctic krill oil high internal phase Pickering emulsion stabilized by bamboo protein gels and the anti-inflammatory effect in vitro and in vivo. *Journal of Functional Foods*, 94.

ZOU, L., XIE, A., ZHU, Y. & MCCLEMENTS, D. J. 2019. Cereal proteins in nanotechnology: formulation of encapsulation and delivery systems. *Current Opinion in Food Science*, 25, 28-34.

Appendix A

Supporting information of Chapter 3

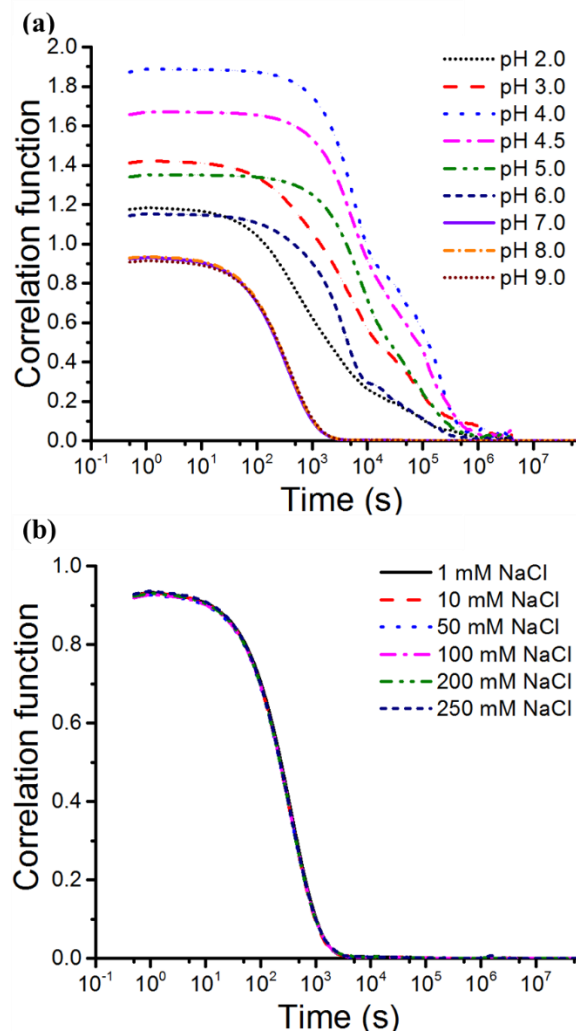


Figure S3.1. Correlation function of PPM as function of pH (a) and as function of ionic strength (b), respectively.

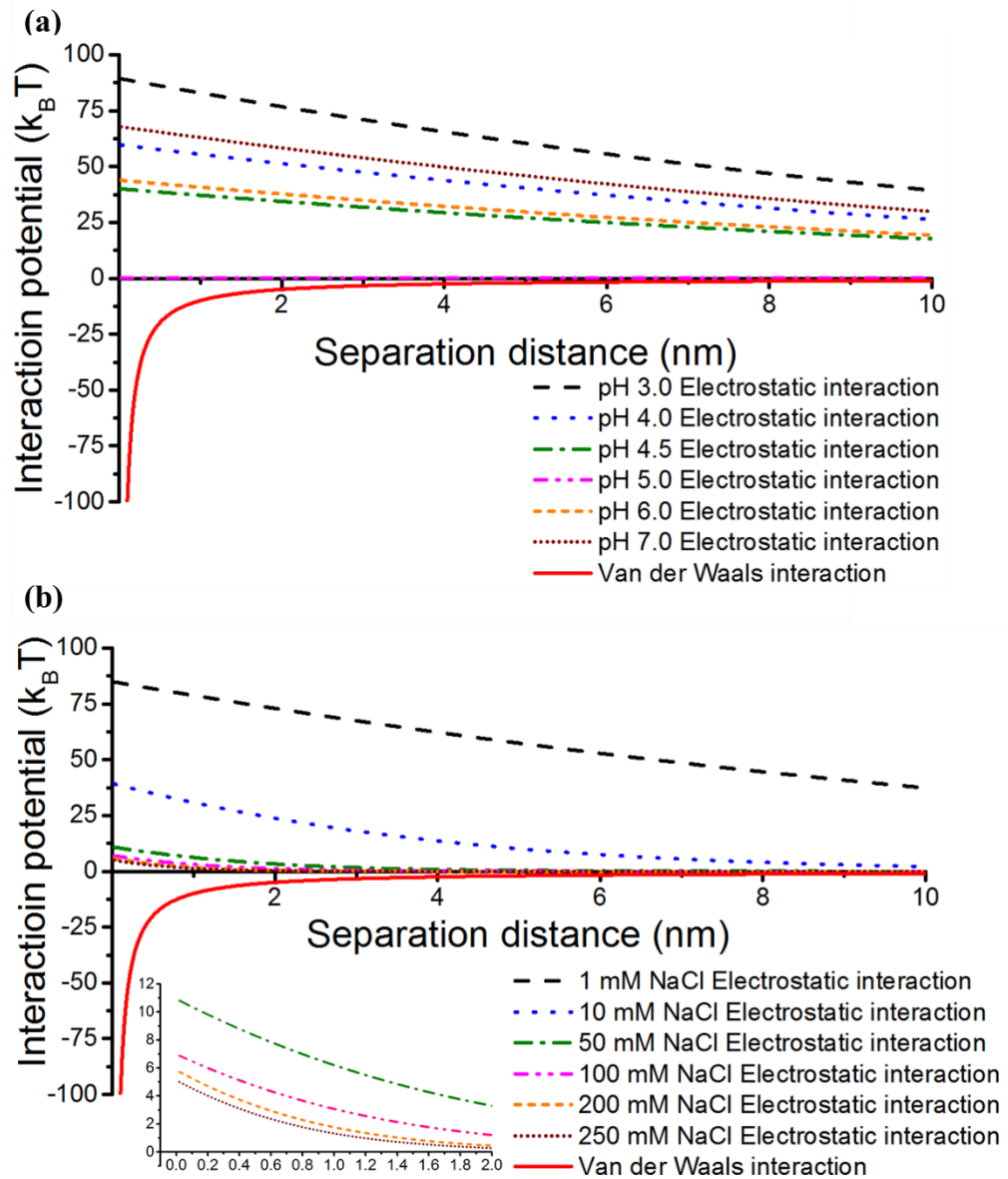


Figure S3.2. Electrostatic ($U_R/k_B T$) and Van der Waals interaction ($U_{VW}/k_B T$) of PPM at various pH (a) and at different ionic strengths (b), calculated as a function of separation distance (h).

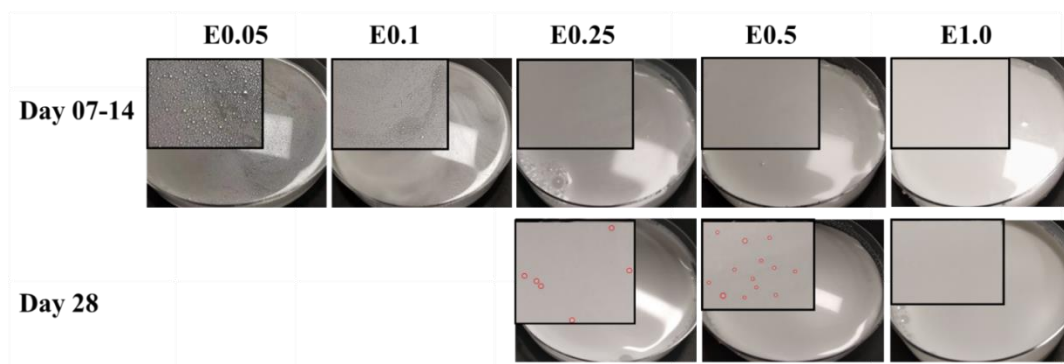


Figure S3.3. Visual images of coalescence stability of diluted PPM-stabilized Pickering emulsions (E0.05-E1.0) (1:4 w/w with buffer) prepared using different concentrations of PPM (0.05-1.0 wt%) during 28 days of storage at 4 °C. Red circles indicate the oil droplets.

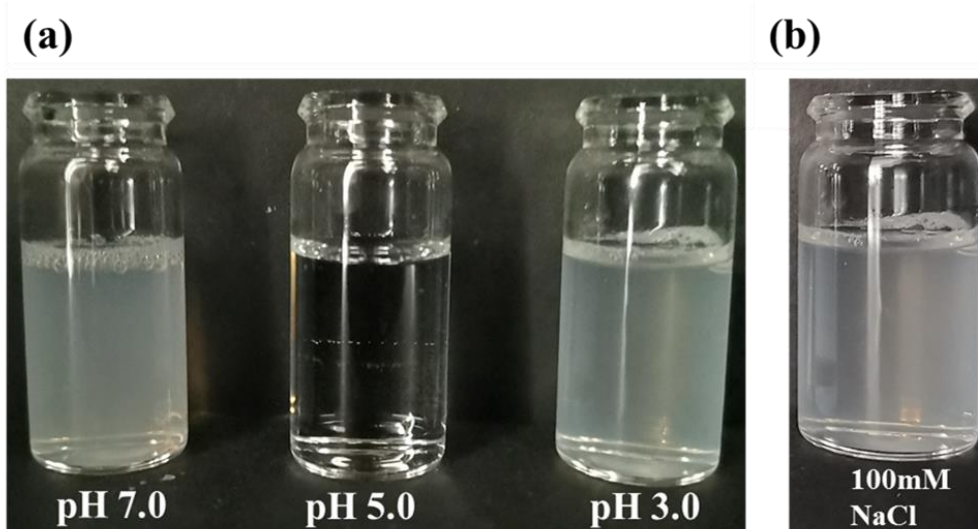


Figure S3.4. Visual images of centrifuged and diluted subnatants of PPM-stabilized Pickering emulsion (E1.0) (1:4 w/w buffer) at different pH values (a) or 100 mM NaCl (b), respectively.

Appendix B

Supporting information of Chapter 4

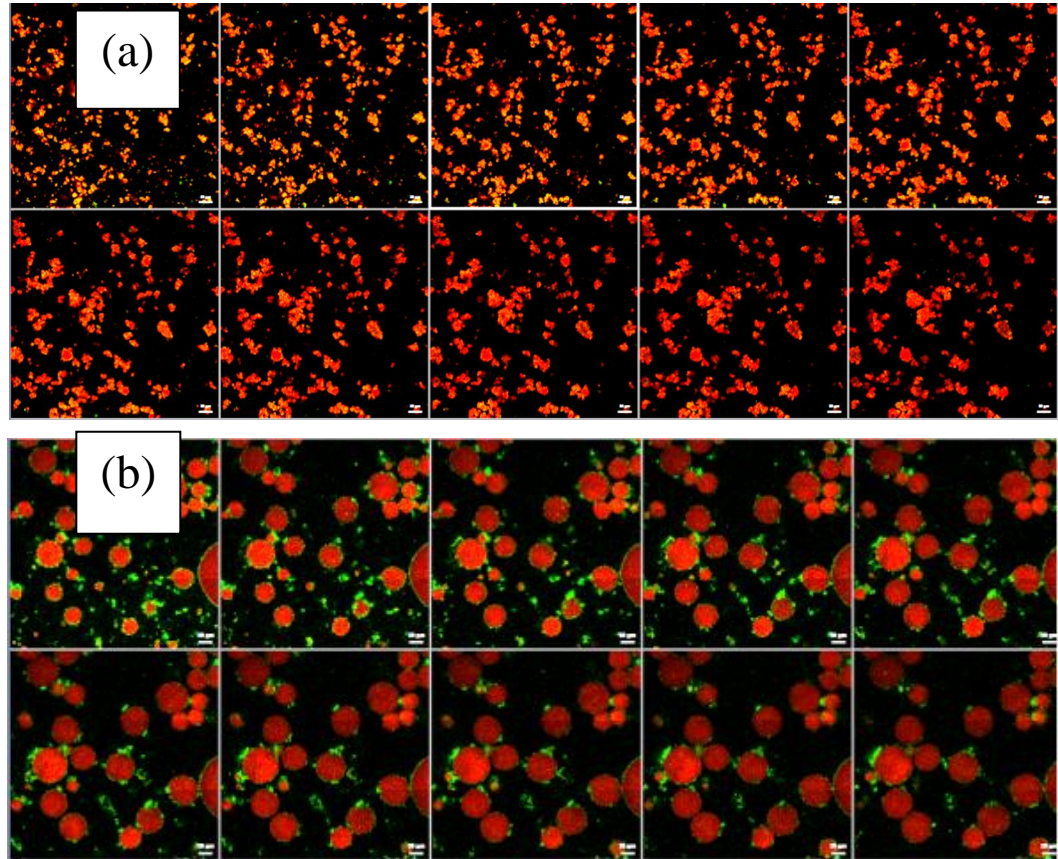


Figure S4.1. Confocal micrograph tiles covering different fields within the sample of 20 wt% oil-in-water emulsions stabilized by PPM (PPM-E) after (a) 0 min and (b) 120 min of *in vitro* gastric digestion at pH 3.0. Green colour represents PPM (stained by Nile Blue); red colour represents the oil phase (stained by Nile Red); black colour represents air or water. Note 0 min in Figure (a) represents the PPM-E+SGF mixture at pH 3.0 *without* the addition of pepsin. Scale bar represents 20 μm.

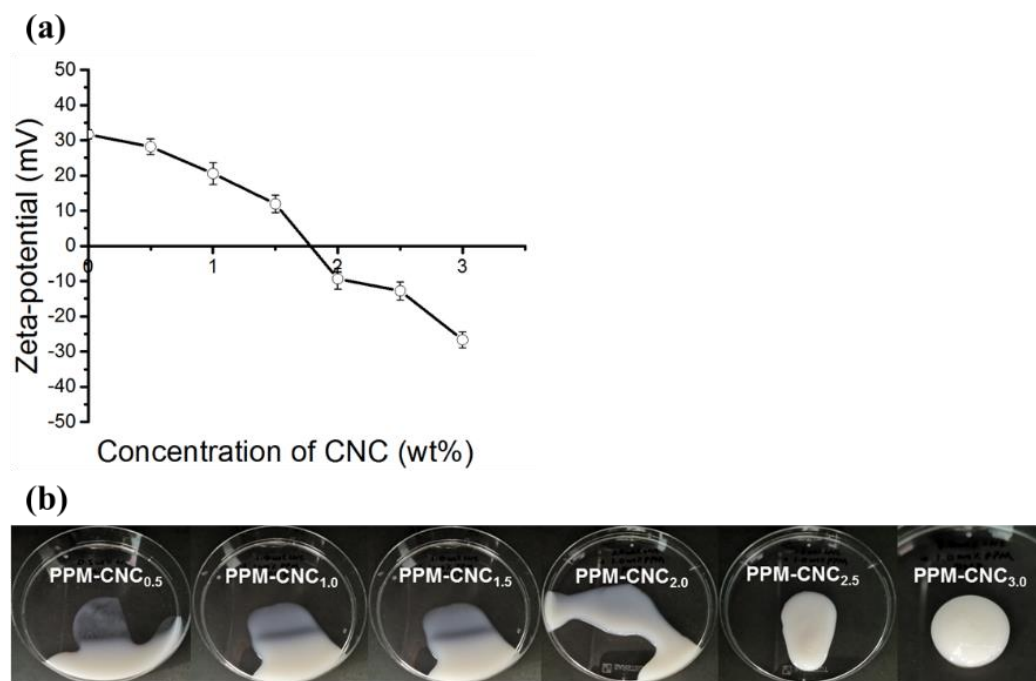


Figure S4.2. Influence of concentration of cellulose nanocrystals (CNC) on: (a) the mean ζ -potential values (\circ) of aqueous dispersion of PPM and (b) the flowability of these mixtures. Error bars represent standard deviations.

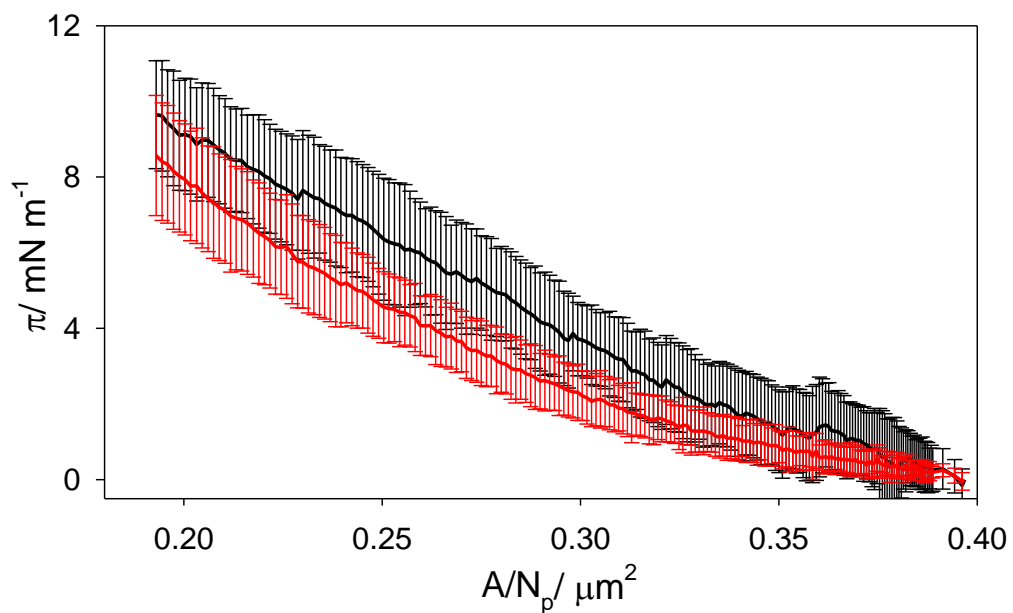


Figure S4.3. Surface pressure (π) versus area per particle (A/N_p) spread at the A-W interface for 0.466 wt% PPM: standard deviations about the means are shown for 9 separate compressions at pH 7.0 (black line and error bars) and pH 3.0 (red line and error bars).

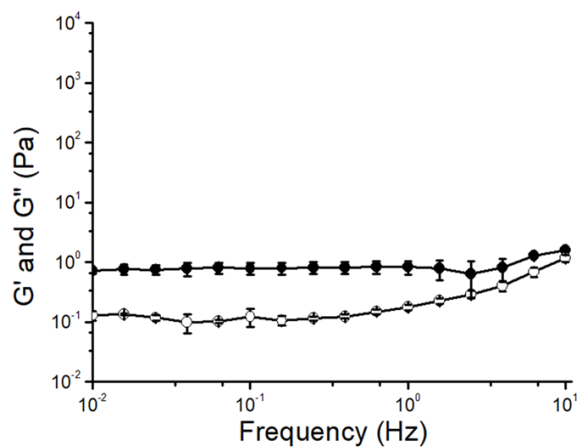


Figure S4.4. Frequency sweep curves of freshly prepared 20 wt% O/W emulsions stabilized by PPM (PPM-E) at pH 3.0 (G' ●, G'' ○). Error bars represent standard deviations.

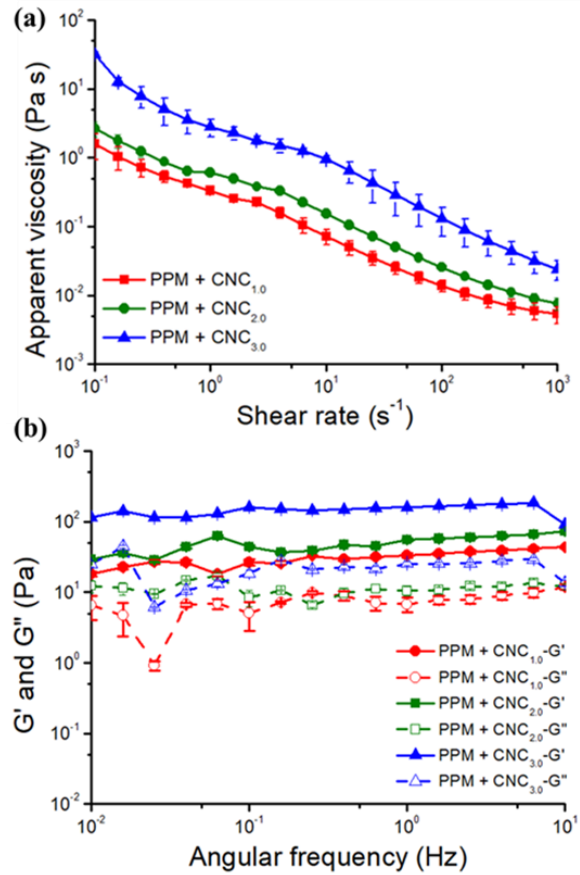


Figure S4.5. (a) Flow curves and (b) frequency sweep curves of freshly prepared PPM (1 wt%) at pH 3 mixed with 1 wt% CNC (PPM + CNC_{1.0}) (●), 2 wt% CNC (PPM + CNC_{2.0}) (■) and 3 wt% CNC (PPM + CNC_{3.0}) (▲). These samples are aqueous dispersions of particles without any oil droplets. Error bars represent standard deviations.

Table S4.1. Mean droplet size of PPM-E with 1, 2 and 3 wt% CNC after 0, 30 and 120 min *in vitro* gastric digestion. Time 0 min represents the emulsion + SGF mixture at pH 3.0 without the addition of pepsin. Different superscripts (a-b) in the same column indicate significant differences between different samples at $p < 0.05$ level.

Size (μm)		Digestion time (min)		
		0	30	120
PPM-E + CNC _{1.0}	d_{32}	4.0 ± 0.1^a	3.3 ± 0.2^b	3.2 ± 0.3^b
	d_{43}	18.0 ± 4.7^a	14.6 ± 3.7^a	12.3 ± 1.8^a
PPM-E + CNC _{2.0}	d_{32}	3.2 ± 0.2^a	3.1 ± 0.2^a	2.7 ± 0.2^b
	d_{43}	13.9 ± 1.9^a	13.1 ± 1.9^a	9.4 ± 1.7^b
PPM-E + CNC _{3.0}	d_{32}	3.2 ± 0.4^a	3.1 ± 0.3^a	2.4 ± 0.1^b
	d_{43}	17.6 ± 4.9^a	16.4 ± 4.9^a	8.1 ± 1.4^b

Different superscripts (a and b) in the same row / column represent significant differences between different samples at $p < 0.05$ level.